



The University of
Nottingham

Microwave assisted synthesis of chalcogenide glasses.

Nupur Prasad

May 2010

GEORGE GREEN LIBRARY OF
SCIENCE AND ENGINEERING

Supervisors

Prof. A. B. Seddon

Prof. S. Kingman

Prof. D. H. Gregory

Microwave assisted synthesis of chalcogenide glasses.

by

Nupur Prasad

**A thesis submitted to the University of Nottingham under the supervision of
Prof. A. B. Seddon, Prof. D. H. Gregory and Prof S. Kingman in partial
fulfilment of the requirements of the degree of Doctor of Philosophy.**

May 2010

**School of Chemistry
University of Nottingham
Nottingham,
NG2 7RD,
United Kingdom.**

**GEORGE GREEN LIBRARY OF
SCIENCE AND ENGINEERING**

Acknowledgements

I am grateful to all those who gave me an opportunity to work over this project. I wish to express my respect and gratitude to my supervisor Prof. AB. Seddon first for her constant guidance, support and inspiration. I thank Dr. David Furniss (Senior Research Office with the Novel Photonic Glasses Group) for his constant guidance and support. I thank my supervisors Prof. D. H. Gregory and Prof. S. Kingman for their guidance.

I am thankful to Dr. Mukul K. Sinha (Director, Expert Software Consultants Ltd., New Delhi, India), my ex-supervisor for his constant encouragement.

I thank Mr. Keith Dinsdale (Senior Experimental Officer in the Wolfson Centre for Materials Research) for his help in obtaining selected area electron diffraction data and Dr. Nigel Neate and Mrs. Nikki Weston (Technical Support Staff) for their help with environmental scanning electron microscopy. I also thank the Department of Chemistry and Department of Mechanical, Materials, and Manufacturing Engineering, University of Nottingham, for providing all the facilities necessary for the research.

I thank my elder brother and his family for their emotional, educational and financial support. I express my respect and gratitude to my parents who have always been a constant source of inspiration. I thank Helen, WeiJian and all my friends who always helped in the lab.

I thank University of Nottingham for their financial support.

Abstract

Chalcogenide glasses have several potential uses for new photonic devices for two reasons: i) their infrared (IR) transparency and ii) viscous flow at the glass transition temperature (T_g). Because of the latter, these glasses can be drawn to optical fibre and polished glass discs can be patterned above T_g for instance as planar waveguides. The fibre or waveguide shaped chalcogenide glasses have several potential uses as chemical sensors, biosensors, laser power delivery *etc.* and hence efforts have been made to synthesise high optical quality chalcogenide glasses.

The well-established melt-quenching method was used as a comparative to prepare chalcogenide glass-melts in this project. Conventionally, the chalcogenide glass-melts are prepared using a rocking resistance furnace but this process is very long and cumbersome. To make the glass-melting process fast, simple and cost effective microwave heating was investigated instead in this project, and this was the main aim of the project. As_2S_3 , $Ge_{33}As_{12}Se_{55}$, $Te_{20}As_{30}Se_{50}$ glasses were made with partial success and As_2Se_3 , $Ge_{17}As_{18}Se_{65}$ glasses successfully, for the first time to the author's knowledge, through microwave heating in a domestic microwave oven (DMO) working at a frequency 2.45 GHz in less than an hour while the resistance heating method took about 1.5 days. The DMO output power was 800 W or 1000 W, and co-heating using both the microwaves and convection current heating to 220°C enabled some glass preparations to be carried out in *ca.* 10 minutes. The reactants were crushed manually for the DMO preparation of chalcogenide products keeping in mind that electric current tends to flow at the surface of the material which is known as 'skin effect'. The size of the silica glass melt-ampoule was kept as small as possible (normally ~ 10 cm) so that the DMO chalcogenide-melt could collect at the bottom of the ampoule and form a DMO chalcogenide rod product.

The increased rate of reaction in the DMO compared to the rate of reaction in the rocking resistance furnace was attributed to the formation of plasma which caused a very high temperature ($> 1000^\circ C$) of the reaction system leading to the almost instant melting of the some reactants. The boiling DMO chalcogenide-melt was seen in several cases but $As/S = 2:3$ (at%) did not boil when exposed to microwaves .

Visually homogenous DMO chalcogenide-products were formed in each of the above stated compositions except in the case of DMO As-S product when four distinct layers could be seen.

The red transparent portion of the DMO As-S sample was X-ray amorphous and showed no crystal feature in SAED (Selected area electron diffraction) using TEM (Transmission electron microscopy) whereas the non-glassy portion showed some crystalline peaks in XRD (X-ray diffraction) but showed no crystalline features in SAED. The DMO Ge/As/Se=33/12/55 (at%) rod product showed a single crystalline peak in the XRD pattern but it was completely amorphous according to SAED. On the other hand, the DMO Te/As/Se = 20/30/50 (at%) rod product showed slight evidence of crystallinity from SAED but was completely amorphous in XRD. DMO As/Se = 40/60 (at%) rod product and DMO Ge/As/Se=17/18/65 (at %) rod did not show any crystalline structure from XRD and from SAED.

The inhomogeneity of the DMO As-S glass was further reflected in the multiple T_gs observed using DTA (Differential thermal analysis) viz.: 166°C, ~194°C (broad) and 300°C in the first DTA run. Though, the sample showed a single T_g value of 202°C during the second DTA run after quenching in-situ the sample from the first DTA run. The stoichiometry of this glass was As_{43.9}S_{56.1} when observed through EDX (Energy dispersive X-ray analysis) which was performed using ESEM (Environmental scanning electron microscopy) showing that the glass was inhomogeneous. The DMO As/Se = 2:3 (at%) rod product showed a single T_g value of 180°C ± 5°C and the stoichiometry was found to be As_{40.1}Se_{59.9} from EDX analysis which was very close to the desired value. The DMO rod product obtained from the composition Ge/As/Se = 17/18/65 showed a single T_g value of 246°C ± 5°C and the observed stoichiometry of the DMO chalcogenide product was Ge_{17.6}As_{19.2}Se_{63.5}. Whereas the Ge_{32.8}As_{11.0}Se_{56.4} DMO rod product could be made from the batch composition Ge/As/Se= 33/12/55 with a T_g value of 368°C ± 5°C but the conventionally prepared glass exhibited a stoichiometry Ge_{33.8}As_{12.5}Se_{53.6} with T_g value 371°C ± 5°C showing that a slight increase in percentage of germanium in the glass composition increases the T_g value. The Te_{19.6}As_{30.4}Se_{50.0} DMO rod product was obtained from Te/As/Se = 30/20/50 batch composition having a T_g value of 371°C ± 5°C showing that the experimental values for the stoichiometry and T_g of the product were very close to the desired value. A sample of Te/As/Se = 20/30/50 was heated in the DMO only for 5 minutes when stoichiometry of the product was found to be Te_{19.6}As_{32.6}Se_{47.8} showing that prolonged exposure of microwaves, which facilitated boiling, was important for homogenisation of the product (note that DMO As-S product never boiled) since the ampoule was not rocked inside the DMO.

It was observed that optical absorption at 2.9 μm wavelengths due to hydroxide contamination for the DMO As-S product was reduced to ~ 3% of that of the As₂S₃ glass made through conventional heating. The absorption bands for –OH group at 2.9 μm and H₂O

at 6.3 μm were very low in almost all the DMO products. Some carbon and silica contamination was found to be slightly larger in DMO products than that present in the conventionally prepared products and the reasons for this are not known at present. The DMO chalcogenide products were obtained reproducibly except in the cases of the DMO As-S product.

Table of Contents

Table of Contents	vii
Glossary of Symbols and Abbreviations.....	xii
Chapter 1	1
Introduction.....	1
1.1 Background of the project.....	1
1.2 Aims and objectives of the project.....	2
1.3 Thesis Layout.....	2
References:.....	4
Chapter 2	5
Literature Review.....	5
2.1 Arrangement of atoms or ions in a glass.....	5
2.2 Definition of a glass.....	6
2.3 Amorphous nature of glass.....	7
2.4 The thermal properties of glass.....	7
2.4.1 The glass transition temperature (T_g).....	8
2.4.1.1 The dependence of T_g on bond strength of the chalcogenide molecular structure. ...	9
2.4.2 The liquidus temperature (T_L).....	11
2.4.3 The fictive temperature (T_f).....	11
2.5 The optical properties of chalcogenide glasses.....	12
2.5.1 The optical loss due to intrinsic factors.....	12
2.5.1.1 Intrinsic absorption.....	12
2.5.1.1.1 Absorption due to electronic transitions.....	13
2.5.1.1.2 Multiphonon absorption.....	14
2.5.1.2 Intrinsic scattering.....	14
2.5.2 Optical loss due to extrinsic factors.....	15
2.5.2.1 Absorption due to extrinsic factors.....	15
2.5.2.2 Scattering due to extrinsic factors.....	18
2.6 Types of inorganic compound glasses.....	18
2.7 Applications of chalcogenide glasses.....	19
2.7.1 Potential passive optical applications of chalcogenide glasses.....	20
2.7.1.1 Laser power delivery.....	20
2.7.1.2 Chemical sensors and biosensors.....	21
2.7.2 Potential active optical applications of chalcogenide glasses.....	22
2.8 Methods of preparation of chalcogenide glasses.....	22
2.8.1 The melt-quenching procedure.....	23
2.8.1.1 Formation of the glass-melt.....	23
2.8.1.2 Glass-melt quenching.....	23
2.8.1.3 Annealing.....	24
2.8.2 Sol-gel procedure.....	25
2.8.3 Sputtering procedures.....	25
2.8.4 Chemical and physical vapour deposition.....	25
2.9 The microwave heating mechanism and its application.....	26
2.9.1 Microwave heating due to molecular polarisation.....	26
2.9.2 Heating effects due to conduction.....	28
2.9.3 Microwave heating in metals.....	29
2.9.4 A review of synthesis of materials using microwave heating.....	29
2.10 Summary.....	31
References:.....	32
Chapter 3	35
Experimental.....	35
3.1 Glass-melting.....	35
3.1.1 Glass-melting process in rocking resistance furnace.....	36
3.1.1.1 Ampoule preparation.....	36
i) HF etching.....	36
ii) Oven drying.....	36

iii) Air baking.....	37
iv) Vacuum baking.....	37
3.1.1.2 Starting materials and their purification.....	38
i) The arsenic purification process.....	38
ii) The sulfur purification process.....	40
3.1.1.3 Glass-batching procedure.....	42
3.1.1.4 Formation of the glass-melt.....	43
3.1.2 Glass-melting in domestic microwave oven (DMO).....	45
3.1.2.1 Ampoule preparation.....	45
(a) Ampoule for the synthesis of arsenic sulfide glass.....	45
(b) Ampoule preparation for the synthesis of arsenic selenide, germanium arsenic selenide (GAS), tellurium arsenic selenide (TAS) and germanium arsenic selenium telluride (GAST) glass.....	45
3.1.2.2 The starting materials and their purification.....	46
3.1.2.3 Glass batching.....	46
3.1.2.4 Initial trials of glass melting in DMO.....	46
3.1.2.5 Formation of the chalcogenide melt in DMO.....	47
(i) Optimising the precise location of melt ampoule in DMO.....	47
3.2 Quenching, annealing and sample preparation.....	51
3.2.1 Quenching and annealing of the chalcogenide melt.....	51
3.2.2 Removal of chalcogenide glass rod from silica glass ampoule.....	53
3.2.3 Sample preparation.....	53
3.2.3.1 Sectioning of all glass samples.....	53
3.2.3.2 Chalcogenide glass polishing procedure.....	54
3.3 Characterisation techniques.....	55
3.3.1 X-ray diffractometry (XRD).....	56
3.3.1.1 Theory of operation.....	56
3.3.1.2 Equipment.....	57
3.3.1.3 Sample preparation.....	58
3.3.1.4 Procedure and equipment.....	58
3.3.2 Selected area electron diffraction (SAED) using transmission electron microscopy (TEM).....	58
3.3.2.1 Theory of operation.....	59
3.3.2.2 Equipment.....	59
3.3.2.3 Sample preparation.....	60
3.3.2.4 Procedure and equipment.....	60
3.3.3 Glass transition temperature and differential thermal analysis (DTA).....	60
3.3.3.1 Theory of operation.....	60
3.3.3.2 Equipment.....	61
3.3.3.3 Sample preparation.....	62
3.3.3.4 Procedure.....	63
3.3.3.4 Data handling.....	63
3.3.4 Differential scanning calorimetry (DSC).....	64
3.3.4.1 Theory of operation.....	64
3.3.4.2 Sample preparation.....	64
3.3.4.3 Procedure and equipment.....	65
3.3.4.4 Data handling.....	65
3.3.5 Fourier transform infrared (FTIR) spectroscopy.....	66
3.3.5.1 Theory of operation.....	66
3.3.5.2 Equipment.....	66
3.3.5.3 Sample preparation.....	67
3.3.5.4 Procedure.....	67
3.3.5.5 Data handling.....	67
3.3.6 Field emission gun environmental scanning electron microscopy (FEG ESEM) with energy dispersive X-ray analysis (EDX).....	68
3.3.6.1 Theory of operation.....	68
3.3.6.2 Equipment.....	68
3.3.6.3 Sample preparation.....	68
3.3.6.4 Procedure.....	69

3.4 Further processing of chalcogenide glasses made by microwave heating for photonic applications.....	69
3.4.1 Fibre drawing.....	70
3.4.2 Vacuum pressing.....	71
References:.....	72
 Chapter 4.....	 73
Microwave assisted synthesis of arsenic sulfide.....	73
4.1 Microwave irradiation of arsenic and sulfur.....	73
4.1.1 Microwave irradiation of arsenic pellets of diameter ca. 4 mm to 7 mm with sulfur flakes in atomic ratio As_2S_3 (id: MW(I)).....	73
4.1.2 Microwave irradiation of arsenic pellets with diameter < 2 mm with powdered sulfur in atomic ratio As_2S_3 (id: MW6).....	74
4.1.3 XRD and TEM SAED of the unannealed deep-red, glass mass (portion 'A' of id: MW6 (fig. 4.1)) and orange friable bits (portion 'D' of id: MW6 (fig. 4.1)).....	75
4.1.4 Differential thermal analysis (DTA) of the unannealed deep red glassy mass (portion 'A' of id: MW6 (fig. 4.1)).....	76
4.1.5 Annealing of the deep red glassy mass (portion 'A' of id: MW6 (fig 4.1)).....	78
4.1.6 X-ray diffractometry (XRD) and optical microscopy of the deep red glassy mass (portion 'A' of id: MW6 (fig. 4.1)) annealed at 212 °C.....	79
4.2 Synthesis of arsenic sulfide glass via resistance heating.....	81
id: CF 074.....	82
4.2.2 Thermal analysis of the conventionally prepared arsenic sulfide id: CH 25.....	82
4.2.3 Optical microscopy of the conventionally prepared arsenic sulfide id:CF 074.....	83
4.3 The optical transmission window measurement using FTIR of the conventionally prepared arsenic sulfide and as-annealed DMO arsenic sulfide.....	84
4.4.1 ESEM EDX for stoichiometry of the as-annealed DMO As-S glassy portion 'A' id: MW6 (see section 4.1.5).....	87
4.4.2 ESEM EDX for stoichiometry of the DTA 'homogenised' DMO As-S glassy portion 'A' id: MW6 (see section 4.1.4).....	88
4.4.3 ESEM EDX for stoichiometry of the conventionally prepared As-S id: CF074.....	91
4.5 The irreproducibility of the glass-melting reaction in the DMO.....	92
4.6 Summary.....	93
References:.....	94
 Chapter 5.....	 95
Microwave assisted synthesis of arsenic selenide.....	95
5.1 Microwave irradiation of the arsenic and selenium and formation of DMO As-Se rods.....	96
5.1.1 Product id: MW8.....	96
5.1.2 Products id: MW9; MW10; MW18; MW19.....	97
5.1.3 Product id: MW39, MW55.....	102
5.2 Synthesis of arsenic selenide glass via resistance heating.....	102
5.3 Characterisation.....	104
5.3.1 Amorphicity of the DMO As-Se products (id: MW8, MW9; MW10; MW18; MW19; MW39) and conventionally prepared product id: CH12 by means of XRD and TEM SAED.....	104
5.3.2 Thermal analysis of the As-Se products.....	106
5.3.2.1 DMO As-Se products.....	106
(a) Evaluation of T _g using DTA.....	106
(b) Evaluation of T _g using DSC.....	107
5.3.2.2 As-Se product made via conventional heating (id: CH12).....	108
5.3.3 Stoichiometry of the DMO and conventionally prepared As-Se products by means of ESEM EDX.....	109
5.3.3.1 DMO As-Se product.....	109
5.3.3.2 Conventionally prepared As-Se product.....	111
5.3.3.3 Conclusions.....	113
5.3.4 Measurement of the optical infrared transmission window of DMO and conventionally prepared As-Se products.....	113
5.3.5 Refractive indices.....	116
5.4 Further discussion.....	118
5.5 Summary.....	119

References.....	120
Chapter 6.....	121
Microwave assisted synthesis of germanium arsenic selenide.....	121
6.1 Microwave irradiation of the starting materials and the formation of product rods.....	121
6.1.1 Formation of DMO Ge/As/Se = 17/18/65 (at%) rod (id: MW29).....	123
6.1.2 Formation of Ge/As/Se = 33/12/55 (at%) rod (id: MW38 and MW46).....	125
6.2 Synthesis of $Ge_{17}As_{18}Se_{65}$ and $Ge_{33}As_{12}Se_{55}$ glasses via resistance heating.....	126
6.2.1 Synthesis of $Ge_{17}As_{18}Se_{65}$ glasses (id: CH13 and CH14) via resistance heating.....	126
6.2.2 Synthesis of $Ge_{33}As_{12}Se_{55}$ glass (id: CH15) via resistance heating.....	127
6.3 Product characterisation.....	128
6.3.1 Characterisation of DMO Ge/As/Se = 17/18/65 products (id: MW29, MW31 and MW41) and conventionally prepared products (id: CH13 and CH14).....	128
6.3.1.1 Amorphicity.....	128
6.3.1.1.1 XRD.....	128
6.3.1.1.2 TEM SAED.....	131
6.3.1.2 Thermal analysis of DMO Ge/As/Se = 17/18/65 products (id: MW29, MW31) and conventionally melted product Ge/As/Se = 17/18/65 (id: CH13).....	131
6.3.1.2.1 Evaluation of Tg of DMO Ge/As/Se = 17/18/65 (id: MW31) using DTA.....	132
6.3.1.2.2 Evaluation of Tg Ge/As/Se = 17/18/65 (at %) products.....	132
6.3.1.3 The stoichiometry of the DMO and conventionally prepared Ge/As/Se = 17/18/65 (at%) products (id: MW29 and MW31, and CH13, respectively).....	134
6.3.1.3.1 EDX analysis of the DMO Ge/As/Se = 17/18/65 (at%) rod product(id: MW31) that had adhered to the silica glass melting ampoule.....	134
6.3.1.3.2 EDX analysis of the middle part of the DMO Ge/As/Se = 17/18/65 (at%) rod product (id: MW31) compared to that of the conventionally prepared Ge/As/Se = 17/18/65 (at%) product (id: CH13).....	136
6.3.1.4 Measurement of optical transmission window using FTIR.....	138
6.3.2 Characterisation of DMO Ge/As/Se = 33/12/55 product (id: MW38) and conventionally prepared product (id: CH15).....	141
6.3.2.1 Amorphicity.....	141
6.3.2.1.1 XRD.....	141
6.3.2.1.2 TEM SAED.....	142
6.3.2.2 Thermal analysis of DMO Ge/As/Se = 33/12/55 (at%) product (id: MW38) and conventionally melted product $Ge_{33}As_{12}Se_{33}$ (id: CH15).....	142
6.3.2.3 ESEM EDX analysis of the DMO Ge/As/Se = 33/12/55 product (id: MW38 and id: CH15).....	143
6.3.2.4 The optical transmission window measurement by means of FTIR.....	145
References:.....	150
Chapter 7.....	151
Microwave assisted synthesis of.....	151
tellurium arsenic selenide.....	151
7.1 Microwave irradiation of the starting materials and the formation of a chalcogenide rod product.....	151
7.1.1 $Te_{20}As_{30}Se_{50}$ product (id: MW30).....	153
7.1.2 $Te_{20}As_{30}Se_{50}$ products (id: MW33 and MW36).....	154
7.2 The synthesis of Te/As/Se = 20/30/50 in a rocking resistance furnace.....	155
7.2.1 $Te_{20}Se_{30}Te_{50}$ product (id: CH20).....	155
7.3 Characterisation of the DMO, and conventionally prepared, Te/As/Se = 20/30/50 (atomic %) products.....	156
7.3.1 Amorphicity of the DMO Te/As/Se = 20/30/50 (atomic %) products (MW30, and MW33) and conventionally prepared Te/As/Se = 20/30/50 (atomic %) product (id: CH20).....	156
7.3.1.1 Powder XRD.....	156
7.3.1.2 TEM SAED.....	157
7.3.2 Thermal analysis of the glass.....	158
7.3.3 Stoichiometry of the DMO and conventionally prepared $Te_{20}As_{30}Se_{50}$ products (id: MW30 and MW36 respectively).....	159
7.3.4 Optical transmission using FTIR.....	161
7.4 Further discussion.....	165

7.5 Summary.....	166
References.....	167
Chapter 8.....	168
<i>Processing of the DMO As₂Se₃ glass for photonic use.</i>	168
8.1 <i>The fibre drawing of the DMO As₂Se₃ glass.</i>	168
8.2 <i>The vacuum pressing of the DMO As₂Se₃ glass</i>	169
8.3 <i>Summary</i>	172
Chapter 9.....	173
<i>Conclusions</i>	173
9.1 <i>Conclusions</i>	173
9.2 <i>Future work</i>	178
<i>References:</i>	179
APPENDICES.....	180

Glossary of Symbols and Abbreviations

ASTM	American Society for Testing Materials
DMO	Domestic microwave oven
ID	Internal diameter
OD	Outer diameter
MW	Microwave
CH	Conventional heating
CF	Chalcogenide fibre
As-S	Arsenic and sulfur
As-Se	Arsenic and selenium
GAS	Germanium, arsenic and selenium
TAS	Tellurium, arsenic and selenium
CVD	Chemical vapour deposition
DSC	Differential scanning calorimetry
DTA	Differential thermal analysis
EDX	Energy Dispersive X-Ray Analysis
ESEM	Environmental scanning electron microscopy
FTIR	Fourier transform infrared spectroscopy
TEM	Transmission electron microscopy
TMA	Thermomechanical analysis
XRD	X-ray diffractometry
B	Rayleigh coefficient
c	Velocity of light
d	Inter-planer spacing
E_g	Photon energy of the band gap
h	Plank's constant
I	Intensity of light
IR	Infrared

K	Force constant
λ	Wavelength
λ_c	Short wavelength cut-off
m_1, m_2	Point masses of a molecule
MCT	Mercury-cadmium-telluride
mIR	Mid-infrared
n	Refractive index
nIR	Near infrared
T_g	Glass transition temperature
T_l	Liquidus temperature
T_c	Crystallisation temperature
V_{fibre}	Drum take-up speed
V_{preform}	Preform feed-in speed
Z	Average coordination number

Chapter 1

Introduction.

1.1 Background of the project.

Chalcogenide glasses are composed of one or more chalcogen elements, (Group 16 of the Periodic Table) such as sulfur, selenium and tellurium, in conjunction with arsenic, germanium, gallium, lanthanides *etc.*. These glasses have potential optical transmission windows within the range of the far-visible ($\sim 0.6 \mu\text{m}$ wavelength) to the mid-infrared ($\sim 20 \mu\text{m}$ wavelength) [1]. In addition to that, they can be moulded at their glass transition temperatures such that they can be drawn to optical fibre (see section 3.5.1) or their polished discs can be patterned by hot pressing methods (see section 3.5.2) [2-4]. Chalcogenide optical fibres can be used as infrared radiation carriers for several potential applications. For example, they could be used for infrared laser power delivery which has several uses such as microsurgery, industrial welding *etc.*. Fourier transform infrared spectroscopy is one of the most sensitive and handy tools to detect infrared radiation. A combination of Fourier transform infrared spectroscopy and chalcogenide fibre makes for potential devices for infrared sensing, such as biosensors, environmental sensors *etc.*. The patterned discs can be used as rib-waveguides [2-15]. Due to the potential optical applications there is a need to prepare high optical quality chalcogenide glasses. Chalcogenide glass melting is normally done by means of resistance furnace heating to form a liquid melt which is quenched to form glass.

There are several sources of impurities that can be incorporated in the chalcogenide glass during its formation. For example, sulfur can be a source of water and carbon in sulfide glasses, arsenic inevitably contains its oxide on its upper surface. The chalcogenide glasses tend to volatilise above the liquidus and so must be contained during the melting. The silica glass melt-ampoules used can be a source of carbon and hydroxide impurity. It is suggested that the dangling chemical $\equiv \text{Si} - \text{O}^-$ bonds of the inner walls of the silica glass melt-ampoules react with atmospheric moisture and also the ampoule inner surface can be contaminated with carbonaceous material, both of which can be dissolved in the chalcogenide glass-melt at a high temperature on prolonged heating during the formation of the chalcogenide glass-melt.

These impurities are infrared active and they absorb energy from the launched infrared beam in the chalcogenide optical devices. The loss of energy from the total energy launched in the form of infrared electromagnetic radiation in a chalcogenide optical device due to impurities present in the chalcogenide glass is known as optical loss due to extrinsic factors. Extrinsic factors determine in practice the percentage of light transmitted through a chalcogenide optical device. The optical loss due to extrinsic factors can theoretically be eliminated [16]. Due to the potential optical applications there is a need to synthesise impurity-free chalcogenide glasses.

1.2 Aims and objectives of the project.

The overall aim of this work was to investigate whether high optical quality chalcogenide glasses can be prepared in a domestic microwave oven (DMO). The potential advantage of using a DMO rather than conventional resistance heating is speed of reaction [17-19] as the conventional melting schedule for making the chalcogenide glasses is typically 1.5 days. However there have been few reports of making inorganic compound glasses in a DMO and only one report of making chalcogenide glasses which resulted, according to the authors [20], in a phase separated glass.

The objectives to achieve the overall aim were to investigate the melting of several binary and ternary chalcogenide glass compositions *viz.*: arsenic sulfide; arsenic selenide; germanium arsenic selenide and tellurium arsenic selenide to compare the products made in a DMO with those made by the conventional method. The product comparison was carried out by investigating the amorphicity, homogeneity, T_g and glass transmission window of products made from the same nominal batch but by the alternative methods of DMO or resistance heating. The melt was encapsulated in a silica glass melting ampoule in both heating techniques.

1.3 Thesis Layout.

Chapters 1, 2 and 3 comprise the first part of the thesis. Chapter 1 is the introduction of the thesis. The literature reviewed in this project is summarised in Chapter 2. The experimental procedures used for the preparation of chalcogenide glasses and the characterisation techniques used in this project are discussed in Chapter 3.

The second part of the thesis comprises Chapters 4 to 8. In these Chapters the project results are presented and discussed. The results obtained while making arsenic sulfide through microwave heating are discussed in Chapter 4. In Chapter 5 is discussed the microwave assisted synthesis of arsenic selenide whereas the further processing of the arsenic selenide made through microwave heating for photonic uses is described in Chapter 8. The results obtained for the microwave assisted synthesis of $\text{Ge}_{17}\text{As}_{18}\text{Se}_{65}$ and $\text{Ge}_{33}\text{As}_{12}\text{Se}_{55}$ are elucidated in Chapter 6. The preparation of tellurium arsenic selenide ($\text{Te}_{20}\text{As}_{30}\text{Se}_{50}$) through microwave heating was investigated and the results obtained are discussed in Chapter 7.

The third part of the thesis is Chapter 9 which summarises the conclusion drawn from the overall work done in this project.

References:

- [1] D. Lezal, *J. Optoelect. & Adv. Mat* **5** (2003), p. 23.
- [2] S. Hocdé, C.B. Plédel, D.L. Coq, H.L. Ma and J. Lucas, *J. Non-Cryst. Solids* **274** (2000), p. 17.
- [3] A.B. Seddon, W.J. Pan, D. Furniss, C.A. Miller, H. Rowe, D. Zhang, E. McBrearty, Y. Zhang, A. Loni, P. Sewell and T.M. Benson, *J. Non-Cryst. Solids* **352** (2006), p. 2515
- [4] X. Zhang, H. Ma and J. Lucas, *J. of Optoelect. and Adv. Mat.* **5** (2003), p. 1327.
- [5] J.S. Sanghera and I.D. Aggarwal, *J. Non-Cryst. Solids* **256-257** (1999), p. 6.
- [6] J.S. Sanghera, L.B. Shaw, L.E. Busse, V.Q. Nguyen, P.C. Pureza, C.B. C., B.B. Harrison, I.D. Aggarwal, R. Mossadegh, F. Kung, D. Talley, D. Roselle and R. Miklos, *Fiber Integr. Opt.* **19** (2000), p. 251
- [7] J.S. Sanghera, L.B. Shaw and I.D. Aggarwal, *C. R. Chemie* **5** (2002), p. 873.
- [8] J.A. Moon and D.T. Schaafsma, *Fiber Integr. Opt.* (2000), p. 201.
- [9] K. Michel, B. Bureau, C. Pouvreau, J.C. Sangleboeuf, C. Boussard-Plédel, T. Jouan, T. Rouxel, J.-L. Adam, K. Staubmann, H. Steinner, T. Baumann, A. Katzir, J. Bayona and W. Konz, *J. Non-Cryst. Solids* **326-327** (2003), p. 434.
- [10] S. Hocde, C.B. Pledel, G. Fonteneau and J. Lucas, *Solid State Sci.* **3** (2001), p. 279.
- [11] J. Keirsse, C.B. Plédel, O. Loreal, O. Sire, B. Bureau, B. Turlin, P. Leroyer and P. Lucas, *J. Non-Cryst. Solids* **326-327** (2003), p. 430.
- [12] P. Lucas, M.R. Riley, C.B. Plédel and B. Bureau, *Anal. Biochem.* **351** (2006), p. 1.
- [13] D.L. Coq, K. Michel, J. Keirsse, C.B. Plédel, G. Fonteneau, B. Bureau, J.M.L. Quéré, O. Sire and J. Lucas, *Comptes Rendus Chimie* **5** (2002), p. 907.
- [14] D.L. Coq, K. Michel, G. Fonteneau, S. Hocde, C.B. Plédel and J. Lucas, *Inter. J. Inorg. Mater.* **3** (2001), p. 233.
- [15] H. Fabian, M. Jackson, L. Murphy, P.H. Watson, I. Fichtner and H.H. Mantsch, *Biospectroscopy* **1** (1995), p. 37.
- [16] N.J. Pitt, *New Materials for Optical Waveguides* **799** (1987), p. 25.
- [17] R. Meredith, *Engineers' handbook of industrial microwave heating*, Institution of Electrical Engineers, London., (1998).
- [18] <http://www.tan-delta.com/>, Last accessed 28/1/2009.
- [19] S.A. Galema, *Chem. Soc. Rev.* **26** (1997), p. 233.
- [20] K. Sivakumaran and C.K.S. Nair, *J. Phys. D: Appl. Phys.* **38** (2005), p. 2476.

Chapter 2

Literature Review.

Glasses are solids having 'frozen-in', liquid-like properties for example there is no long range order of molecular arrangement leading to the amorphous nature of glass (section 2.1 to 2.3). Glasses have distinct thermal properties such as viscous flow at, and above, the glass transition temperature (T_g) (see section 2.4) that defines a material as glassy and allows shaping to be carried out. Inorganic compound glasses exhibit optical transparency in some wavelength range (see section 2.5) and such glasses can be classified on the basis of their optical transparency range (see section 2.6). Due to their unique thermal and optical properties inorganic compound glasses have several potential applications (see section 2.7) and hence there is a need to prepare impurity free, homogenous glasses. The most commonly used melt-quenching method was used for preparation of the chalcogenide glasses in this project. Conventionally, a chalcogenide glass melt can be prepared by heating the reactants using a rocking resistance furnace which is a long process and takes about 1.5 days. The aim of this project was to reduce this reaction time and to make the chalcogenide glass melts *via* microwave heating and chalcogenide glasses on melt-quenching. The microwave heating mechanism is introduced in section 2.9. The chapter 2 is summarised in section 2.10.

2.1 Arrangement of atoms or ions in a glass.

Several cations (such as Zn^{2+} , Na^+ , Fe^{3+} *etc.*) and anions (such as halide, oxide, chalcogens *etc.*) can be melted to form liquids which are referred to as inorganic compound melts. The viscosities of some of these melts (*e.g.* the fluoride melts) are of the same order as that of water (10^{-2} Pa s) on cooling these crystallise at or, a little below, the freezing point leading usually to a sharp decrease in the volume per unit mass. A few inorganic compound melts have very high viscosities and, upon cooling, these melts solidify without crystallising as the process of crystallisation needs rearrangement of atoms to their appropriate crystal lattices and the high viscosity restricts the movement of atoms. This viscous liquid below the freezing point is known as a "super-cooled liquid". It is possible to cool the super-cooled liquid further with a rise in viscosity of the liquid without crystallisation. At viscosities of 10^{12} Pa s to 10^{13} Pa s the super-cooled melt becomes visco-elastic and then freezes to a disordered solid, with mechanical properties often close to an ideal elastic solid, in the glass transformation region (T_g) [1]. The cooling thus reduces the mobility of the material's atoms or ions before they can

pack into a more thermodynamically favorable crystalline state. Formation of an ordered system takes a certain amount of time since atoms/ions must move from their current location to a more energetically preferred point at crystal nodes. As the temperature falls molecular motion slows and if the cooling rate is fast enough the atoms/ions never reach their equilibrium destination - the substance enters into dynamic arrest leading to a disordered arrangement of atoms in a solid - a glass forms. A glass can also be synthesised by slight change in the stoichiometry of the composition of a compound since the change in exact stoichiometry prevents the system acquiring a regular crystalline structure. In a glass the species are disordered but are rigidly bound.

An example of crystalline and amorphous material is given in fig. 2.1 showing the difference between the atomic arrangements. Zachariasen proposed this model of a relatively open structure of glass (see fig. 2.1 (b)) as compared to the crystalline structure (see fig. 2.1 (a)) of the same material, in this case silica [2].

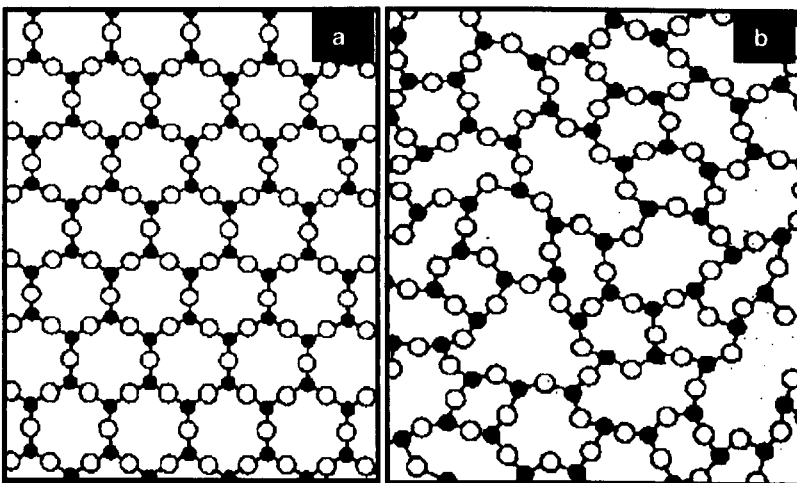


Fig. 2. 1 Schematic molecular arrangement in (a) crystalline (quartz) and (b) amorphous silica [2].

2.2 Definition of a glass.

In 1945, American Society for Testing Materials (A.S.T.M) defined glass as: “Glass is an inorganic product of fusion which has cooled to a rigid condition without crystallising [1].”

This definition has the following limitations:

- According to the above definition a glass must be an “inorganic material” which is not always true. Glycerol forms a glass.
- A glass should always be synthesised after “cooling of its melt” that is not always true as glass can be synthesised *via* other methods such as chemical vapour deposition, sol-gel route and evaporation and sputtering.

In order to broaden the definition of glass the U.S National Research Council defined glass as: “Glass is an X-ray amorphous material which exhibits the glass transition [1], this being defined as that phenomenon in which a solid amorphous phase exhibits with changing temperature a more or less sudden change in the derivative thermodynamic properties, such as heat capacity and expansion coefficient, from crystal like to liquid like values” [3].

The above definition requires two important properties of a material in order to be called a glass and these are: i) a glass should be X-ray amorphous and ii) it should exhibit a glass transition temperature. The amorphous nature of glass is discussed in section 2.3 and the glass transition temperature is discussed in section 2.4.1.

2.3 Amorphous nature of glass.

The basic difference between an X-ray diffraction pattern of a crystalline solid and an amorphous glassy solid is the absence of sharp peaks for the glassy material due to the absence of long range order in glasses. An example of the X-ray diffraction patterns of cristobalite and silica glass is shown in fig. 2.2, demonstrating also that the broad diffuse halo for the glass is centred close to the maximum intensity sharp peak for cristobalite.

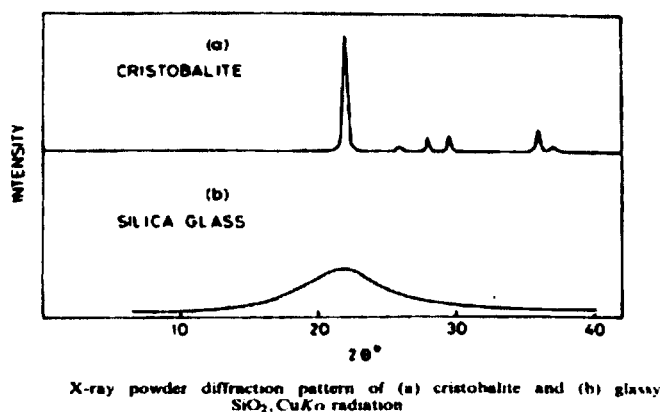


Fig. 2.2 X-ray diffraction pattern of crystalline and glassy silica [4].

2.4 The thermal properties of glass.

The three characteristic temperatures *viz.* the glass transition temperature, liquidus temperature and fictive temperature of a glass are discussed below:

i) The glass transition temperature or temperature range (T_g) – When a glass is heated it becomes soft at T_g . T_g is a characteristic temperature of a glass and is discussed in subsection 2.4.1 [1-3].

ii) The liquidus temperature (T_L) – This is the lowest temperature at which every single crystal is melted to give a liquid. This temperature is called liquidus temperature and is discussed in subsection 2.4.2 [1, 5].

iii) The fictive temperature (T_f) – This is the temperature which is close to T_g and which the glass-melt can be considered to have cooled instantaneously from, increasing the viscosity of the glass-melt such that molecular motion is hindered to produce a glass. This temperature is known as fictive temperature and is discussed in subsection 2.4.3 [1].

2.4.1 The glass transition temperature (T_g).

In fig 2.3 considering a single material in the molten state at point 'a', the density of the melt will start increasing gradually along the line 'ab' as the melt is cooled down but at the liquidus temperature T_L the density of most melts increases substantially and instantaneously at 'bc' in fig. 2.3 leading to the formation of a crystalline solid. Whereas some melts behave differently with no sharp change of density as in the previous case. The change in the density of these melt is along the line 'a' to 'b' to 'e' and they form a super-cooled liquid. A glass is formed when this super-cooled liquid is further cooled to obtain a solid at a viscosity 10^{13} Pa s.

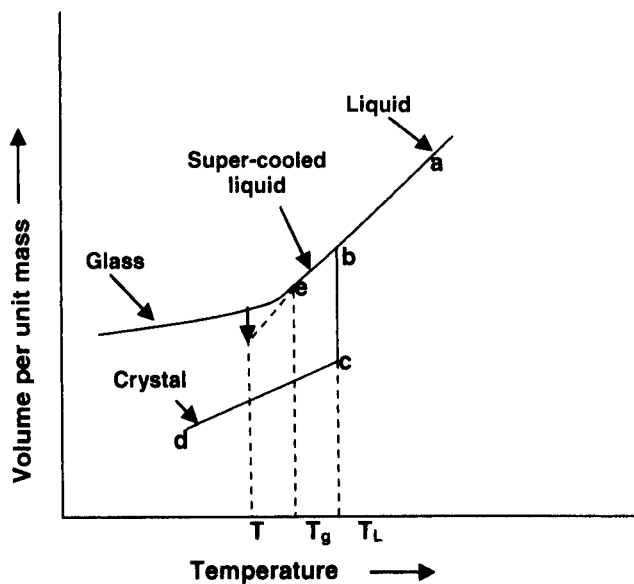


Fig. 2. 3 Volume-temperature diagram showing the difference between a glass-forming material and one that crystallises on cooling [1].

The temperature at which the change in the slope occurs is called the glass transformation temperature or glass transition temperature (T_g) but more commonly T_g is a small range of temperatures. The heat energy absorbed by a glass sample at its T_g is consumed in a phase transition from a solid-like visco-elastic material to a liquid material and the rise in the temperature of the glass sample during heating is less than the value expected if there had

been no phase transition. In fact this is called a pseudo-second order phase transition. This is because there is only a change in the heat capacity from solid-like value to a liquid-like value.

The viscosity of the glass-forming liquid at T_g is approximately $10^{12.5}$ Pa s. The material is then called a super-cooled liquid and, as discussed above, the relative molecular motion is hindered at this temperature due to high viscosity [1]. The T_g of a chalcogenide glass depends upon the bond strength of the chalcogenide molecular bonds making up the chalcogenide glass. The relation between the bond strength and T_g value is discussed in section 2.4.1.1.

2.4.1.1 The dependence of T_g on bond strength of the chalcogenide molecular structure.

T_g of a chalcogenide glass depends upon the average bond strength of the chalcogenide molecular structure and hence is directly related to the composition of the glass. The chalcogenide glass structure is weakly linked forming a cross linked network. The strength of this network is assessed by the average co-ordination number of glass. The average coordination number (Z) a glass having molecular formula $A_xB_yC_z$ is given by:

$$Z = \frac{4x + 3y + 2z}{x + y + z} \dots\dots\dots 2.1$$

where 'A' is an element of Group 14 of Periodic Table such as germanium,

'B' is an element of Group 15 of Periodic Table such as arsenic and antimony,

'C' is an element of Group 16 of Periodic Table such as sulfur, selenium and tellurium.

The factors 4, 3 and 2 are the coordination numbers of the respective elements and 'x', 'y' and 'z' is the atomic percentage of the corresponding elements present in the chalcogenide glass as given by the overall glass composition or stoichiometry. The coordination number of the constituent elements is calculated according to equation 2.2.

$$\text{Coordination number of an element} = 8 - n \dots\dots\dots 2.2$$

where, n = no. of electrons in its outermost shell [6-8]. The coordination numbers of the elements used for the preparation of chalcogenide glass have been calculated using equation 2.2 and are listed in Table 2.1.

Table 2.1 The coordination number of the elements used in the synthesis of chalcogenide glasses in this project.

Elements	No. of electrons in outmost shell (n)	Coordination number of the elements (8 - n)
Germanium	4	4
Arsenic	5	3
Sulfur	6	2
Selenium	6	2
Tellurium	6	2

The average coordination numbers of the chalcogenide glass compositions are listed in the Table 2.2 calculated by using equation 2.1 and using the values predicted in Table 2.1.

Table 2.2 The average coordination numbers and the T_g values of the chalcogenide glasses prepared in this project are shown below.

Composition / atomic %	x + y + z	The average coordination number of the glass (Z)	T _g / °C	Ref.
As ₄₀ S ₆₀	100	2.40	202	[9]
As ₄₀ Se ₆₀	100	2.40	180	[10, 11]
Te ₂₀ As ₃₀ Se ₅₀	100	2.30	135	[12]
Ge ₁₇ As ₁₈ Se ₆₅	100	2.52	236 ± 3	[13]
Ge ₃₃ As ₁₂ Se ₅₅	100	2.78	362	[14]

It is evident from the above Table 2.2 that the average coordination number of the chalcogenide glass increases with the increase in the atomic percentage of germanium which in turn increases the T_g of the chalcogenide glass as germanium has four fold coordinate geometry. The T_g values of the stated composition of glasses above are listed above in the Table 2.2.

The glass transition temperature of arsenic sulfide glass is higher than the glass transition temperature of arsenic selenide glass as sulfur is a smaller atom than the selenium atom and hence a stronger arsenic chalcogenide bond exists in the glassy network. Though for these respective glasses, an increase in the percentage of sulfur or selenium in the composition shows slight increase in T_g value [13].

2.4.2 The liquidus temperature (T_L).

When a complex liquid is cooled, at some temperature and pressure the melt becomes saturated with a crystalline phase. The equilibrium temperature at which this process begins is known as the liquidus temperature at that pressure. When a devitrified glass is heated, and at each temperature sufficient time is given for enough crystals to dissolve to saturate the liquid, the crystals will gradually and continuously decrease in amount, and finally disappear. The lowest temperature at which the last trace of the crystal disappears also is the liquidus temperature; and the experiments in which the liquid is cooled give the same temperature for the liquidus as experiments in which the devitrified glass is heated [5]. The liquidus temperature is a characteristic temperature of a glass.

2.4.3 The fictive temperature (T_f).

It is possible to attain a glassy material at temperatures well below glass transition temperature having an atomic configuration similar to that of the atomic configuration at a higher temperature (in the glass transition temperature region). Suppose

T' = a particular temperature above T_g

T = a particular temperature much below T_g

when a melt at a particular temperature T' (above T_g) is cooled to a temperature T (below T_g) infinitely quickly so that the glass can form but the atomic configuration remains the same as that at temperature T' down at temperature T , then the T' is termed the fictive temperature at temperature T [1]. As discussed in section 2.1 fast cooling results in a dynamic arrest of the “molecules” of the system leading to the formation of glass rather than an ordered arrangement of crystalline structure hence the higher the viscosity of the melt the easier it will be to obtain a glass.

Thermal properties such as T_g are important while fabricating an optical device made of a chalcogenide glass, as it is at, or above, T_g that a the glass-forming melt can be given a shape, for example it can be drawn into a fibre or can be pressed so that it can be given a shape. Similarly, the optical properties of a glass are important while fabricating an optical device using a chalcogenide glass as the optical properties of a chalcogenide glass determine the use of a particular chalcogenide glass for a particular optical application; for example only an infrared transmitting glass can be used as CO_2 laser power delivery working at $10.6 \mu m$ [15]. Hence, a glass for passive optical applications is chosen for fabrication based on its T_g and its optical transmission window. The optical properties of a chalcogenide glass are discussed in section 2.5.

2.5 The optical properties of chalcogenide glasses.

Chalcogenide glasses are infrared transmitting. When infrared radiation is passed through the chalcogenide glass molecular structure only a part of the light is transmitted through the glass and rest of it is lost by several mechanisms [16].

The optical losses in chalcogenide glasses are either due to the inherent properties of the material, which is termed as due to intrinsic factors, or due to impurities and imperfections incorporated during the fabrication of the chalcogenide glass, which is termed as due to extrinsic factors. These factors are summarised in fig. 2.4.

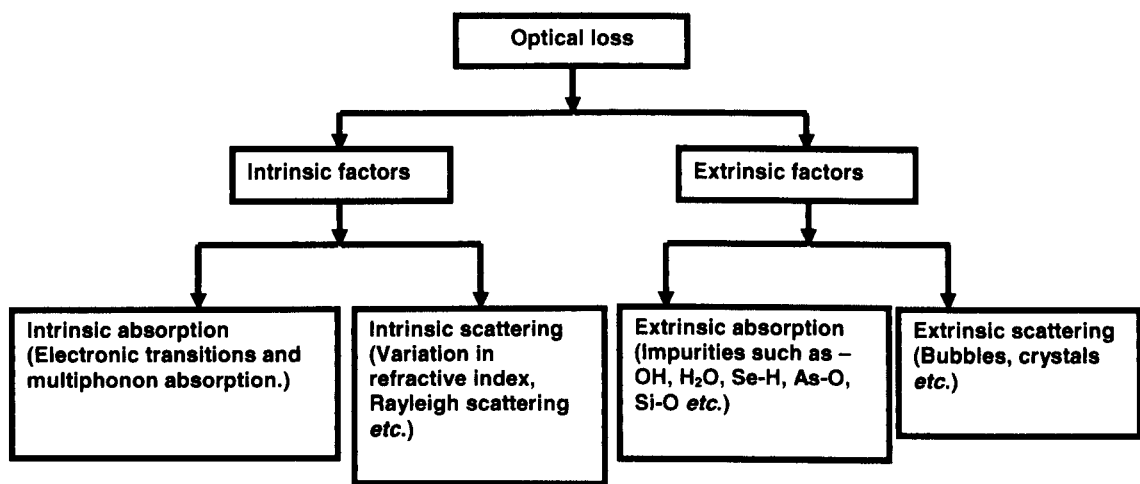


Fig. 2. 4 The various optical losses in chalcogenide glass.

Intrinsic factors are discussed in section 2.5.1 and extrinsic factors are discussed in section 2.5.2.

2.5.1 The optical loss due to intrinsic factors.

The losses due to intrinsic factors depend upon the inherent properties of the material and hence are unavoidable. The intrinsic attenuation can be divided into two main sections the intrinsic absorption and the intrinsic scattering. The intrinsic absorption is discussed in section 2.5.1.1 and the intrinsic scattering is discussed in section 2.5.1.2.

2.5.1.1 Intrinsic absorption.

The region of wavelength over which a chalcogenide glass is transparent, is determined by the intrinsic properties of the material. It is known as the optical transmission window. The short wavelength limit of transparency is determined by electronic transitions (see section 2.5.1.1.1)

whereas the long wavelength limit of transparency is governed by coupling of radiation to infrared active vibrational modes (see section 2.5.1.1.2) [16, 17].

2.5.1.1.1 Absorption due to electronic transitions.

The chalcogenide glasses have electronic band gaps. When a chalcogenide glass is exposed to electromagnetic radiation, electrons below the electronic band gap absorb energy from the incident electromagnetic radiation and jump to across the band gap to a higher energy level. Hence, electromagnetic radiation with sufficient energy or short enough wavelength interacts with the chalcogenide glasses and is absorbed by this electronic mechanism and cannot be transmitted through it. This short wavelength cut-off is defined by the relationship given by equation 2.3,

$$\lambda_c = hc/E_g \quad \dots\dots\dots 2.3$$

Where, λ_c = short wavelength cut-off with sufficient energy to enable the electronic transition and hence absorption.

h = Planck's constant

c = velocity of light

E_g = minimum energy required for electronic transition across the band gap

For chalcogenide glasses, the value of E_g depends upon the bond strength of the chalcogenide molecule. As we go down a Group of the Periodic Table, the size of the atom increases, thus in the chalcogen group (Te > Se > S), hence the bond strength of the chalcogenide molecular structure decreases as we go down the group. Hence sulfur-based chalcogenide glasses require higher energy (*i.e.* electromagnetic radiation of higher frequency and shorter wavelength) for electronic transition than selenium or tellurium based chalcogenides. Thus sulfide-based glasses are transparent at shorter wavelengths (and hence red in colour) as compared to selenide or telluride glasses.

The transmission does not cut-off sharply at a particular wavelength but it extends slightly into the transparent region of a material and is known as the Urbach tail and is mathematically expressed as equation 2.4 [16]:

$$\beta \propto e^{c\omega/kT} \quad \dots\dots\dots 2.4$$

where,

β = absorption coefficient

k = Boltzmann's constant

T = absolute temperature

ω = frequency of electromagnetic radiation

c = velocity of light

This exponential tail would only be of major significance where infrared transmittance is concerned if it was in close proximity to the wavelengths of interest [16, 17]. The mechanism of long wavelength cut off in the chalcogenide glasses is discussed in section 2.5.1.2.

2.5.1.1.2 Multiphonon absorption.

The long wavelength edge on transmission is due to the coupling of electromagnetic radiation to infrared-active vibrational modes. The strongest absorption occurs at the fundamental vibrational frequency ν_0 which is mathematically expressed as eqⁿ 2.5:

$$\nu_0 = \frac{1}{2\pi} (k/\mu)^{1/2} \dots\dots\dots 2.5$$

where, k = force constant which is bond strength here and

μ = effective mass or reduced mass and is mathematically expressed as eqⁿ 2.6:

$$\frac{1}{\mu} = [1/m_1 + 1/m_2] \dots\dots 2.6$$

where, m_1 and m_2 are the masses of two atoms in a diatomic molecule or simple chemical bond.

From the above relation it is clear that the chalcogenide glass molecular structure composed of heavier elements should have a transparency at longer wavelengths than the chalcogenide glasses composed of lighter elements in their molecular structure. The sulfide based chalcogenide glasses transmit to shorter wavelength, at the longer wavelength side of their transparent window than the selenide glasses and telluride glasses.

As discussed in the above two subsections (2.5.1.1 and 2.5.2.2) it is clear that the intrinsic absorptions, that is electronic transition absorption and the multiphonon absorption, determine the optical transmission window for chalcogenide glasses.

The part of incident electromagnetic radiation scattered due to the inherent properties of the material is discussed in section 2.5.1.2.

2.5.1.2 Intrinsic scattering.

Some degree of intrinsic scattering is expected in all homogenous chalcogenide glasses due to perturbation of refractive indices. The phenomenon of scattering (intrinsic or extrinsic) is

dependent upon the size of the centre of scatter. It can be divided in three main groups as described below:

- i) If the scattering centres are much smaller than the wavelength of the incident radiation then Rayleigh scattering theory can be used [16].
- ii) If the scattering centres are approximately equal to the wavelength of the incident radiation then Mie forward scattering theory can be used to explain the phenomenon [16].
- iii) If the scattering centres are much larger than the wavelength of the incident radiation then the scattering can be described as non-selective and is independent of the wavelength of the incident radiation [16].

Normally for chalcogenide glasses it is assumed that micro-fluctuations in density and composition 'frozen-in' at T_g during glass-making give rise to Rayleigh scattering. It is also usually found that this Rayleigh scattering gives rise to less optical loss than the intrinsic absorption loss mechanisms discussed in section 2.5.1.1.

2.5.2 Optical loss due to extrinsic factors.

The optical loss due to impurities incorporated or imperfection created during the formation of the chalcogenide glass is termed as loss due to extrinsic factors. The extrinsic loss mechanisms determine the percentage of the theoretical level of transparency attainable in a chalcogenide glass in practice. The affect of these factors can be limited by controlling fabrication techniques. These extrinsic loss mechanisms are basically scatter and absorption. The extrinsic absorption is discussed in subsection 2.5.2.1 and the extrinsic scattering is discussed in subsection 2.5.2.2.

2.5.2.1 Absorption due to extrinsic factors.

The raw materials and the vessel (normally a silica glass ampoule) used to synthesise the chalcogenide glasses contain impurities such as physisorbed and chemisorbed water present in the silica glass melt-ampoules or in the starting materials used to prepare the chalcogenide glass. Also, carbon, oxides of silica, oxides and hydrides of the starting materials are some of the source of impurities present in the chalcogenide glass. When an electromagnetic wave of the infrared region passes through the glass, energy is absorbed by these species (impurities). For instance, the O-H bond absorbs energy in the infrared region thus causing a net loss in the output from the chalcogenide glass. Similarly, absorption due to As-O, Ge-O, Se-H, C-O, Se-

H *etc.* are observed in infrared region thus causing a net optical loss in, for instance, chalcogenide optical devices [17]. These impurities are in fact the main source of attenuation in chalcogenide glasses which is thus due to extrinsic factors. A list of common impurities in chalcogenide glasses having absorption bands in the infrared region, with band position, is given in Table 2.3.

Table 2.3 Impurities commonly present in the chalcogenide glass causing loss due to absorption in the infrared region.

Band position		Assignment	Reference
μm	cm^{-1}		
2.7	3704	O-H	[18-20]
		H ₂ O	[10]
2.8	3571	O-H	[18-23]
		H ₂ O	[10, 24, 25]
2.9	3448	O-H	[10, 20, 21, 24-27]
		SeO-H	[23]
3.1	3226	S-H	[20, 21, 28]
3.4	2941	C-H	[21]
3.5	2857	Se-H	[23]
		Se-H/C-H	[21]
		H ₂ S/Se-H	[10, 19, 25]
4.0	2500	S-H	[21, 28]
4.1	2439	Se-H	[21, 23, 24]
		S-H	[26]
		H ₂ S/Se-H	[10, 19, 25]
4.3	2326	C-O	[28]
4.5	2222	Se-H	[18, 28]
4.6	2174	Se-H	[19, 21, 23, 24, 26]
		H ₂ S/Se-H	[10, 25]
4.7	2128	H ₂ S/Se-H	[19]
		C-O	[28]
4.9	2041	Ge-H	[26]
5.0	2000	As-H	[26]
		Ge-H	[28]
5.1	1961	Te-C	[21]
5.5	1818	AsO-H	[23]
6.2	1613	H-O-H	[19]
6.3	1587	H ₂ O	[10, 20, 23, 25, 28]
		O-H	[18, 21, 27]
		H-O-H	[22]
7.0	1429	As-S/S-S	[20]
7.1	1408	As-S/S-S	[20]
7.2	1389	As-S/S-S	[20]
7.3	1370	As-S/S-S	[20]
7.4	1351	As-S/S-S	[20]
7.5	1333	As ₄ O ₆	[10, 19, 25]
		As-S/S-S	[20]
7.6	1316	As-S/S-S	[20]
7.7	1299	As-S/S-S	[20]
7.8	1282	H ₂ Se/Se-H	[10, 25]
		As-S/S-S	[20]

Band position		Assignment	Reference
μm	cm^{-1}		
		Ge-O	[23]
		P-O	[27]
7.9	1266	As ₄ O ₆	[10, 25]
		Ge-O	[24, 28]
		As-O	[21, 27]
		As-S/S-S	[20]
		As ₄ O ₆ /Ge-O	[19]
8.0	1250	Ge-O	[27]
		SeO ₂	[10, 19]
		As-S/S-S	[20]
8.1	1235	Ge-O	[23]
8.2	1220	P-O	[27]
8.3	1205	P-O	[27]
8.7	1149	As-O	[27]
		SeO ₂	[10, 19]
8.9	1124	As-O-As	[10, 25]
9.0	1111	Si-O	[26]
9.1	1099	Si-O	[26, 27]
9.2	1087	Si-O	[10, 26]
9.3	1075	Si-O	[21, 26]
9.4	1064	Si-O	[26]
9.5	1053	As ₄ O ₆	[19, 25]
		As-O	[21, 27]
		Si-O	[26]
		As ₄ O ₆ /Si-O	[10]
9.6	1042	Si-O	[26]
		As-O	[27]
9.7	1031	Si-O	[26]
9.8	1020	Si-O	[26]
		P-O	[27]
9.9	1010	Si-O	[26]
10.0	1000	Si-O	[10, 26]
10.4	962	-Se-O-	[25]
		Si-O/Se-O	[10]
		Ge-O	[21]
10.7	935	-Se-O-	[19]
10.8	926	P-O	[27]
		AsO-H	[23]
		As-O-H	[10]
		Ge-O	[21]
11.0	909	-Se-O-	[19]
11.1	901	Se-O	[21]
11.4	877	Ge-O	[21]
11.5	870	Ge-O	[19]
12.3	813	As-O	[21]
12.4	806	Ge-O	[21]
12.5	800	Ge-O	[23]
		Ge-O/As-O	[18]
		As ₂ O ₃	[19]
		Si-O	[21]
12.7	794	As ₄ O ₆	[10, 25]

Band position		Assignment	Reference
μm	cm^{-1}		
		Ge-O/As-O	[18]
12.8	781	Ge-O	[22, 24]
		Ge-O/As-O	[27]
		As ₄ O ₆ /SeO ₂ /Ge-O	[19]

2.5.2.2 Scattering due to extrinsic factors.

Bubbles or crystals or inclusions formed during the synthesis of chalcogenide glass causes scattering. The mechanism of scattering can be explained in as in subsection 2.5.1.2.

2.6 Types of inorganic compound glasses.

Glasses may be subdivided into two main groups according to their transmission window:

i) silica and multicomponent silicate glasses and ii) special glasses [21]. These glasses are described as follows:

1) Silica and multicomponent silicate glasses: the glasses which are normally used for bulk commercial applications for: windows; lamp envelopes; camera lenses; glass containers *etc.* are both silica and multicomponent silicate glasses. Silica glass itself is transparent from the near-ultraviolet (near-UV, that is wavelengths in the range of 200 nm to 350 nm) to the near-infrared (that is wavelengths in the range of 0.7 μm to 2.5 μm) for samples of mm optical pathlength.

2) Special glasses: these glasses exhibit transparent windows within a range which spans the near-UV (200 nm) to the mid-IR (>10 μm) and include:

- Heavy metal fluoride glasses – in 1974, Poulain and co-workers discovered heavy metal fluoride glasses based on zirconium and/or hafnium fluoride. These glasses exhibit transparency over the wavelength range from the near UV (0.25 μm) to the mid IR (6.5 μm) [21] in mm optical pathlength. They also possess low refractive index, low material dispersion, low linear scattering loss but poor aqueous chemical durability [29]. These properties make them potentially a promising candidate for a wide variety of applications, if hermetically sealed, ranging from laser windows, infrared sensing, laser surgery and infrared fibre optics. ZBLAN is one of the most popular compositions and is a fluoride glass based on ZrF₄, BaF₂, HfF₄, LaF₄, AlF₄ and NaF.

- Heavy metal oxide glasses – The vitreous solidification of GeO_2 melts was first reported by Dennis and Laubengayer [3]. Examples of multicomponent heavy metal oxide glasses are $\text{GeO}_2\text{-PbO}$ and $\text{TeO}_2\text{-ZnO-Na}_2\text{O}$. These glasses exhibit transparency over the approximate wavelength range from the near-UV ($0.4\ \mu\text{m}$) to the mid-IR ($7\ \mu\text{m}$) [21]. The heavy metal oxide glass fibres based on GeO_2 can be used as an alternative to heavy metal fluoride glass fibre for $3\ \mu\text{m}$ laser power delivery.
- Chalcogenide glasses – These glasses are based on one or more chalcogenide elements such as S, Se and Te in conjunction with As, Ge, Ga, lanthanides *etc.* Chalcogenide glasses have transmission windows in the range of the mid-visible ($0.5\ \mu\text{m}$) to the mid-IR ($\sim 20\ \mu\text{m}$). Tellurium containing chalcogenide glasses are potentially transparent to wavelengths of more than $15\ \mu\text{m}$ [21].

The chalcogenide glasses have several potential applications, due to their unique thermal (see section 2.4) and optical properties (see section 2.5), which are discussed in section 2.7.

2.7 Applications of chalcogenide glasses.

It is well known that most types of inorganic compound glasses (section 2.6) are soft enough at, or above, their T_g s to be moulded, including fibre drawing (see section 3.5.1) and hot embossing (see section 3.5.2) [30-32]. The advantages of chalcogenide glasses over other glasses (section 2.6) include: a large transparent window in the mid-infrared region (from $\sim 2.5\ \mu\text{m}$ to potentially $20\ \mu\text{m}$) [15, 32] and a wide range of fibre diameter (at least $100\ \mu\text{m}$ to $400\ \mu\text{m}$) can be drawn using chalcogenide glasses [32].

Well developed silica glass fibres can transmit only up to $3\ \mu\text{m}$ wavelength where as some compositions of chalcogenide glass fibres can potentially transmit light up to $20\ \mu\text{m}$ wavelength, depending upon the composition (see fig. 2.5) of the glass. For example, according to Sanghera *et al.* [33], sulfide based glasses are transparent in the wavelength region $0.8\ \mu\text{m}$ to $7\ \mu\text{m}$, selenide glasses transmit in the region of $1\ \mu\text{m}$ to $10\ \mu\text{m}$ and telluride based glasses transmit in the region of $2\ \mu\text{m}$ to $12\ \mu\text{m}$. However, these reported transparency regions are the transparent window practically accessible for use between the impurity absorption bands; the intrinsic transparency of telluride chalcogenide glasses can be up to $\sim 20\ \mu\text{m}$ wavelength, as shown in fig. 2.5 [33].

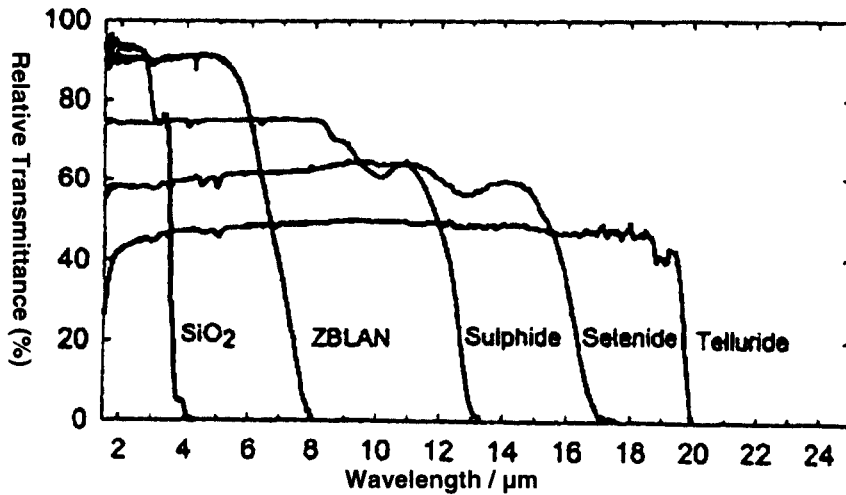


Fig. 2. 5 Transmission spectra of several inorganic compound glasses (optical path length of about 2-3 mm) [33].

Due to their above mentioned unique optical and thermal properties, the chalcogenide glasses have numerous potential optical applications in civil, military and medical areas. These potential optical applications can be classified into mainly two groups: i) passive applications and ii) active applications [15]. The potential passive optical applications are discussed in section 2.7.1 and some potential active optical applications are introduced in section 2.7.2.

2.7.1 Potential passive optical applications of chalcogenide glasses.

In passive fibre optic applications the chalcogenide optical fibres are used as “light pipes”. The chalcogenide fibre has no role other than transporting infrared radiation from one point to another. The chalcogenide glass does not interact with the incoming electromagnetic radiation other than by absorption and scattering due to extrinsic factors, and intrinsic factors of the material which are inevitable [15] (see section 2.5).

Laser power delivery, chemical sensing, temperature monitoring and thermal imaging, near-field microscopy, fibre multiplexing for imaging are a few of the examples of potential passive optical applications. Laser power delivery, chemical sensing and use of fibre as biosensors are discussed in brief in the following sections 2.7.1.1 and 2.7.1.2.

2.7.1.1 Laser power delivery.

Laser power can be used for medical surgery and hence chalcogenide glass optical fibres can potentially be used for infrared transmission [15, 30, 32-36] for example ophthalmic surgery requires operation at 2.94 μm [33].

The carbon monoxide and carbon dioxide laser operating at 5.4 μm and 10.6 μm , respectively, and can be potentially used for laser medical surgery, and for industrial welding and cutting [33]. As the laser power can be used in remote places only if it can be transported to the desired place, chalcogenide optical fibres such as selenides and tellurides could be used for carrying the radiation since chalcogenide glasses are transparent in both these regions of the electromagnetic spectrum (see section 2.5).

Arsenic sulfide fibreoptics transmit in the atmospheric window region of 2-5 μm and can be used for transmission of laser power in this region whereas selenide and telluride fibreoptics transmit in the atmospheric window of 8-12 μm .

It has been found that in some cases laser medical surgery at 6.4 μm wavelength leaves less denatured tissue than the conventionally available laser surgery wavelengths such as the Er:III doped YAG laser used for surgery at $\sim 2.9 \mu\text{m}$ [15, 33, 34]. Thus chalcogenide glass optical fibres could be used to deliver the 6.4 μm wavelength radiations, however the lasers available at 6.4 μm are expensive and generally unavailable.

2.7.1.2 Chemical sensors and biosensors.

It is a well-established fact that biological materials exhibit absorption spectra in the region from $\sim 2.5 \mu\text{m}$ to 10 μm which corresponds exactly to the transparency range of the chalcogenide glasses [37]. For example, for nucleic acids the region between 6.66 μm to 8.33 μm is populated by a number of sharp but weak absorptions. The major absorptions in spectra of DNA arise from vibrational modes of the phosphate groups at $\sim 8.16 \mu\text{m}$. RNA shows an absorption peak at 8.06 μm due to P-O bond. Ethanol molecules show absorption bands in the 8 μm to 12 μm region. The C-O bond vibrates in the region of $\sim 5.55 \mu\text{m}$ to $\sim 6.55 \mu\text{m}$. Similarly, CH_2 and CH_3 , C=O, N-H, amide I and amide II, C-N, COO^- etc. groups are infrared active [37, 38].

Several other species such as oil, soap, paint, benzene and its derivatives, chlorinated hydrocarbons, alcohols, carboxylic acids, aqueous acids, perfumes and pharmaceutical products are infrared active and can be identified using the spectra obtained in FTIR [15].

The most widely used infrared spectroscopic tool is FTIR (see section 3.3.5). The infrared spectroscopy technique is fast, highly selective and provides quantitative analysis of a wide range of samples. It can be used to distinguish and classify microorganisms, study metabolic activities, to detect toxicants and to characterise tissues and fluids [39]. But FTIR can be used

for remote sensing only with a solution like using infrared transmitting optical fibres so that these fibres can carry radiation to and from an infrared spectrometer to obtain the spectra which can be studied as the source of information. Chalcogenide glasses are transparent in the infrared region and can be drawn to a fibre hence chalcogenide glass optical fibres could be used as the infrared carrier between the remote place and the FTIR spectrometer, which is sensitive enough to detect the presence of infrared active species [39].

According to the review by Sanghera *et al.* [15], as described above these techniques can be exploited for use as biosensors and chemical sensors. For example spectroscopic differences between normal and malignant tissues have been identified in a variety of infrared vibrational absorption bands. Condition based maintenance is important, for example the need to change engine oil can be monitored using a fibre optic 'dipstick'. Thus a fibre optic probe can be used to monitor the quality of oil and can provide information whether a change in oil is needed or not [15, 33]. Fibre Evanescent Wave spectroscopy (FEWS) may be used to study the in-situ analysis remotely and virtually instantaneously using optical fibres [39].

2.7.2 Potential active optical applications of chalcogenide glasses.

In active applications the light, propagating through the chalcogenide optical fibre, interacts with the material of the fibre other than due to scattering and absorption. The glasses used here are most commonly doped with rare earth ions, such as erbium III. The potential applications of such fibres are amplifiers, bright sources, gratings *etc.* [15]. The detailed discussion of active applications of chalcogenide glasses is beyond the scope of this thesis.

Due to the extensive potential optical applications of chalcogenide glasses as discussed in section 2.7, efforts have been made in the present work to prepare high purity chalcogenide glasses with as good optical properties as possible. The methods of preparation of chalcogenide glasses are discussed in section 2.8.

2.8 Methods of preparation of chalcogenide glasses.

Chalcogenide glasses can be synthesised using the following methods [21]:

- Melt-quenching
- Sol-gel
- Sputtering
- Chemical and physical vapour deposition

These methods will be discussed in the following subsections.

2.8.1 The melt-quenching procedure.

The three main steps of melt-quenching procedure are: i) formation of the glass-melt from the glass batch (see section 2.8.1.1) ii) glass-melt quenching (see section 2.8.1.2) iii) annealing of the super-cooled liquid (see section 2.8.1.3).

2.8.1.1 Formation of the glass-melt.

From earlier discussion (section 2.1 and 2.2) it is clear that the initial requirement of the melt-quenching procedure is to obtain a homogenous melt of the glass above the liquidus. Conventionally this is done by heating chalcogenide and metalloid reactants through resistance heating. The starting materials are taken in atomic % (according to the required molecular formula of the chalcogenide glass) and then melted in a silica glass melt-ampoule in a rocking resistance furnace as discussed in detail later in section 3.1 to prepare a chalcogenide glass-melt. The furnace is rocked (and sometime also rolled) in order to attain the mechanical mixing of the reactants to get a homogenous melt. This is a long process and takes approximately 1.5 days as heat flow occurs from the surface of the reactants to their centre. The surface of the reactants is heated *via* radiation, convection or conduction or, commonly, a poorly controlled mixture of all three and hence the rate of heating is slow. The process time is limited by the rate of heat flow into the body from the surface, which is determined entirely by the physical properties of the reactants *viz*: i) specific heat; ii) thermal conductivity and iii) density. The combination of these three is called the “thermal diffusivity”. Thermal diffusivity uniquely determines the temperature rise within a material as a function of time and depth from the surface, at a particular set of conditions at the surface. Nothing can be done in the application of the surface heating to accelerate heating once the surface has reached to a specified maximum temperature. Internal temperature is then limited by thermal diffusivity of the material [40]. To improve this process and to reduce the reaction time, microwave heating is investigated here for the preparation of chalcogenide glass-melts. The microwave heating mechanism is explained and its applications are discussed briefly in section 2.9.

2.8.1.2 Glass-melt quenching.

As discussed in section 2.1 the glass-melt has to be cooled suddenly to produce a super-cooled liquid and this process is known as glass-melt quenching. The quenching conditions should be such that an adequate amount of heat can be extracted from the melt, taking the melt from a temperature at, or above, the liquidus to below the liquidus. This leads to the formation of a viscous material below the liquidus where atoms can no longer move quickly

relative to one another. The decrease in volume with temperature is then due to the decrease in atomic vibration only. Further cooling of the super-cooled melt could produce a visco-elastic material which, on reaching T_g *i.e.* a viscosity of $\sim 10^{12.5}$ Pa s can be termed a glass (see section 3.1).

2.8.1.3 Annealing.

The super-cooled liquid is then annealed. The purpose of annealing is to attain uniform temperature through out the system and to retain this even temperature whilst cooling within the T_g temperature region. It is noted that the super-cooled liquid may achieve an uneven temperature during quenching.

For example, the formation of contraction cone in the top surface of a melt (see section 4.2), contained within a long, narrow container during the quenching, is actually a result of attainment of uneven temperature in the system during quenching through T_g . Thus, it is suggested that the liquid melt present near the walls of the silica glass melt-ampoule is cooler than the material present in the interior of the melt during quenching. This is because the material present near walls of the silica glass melt-ampoule is more exposed to the cold quenching medium (air or water) outside the containment. Hence, the liquid melt present near the walls is at a higher viscosity relative to the material present in the interior of the melt. As T_g is approached, the outside material sets solid as a glass whilst the inner melt is still contracting as a liquid above T_g , forming a permanent contraction cone. This uneven temperature distribution may also cause high molecular strain in the glass formed after cooling leading to a poor mechanical quality of the chalcogenide glass.

Therefore, a super-cooled liquid formed after quenching of the glass-forming melt is kept for a certain length of time (for approximately for one hour for specimens which have their minimum thickness of up to about 10 mm, see section 3.2) at a temperature slightly above (usually) its T_g to attain uniform temperature throughout the super-cooled liquid mass which helps in making stable, strain-free *i.e.* annealed glasses.

The choice of temperature for annealing is important as, if a super-cooled liquid is annealed at too high a temperature above its T_g , or for too long a time, it may crystallise. After annealing, the product is then cooled relatively slowly so that the temperature within the system should be uniform thus preventing any further introduction of even temporary strain.

2.8.2 Sol-gel procedure.

The sol-gel technique allows processing of glasses at low temperature in different shapes, *i.e.* monoliths, films, fibres or nano-sized powders. In contrast to the melt-quenching method, in the sol-gel approach, the reaction is carried out in the presence of water and / or solvents such as toluene. Seddon *et al.* showed that although amorphous germanium disulphide can be prepared *via* sol-gel route, contamination due to oxide was difficult to avoid [41].

2.8.3 Sputtering procedures.

Sputtering is a physical process in which atoms in a solid target material are ejected into the gas phase due to bombardment of the target material with energetic ions or atoms. The ions for the sputtering process are supplied by a plasma that is induced within the sputtering equipment. The process can be visualised as ‘atomic billiards’, with the ions striking a large cluster of closed packed atoms. The atoms present on the surface of the substrate are ejected from the surface and are deposited on a substrate in the line-of-sight as a thin film of glass. This process is largely driven by the exchange of momentum between the atoms of the bombarding material and the substrate. In our laboratory, recent work has shown that sample of porous Si-on-Si wafer can be coated by chalcogenide glass. A 6 μm thick film of $\text{Ge}_{17}\text{As}_{18}\text{Se}_{65}$ was grown onto the surface of Si-on-Si wafer and a 4 μm thick film of $\text{Ge}_{15}\text{As}_{15}\text{Se}_{17}\text{Se}_{53}$ was grown over a GaAs substrate *via* sputtering [31].

2.8.4 Chemical and physical vapour deposition.

This involves the deposition of solid from its gaseous phase. Precursor gases are passed over hot substrate where they are deposited as thin films. The precursor chemicals should be volatile but easily condensable as well so that they can be deposited over a substrate. The process of deposition may be fairly slow but very thin layer of glass can be deposited over the substrate. This glass can be impervious and of high purity and hence this method can be used for the production of wave guides, coatings, semiconductors and powder production.

Physical vapour deposition may involve evaporation under vacuum of a bulk glass target or of the individual elements making up the required glass film composition.

An example of chemical vapour deposition is that Ge_2S_3 glass was fabricated as a thin film through chemical vapour deposition over CaF_2 and Schott N-PSK58. Thus, GeCl_4 was vaporised by passing argon gas and then mixed with H_2S and passed over the substrate glass (CaF_2 and Schott N-PSK58 glasses) in the temperature range: 450°C to 600°C, when a few micron thick germanium sulfide glass film was fabricated on the substrate [42].

2.9 The microwave heating mechanism and its application.

Microwaves are electromagnetic waves with wavelengths ranging from 1 mm to 1 m, and frequencies between 0.3 GHz and 300 GHz. Microwaves have electric and magnetic field components oscillating at a very high speed. The reason for interaction of the molecules with the microwaves can be attributed to the nature of the molecule: that a molecule contains both positive and negative charges. The cause of microwave heating can be explained through:

- i) microwave heating due to molecular polarisation (see section 2.9.1)
- ii) microwave heating due to conduction (see section 2.9.2)
- iii) microwave heating in metal powder (section 2.9.3).

2.9.1 Microwave heating due to molecular polarisation.

When a material is irradiated with microwaves the constituent molecules of the material interact with the microwaves. The reason for interaction of the molecules with the microwaves can be attributed to the nature of the molecule. A molecule contains both positive and negative charges. The bound charges attempt to align themselves with the field. The applied field provides the energy of this rotation. The “right frequency” of the applied irradiation is when the dipoles have the time to respond to the alternating electric field but the rotation lags behind the field. This gives rise to a phase difference. This phase difference causes energy to be lost from the dipole, by molecular friction and random collisions, giving rise to heat into the body. Thus the tendency of displacement of charges within the material due to application of microwaves is one of the main causes of generation of heat. This is explained in more detail below.

The total polarisation of the material arising from the displacement of charges can be expressed as follows:

$$a_t = a_e + a_a + a_i + a_d \dots\dots\dots\text{eq. 2.7}$$

where, a_t = total polarisation

a_e = polarisation due to electronic displacement also known as electronic polarisation.

a_a = polarisation due to displacement of nuclei with respect to one another.

a_i = interfacial polarisation which arises from the interfacial phenomena in inhomogeneous material.

a_d = polarization due to polar molecules present in the material which is known as dipolar polarisation [43-45].

The mechanisms of molecular polarisation on application of microwaves leading to the generation of heat are explained as follows:

i) The electronic polarisation (a_e): The movement of electron around the nuclei is known as electronic polarisation. Since it arises due to the relative displacement of the orbital electron it is observed in neutral atoms as well, for example in germanium and silicon covalent crystals the polarisability is entirely electronic in nature. The electronic polarisation can be shown as in fig. 2.6.

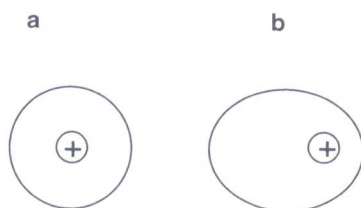


Fig. 2. 6 (a) Unpolarised atom. (b) Polarised atom due to the application microwaves.

The electronic displacement is in the same phase when irradiated to microwaves thus practically does not participate in microwave heating.

ii) Polarisation due to inter-nuclear displacement (a_a): The movement of nuclei relative to each other is almost in the phase of the applied electromagnetic field and hence does not participate in microwave heating.

iii) Dipolar polarisation (a_d): If a molecule with a permanent dipole moment is exposed to microwaves, the molecular dipole tends to align with the field. It can be visualised as in fig. 2.7.

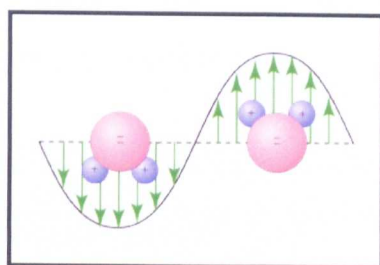


Fig. 2.7 Change of dipole on application of microwaves.

The “right frequency” of the applied irradiation for producing heat is when the dipoles have the time to respond to the alternating electric field but the rotation lags behind the field. This gives rise to a phase difference. This phase difference causes energy to be lost from the dipole, by molecular friction and random collisions, giving rise to heat into the body (fig. 2.7). This is called dipolar polarisation. It is important to irradiate the The “right frequency” of the applied irradiation for producing heat is when the dipoles have the time to respond to the alternating

~~electric field but the rotation lags behind the field.~~ This gives rise to a phase difference. This phase difference causes energy to be lost from the dipole, by molecular friction and random collisions, giving rise to heat into the body (fig. 2.7). This is electromagnetic wave of a frequency in which these dipolar molecules can respond because if an electromagnetic wave of a very high frequency is used, then the dipoles do not have enough time to rotate and so do not respond, leading to no microwave heating. Similarly if an electromagnetic wave of a very low frequency is used for the purpose the dipole may align themselves, hence leading to no molecular friction and hence no heating. Microwaves are in the correct frequency region where these dipoles respond but cannot align exactly leading to the generation of heat energy.

iv) Interfacial polarisation (a_i): This mechanism is important for systems comprised of conducting inclusions in a second non-conductive material. An example would be a dispersion of metal particles in a microwave transparent material such as sulfur. Sulfur is microwave transparent and the metals reflect microwaves yet the combination of the two makes the heterogeneous phase mixture microwave absorbent. It can be viewed as a combination of the conduction and dipolar polarisation. The formation of a few of the chalcogenides *via* microwave heating such as synthesis of arsenic sulfide (see Chapter 4) may be explained by this mechanism. Although arsenic is generally viewed as being a metalloid, rather than being a true metal, being located in the middle of the 'p' block of the Periodic Table.

The above discussed mechanisms can be explained simply as that the oscillating electric and magnetic field of the electromagnetic field applies a force on the charged particles thus compelling the molecules to migrate and rotate. This molecular movement creates intermolecular friction which in turn produces heat.

The microwave heating mechanism when a conducting material is exposed to microwaves is explained by the conduction mechanism. The conduction mechanism is discussed in section 2.9.2.

2.9.2 Heating effects due to conduction.

When a material having loosely bound charged particles which are free to travel in the material, for example electrons in a sample of carbon such as graphite where labile electrons present in the system, or a solution containing ionic salts such as sodium chloride solution in water, are exposed to microwaves the oscillating electromagnetic field generates an oscillation of electrons or ions in the material, resulting in an electric current. This current faces internal resistance, which heats the material [43].

Heat is generated when a metal is exposed to microwaves. The mechanism of heat generation in metals can be explained by 'skin effect' which is discussed in section 2.9.3.

2.9.3 Microwave heating in metals.

Metals contain labile electrons on their outer surface. The electronic structure of metal can be visualised as positively charged ions submerged in a "sea" of electrons. When the metal is exposed to microwaves, there is tendency of the microwaves to disperse on the surface of the metal. Electric current tends to flow at the surface of the material which is known as the 'skin effect' and the measure of the distance over which the current falls to 1/e of its original value is known as the 'skin depth' [43, 45-47]. The mechanism of heat production can be explained using Joule's law or Ohmic heating. The microwave heating of metals often is accompanied by the formation of a plasma.

Taking these concepts into consideration, the starting materials were crushed in this work before exposing them to microwaves inside the DMO (domestic microwave oven). A list of electrical resistivities and dielectric constant of the starting material is given below in Table 2.4 and Table 2.5 respectively.

Table 2.4 List of electrical resistivities of the starting materials.

Elements	Electrical resistivity/ $\mu\Omega\text{cm}$ at 20°C	Reference
Ge	4.6×10^7	[48]
As	33.3	[49]
S	2×10^{27}	[46]
Se	2×10^{13}	[46]
Te	4.36×10^5	[50]

Table 2.5 List of dielectric constants of the starting materials.

Elements	Dielectric constant			Reference
	Dielectric constant value	Applied temperature	Applied frequency	
Ge	16.0 ± 0.3	20°C	9.2×10^9 Hz	[51]
	15.8 ± 0.2	Room temperature	500 - 3×10^{10} Hz	
As	10.23	20°C	60 Cycles	[48]
S (powder)	3.5	Unspecified	Unspecified	[48]
Se	5.4	482°F	Unspecified	[48]
Te	-	-	-	-

2.9.4 A review of synthesis of materials using microwave heating.

Microwave heating provides potentially a cleaner, faster, and cheaper heating aid. It has been used in the food industry for decades. In recent years, this technique has been used in

scientific laboratories for accelerating organic reactions [52, 53]. The application of microwaves in accelerating organic reactions is not discussed further in this thesis.

The reported applications of microwave heating for the synthesis of inorganic solids are summarised as follows.

Baghurst and Mingos [54] reported that some oxides *eg.* ZnO, CuO, MnO₂ and V₂O₅ absorb microwaves very strongly. It has been found that solid state inorganic oxides can be synthesised through microwave heating, for instance ternary oxides were formed by microwave heating of a mixture of oxides which do and do not absorb microwave strongly. A commercially available microwave oven operating at 2.45 GHz and power levels 50-500 W was used.

Vidhyanathan and Rao [55] synthesised Ti, Ga and V nitrides through microwave-assisted carbothermal reduction and nitridation. Ti, Ga and V oxides were mixed with amorphous carbon and exposed to microwave radiations under a flowing ammonia and gaseous nitrogen environment. It was believed that the amorphous carbon acted both as a microwave absorber and as a reducing agent for the metal oxides. The domestic microwave oven (Battliboy, Eddy) operating at 2.45GHz with a maximum power level of 980 W was used.

Whittaker and Mingos [56] carried out microwave-assisted solid-state reactions involving metal powders and gases. Metals powders (Cr, W, In, Te, Ti and Cu) were allowed to react with gaseous halogens, ammonia and nitrogen (Cl₂, Cl₂ with O₂, Br₂ with Ar, NH₃ and N₂) in an appropriate microwave environment when the corresponding metal halides, metal oxyhalides and nitrides were formed. A multimode domestic microwave oven operating at 2450 MHz was used for heating.

Carbides, nitrides, zeolites and silicide have all been prepared [57]. Oxide-based glasses have been made [58]. A few polycrystalline chalcogenides such as zinc sulphide, zinc selenide, lead telluride, lead selenide and silver sulfide were made through microwave heating. The microwave exposure times varied from 5 to 20 minutes [59]. Crystalline molybdenum selenide was synthesised through microwave heating. The reaction was carried out in a Spectra 900 W microwave oven, with a 2.45 GHz working frequency. The total power of the microwave oven was maintained as 900 W throughout the reaction [60].

Very few chalcogenide glasses have been reported to have been synthesised *via* microwave heating. Shivkumaran and Nair [61] synthesised tellurium and selenium based glasses at 700

Watts in a multimode cavity ordinary domestic microwave oven having a frequency 2.45 GHz. The samples were exposed to microwave radiation for 3 to 9 minutes when travelling hot spots and sparks were observed during heating. The melt was quenched. The product was X-ray amorphous and two glass transition temperatures (T_g) were observed by means of differential thermal analysis. According to these authors, the two observed T_g s showed that two types of glass were formed and indicating that phase separation had occurred during the glass synthesis.

2.10 Summary.

A glass is defined as an X-ray amorphous material with a glass transition temperature (T_g). Inorganic compound glasses have several exceptional thermal properties such as viscous-flow at T_g which can be exploited in making optical fibres *etc.* Inorganic compound glasses exhibit optical transparency and can be used as light carriers. Chalcogenide glasses are transparent in the mid-infrared region and hence a chalcogenide fibre can be used as for infrared transmission, for example for laser power delivery, biochemical sensing, chemical sensing *etc.* The potential optical applications of these glasses demand the necessity of synthesising high optical quality chalcogenide glasses. The well-established melt quenching method is usually used for the formation of chalcogenide glasses. Since this a long process and takes about 1.5 days, microwave heating was used in this project for the preparation of chalcogenide glasses with the aim to reduce the time of reaction. It is suggested that the microwave heating is due to the interaction of microwaves with the material and heat is generated due to molecular agitation or interaction of the free charges present in the reactants. Research has been reported using microwave heating to make organic materials, crystalline metal oxides and metal chalcogenides and oxide glasses. However, very little work has been reported on making chalcogenide glasses *via* microwave heating and the in the only reported work identified it was concluded by the authors that phase separated glasses had been produced.

References:

- [1] H. Rawson, *Glass science and technology 3, Properties and applications of glass*, Elsevier Scientific Publishing Company, Amsterdam, (1980).
- [2] H. Rawson, *Glasses and their applications*, Institute of Metals, London, (1991).
- [3] W. Vogel, *Glass chemistry*, Springer-Verlag, 2nd edition, Berlin, (1994).
- [4] A.R. West, *Basic solid state chemistry*, John Wiley and Sons, 2nd edition, England, (1999).
- [5] G.W. Morey, *The properties of glass*, Reinhold Publishing Corporation, 2nd edition, New York, (1954).
- [6] J.E. Shelby, *Introduction to glass science and technology*, Royal Society of Chemistry, 2nd edition, Cambridge, (2005).
- [7] P. Kumar and R. Thangaraj, *J. Non-Cryst. Solids* **352** (2006), p. 2288.
- [8] A.B. Seddon, *J. Non-Cryst. Solids* **213-214** (1997), p. 22.
- [9] M.B. Myers and E.J. Felty, *Mater. Res. Bull.* **2** (1967), p. 535.
- [10] W.A. King, A.G. Clare and W.C. LaCourse, *J. Non-Cryst. Solids* **181** (1995), p. 231.
- [11] M.F. Churbanov, V.S. Shiryayev, I.V. Scripachev, G.E. Snopatin, V.V. Gerasimenko, S.V. Smetanin, I.E. Fadin and V.G. Plotnichenko, *J. Non-Cryst. Solids* **284** (2001), p. 146.
- [12] D.L. Coq, C.B. Plédel, G. Fonteneau, T. Pain, B. Bureau and J.L. Adam, *J. Non-Cryst. Solids* **326-327** (2003), p. 451.
- [13] S.D. Savage, C.A. Miller, D. Furniss and A.B. Seddon, *J. Non-Cryst. Solids* **354** (2008), p. 3418.
- [14] J.T. Gopinath, M. Soljagic, E.P. Ippen, V.N. Fuflyigin, W.A. King and M. Shurgalin, *J. Appl. Phys.* **96** (2004), p. 6931.
- [15] J.S. Sanghera and I.D. Aggarwal, *J. Non-Cryst. Solids* **256-257** (1999), p. 6.
- [16] J.A. Savage, *Infrared optical materials and their antireflection coatings*, Adam Hilger Ltd., Bristol, (1985).
- [17] N.J. Pitt, *New Materials for Optical Waveguides* **799** (1987), p. 25.
- [18] P.J. Webber and J.A. Savage, *J. Non-Cryst. Solids* **20** (1976), p. 271.
- [19] A.M. Reitter, A.N. Sreeram, A.K. Varshneya and D.R. Swiler, *J. Non-Cryst. Solids* **139** (1992), p. 121.
- [20] J. Kobelke, J. Kirchhof, K. Schuster and A. Schwuchow, *J. Non-Cryst. Solids* **284** (2001), p. 123.
- [21] D. Lezal, *J. Optoelect. & Adv. Mat* **5** (2003), p. 23.

- [22] W. Chen, J. Cheng and G. Chen, *J. Non-Cryst. Solids* **221** (1997), p. 274.
- [23] J.S. Sanghera and I.D. Aggarwal, *Infrared fiber optics*, CRC Press LLC, Washington D.C., (1998).
- [24] D.S. Ma, P.S. Daniels and C.T. Moynihan, *J. Non-Cryst. Solids* **37** (1980), p. 181.
- [25] C.T. Moynihan, P.B. Macedo, M.S. Maklad, R.K. Mohr and R.E. Howard, *J. Non-Cryst. Solids* **17** (1975), p. 369.
- [26] M.F. Churbanov, *J. Non-Cryst. Solids* **184** (1995), p. 25.
- [27] J.A. Savage, P.J. Webber and A.M. Pitt, *Infrared Phys.* **20** (1980), p. 313.
- [28] J.S. Sanghera and I.D. Aggarwal, *J. Non-Cryst. Solids* **213-214** (1997), p. 63.
- [29] L.G. Hwa and C.K. Shu, *Chin. J. Phys.* **34** (1996), p. 1270
- [30] X. Zhang, H. Ma and J. Lucas, *J. of Optoelect. and Adv. Mat.* **5** (2003), p. 1327.
- [31] A.B. Seddon, W.J. Pan, D. Furniss, C.A. Miller, H. Rowe, D. Zhang, E. McBrearty, Y. Zhang, A. Loni, P. Sewell and T.M. Benson, *J. Non-Cryst. Solids* **352** (2006), p. 2515
- [32] S. Hocdé, C.B. Plédel, D.L. Coq, H.L. Ma and J. Lucas, *J. Non-Cryst. Solids* **274** (2000), p. 17.
- [33] J.S. Sanghera, L.B. Shaw and I.D. Aggarwal, *C. R. Chemie* **5** (2002), p. 873.
- [34] J.S. Sanghera, L.B. Shaw, L.E. Busse, V.Q. Nguyen, P.C. Pureza, C.B. C., B.B. Harrison, I.D. Aggarwal, R. Mossadegh, F. Kung, D. Talley, D. Roselle and R. Miklos, *Fiber Integr. Opt.* **19** (2000), p. 251
- [35] J.A. Moon and D.T. Schaafsma, *Fiber Integr. Opt.* (2000), p. 201.
- [36] K. Michel, B. Bureau, C. Pouvreau, J.C. Sangleboeuf, C. Boussard-Plédel, T. Jouan, T. Rouxel, J.-L. Adam, K. Staubmann, H. Steinner, T. Baumann, A. Katzir, J. Bayona and W. Konz, *J. Non-Cryst. Solids* **326-327** (2003), p. 434.
- [37] S. Hocde, C.B. Pleedel, G. Fonteneau and J. Lucas, *Solid State Sci.* **3** (2001), p. 279.
- [38] H. Fabian, M. Jackson, L. Murphy, P.H. Watson, I. Fichtner and H.H. Mantsch, *Biospectroscopy* **1** (1995), p. 37.
- [39] P. Lucas, M.R. Riley, C.B. Plédel and B. Bureau, *Anal. Biochem.* **351** (2006), p. 1.
- [40] R. Meredith, *Engineers' handbook of industrial microwave heating*, Institution of Electrical Engineers, London., (1998).
- [41] A.B. Seddon, S.N.B. Hodgson and M.G. Scott, *J. Mater. Sci.* **26** (1991), p. 2599.
- [42] C.C. Huang and D.W. Hewak, *Opt. Exp.* **12** (2004), p. 2501.
- [43] <http://www.tan-delta.com/>, Last accessed 28/1/2009.
- [44] S.A. Galema, *Chem. Soc. Rev.* **26** (1997), p. 233.

- [45] R.P. Feynman, R.B. Leighton and M. Sands, *The Feynman lectures on physics*. Volume 2, mainly electromagnetism and matter, Reading, Mass.: Addison-Wesley, US, (1964).
- [46] A.G. Whittaker and D.M.P. Mingos, *J. Chem. Soc. Dalton Trans.* (1995), p. 2073.
- [47] A.G. Whittaker and D.M.P. Mingos, *J. Chem. Soc., Dalton Trans.* (2002), p. 3967.
- [48] http://clippercontrols.com/info/dielectric_constants.html#S, Last accessed 2/6/2009.
- [49] <http://www.americanelements.com/as.html>, Last accessed 2/6/2009.
- [50] <http://www.americanelements.com/tellurium.html>, Last accessed 20/10/2009.
- [51] CRC Handbook of Physics and Chemistry, Section 4, Properties of the Elements and Inorganic Compounds, 87th edition, (2006-2007).
- [52] D.M.P. Mingos and D.R. Baghurst, *Chem. Soc. Rev.* **20** (1991), p. 1.
- [53] A.G. Whittaker and D.M.P. Mingos, *J. Microwave Power and Electromag. Eng.* **29** (1994), p. 195.
- [54] D.R. Baghurst and D.M.P. Mingos, *J. Chem. Soc., Chem. Commun.* (1988), p. 829.
- [55] B. Vaidhyanathan and K.J. Rao, *Chem. Mater.* **9** (1997), p. 1196.
- [56] A.G. Whittaker and D.M.P. Mingos, *J. Chem. Soc. Dalton Trans.* (1993), p. 2541
- [57] K.J. Rao, B. Vaidhyanathan, M. Ganguli and P.A. Ramakrishnan, *Chem. Mater.* **11** (1999), p. 882.
- [58] B. Vaidhyanathan, M. Ganguli and K.J. Rao, *J. Solid State Chem.* **113** (1994), p. 448.
- [59] B. Vaidhyanathan, M. Ganguli and K.J. Rao, *Mater. Res. Bull.* **30** (1995), p. 1173.
- [60] R. Harpeness, A. Gedanken, A.M. Weiss and M.A. Slifkin, *J. Mater. Chem.* **13** (2003), p. 2603
- [61] K. Sivakumaran and C.K.S. Nair, *J. Phys. D: Appl. Phys.* **38** (2005), p. 2476.

Chapter 3

Experimental.

The aim of this work was to explore chalcogenide glass making by microwave processing. However, the well-established, conventional resistance furnace glass melting method was also used here to prepare the chalcogenide glasses. Thus conventional glass melting in a resistance furnace was carried out of: As_2S_3 , As_2Se_3 , $\text{Ge}_{17}\text{As}_{18}\text{Se}_{65}$, $\text{Ge}_{33}\text{As}_{12}\text{Se}_{55}$, $\text{Te}_{20}\text{As}_{30}\text{Se}_{50}$ in order to have a benchmark for comparison of products made during microwave processing of the same starting materials. General observations of the microwave processing are presented here in section 3.1.2. More details may be found in later chapters 4 to 7. Efforts were made to prepare impurity free glasses. Towards achieving this goal the melting ampoules, used here for both the microwave processing and conventional glass melting were, in general cleaned and baked, and the raw materials were purified. The glass melting procedures, which included purification of raw materials and ampoule baking, glass batching, formation of glass-melt *etc.*, are described in section 3.1. The glass-melt was quenched and annealed and the processes of quenching and annealing are described in section 3.2. The product thus formed was taken out of the ampoule and characterised. The techniques used to characterise the products are discussed in section 3.3 whereas the procedures used for processing of glass products for photonic uses are described in section 3.4.

3.1 Glass-melting.

The procedures used in an effort to prepare homogenous and impurity free glass-melts are described in this section. The glass melting procedure using the resistance rocking furnace is described in section 3.1.1 whereas the procedure used for melting in a domestic microwave oven is described in section 3.1.2. These procedures included ampoule preparation (see section 3.1.1.1), purification of raw materials (see section 3.1.1.2), glass batching (see section 3.1.1.3) and the formation of glass-melt (see section 3.1.1.4).

3.1.1 Glass-melting process in rocking resistance furnace.

3.1.1.1 Ampoule preparation.

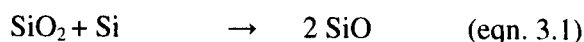
Silica glass ampoules (OD/ID = 14/10 mm, length = 250 to 300 mm) to hold the chalcogenide glass-melts were sourced from Multilab Ltd.. The ampoule was cleaned following four steps, before taking it to the chalcogenide glove box, as follows:

i) HF etching.

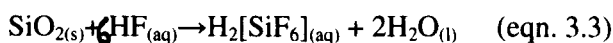
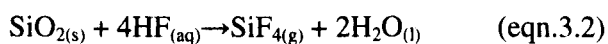
The as-received silica ampoule was filled with 1% vol. /vol. hydrofluoric acid and left for about 10 minutes at ambient temperature. The acid was then discarded in a separate bottle. This process was repeated three times. The ampoule was then rinsed with plenty of distilled water and the used water was neutralised and poured down through the sink in a fume cupboard.

This step was done for two reasons:

- It was believed that the ampoules as-received from Multilab may not have been HF etched and the silica fume (produced during the fabrication process) would have been left in the ampoule. As hydrofluoric acid attacks silica [1] it was used here to remove any silica fume left in the ampoule after manufacture. It is known that at about 950°C and normal pressure silica breaks down as follows [2]:



- In some of the experiments the silica ampoule broke during annealing. Perhaps, the chalcogenide glass-melt at a high temperature suspended on the uneven silica surface put some stress on the silica ampoule during cooling below T_g and, due to thermal expansion mismatch, the ampoule broke. In order to make the ampoule inner surface smooth (and to remove any silica fume, as eqn. 3.1) the ampoule was etched with aqueous (aq.) hydrofluoric acid since HF reacts with SiO_2 according to the following reactions:



(s = solid; g = gaseous; l = liquid; aq = aqueous)

ii) Oven drying.

The silica glass ampoule was then dried at 70°C in an oven (Heraeus Instruments/Lot1174), kept in a class 10000 clean room, for 6 hours to remove any adherent water from the inner surface of the ampoule.

iii) Air baking.

The dried silica glass ampoule was then air baked in a resistance furnace (Instron STL) to remove any carbon impurity present. The following reaction was believed to have taken place:



The silica-glass ampoule was heated according to the heating schedule in Table 3.1.

Table 3.1 Silica glass ampoule heating schedule during the air bake step of the ampoule pre-cleaning.

Stage	Heating schedule
1.	Step to 70°C from room temperature (RT)
2.	From 70°C to 1000°C @ 200°C/h
3.	Dwell at 1000°C for 6 h
4.	From 1000°C to 70°C @ 200°C
5.	Ampoule withdrawn at 70°C and cooled to RT

iv) Vacuum baking.

The air baked, silica glass ampoule was then baked in the resistance furnace (Instron STL) under vacuum (~ 1 Pa) using a turbo-pump (Pfeiffer vacuum) and according to the same heating schedule as for the air baking (Table 3.1) in order to try to remove any physi-sorbed (H_2O) and chemi-sorbed (hydroxide) impurity present on the inner surface of the silica ampoule. For removal of hydroxide, the following reaction was believed to take place:

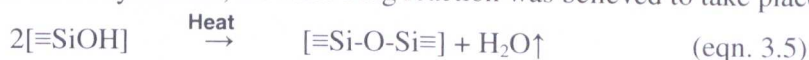


Figure 3.1 shows the silica gas ampoule attached *via* the valve to the evacuation line for the vacuum baking step.

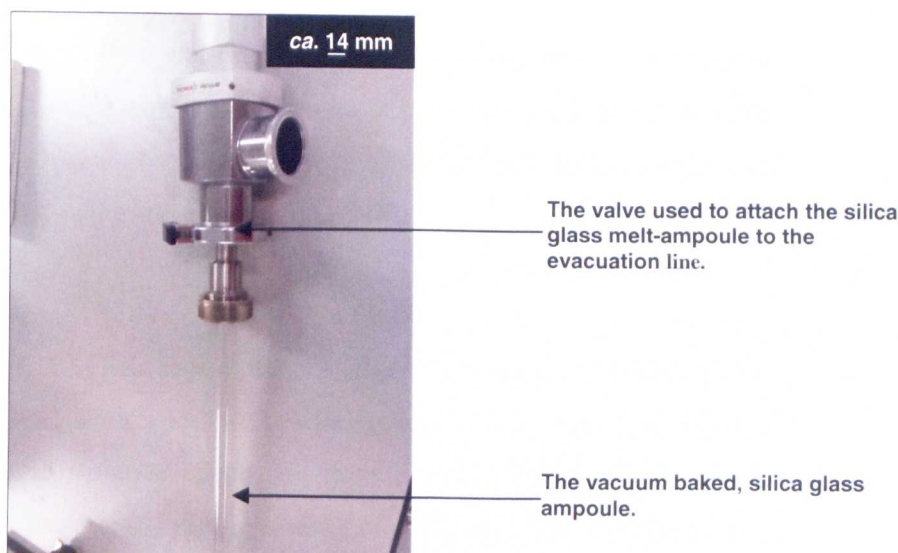


Fig. 3. 1 The vacuum baked silica glass ampoule attached to the evacuation line with the evacuating valve.

3.1.1.2 Starting materials and their purification.

Chalcogenide glasses were synthesised from one or more chalcogen elements such as S, Se and Te in conjunction with As, Ge, Ga or lanthanide chalcogenides [3]. The chemicals, used for the formation of glass-melts, with their purity level, physical state (that is size of the chunks or beads or powder *etc.*) and source (name of the company from where it was bought) are listed in Table 3.2.

Table 3.2: Chemicals precursors and their purity level used for making chalcogenide products.

Chemicals	Purity (%) / grade (metals – based)	Physical state (as received)	Source
As	99.99999	*Chunks (2 to 8 mm)	Furukawa
As	99.999995	*Powder (100 mesh)	Alfa Aesar
As amorphous	99.999	Up to 7 mm chunks	All Chemie Ltd.
Ge	99.999	*Chunks (3 to 6 mm)	Cerac
S	99.99	?Flakes (1 to 6 mm)	Cerac, Aldrich, Alfa Aesar
Se	99.999	*Beads (3 mm)	Cerac
Te	99.9999	?Shot (1 to 6 mm)	Cerac
Ga	99.999	*Shot (3mm)	Testbourne Ltd.
Er ₂ S ₃	99	?Powder (Grain size could not be estimated through visual inspection.)	Prochem Inc.

Key: *Size of the chunks, shot or beads, or grain size of the powder, as stated on the bottle.? Size of the chunks or powder not stated on the bottle, estimated size through visual inspection is stated here.

Germanium, selenium, tellurium, gallium and erbium sulfide were used as-received without further purification. Arsenic and sulfur were purified in-house to reduce oxide and, and oxide, hydride and water, impurity respectively. The arsenic purification and sulfur purification processes are described in the following subsections (i) and (ii):

i) The arsenic purification process.

Arsenic as received (Furukawa, 7n5) was kept in the chalcogenide glove box (Mbraun 150B-G) circulated with nitrogen (BOC white spot) with reduced oxygen and water level (each \leq 0.1 ppm). ~ 8 g of arsenic was weighed inside the glove box using a chemical balance (Sartorius model BP221S, accuracy \pm 0.1 mg) in a weighing boat (Fischer) and poured in a silica glass ampoule (Multilab, OD/ID = 14/10) cleaned and baked as described in section 3.1.1. The open end of the silica glass ampoule was fitted with a Saunder's valve and the screw was closed in order to prevent it from direct contact with the open atmosphere. The arsenic-containing closed silica glass ampoule was taken out of the glove box. It was then

attached to the evacuation system consisting of a rotary pump (VRC 200-7.0) and a diffusion pump (Edwards, B 30207240) and was evacuated to a pressure of $\sim 10^{-4}$ mbar. The evacuated ampoule containing arsenic was heated using a vertical resistance tube furnace (ID = 27 mm) inside a fume cupboard. The open end of the furnace was closed using thermal blanket (Superwool™ 607™ Blanket) in order to generate the desired temperature throughout the furnace. A small amount of the upper part of the silica glass ampoule was exposed to the open atmosphere and was not covered by thermal blanket in order to keep it at a slightly lower temperature since it was believed that the impurities that were mainly the oxides of arsenic where what was deposited at the colder part of the ampoule. The set up for the arsenic purification process is shown in fig. 3.2.

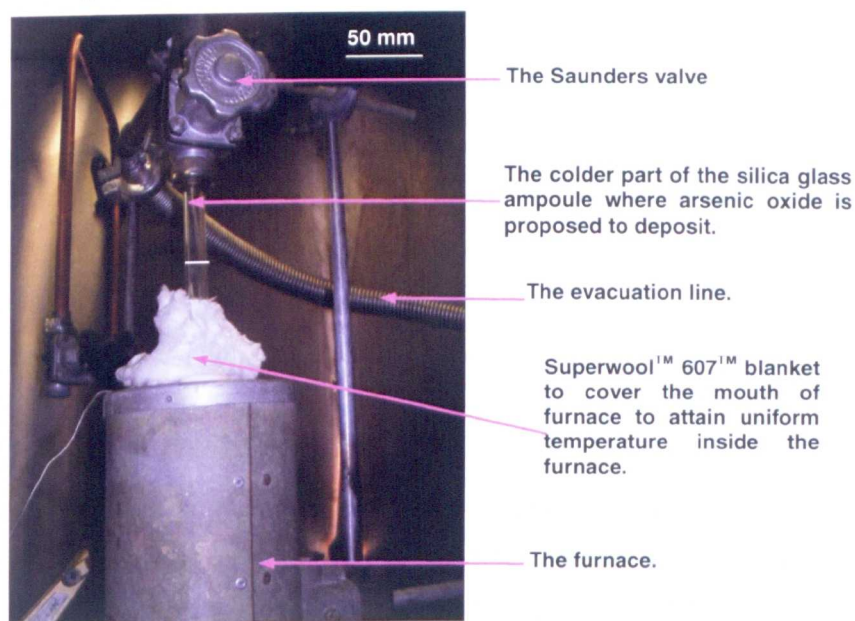


Fig. 3.2 The arsenic purification process in progress.

The arsenic was then heated according to the heating schedule indicated in Table 3.3.

Table 3.3 The arsenic purification heating schedule.

Stage	Schedule	Vacuum reading /mbar (Pa)
1	25°C → 200°C @ 200°C/h	10^{-4} (10)
2	200°C → 250°C @ 100°C/h	“
3	Hold at 250°C for 1h	
4	250°C → 300°C @ 100°C/h	
5	Hold at 300°C for 1h	“
6	At 180°C, withdrew furnace and allowed ampoule to cool to RT	

The furnace was withdrawn from the silica glass ampoule containing the arsenic at about 180°C. The ampoule was allowed to cool under vacuum. It was then detached, still protected from the open atmosphere by the Saunders valve, from the evacuation line and kept in the chalcogenide glove box (<0.1 ppm H_2O , <0.1 ppm O_2). The ampoule was opened inside the

glove box and each purified arsenic batch was kept in separate bottles. Red and white powdery oxides of arsenic could be seen at the top and colder part of the ampoule. The arsenic looked “shinier” after purification.

ii) The sulfur purification process

Sulfur was purified by two methods here:

Method (a):

- All the batch components, in the desired amounts, were weighed and placed in a silica glass ampoule inside the chalcogenide glove box. The glass batching procedure is described in section 3.1.1.3. The silica glass ampoule had been air baked and vacuum baked (section 3.1.1.1). All the other batch components were kept underneath the sulfur. The open end of the ampoule was closed with a Saunder’s valve whilst the ampoule was still inside the glove box. The ampoule with valve attached was then removed from the glove box and connected to the above described (this section 3.1.1.2 (i)) evacuation system. The sulfur was then boiled using an oxypropane torch (GIS, Junior Jet 7). Oxygen (BOC, Industrial grade, 99.5%) and propane (CALOR Gas) was used for obtaining a mild blue flame which was played over the outside of the ampoule at the place where sulfur was on the inside. The sulfur first melted to a yellow, visually transparent liquid. The sulfur-melt was boiled when bubbles formed. It is believed that the oxide and hydrogen containing impurities in the form of bubbles of H_2O , H_2S , SO_2 , SO_3 , and CO_2 etc. evaporated or volatilised during heating. The constant evacuation process facilitated this process. On further heating the sulfur-melt became thick and viscous (according to visual inspection) and bright orange (see fig 3.3). The heating was then stopped and the ampoule was sealed using the above oxypropane torch. This part of the process was done by Dr. David Furniss.

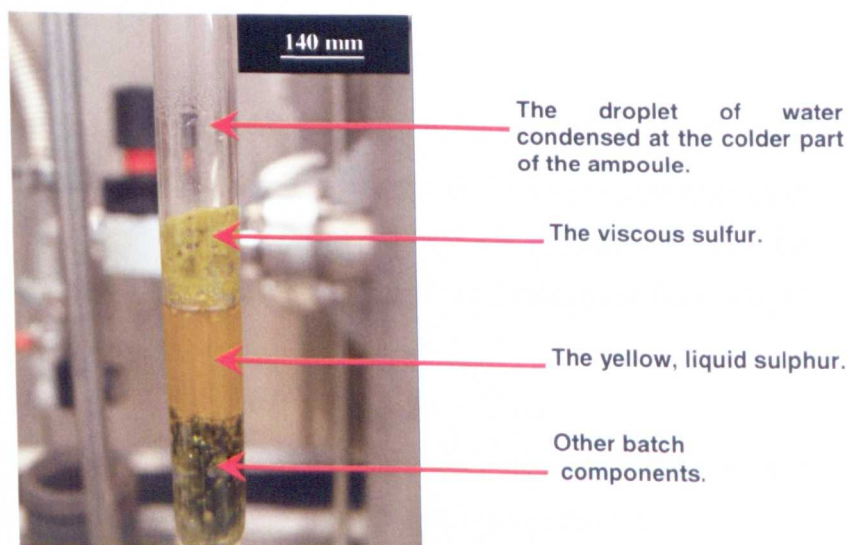


Fig 3.3 The sulfur purification process method (a) in progress.

Method (b):

• In the above described process sulfur was boiled in the presence of the other batch components. It was thought that the impurities, such as water, released from the sulfur may contaminate the other batch components present in the ampoule. In order to improve this process, and to prevent the other batch components becoming contaminated by the contamination released from sulfur, the following procedure was employed:

i) The silica glass ampoule was weighed inside the glove box (<0.1 ppm H_2O , <0.1 ppm O_2).

Let, W_A = weight of the silica glass ampoule.

ii) Amount of the sulfur required was calculated using Batch software (see section 3.1.1.3).

Let, W_R = amount of the sulfur required.

iii) An excess amount of the sulfur was weighed as it was thought that some of the sulfur would be lost in boiling. The sulfur might be lost in the form of H_2S , SO_2 or evaporated as sulfur vapour. Let, W_T = amount of sulfur taken (such that $W_T - W_R = +ve$).

iv) The sulfur was poured in the ampoule inside the chalcogenide glove box (<0.1 ppm H_2O , <0.1 ppm O_2) and the ampoule fitted with Saunders valve (this section 3.1.1.2 (ii) (a)).

v) The final weight of the ampoule with sulfur was measured. Let, W_F = weight of ampoule with raw sulfur.

vi) The ampoule with sulfur (excess amount) and fitted with Saunders valve (to prevent sulfur from direct contact with atmosphere) was taken out of the chalcogenide glove box. Sulfur was boiled as described above (this section 3.1.1.2 (ii) (a)).

vii) The ampoule was then allowed to cool and was taken inside the chalcogenide glove box. It was then detached from the Saunder's valve. The sulfur deposited on the upper part of the ampoule was scratched gently and removed using a stainless steel spatula (Fischer). The ampoule with remaining sulfur (left after boiling) was weighed inside the glove box. Let, W_L = weight of ampoule after the sulfur was boiled.

viii) The amount of sulfur present in the ampoule was calculated by subtracting from W_L (weight of ampoule after the sulfur had boiled) the weight of empty ampoule W_A .

The desired mass of each of the components was weighed in a separate plastic weighing boat (Fischer) using a stainless steel spatula (Fischer). Separate stainless steel spatulas (Fischer) were used for each different elemental precursor to take out the chemical from the bottle and transfer it into the weighing boat. The reactants were then poured into the cleaned and baked (as described in the above section 3.1.1) silica glass ampoule. Still inside the glove box, the Saunder's valve was attached to the open end ampoule with the help of an 'O' ring in order to prevent the any leak of atmospheric air inside the ampoule. The silica ampoule was then taken out of the glove box and attached to an evacuation system consisted of a rotary pump (VRC 200-7.0) and a diffusion pump (Edwards, B 30207240). The rotary pump was used for evacuation of the silica glass ampoule at high pressures followed by the diffusion pump which was used to evacuate it to lower pressure. The diffusion pump was attached to the ampoule through a cold trap. The cold trap was filled with liquid nitrogen (Fischer) with the aim of reducing the flow of evaporated chemicals, especially sulfur and selenium present in the ampoule, to the diffusion pump. It is suggested that sulfur and selenium polymerise with the oil present in the diffusion pump which makes it non-functioning and arsenic is hazardous for health. The ampoule was evacuated to $\sim 10^{-5}$ mbar (1 Pa) and was sealed using an oxy-propane torch (GIS, Junior Jet 7). Oxygen (BOC, Industrial grade, 99.5%) and propane (CALOR Gas) was used for obtaining a hot blue flame for sealing the ampoule (fig. 3.6).

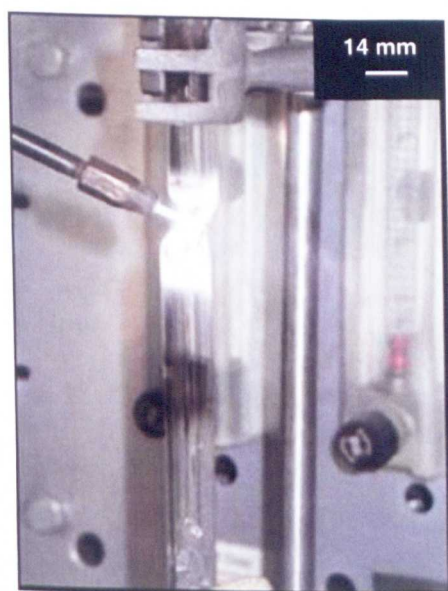


Fig 3.6 The silica ampoule sealing in process.

3.1.1.4 Formation of the glass-melt.

The evacuated and sealed silica glass ampoule, containing the reactants, was then heated to obtain a chalcogenide glass-melt. Thus the silica glass ampoule was wrapped in thermal blanket (Superwool™ 607™ Blanket) and then tied with Ni-chrome wires (~ 1 mm in diameter) to secure the blanket and was inserted in a rocking furnace (Instron, TF105/4.5/1 ZF with controller Eurotherm 2408, ID 86 mm) where the reactants were heated by resistance heating. The furnace had been modified in-house to provide a rocking movement. The furnace

was rocked at $30^\circ \pm 5^\circ$ about the horizontal axis during heating in order to prepare a homogenous melt. Rocking provided mechanical mixing of the reactants, especially when they become molten.

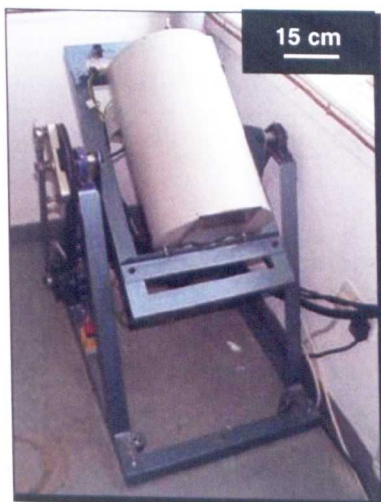


Fig. 3.7 The resistance rocking furnace (length = ~ 630 mm).

An example of the heating schedule for the melting of arsenic selenide (As_2Se_3) in the resistance rocking furnace is presented in Table 3.4 and shown schematically in fig. 3.8.

Table 3.4: The melting schedule for arsenic selenide (As_2Se_3) glass in resistance rocking furnace.

Stage	Heating schedule
1.	From room temperature (RT) to 200°C @ $200^\circ\text{C}/\text{h}$
2.	From 200°C to 800°C @ $40^\circ\text{C}/\text{h}$
3.	Dwell at 800°C for 12 h
4.	From 800°C to 650°C @ 40°C
5.	Dwell at 650°C until withdrew for annealing

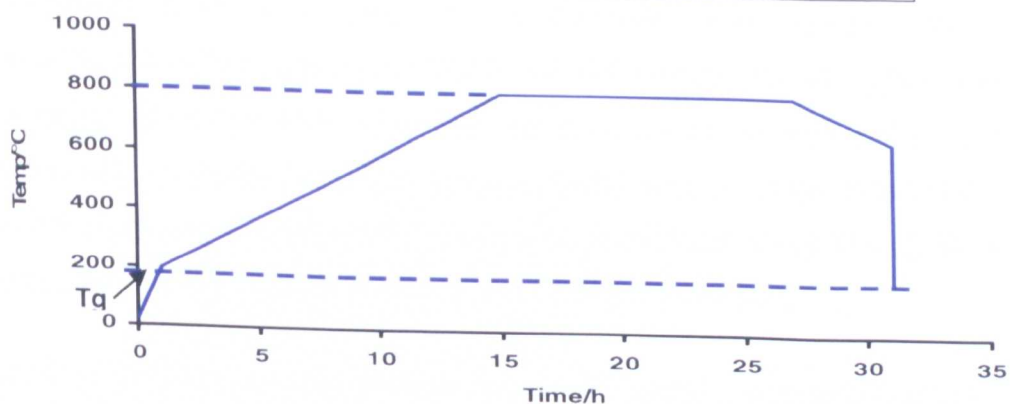


Fig 3.8 The heating trend for the preparation of As_2Se_3 chalcogenide glass-melts.

The whole melting procedure took *ca.* 32 to 44 hours, depending on the particular chalcogenide glass to be melted. The heating schedule was different for different glass compositions and will be discussed separately in subsequent chapters. The key principle is to heat the glass composition above its liquidus temperature (T_L) during melting. The general melting schedule is depicted in Table 3.5.

Table 3.5: The general melting schedule for chalcogenide glass in the resistance rocking furnace.

Stage	Ramp Type/Dwell	Heating schedule
1.	Fast ramp	(200°C/h) from RT
2.	Slow ramp	40°C/h to $(T_L + \geq 200)^\circ\text{C}$
3.	Dwell	Dwell at $(T_L + \geq 200)^\circ\text{C}$ for 12 to 24 h
4.	Ramp before quenching	60°C/h or 40°C/h to $(T_L + \geq 50)^\circ\text{C}$

Key: T_L = liquidus temperature

The furnace was rocked to the new end-of-cycle position once after every 5 minutes and remained static at the new position for just under 5 minutes. At the end of the heating schedule (at stage 5 of Table 3.1) the furnace was held vertical for about 5 minutes in order to collect the melt at the bottom of the ampoule before quenching.

3.1.2 Glass-melting in domestic microwave oven (DMO).

As stated above, general observations are made here about the ampoule preparation, starting materials, glass batching, initial trials and glass melting in the DMO followed by general information on melt quenching and annealing. More details may be found in chapters 4 to 7.

3.1.2.1 Ampoule preparation.

(a) *Ampoule for the synthesis of arsenic sulfide glass.*

Silica glass tube of length 1 m, ID 10 mm and OD 14 mm, (Multilab Ltd.) was split into two equal parts by scoring around the tube circumference with a tungsten carbide knife (Le WTHAM Products) to obtain two pieces of silica tube each about 500 mm length. The score mark was made wet with a drop of distilled water which helped in cutting the silica tube in two equal halves. Each half of the silica tube was then sealed (see section 3.1.1.3) using the oxy-propane torch to obtain two silica glass ampoules each of length about 250 mm. The ampoule to be used was then rinsed three times with distilled water and then air dried in air in the ambient atmosphere but it was neither dried nor baked in an oven.

(b) *Ampoule preparation for the synthesis of arsenic selenide, germanium arsenic selenide (GAS), tellurium arsenic selenide (TAS) and germanium arsenic selenium telluride (GAST) glass.*

The ampoule preparation procedure was as discussed above in section 3.1.1.

3.1.2.2 The starting materials and their purification.

The starting materials for the DMO processing were the same as used for the conventional glass melting in the rocking resistance furnace. The source, purity and particle size of the starting materials as-received are listed in Table 3.2. All the starting materials such as arsenic, germanium, sulfur, selenium and tellurium were crushed separately using a clean agate mortar and pestle (Fisher) manually inside the glove box (MBraun 150B-G) to powder. The powdered germanium, selenium, tellurium was used without any further purification but powdered arsenic was purified as described in section 3.1.1.2 before use.

3.1.2.3 Glass batching.

Again the glass batching for the DMO processing was the same as used for the conventional glass melting in the rocking resistance furnace. Thus the powdered elemental materials arsenic, germanium, sulfur, selenium and tellurium were weighed in separate weighing boats as described in section 3.1.1.3. The weighed materials were then mixed in a plastic weighing boat (Fischer) using a stainless steel spatula (Fischer) and then poured in the cleaned silica ampoule. The ampoule was then taken out of the chalcogenide glove box and was sealed as described in section 3.1.1.3.

3.1.2.4 Initial trials of glass melting in DMO.

During the early stage of the project arsenic selenide (4 g) was made in *ca.* 140 mm long ampoule when tiny glossy hemispheres were obtained (see fig. 3.9).

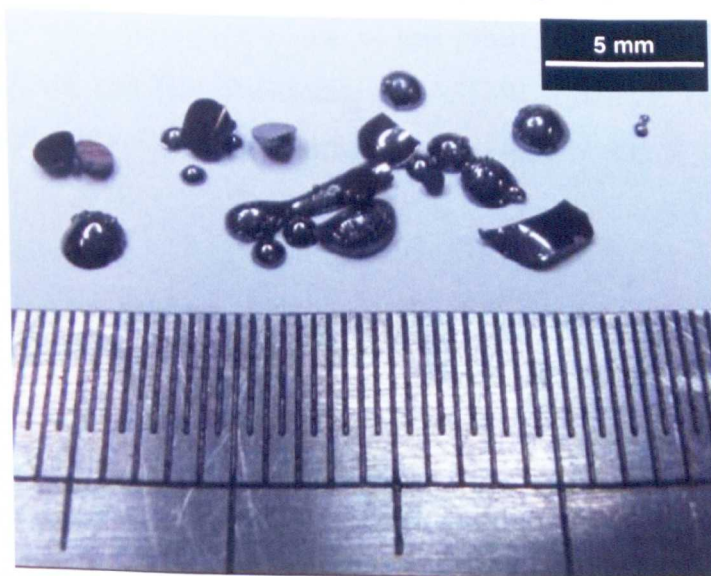


Fig. 3.9 The tiny hemispheres of product formed during initial trials of glass melting in the DMO.

The glass-melt could not collect at the bottom of the silica ampoule as the melt had boiled during microwave heating. Heating stopped as soon as the domestic microwave oven (DeLonghi/ M8021P-B1) was turned off. The glass-melt in contact with the silica ampoule

quenched immediately and stuck to the wall of the ampoule. The wall of the silica ampoule was coated with chalcogenide melt. A few droplets of the chalcogenide melt quenched and small shining hemispheres of product of diameter *ca.* 0.5 mm to *ca.* 3 mm (fig. 3.9) were obtained (see later sections 5.1.1 and 5.1.2).

In order to get a glass rod and reduce waste of the chalcogenide melt the length of silica ampoule was kept as small as possible so that the chalcogenide glass-melt could collect at the bottom of the ampoule and could be quenched in an effort to obtain a monolithic rod product (see later section 5.1.3). Fig 3.10 shows a typical Ge-As-Se chalcogenide product (id: MW31) coated silica ampoule formed during microwave heating. The length of the ampoule was kept to 100 mm to 110 mm long for 10 g of glass batch.

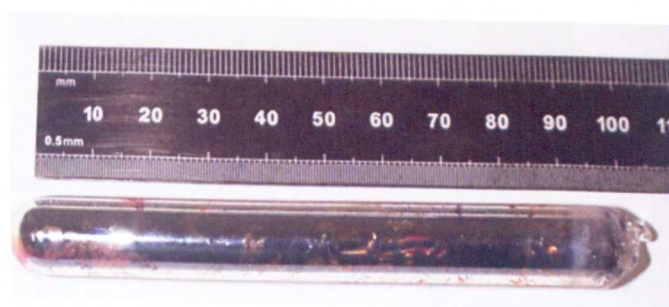


Fig. 3.10 An example of chalcogenide product coated silica ampoule formed during microwave heating of 10 g of starting materials Ge, As and Se in ~100 mm of ampoule (id: MW31).

3.1.2.5 Formation of the chalcogenide melt in DMO.

(i) Optimising the precise location of melt ampoule in DMO.

The chalcogenide melt was prepared using a domestic microwave oven (DMO). Three different DMOs were used during the course of this project: (i) DeLonghi/ M8021P-B1 (ii) DeLonghi/ EM821AAN and (iii) Panasonic/ NNA554W. All the three DMOs were a multimode cavity with eddy cycle and maximum power rating of 800 W, 800 W and 1000 W, respectively.

To prepare a DMO As-S product (DMO make/model = DeLonghi/ M8021P-B1) is now discussed. In the later experiments a beaker containing sand was used for the placing the ampoule and the method to decide the position of the beaker inside the DMO is subsequently also discussed below.

In initial experiments, for the microwave assisted synthesis of As-S glass, the ampoule was supported in a deep circular groove (diameter = ~ 16 mm, ~ 15 mm deep) made in a mullite brick (length = ~ 80 mm, breadth = ~ 18 mm, height = ~ 20 mm) inside the DMO. The batch was 4 g of atomic stoichiometry 2As:3S. The sealed silica ampoule was placed in the middle

of the groove (off vertical) of the mullite brick. The mullite brick was kept in the middle of the DMO (make/model = DeLonghi/M8021P-B1) as a trial position (see fig. 3.11) as this position was used by some senior researchers (preparing very different products) previously. Several blue glows were seen as soon as the heating started.

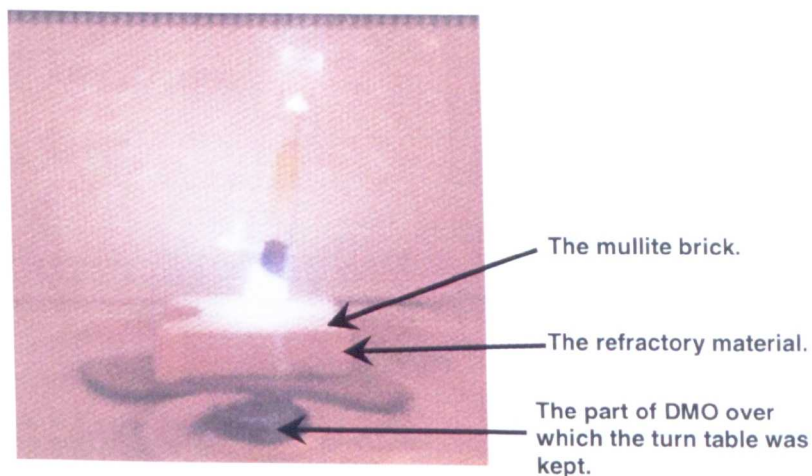


Fig. 3.11 The blue glow formed during the formation of As-S glass (MW6) inside the DMO (make/model = DeLonghi/M8021P-B1). The sealed silica glass ampoule containing the As-S batch was kept in the groove (diameter = ~ 16 mm, depth = ~ 15 mm) placed over a refractory material in a mullite brick ($l = \sim 80$ mm, $b = \sim 18$ mm, $h = \sim 20$ mm) as a trial position. 4g of batch was in atomic stoichiometry $2As:3S$.

Fig. 3.11 shows the set up early in the project and was used only for As_2S_3 .

For the preparation of the chalcogenide melts in the remaining two DMOs of make model DeLonghi/ EM821AAN and Panasonic/ NNA554W in the rest of the experiments, the ampoule with reactants was placed in a silica glass beaker (50 ml ($50 \times 10^{-3} dm^3$), Multilab, diameter = ~ 65 mm and height = ~ 85 mm) which was approximately half-filled with sand. The beaker was placed inside the DMO after determining the position of anti-nodes of the standing waves present in the DMO. The position of anti-node was decided by keeping an unsealed silica glass ampoule containing < 2 g of amorphous carbon standing in the 50 ml beaker (as above) containing the sand. The beaker with the ampoule containing amorphous carbon was placed inside the DMO and the DMO was switched on. The place in the DMO where the carbon started glowing to deep orange red in less than 10 seconds was chosen for placing the beaker. This method was used for every experiment irrespective of the DMO make and model. It was found that one of the corners of the DMOs was usually suitable for placing the beaker containing sand. The beaker had to be kept at the left hand corner near to the door of the DMO for the DMO of make/model = DeLonghi/ EM821AAN whereas the beaker had to be kept in the left hand corner furthest from the door for the DMO of the make/model = Panasonic/ NNA554W (see fig. 3.12). The ampoule with the reactants was

leaned just off vertical on the sand as shown schematically in the fig. 3.12 and the photographs shown in figs. 3.13 and 3.14.

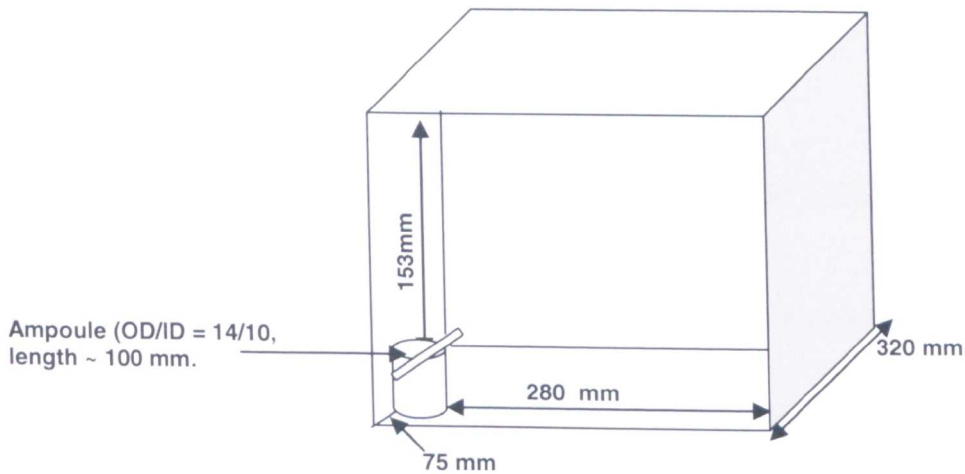


Fig. 3.12 A schematic of the optimum position of the silica glass ampoule containing the chalcogenide batch inside the DMO (DeLonghi/ EM821AAN). The ampoule was supported just off vertical by means of a 250 ml ($250 \times 10^{-3} \text{ dm}^3$) capacity beaker (Multilab). The diagram is not to scale.

Fig. 3.13 shows the photographs of the position of the beaker with the silica glass ampoule leaned off vertical inside the DMO. When DMO with make/model DeLonghi/ EM821AAN (see fig. 3.13 (a)) was used the beaker was kept far near the front end whereas when Panasonic/ NN A554W was used the beaker was kept far from the front end (see fig. 3.13 (b)).

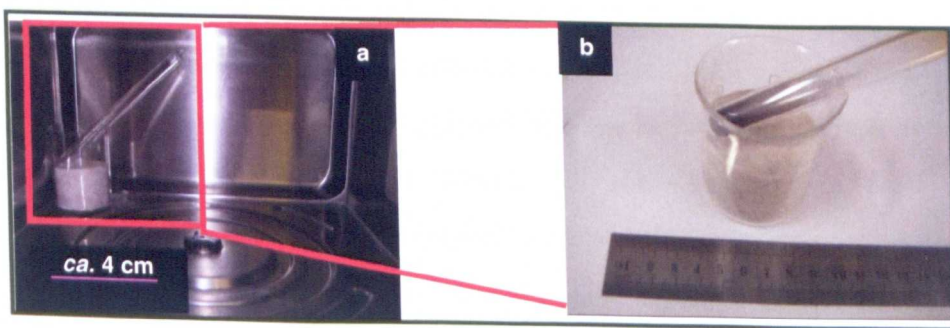


Fig 3.13 Photographs showing the position of the sealed ampoule (b) placed on a beaker containing sand (a) inside the DMO (make/model = Panasonic/ NNA554W).

The dimensions of all of the DMOs used in this project and the relative position of the silica glass ampoule, containing the chalcogenide glass melt, are listed in Table 3.6.

Table 3.6 Dimensions of the DMOs used in this project with the approximate position of the glass beaker, containing sand, used to support the silica glass ampoule, containing the chalcogenide glass melt, inside the DMO.

DMO Make/Model	Dimension (L x W x H) / (mm)		Position of beaker inside the DMO
	External	Internal	
DeLonghi/M8021P-B1	Not recorded.	Not recorded.	Not recorded.
DeLonghi/ EM821AAN	485 x 395 x 287	305 x 305 x 203	280 mm across from the

DMO Make/Model	Dimension (L x W x H) / (mm)		Position of beaker inside the DMO
	External	Internal	
			right hand side, 153 mm from the top, 75 mm from the front (see fig 3.11).
*Panasonic/ NN A554W	500 x 305 x 250	290 x 320 x 210	290 mm across from the right hand side, 130 mm from the top, 210 mm from the front.

Key: * This was a convection DMO and the DMO cavity could be heated to 220°C through the convection current alone.

(ii) Further general comments on the success of the DMO glass melting.

During the preparation of DMO As-S chalcogenide product the chalcogenide melt could be seen at the bottom of the ampoule but the DMO chalcogenide melt never boiled.

During the synthesis of arsenic selenide, germanium arsenic selenide glasses and tellurium arsenic selenide glass, a boiling melt was observed irrespective of the type (here the term 'type' is used to indicate different makes and models of DMOs used during the preparation of these DMO chalcogenide products) of the DMO used. Fig. 3.14 shows an example of a boiling chalcogenide melt (As-Se) inside the DMO. It was also observed that during the preparation of Ge-As-Se chalcogenide product that the walls of the ampoule were less coated with chalcogenide glass melt when the DMO was preheated, and heated simultaneously with the application of microwaves, using the convection current both prior to, and at the same time, as the microwave irradiation. It is believed that the higher temperature of the walls of the silica glass ampoule reduced the viscosity of the chalcogenide melt and DMO chalcogenide melt dripped down to the bottom of the ampoule.

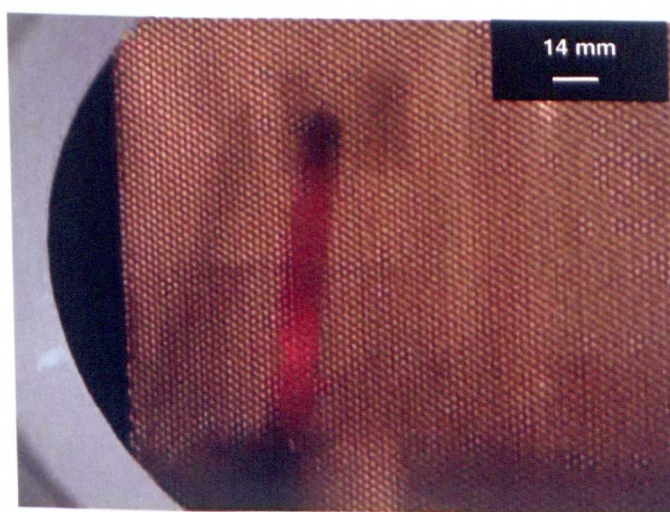


Fig 3.14 An example of a boiling chalcogenide melt under microwave irradiation in the DMO. This particular case was during the formation of As_2Se_3 glass (MW18). The sealed ampoule was kept in a silica glass beaker over sand. 10 g of batch was in atomic stoichiometry 2As:3Se. The perforated sheet visible in the photograph is the door of the microwave oven.

The preparation of two compositions of chalcogenide DMO product composed of germanium, arsenic, selenium and tellurium was attempted using the DMO. It was observed that the composition $\text{Ge}_{30}\text{As}_{10}\text{Se}_{30}\text{Te}_{30}$ (id: MW57) boiled well in the DMO at 1000 W while the convection heating was switched on *in-situ* with the microwave heating when DMO make/model = Panasonic/ NN A554W was used whereas, however, $\text{Ge}_{15}\text{As}_{15}\text{Se}_{17}\text{Te}_{53}$ (id: MW54) did not boil even when the convection heating was operated in-situ of the microwave heating.

In addition, Ge-As-Te (with the exact composition $\text{Ge}_{10}\text{As}_{50}\text{Te}_{40}$, id: MW59) DMO melt did not boil in the DMO. Though a melt was formed and melting could be seen. When this DMO chalcogenide product was taken out of the ampoule few fragments with metallic lustre could be seen at the contraction cone. (Please note that the work on Ge-As-Se-Te and Ge-As-Te compositions is not further reported in this thesis.)

The time of exposure to microwaves for each particular chalcogenide glass system is discussed in the following chapters 4 to 7. The chalcogenide melts obtained with this method were quenched and annealed to try to make monolithic glasses. The methods of quenching, annealing and sample preparation of the products made in DMO are discussed in the following section 3.2.

3.2 Quenching, annealing and sample preparation.

General comments are made here regarding the quenching and annealing of melts made either by conventional heating in the rocking resistance furnace or in the DMO in an effort to obtain monolithic chalcogenide glass rods. Further details are to be found in future chapters 4 to 7. The process used for quenching and annealing of the glass-melt is discussed in section 3.2.1 whereas the procedure used for the removal of glass rod from the silica ampoule is discussed in section 3.2.2. The glass rod was then sliced and polished to prepare a polished glass samples (see section 3.2.3).

3.2.1 Quenching and annealing of the chalcogenide melt.

The chalcogenide-melt was cooled *in situ* inside the silica glass ampoule by removing the ampoule from the heat source (*i.e.* the ampoule was taken out of the rocking resistance furnace (section 3.1.1.4) or the DMO (section 3.1.2.5)) and cooling in either ambient air, cold water or boiling water for of the order one minute. The quenching condition was decided according to the T_g of the glass and further details are given in chapter 4 to 7. During, quenching it was aimed to prepare a super-cooled liquid and the process of instant or fast

cooling of the melt to form a super-cooled liquid is called quenching. The quenched super-cooled liquid was then annealed by placing it in a preheated furnace at $(T_g + 10)^\circ\text{C}$ for one hour to release the molecular stress built up due to quenching where different parts of the glass-melt sample cool at different rates. (Note - T_g was taken as that measured using differential thermal analysis (DTA) (section 3.3.3)).

The super-cooled liquid was then cooled down slowly ramp with a first slow ramp of 5°C/h to $(T_g - 40)^\circ\text{C}$ where it would have had the opportunity to transform fully to a glass and a second fast ramp of 15°C/h to room temperature. An example of the annealing schedule as a general cooling trend is depicted in fig. 3.15.

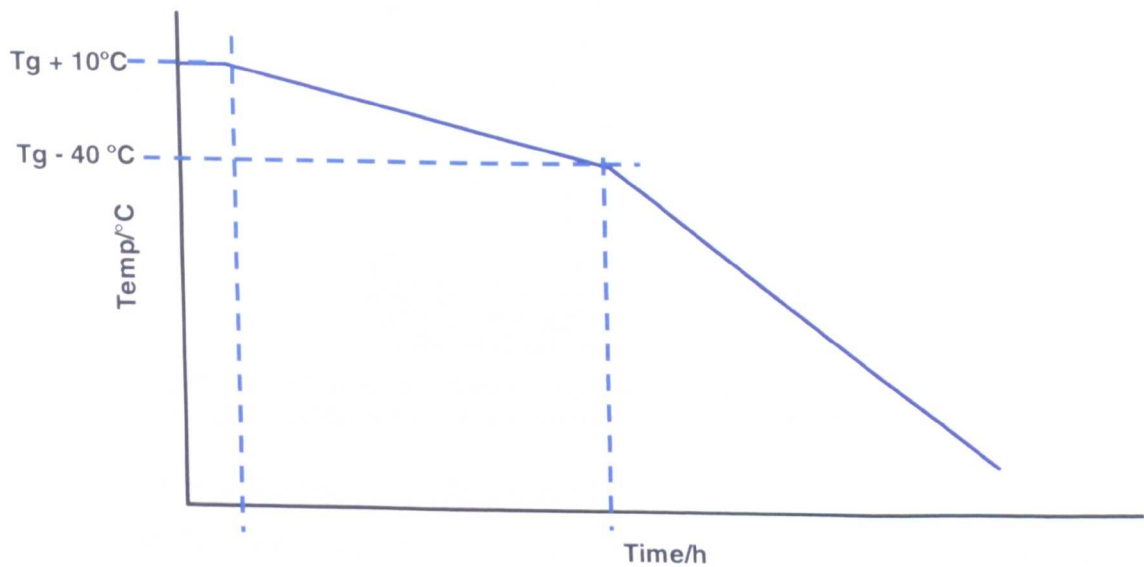


Fig. 3.15 The general cooling trend during annealing of chalcogenide glasses made either in the rocking resistance furnace or the DMO.

The following fig. 3.16 shows a typical annealed chalcogenide glass sample, still inside the silica glass ampoule, made in the resistance rocking furnace.



Fig. 3.16 Typical annealed chalcogenide glass sample, in a silica glass ampoule, prepared in the resistance rocking furnace (20 g of batch was in atomic stoichiometry 40As:60Se, id: CF 111). (Note: photograph kindly supplied by Zheng Lian (PhD student) of University of Nottingham and this glass was made by him.)

3.2.2 Removal of chalcogenide glass rod from silica glass ampoule.

If a monolithic chalcogenide glass rod was obtained after quenching and annealing, the rod was taken out of the silica glass melting ampoule. The silica glass ampoule was cut using a diamond cutting saw (Buehler, Isomet low speed saw) and diamond wafering blade (150 HC with diameter = 100 mm, thickness = 0.35 mm). Fig. 3.17 shows the the diamond cutting saw with the diamond wafering blade.



Fig. 3.17 The silica ampoule cutting (the process of vacuum release) using the diamond cutting saw and diamond wafering blade, to release the chalcogenide glass rod from the ampoule.

A lubricant oil was used to reduce the temperature of the blade raised due to friction between the blade and the silica ampoule. The ampoule was first cut above the top of the chalcogenide product inside the silica glass ampoule to release the vacuum. The release of vacuum was accompanied by an in-spill of oil with bubbles inside the ampoule. The ampoule was then cut to about 1.8 mm deep at three places along the length at regular intervals around the circumference of the ampoule. The chalcogenide glass was removed out of the ampoule without any difficulty. Normally, this process was carried out in the fume cupboard under ambient air flow.

3.2.3 Sample preparation

Sample preparation included the sectioning of the chalcogenide glass rod (see section 3.2.3.1) and polishing (see section 3.2.3.2) to get a flat chalcogenide glass disc with optically finished surfaces for analysis.

3.2.3.1 Sectioning of all glass samples.

The chalcogenide glass rod was sectioned orthogonally to the length into several pieces. Extra care was taken to keep the two opposite sides of the cut-out glass pieces parallel to each other.

The same diamond cutting saw and wafering blade as described in section 3.2.2 were used to cut the glass sample (see fig. 3.18).

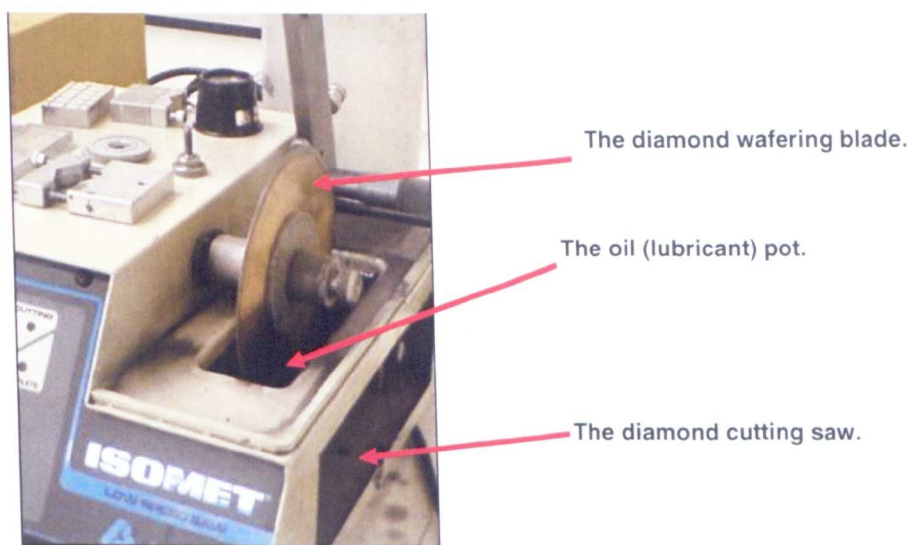


Fig 3.18 The diamond cutting saw with the diamond wafering blade used for sectioning the chalcogenide glass rod into samples for analysis.

3.2.3.2 Chalcogenide glass polishing procedure.

To obtain a smooth, flat surface the chalcogenide glass sample was ground and polished. A piece of chalcogenide glass sample, cut as a flat disc from the as-prepared chalcogenide glass rod, was glued using warm wax (Mounting epoxy, Struer) on the flat surface of the brass block which was a part of a home-made polishing jig (fig. 3.19). The chalcogenide glass samples were then initially ground on a flat commercial silicate glass plate using 400 grit SiC powder (Buehler, Coventry, UK) mixed with paraffin oil based lubricant (Buehler, Coventry, UK). The process was repeated with 1000 grit SiC powder mixed with paraffin oil based lubricant (Buehler, Coventry, UK) glass side. The chalcogenide glass sample was washed between each grit type with acetone (>99.99 %, Fischer, UK) and air dried before being polished with a SiC powder of finer grade. Two different sides of the same silicate glass plate were each dedicated to the different grit SiC particle size to avoid cross-contamination.

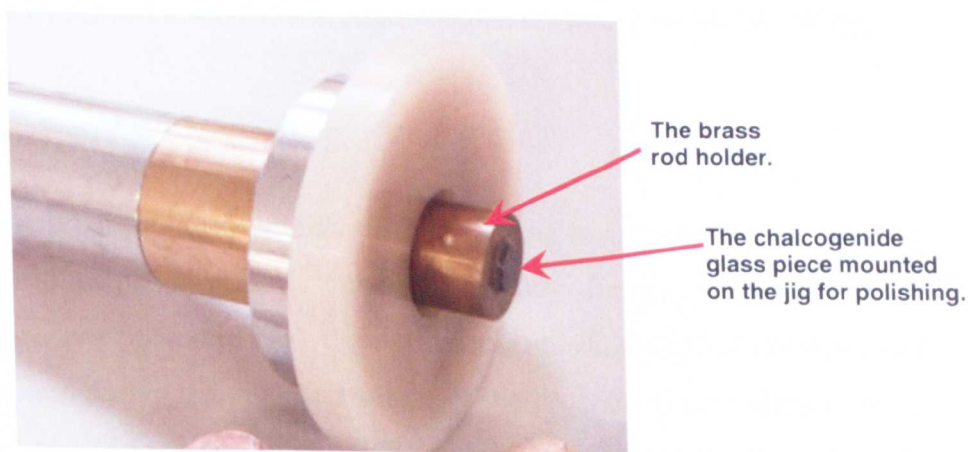


Fig. 3.19 The chalcogenide glass polishing jig.

After grinding, the sample, still supported on the surface of the brass block on the home made polishing rig, was polished on a rotating polishing wheel (Metaserv, 2000, Buehler, Coventry, UK, fig 3.14) using METADI II diamond paste and oil based lubricant (Buehler, Coventry, UK). Three grades of diamond pastes were used successively: 6 μm , 3 μm and 1 μm . The sample was washed each time with acetone (>99.99 %, Fischer, UK) and air dried before being polished with a diamond paste of finer grade. The various steps of grinding and polishing are listed in Table 3.7.

Table 3.7 Steps for chalcogenide glass I grinding and II polishing; the chalcogenide glass sample was acetone (Fisher, 99.99%)-washed carefully after each step and air dried.

I. SiC powder grinding		II. Diamond paste polishing	
Stage	Process	Stage	Process
1.	400 grit glass plate with 400 grit SiC	1.	6 μm diamond paste used over 6 μm plate
2.	1000 grit glass plate with 1000 grit SiC	2.	3 μm diamond paste used over 3 μm plate
	-	3.	1 μm diamond paste used over 1 μm plate
	-	4.	¼ μm diamond paste used over ¼ μm plate

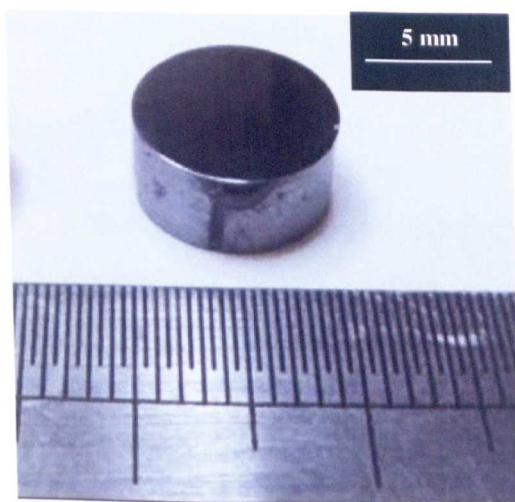


Fig. 3.20 Examples of a polished chalcogenide glass sample: arsenic selenide (id: MW39).

3.3 Characterisation techniques.

Samples of chalcogenide products prepared either in the rocking resistance furnace or in the DMO were characterised using several techniques, including for the determination of amorphicity, glass transition temperature (T_g), the optical transmission window and chemical composition. The main aim during the characterisation of the products was to determine the benchmark material properties for the chalcogenide glass products prepared conventionally *via* the rocking resistance furnace to allow to conclusions to be drawn regarding the material

properties of chalcogenide products prepared in the DMO. Both the conventional and the DMO preparation methods should theoretically yield the same results irrespective of the method of preparation of the glass.

Chalcogenide products were subjected to powder X-ray diffraction (XRD) and selected area electron diffraction (SAED), using transmission electron microscopy (TEM), to confirm the amorphicity of the sample. Differential thermal analysis (DTA) and differential scanning calorimeter (DSC) were performed to determine T_g. The chemical composition of the glass was analysed by energy dispersive X-ray (EDX) analysis using environmental scanning electron microscopy (ESEM). The glass transmission window was measured using Fourier transform infrared spectroscopy (FTIR). These characterisation techniques and the method of sample preparation for each characterisation technique are discussed in the following subsections 3.3.1 to 3.3.6.

3.3.1 X-ray diffractometry (XRD).

To check the amorphicity of the glass overall the sample was subjected to powder X-ray diffraction. The theory of operation, basic construction of diffractometer, procedure for sample preparation and the procedure for carrying out the measurement were as follows.

3.3.1.1 Theory of operation.

Bragg [4] recognized that diffracted X-rays act as though they were “reflected” from planes of atoms in the structure. Contrasting the continuous reflection of light from a mirror however, the X-ray “reflection” took place only at certain angles that were controlled by the spacings between atomic planes and the wavelength of the radiation. He showed that this “reflection” took place only when the equation:

$$n\lambda = 2d \sin \theta \quad \dots\dots\dots \quad (\text{eqn. 3.6})$$

was satisfied, where n is an integer, λ is the wavelength of the radiation, d is the interplanar spacing, and θ is the incident angle relative to the plane of atoms. For “reflection” to occur from a set of parallel planes of atoms in a structure, these “reflections” must be in phase so that they constructively strengthen each other and generate a measurable signal. The geometry necessary for constructive interference can be seen in fig 3.21.

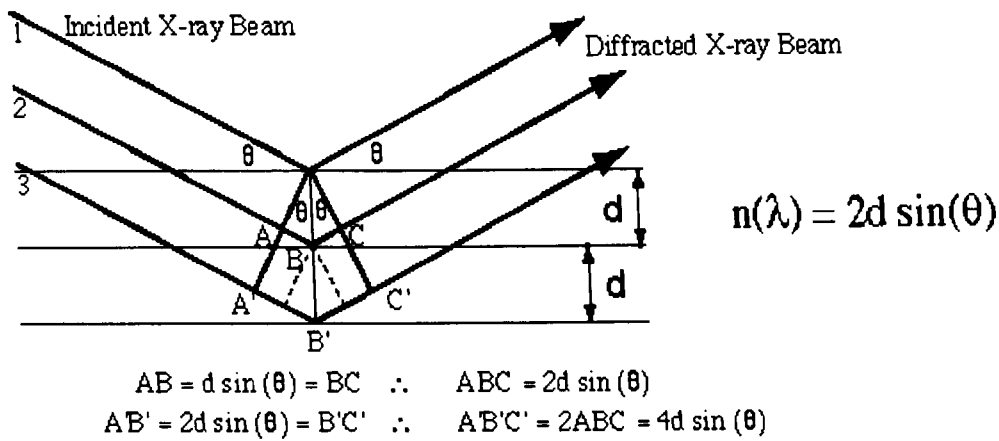


Fig. 3.21 Path of X-rays with respect to atomic planes of a material for the deduction of Bragg's equation (eqn. 3.6).

From fig. 3.21, if the path difference (ABC) for the diffracted rays 1 and 2 is exactly one wavelength then they will reinforce each other by constructive interference. Under these same conditions the path difference ($A'B'C'$) for rays 1 and 3 will be two wavelengths and they also will constructively interfere.

Since, in a glass there is no long term regular arrangement of atoms, the X-ray diffraction pattern shows an amorphous halo or hump in contrast to the sharply peaked X-ray diffraction pattern of crystalline substances.

3.3.1.2 Equipment.

Standard X-ray tubes produce divergent beams and hence most of the high resolution X-ray diffractometers use self-focusing geometries, which improve both the diffracted intensity and the resolution of the instrument. This is usually achieved by highly precise X-ray optics, which are incorporated into the critical part of the powder diffractometer hardware – the goniometer or goniostat.

In the powder diffractometer, both the incident beam and the diffracted beam form the same angle say θ , with the surface of the flat sample and atomic planes are assumed parallel to the flat sample surface. Hence, the angle between the incident ray and the diffracted ray is 2θ .

The incident beam passes through two "Soller slits" before reaching to the sample. These Soller slits limit the divergence of the incident beam and focus it towards the sample. The beam then passes through a divergence slit as a divergent beam has to interact with the sample. The diffracted beam then passes through the second Soller slit before reaching to the detector. The detector is interfaced with a computer for data acquisition. Fig. 3.22 shows the path of X-ray in powder X-ray diffractometer.

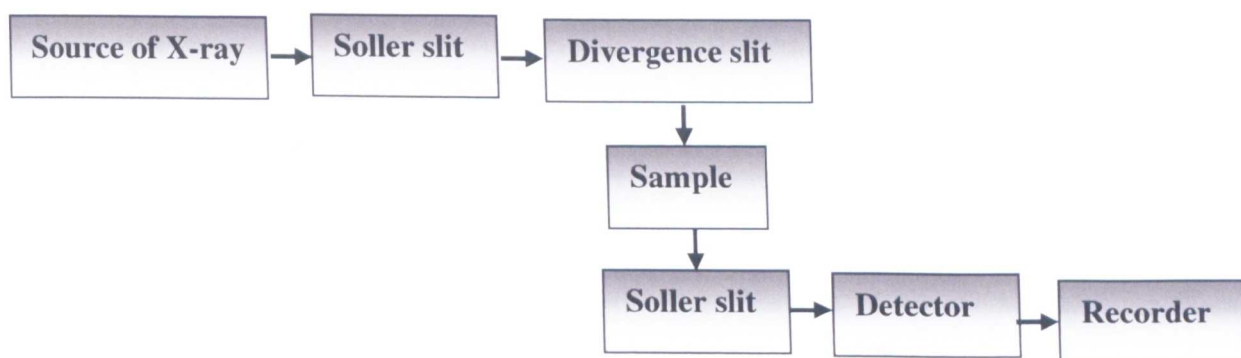


Fig 3.22 Path of X-ray in an X-ray diffractometer.

3.3.1.3 Sample preparation.

A piece of the chalcogenide sample was crushed to fine powder using an agate mortar and pestle (Fischer). The powder was then packed in a sample holder made of aluminium. The shape of the sample holder is shown in fig. 3.23.



Fig 3.23 Side elevation of aluminium sample holder (with sample) for powder X-ray diffraction.

The surface of the powdered sample was made as flat as possible by smoothing a silicate glass microscope slide over the top of the aluminum sample holder.

3.3.1.4 Procedure and equipment.

The sample was scanned from 35° to 70° 2θ and the step size was 0.02° 2θ at using a Siemens, D 500 X-ray diffractometer at 40 kV voltage and 20 mA current.

3.3.2 Selected area electron diffraction (SAED) using transmission electron microscopy (TEM).

Selected area electron diffraction (SAED) was carried out to check whether the prepared glasses exhibited crystallinity at nanometer scale. For SAED, the sample was exposed to a highly energetic beam of electrons by the use of transmission electron microscopy (TEM). An aperture was used to define the area from which a diffraction pattern was formed for the TEM specimen. The highly energised electrons interacted with the sample and were diffracted. An image of the arrangement of atoms in the sample is manifested in the diffraction pattern. The theory of operation, the basic construction of transmission electron microscope, sample preparation and the procedure for taking images are as follows:

3.3.2.1 Theory of operation.

X-ray diffraction was discussed above (section 3.3.1.1) here more general comments are made regarding diffraction. The phenomenon of diffraction is the interference caused by an object in the path of waves, and the pattern of varying intensities that results is called a diffraction pattern. Diffraction occurs when the dimensions of the diffracting object are comparable to the wavelength of the radiation. Thus in X-ray diffraction, the X-ray wavelength is comparable to the interatomic planar spacings. For electron diffraction, the de Broglie wavelength of the electrons is also comparable to the interatomic planar spacings but the electron beam can be focused to a smaller size here allowing detection of smaller volumes of crystalline material. To perform the selected area electron diffraction the microscope is adjusted so that it can collect all of the diffracted electron beams. All diffracted electrons follow Bragg's Law and thus are scattered according to the equation 3.6.

All incident electrons have the same incident energy (thus wavelength) and enter the specimen normal to its surface. The entire incident electrons which are scattered by the same atomic spacing will be scattered by the same angle. These "similar angle" scattered electrons can be collected using magnetic lenses to form a pattern of spots; each spot corresponds to a specific atomic spacing (a plane). This pattern can then yield information about the orientation of atomic arrangements present in the sample. In a glass sample there is no long range periodic, regular atomic arrangement and hence a blurred pattern is observed which encompasses the slightly different bond lengths and angles throughout the glass structure.

3.3.2.2 Equipment

Electron microscopes work in an analogous way to the optical microscope. In the optical microscope the sample is exposed to a source of visible light whereas in the electron microscope the sample is exposed to a beam of electrons. A tungsten filament is used as the source of electrons. Electron microscopes contain several electromagnetic lenses for focussing the electron beam. The basic components of a transmission electron microscope are shown in fig 3.24 and described below.

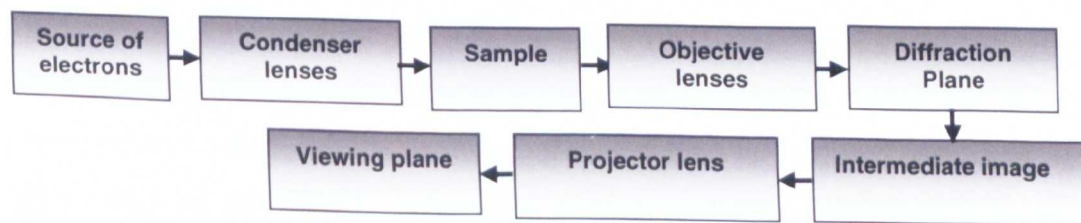


Fig 3.24 The basic components of a transmission electron microscope.

A beam of electrons emitted from a tungsten filament is accelerated towards the sample using electromagnetic lenses called condenser lenses. The condenser lenses control the size of the angular spread of the incident electron beam. The electron beam passes through the sample. The transmitted electron beam passes through a number of lenses – objective, intermediate and projector - in order to form a magnified image. By changing the relative position of the viewing screen the diffraction pattern can be imaged.

3.3.2.3 Sample preparation.

A small piece of chalcogenide product was cut then powdered using a clean, agate mortar and pestle. The powder was then mixed with acetone (99.99 %, Fischer). One drop of this mixture was then transferred on to a carbon coated copper grid using a clean (new) soda-lime-silica-glass capillary tube. This mixture was allowed to dry for a couple of minutes under the ambient.

3.3.2.4 Procedure and equipment.

The copper grid on which the sample was placed was mounted over a sample holder. TEM micrographs were obtained using a Jeol 2000 FXII transmission electron microscope at an operating voltage of 200 KeV.

3.3.3 Glass transition temperature and differential thermal analysis (DTA).

The glass transition temperature (T_g) of the chalcogenide glass products was determined by differential thermal analysis (DTA). The theory of operation, basic construction of the DTA equipment, procedure for sample preparation and the procedure for carrying out the measurement of T_g are described below.

3.3.3.1 Theory of operation.

DTA is a technique in which the temperature of a sample is compared to that of an inert reference material when they are both subjected to a controlled temperature programme. There is a zero temperature difference between the sample and the inert reference material when the sample does not go through any physical or chemical change. On the occurrence of any thermal event, such as melting, decomposition or change in crystal structure the temperature of the sample either lags behind or leads the reference temperature. The equipment is not equipped for mass changes and so the sample and the reference must not undergo decomposition leading to mass change over the temperature regime selected. During

an endothermic change, the sample is at a lower temperature than the reference material, but in the case of an exothermic reaction the sample is at a higher temperature than the reference material. This condition is only temporary because, on completion of the reaction, the sample will again show the zero temperature difference with respect to the reference. The temperature difference ΔT between the sample and the reference material can be depicted as

$$\Delta T = T_S - T_R$$

where,

T_S = Temperature of the sample

T_R = Temperature of the reference

In DTA, a curve of ΔT is usually plotted against the temperature of the reference. Fig. 3.25 shows a typical DTA curve of ΔT versus T for an AlF_3 -based glass obtained by isochronal heating of a small sample of the glass while monitoring the temperature difference (ΔT) of the glass relative to an inert reference supplied with the same rate of heat input [5]. The curve shows the typical endothermic change in baseline at T_g as the molar heat capacity of the supercooled liquid $> T_g$ is larger than the molar heat capacity of the glass $< T_g$. Also exothermic crystallisation peaks T_{c1} and T_{c2} are present and the liquidus when the baseline returns after the melting events. The AlF_3 based glass is ideal as it exhibits all of these phenomena giving an exemplar DTA curve. By convention, DTA exothermic peaks are plotted upwards.

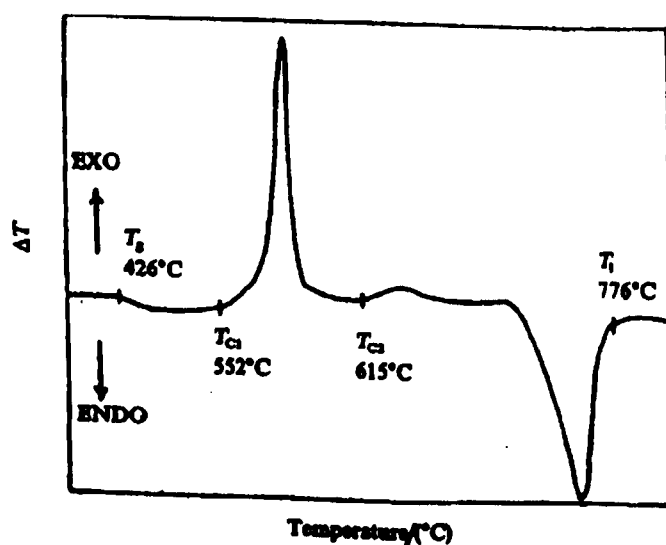


Fig 3.25 DTA curve of composition AMCSBY-7 heated at $10^\circ\text{C}/\text{min}$ under nitrogen. The sample was in the form of fragments of 0.5-3 mm in size. (A is AlF_3 , M is MgF_2 , C is CaF_2 , B is BaF_2 , S is SrF_2 , Y is YF_3) [5].

3.3.3.2 Equipment.

The schematic of conventional DTA equipment is shown in fig. 3.26. The equipment used here was a Perkin Elmer DTA 7 Analyser.

Sample and reference were placed side by side in matched crucibles and cups in a heating block which was heated at a constant rate; identical thermocouples were placed in each and are connected 'back to back'. As long as the sample and the reference were at a same temperature the thermocouple did not experience any net voltage. When a thermal event occurred in the sample a temperature difference, ΔT , existed between sample and reference which was detected by the net voltage of the thermocouple. A third thermocouple was present inside the apparatus to measure the temperature of the heating block.

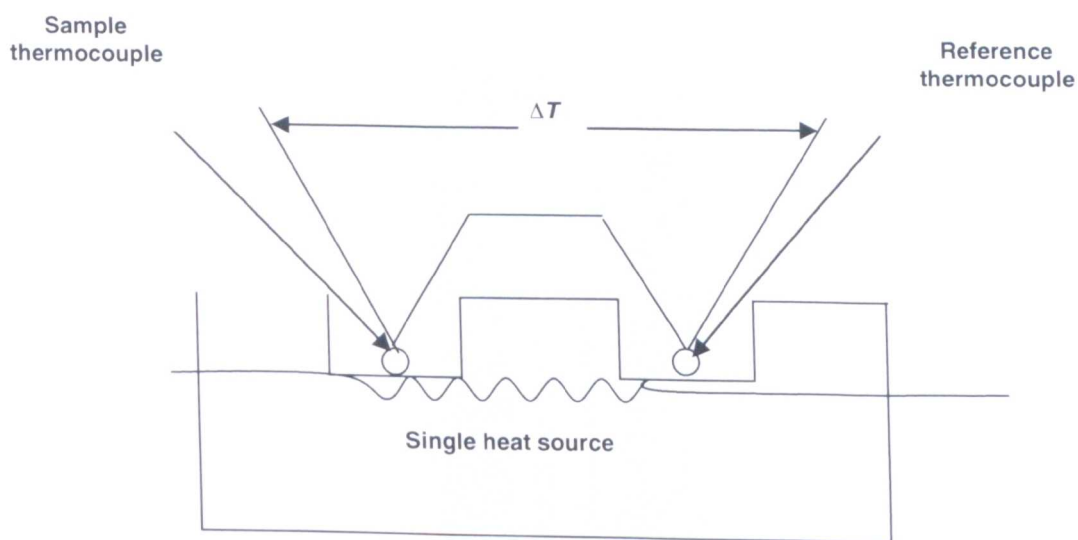


Fig. 3.26 Schematic of DTA equipment.

3.3.3.3 Sample preparation.

The chalcogenide glass sample obtained after annealing was broken into small pieces using a clean agate mortar and pestle. 50-80 mg of the pieces were weighed using a chemical balance (Sartorius, model BP221S accurate to $\pm 0.1\text{mg}$) in ambient conditions. The chalcogenide sample was sealed in an evacuated silica glass ampoule (Brambach, OD 4.7 mm, ID ~ 3 mm) as the sample was volatile. The reference DTA ampoule was prepared by evacuating and sealing an empty silica glass ampoule (Brambach, OD 4.7 mm, ID ~ 3 mm) having approximately the same mass as that of the ampoule used the sample. Fig. 3.27 shows the unsealed DTA ampoules, the sealed DTA ampoule with sample and the reference ampoule.

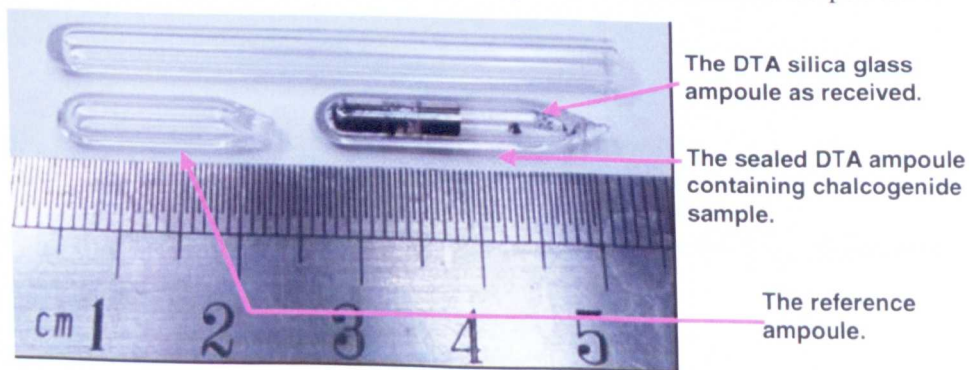


Fig. 3.27 The DTA silica glass ampoules used for characterisation of the chalcogenide sample for instance for determination of T_g .

To evacuate the DTA ampoules, a metallic part with a plastic tube was used. The DTA ampoules were attached to the plastic tube end with the help of a screw. The metallic end was attached to the Saunder's valve with the help of an 'O' ring. The small silica glass ampoule either containing the chalcogenide sample or empty, if it was the reference was then evacuated and sealed as described in section 3.1.1.3.

The arrangement of DTA ampoules inside the DTA machine is shown in photograph 3.28.



Fig. 3.28 The DTA silica glass ampoules (size indicated in fig. 3.27) containing the chalcogenide glass sample were supported in the DTA cups made of platinum inside the DTA head of the Perkin Elmer DTA 7 Analyser.

3.3.3.4 Procedure.

A baseline was first run with both the sample and the reference ampoules sealed and empty. The baseline run was subtracted from the raw DTA curve of the sample versus reference to remove the effect of any instrument artefacts unrelated to the specimen. DTA curves were obtained at a rate of $10^{\circ}\text{C}/\text{min}$ from room temperature to 800°C the maximum temperature depended on composition. All runs were carried out under in a flowing argon (BOC) atmosphere at the rate of $20\text{ ml}/\text{min}$ ($3 \times 10^{-4}\text{ dm}^3/\text{s}$). A baseline run was carried out once in a month during this project.

3.3.3.4 Data handling.

Data handling of the DTA results is discussed together with data handling of differential scanning calorimetry results in section 3.3.4.4.

3.3.4 Differential scanning calorimetry (DSC).

Differential scanning calorimetry (DSC) was used, in addition to DTA, to determine the T_g of chalcogenide samples. DSC is an alternative method to DTA but more quantitative.

3.3.4.1 Theory of operation.

The theory of operation in DSC is similar to the theory of operation of DTA, but allows more accurate knowledge of heat flow during a physical change of the sample. DSC measures the heat energy transferred to or from a sample at constant pressure usually ambient during a physical change. In DTA the change in temperature during the physical or a chemical change is detected by the net voltage of the back-to-back thermocouples detecting temperature of the sample and reference respectively. For DSC, the sample and the reference are maintained at the same temperature during heating and extra heat input or output, in the form of electrical power supplied, to the sample, required in order to maintain this balance, is measured. Enthalpy changes are therefore measured directly using DSC whereas DTA is designed for maximum sensitivity to thermal changes, but this is often at the expense of losing a calorimetric response; thus DTA peak areas are only qualitatively related to the magnitude of the enthalpy changes occurring. Hence, it is better to use DSC for T_g measurement since it should give a more accurate result. The layout of the sample and reference in the Perkin Elmer DSC Pyris 7 calorimeter used is shown in fig. 3.29.

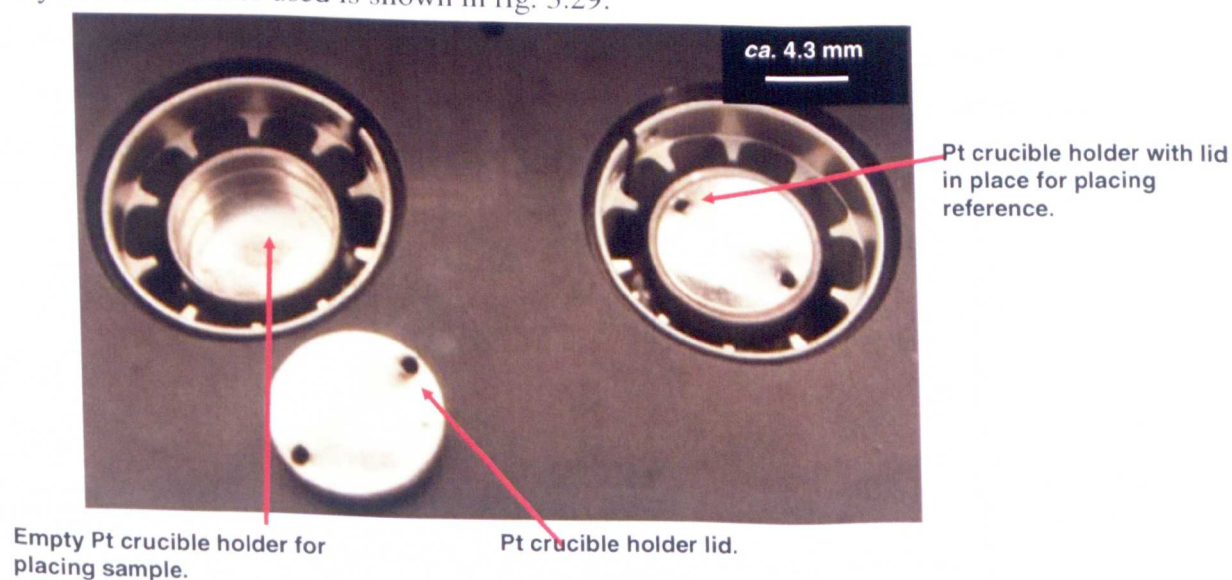


Fig. 3.29 Plan view of the Perkin Elmer DSC Pyris 7 head and sample and reference holder.

3.3.4.2 Sample preparation.

15 to 20 mg of the chalcogenide sample were weighed using a chemical balance (Sartorius, model BP221S accurate to ± 0.1 mg) into the DSC aluminium pan (Perkin Elmer) which was covered with an aluminum lid (Perkin-Elmer) using a Perkin Elmer DSC-pan press in order to

cold-seal the lid with the pan. The sample arrangement is shown in fig. 3.30. An identical, but empty, reference pan was also prepared.

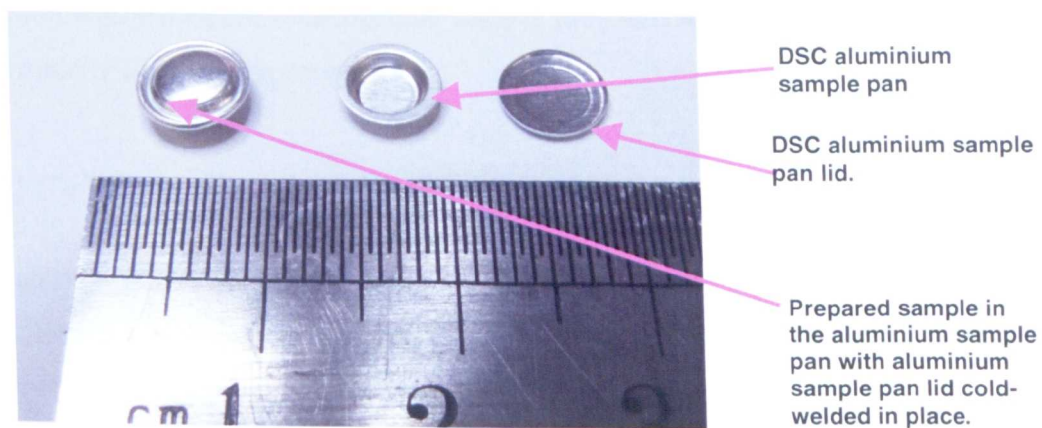


Fig 3.30 The DSC aluminium sample pan, sample lid and the pressed (ready to use) sample lid and pan with the chalcogenide sample inside.

3.3.4.3 Procedure and equipment.

A Perkin Elmer Pyris1 differential scanning calorimetry with water circulating chillers and argon gas flow at the rate of 20 ml/min ($3 \times 10^3 \text{ dm}^3 / \text{s}$), was used to measure T_g in this project. A baseline run was carried out before each experimental session and the resulting baseline curve was subtracted from each DSC sample curve afterwards.

3.3.4.4 Data handling.

The T_g of the chalcogenide sample was evaluated using Perkin Elmer software. The calculation for the onset of T_g was done by using the Perkin Elmer software to draw two tangents to the DSC curve: just before the T_g event and just after (fig. 3.31).

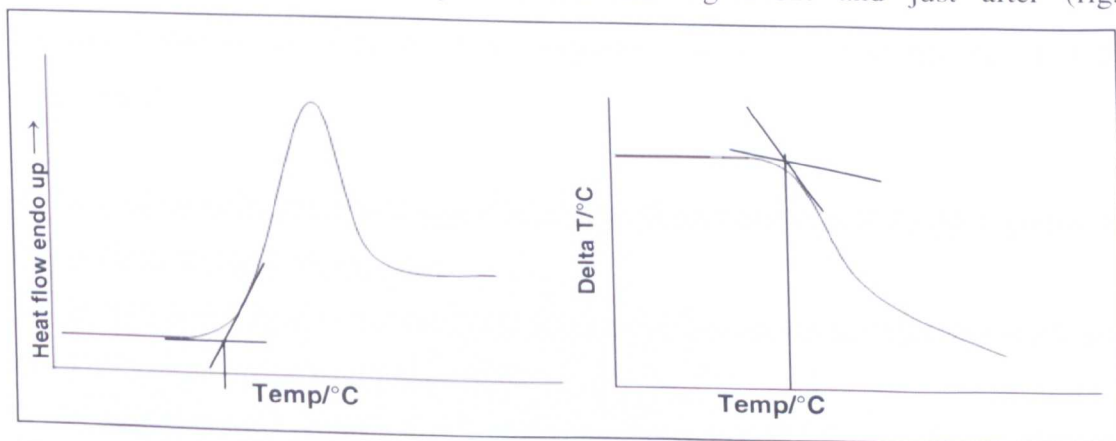


Fig. 3.31 Schematic of a DSC curve.

Fig. 3.32 Schematic of a DTA curve.

The onset T_g was recorded at the intersection of the two tangents. Fig 3.32 shows a DTA curve with the tangents evaluating T_g value.

3.3.5 Fourier transform infrared (FTIR) spectroscopy.

The optical transmission window of the chalcogenide sample prepared was determined using Fourier transform infrared (FTIR) spectroscopy.

3.3.5.1 Theory of operation.

For molecules with an overall electric dipole then the electric dipole moment changes when the atoms of the molecule are displaced relative to each other and this occurs when the molecule vibrates. Such atomic vibrations of a molecule have the capacity to resonate with electromagnetic radiation of the infrared region and hence are known as infrared active vibrations. This property of nature is the basis of infrared spectroscopy. The molecular structure of such resonator materials is therefore revealed when exposed to infrared radiation as material absorbs energy at the same frequency regions as the vibrational frequency of its constituents bonds. The net radiation is monitored during infrared spectroscopy. An important advantage of Fourier transform infrared spectroscopy is that all the radiation emitted by the source is monitored continuously. This is in contrast to conventional dispersive spectrometers where monochromators are used to filter the incident radiation and allow only a part of the radiation to fall on the sample. Thus FTIR is more sensitive than conventional spectrometers. The data are subjected to a Fourier transform when a conventional spectrum is obtained.

3.3.5.2 Equipment.

The basic construction of an FTIR spectrometer is as follows with the main following five components:

1. Source of radiation – a source of electromagnetic radiation with the required frequency that is illuminated on the sample.
2. Sampling component – a device to direct the electromagnetic radiation to the sample and from the sample to the instrument.
3. Signal detector – an optoelectronic device that changes light to a voltage or a current.
4. A computer – used for the acquisition and analysis of data.

Here a Bruker IF 66 FTIR instrument was used. The source of radiation, beam splitter and the detector used during this project for the measurement of the transmission window of the sample across the full IR spectrum are given in Table 3.7.

Table 3.7 Set of light source, beam splitter and detectors used for the FTIR measurement of transmission window for chalcogenide materials prepared during this project.

Category	Type	Wavelength range/ μm	Spectrum	Supplier
Source	Tungsten lamp	0.3-3.3	Visible-NIR	Bruker
	Glow bar	3.3-100	NIR-IR	
Beam splitter	CaF ₂	0.2 – 6	Visible-MIR	Bruker
	CaF ₂ (NIR)	0.9 – 6	NIR-MIR	
	KBr	1.3 – 27	NIR-IR	
Detector	GaP	0.3 -0.55	Visible	Bruker/Judson
	Si	0.4 -1	Visible-NIR	
	InGsAs	0.8-1.7	NIR	
	InSb	0.9-5.4	NIR-MIR	
	DTGS	0.8-27	NIR-MIR	

Key: NIR is near-infrared; MIR is mid-infrared; DTGS is Deuterated triglycine sulphate.

3.3.5.3 Sample preparation.

For bulk optical transmission measurement, a sample of about 2 mm to 3 mm optical path length was cut and polished. The procedure for cutting and polishing of chalcogenide products is discussed in section 3.2.1 (g) and (h) respectively.

3.3.5.4 Procedure.

The FTIR spectrometer was purged for ten minutes with dry air (Parker Filtration, FT-IT purge gas generator, 75-52-12VDC) to remove carbon dioxide and water from the system. Carbon dioxide absorbs at around 4.4 μm and water at $\sim 2.7 \mu\text{m}$ and $\sim 6.3 \mu\text{m}$ in the transparent window of the chalcogenide glasses and were therefore removed from the atmosphere. A background spectrum was taken using the chosen sample holder aperture (3 mm diameter). The sample was fixed in place over the aperture, orthogonal to the beam, using Plasticine©. The sample holder with the sample was inserted in the FTIR chamber which was again purged with dry air to remove carbon dioxide and water vapour before collecting the spectrum.

3.3.5.5 Data handling.

Bruker software was used to remove the background (*e.g.* the contribution to absorbance from the local purged atmosphere) from the sample spectrum. Next, spectra were divided through by path length expressed as cm to give the vertical axis as absorption coefficient. It should be noted that this meant that the baseline absorption had no meaning.

To get an absorption coefficient for a particular absorption band, the absorption/cm just before and just after the band was measured and the average of these taken (A_{av}). Next the

peak absorption/cm of the band was noted (A_{peak}). The absorption coefficient for a particular absorption band was taken as ($A_{\text{peak}} - A_{\text{av}}$).

3.3.6 Field emission gun environmental scanning electron microscopy (FEG ESEM) with energy dispersive X-ray analysis (EDX).

The stoichiometry of the chalcogenide sample was determined by means of energy dispersive X-ray analysis (EDS) of the sample using field emission gun environmental scanning electron microscope (FEG ESEM). It is believed that a typical homogenous sample should have approximately 0.4 standard deviation in the stoichiometry of the different parts of the sample.

3.3.6.1 Theory of operation.

A high energy beam of electrons, produced within an environmental scanning electron microscope, is focused into the sample being studied. Here a beam of electrons was used. The incident beam excites an electron in an inner shell, ejecting it from the shell while creating a vacant energy level in the atom. An electron from a higher-energy shell then fills the vacant energy level, and the difference in energy between the higher-energy shell and the lower energy shell is released in the form of an X-ray. These X-rays are characteristic of the difference in energy between the two shells, and of the atomic structure of the element from which they were emitted.

3.3.6.2 Equipment.

ESEM consists of an electron gun, situated at the top of an electron column that generates an electron beam. A series of magnetic lenses and apertures converge the electron beam. The converged electron beam is accelerated towards the sample. In ESEM the sample chamber is separated from the electron source chamber. In this project the FEI XL30, FEG-ESEM ESEM was used and the sample chamber was filled with nitrogen gas, though the electron chamber was still in the high vacuum mode. The EDX analysis was performed with at 15 kV operating voltage (and hence electrons having 15 keV of energy) and 10 mm working distance and data were obtained in auxiliary mode.

3.3.6.3 Sample preparation.

A few chunks of the chalcogenide glass or a chalcogenide glass sample (broken from a melt boule using an agate pestle and mortar) was placed on a carbon coated sticky tab stuck on to an aluminium disc. The sample was cleaned with acetone (Fischer, 99.99%) and air dried. It

was then cleaned using an air blower. The chalcogenide glass sample was not coated with any conducting material, such as gold.

3.3.6.4 Procedure.

The EDX analysis of the samples was kindly done by Dr. Nigel Neate and Mrs. Nikky Weston (Technicians in the Department of Mechanical, Materials and Manufacturing Engineering). The beam of electrons was focused randomly onto the different parts of the surface of the sample. Samples having defects were studied by focusing the beam at the point of the defect to detect if any impurity was present. The diameter of the electron beam was $\sim 10 \mu\text{m}$. The electron penetration depth was $\sim 1 \mu\text{m}$ to $\sim 2 \mu\text{m}$. A typical EDX spectrum of germanium arsenic selenide is shown in fig. 3.33.

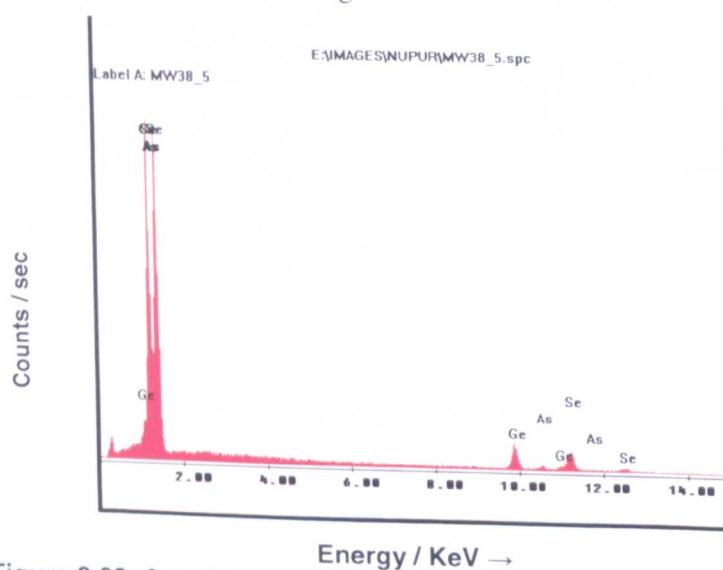


Figure 3.33 A typical EDX spectrum of germanium arsenic selenide.

3.4 Further processing of chalcogenide glasses made by microwave heating for photonic applications.

Chalcogenide glasses successfully made through microwave heating were processed further in two different ways for photonic applications: one glass sample was drawn to fibre and another was hot embossed. The fibre drawing process is discussed in section 3.5.1 and the hot embossing process is discussed in section 3.5.2.

3.4.1 Fibre drawing.

An in-house Heathway fibre drawing tower modified by Dr. David Furniss was used for this purpose (fig. 3.34).

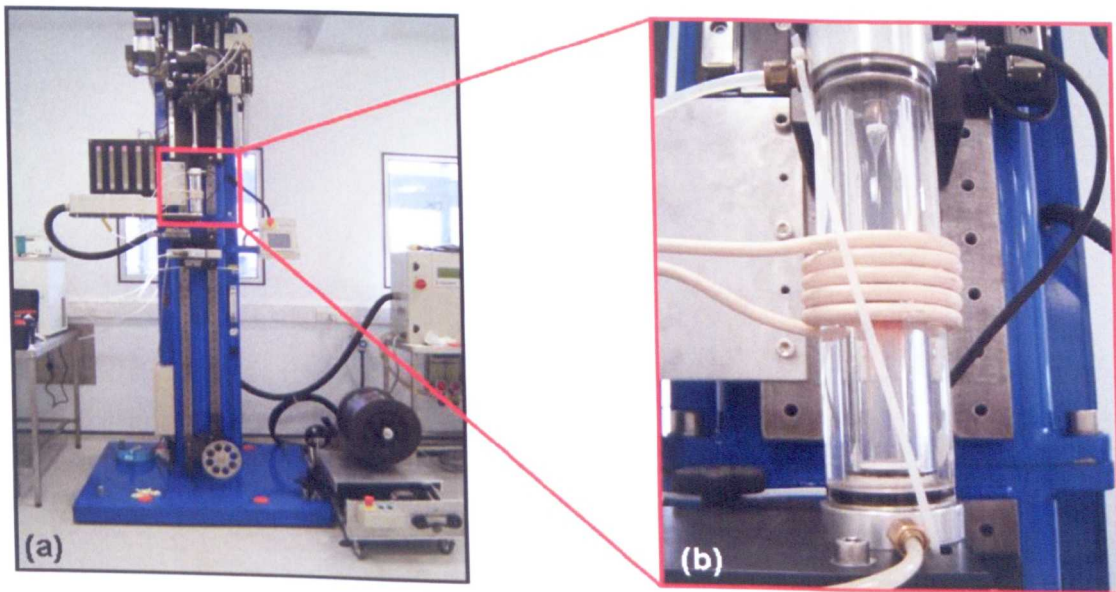


Fig 3.34 (a) The fibre drawing tower (~ 3 m tall) and (b) the new in-house customised radio frequency fibre drawing furnace (~ 0.2m vertical dimension).

The tower was kept in a class 10,000 clean room under controlled temperature and humidity. The chalcogenide glass preform was supported above of the fibre drawing furnace, clamped to the feeding rod. The bottom of the preform was kept a few mm below the carbon ring susceptor. The carbon ring was held within a silica glass enclosure, through which was passed nitrogen gas (BOC 'white spot') and heated by radio frequency waves supplied by a copper coil. As soon as the chalcogenide glass within the carbon ring became soft, a drop of chalcogenide glass fell down through the system, drawing chalcogenide glass fibre behind it. The fibre was immediately passed around a tensioning wheel vertically below the furnace and then wound on a drum by means of a fibre winder (designed and built in-house by Dr David Furniss). The drum was rotated about horizontal axis so that the chalcogenide glass fibre wound on it. The preform feed-in speed and the speed of the drum rotation could be controlled and were used to calculate the diameter of the fibre. The following equation was used:

$$V_{in} \times (D/2)^2 = V_{out} \times (R/2)^2 \quad (\text{eqn. 3.7})$$

Where, V_{in} = preform feed-in speed, V_{out} = drum rotating speed, D = diameter of the preform, R = calculated diameter of the fibre. The fibre diameter was monitored (Beta laser monitor).

3.4.2 Vacuum pressing.

Vacuum pressing equipment made in-house by Dr. David Furniss was used for trial embossing of DMO-prepared chalcogenide glasses. The vacuum pressing equipment is shown schematically in figure 3.29.

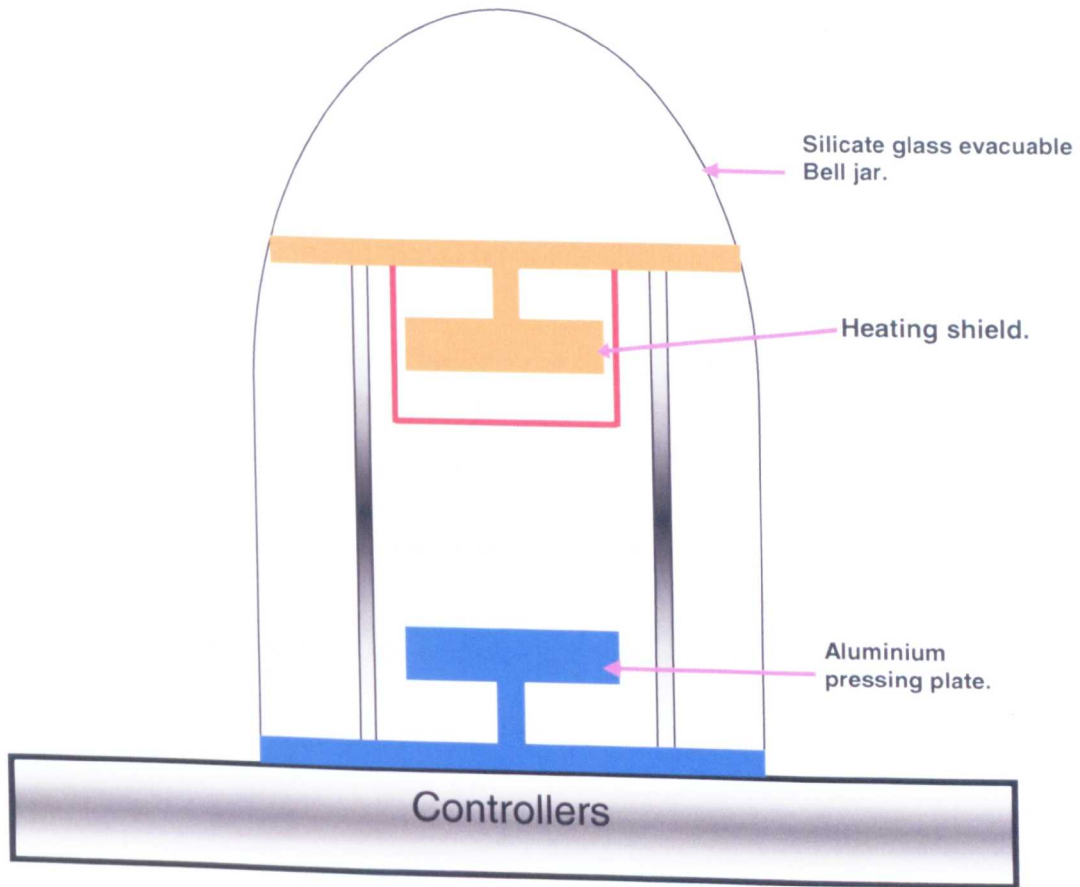


Fig. 3.35 Schematic diagram (not to scale) of vacuum pressing equipment used for trial embossing of DMO-prepared chalcogenide glasses.

The lower aluminium plate, as shown in fig. 3.29, was cleaned with acetone (Fischer, 99%) and allowed to dry in ambient conditions. A silicon wafer mould (supplied by Professor Catrina Bryce, Optoelectronics Research Group, Department of Electronics and Electrical Engineering, The University of Glasgow) was placed on top of the lower Al plate and with the mould surface uppermost. The polished chalcogenide glass sample was placed on top of the silicon wafer mould. The lower aluminium plate could be moved upwards with a controlled speed and the upper aluminium plate was fixed. The two aluminium-plates were heated at the same rate and to the same temperature, heating also the chalcogenide glass sample. The chalcogenide glass sample was kept at $\geq T_g$ for about 30 minutes. Moulding could be carried out $\geq T_g$ where the supercooled chalcogenide liquid exhibits viscous flow on application of pressure. The lower plate was raised at a controlled rate and was allowed to touch the upper plate. The sample was then pressed against the mould. The lower plate was

kept stationary during the process of pressing in order to maintain constant applied pressure. The pressing process was carried for about 1 minute under a controlled load. At the end of the pressing process the lower plate was moved downwards and the chalcogenide glass was cooled to room temperature by adjusting the heat flow to the aluminium plates. The whole process was done under vacuum (10^{-4} mbar ($\sim 10^{-2}$ Pa) achieved by rotary pump (Edward/ 2 Stage, GEC machines, AC motor, BS 5000-11, Type BS 2212) and diffusion pump (PFEIFFER, D35614, Asslar, Vacuum Emmeliusstr. 33 / Mod. Nr. PM 201 280).

References:

- [1] F.A. Cotton and G. Wilkinson, *Advanced inorganic chemistry*, A Wiley Interscience Publication, 5th edition, New York, (1976).
- [2] N.N. Greenwood and A. Earnshaw, *Chemistry of the elements*. Butterworth-Heinemann, Linacre House, Jordan Hill, 2nd edition, Oxford., (1997).
- [3] D. Lezal, *J. Optoelect. & Adv. Mat* **5** (2003), p. 23.
- [4] A.R. West, *Basic solid state chemistry*, John Wiley and Sons, 2nd edition, England, (1999).
- [5] A.B. Seddon, Teaching Handout, for course: High Performance Ceramics and Glasses, 2008.

Chapter 4

Microwave assisted synthesis of arsenic sulfide.

The synthesis of arsenic sulfide glass through microwave heating using a domestic microwave oven (DMO) was investigated. In order to compare the properties of arsenic sulfide made in the domestic microwave oven (hereafter called 'DMO arsenic sulfide') arsenic sulfide glass was independently prepared using a resistance furnace (hereafter named 'arsenic sulfide made through conventional heating'). The prepared samples were cut, polished and characterised as described in chapter 3. The results obtained from the microwave assisted synthesis of chalcogenide glass are reported and discussed in section 4.1 whereas the results obtained from conventional melting are presented in section 4.2. A comparison of results obtained using FTIR are further discussed in section 4.3. The ESEM results which established the stoichiometry of the products is described in section 4.4. The irreproducibility of the reaction in the DMO is discussed in section 4.5. Chapter 4 is summarised in section 4.6.

4.1 Microwave irradiation of arsenic and sulfur.

To determine the optimum reaction conditions for microwave heating of arsenic and sulfur, several experiments were carried out in an attempt to make As_2S_3 glass. These, and the results obtained, are discussed in the following subsections 4.1.1 to 4.1.6. (It should be noted here that original attempts to make DMO arsenic sulfide using As (99.99999%, Furukawa, chunks 2 to 8 mm) were unsuccessful and the reason for this is unclear at present.)

4.1.1 Microwave irradiation of arsenic pellets of diameter *ca.* 4 mm to 7 mm with sulfur flakes in atomic ratio As_2S_3 (id: MW(I)).

Eight As pellets (1.2 g, 99.999 %, All Chemie Ltd. (amorphous)) of diameter *ca.* 4 mm to 7 mm (size range was deliberately selected from the bottle) were added to sulfur flakes (0.78 g, 99.99 + %, Aldrich) in atomic ratio As_2S_3 in a silica glass ampoule (see section 3.1.2.1.1). The ampoule was sealed under vacuum (*ca.* 4×10^{-2} Pa) achieved using a rotary pump and then diffusion pump (see section 3.1.1.3) using an oxy propane flame (see section 3.1.1.3). The batch, sealed in the silica ampoule, was then subjected to microwave irradiation under vacuum for 35 minutes at 440 W using a domestic microwave oven (DMO, DeLonghi/M8021P-B1). A blue flash (once) was observed during the heating. The ampoule

was taken out from the DMO and cooled in air. From the appearance it seemed that chalcogenide glass had not formed. The same ampoule was placed again inside the DMO and heated for another 35 minutes at 440 W; blue flashes were observed at regular intervals of 45 to 60 seconds for the first 15 minutes. The blue flashes stopped after 15 minutes of microwave irradiation. After 35 minutes the ampoule was taken out of the DMO and cooled in air. It was observed that the reactants had not melted completely to give a glass-melt. An orange-red mass was obtained. From visual inspection it appeared that the chalcogenide glass had not formed as the product was not glossy. The sulfur had melted to a certain extent suggesting that arsenic had coupled with the microwaves and the mechanism of interfacial polarisation had taken place which resulted in the heating and melting of sulfur. Moreover, several short periods of blue glow were observed suggesting that the reactants had coupled with the microwaves but glass could not be formed.

4.1.2 Microwave irradiation of arsenic pellets with diameter < 2 mm with powdered sulfur in atomic ratio As_2S_3 (id: MW6).

In the next attempt to synthesise As_2S_3 glass through microwave heating, it was decided to take reactant particles of smaller size than those of the above subsection 4.1.1 to give greater surface area of reaction. As (1.521 g, 99.999 %, All Chemie Ltd. (amorphous)) particles of diameter < 2 mm (size range was deliberately selected from the bottle) were weighed and then mixed with powdered sulfur (0.9866 g, 99.99 + %, Aldrich). Sulfur flakes were powdered using a clean, agate mortar and pestle. The above stated chemicals in atomic ratio As_2S_3 were placed in a silica glass ampoule (see section 3.1.2.1.1) which was sealed under vacuum (*ca.* 2.3×10^{-2} Pa) achieved using a rotary pump and then diffusion pump (see section 3.1.1.3) using an oxy propane flame (see section 3.1.1.3). The mixed reactants were then irradiated with microwaves under vacuum, using the same DMO equipment as reported in section 4.1.1, for 35 minutes at the higher power of 800 W. A few blue flashes were observed during the heating. The melt was air quenched. A yellow liquid was observed that became reddish yellow on cooling and the melt solidified into a reddish, brown glassy substance. On cooling, the product was observed to be inhomogeneous with four distinct portions (fig. 4.1). The physical state of the product can be described as follows:

- A. the lower most part was deep-red, transparent and glassy as shown in portion 'A' of fig. 4.1;
- B. above the portion 'A' a few glassy pellets of diameter 1 mm to 2 mm were observed as shown in portion 'B' of fig. 4.1;
- C. above the portion 'B' an orange friable mass was observed as shown in portion 'C' of fig. 4.1 and

D. the uppermost layer was composed of orange friable bits and is shown as portion 'D' of fig. 4.1.

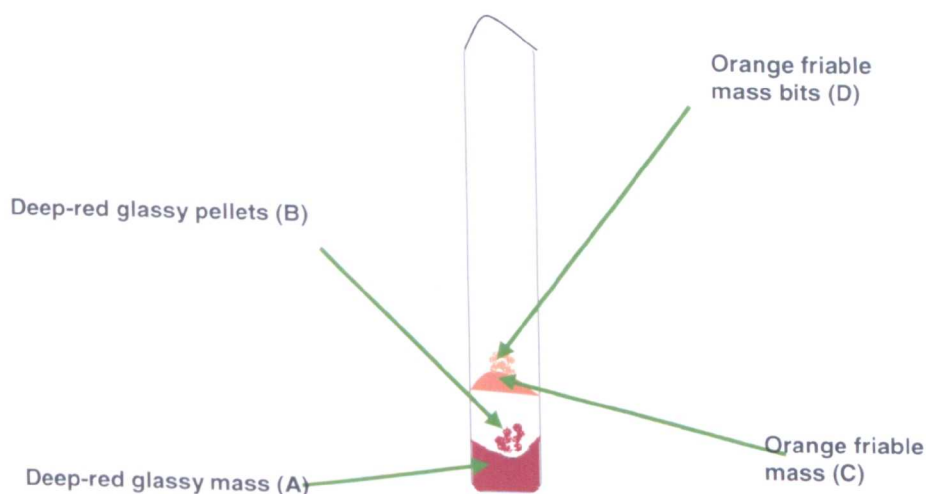


Fig. 4.1 A schematic diagram of the inhomogeneous product (id: MW6) after microwave irradiation (see section 4.1.2) of arsenic (> 2 mm diameter small pieces) and sulfur (powder). The diagram is not to scale.

4.1.3 XRD and TEM SAED of the unannealed deep-red, glass mass (portion 'A' of id: MW6 (fig. 4.1)) and orange friable bits (portion 'D' of id: MW6 (fig. 4.1)).

A small chunk of the deep-red glassy mass (portion 'A' of id: MW6, fig. 4.1) was powdered using a clean agate mortar and pestle (Fischer) and subjected to powder X-ray diffraction (XRD).

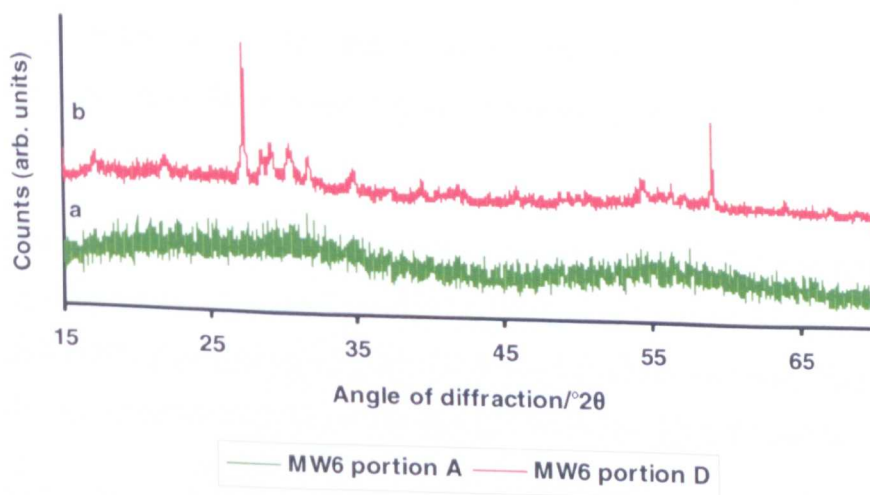


Figure 4.2

- (a) XRD pattern of the as-quenched, unannealed portion 'A' of the As-S product prepared in the domestic microwave oven (DMO) (see Fig. 4.1). Data multiplied by a factor of 12.
- (b) XRD pattern of as-quenched, unannealed portion 'D' of the As-S product prepared in the domestic microwave oven (DMO) (see Fig. 4.1). Data multiplied by a factor of 4.

The amorphous halo obtained in the XRD pattern can be seen in fig. 4.2 (a) showing that a glass had formed. Crystalline peaks were not present in the XRD pattern of the deep red glassy mass (portion 'A' of id: MW6, (fig. 4.1a)). A few sharp peaks were observed in the

XRD pattern (fig. 4.2b) of the upper friable orange mass (portion 'D' of id: MW6, fig. 4.1). The crystalline peaks shown in fig. 4.2b matched slightly with crystalline AsS, As₂S₅ and Al (which could have come from aluminium holder) according to XRD Evaluation software, as shown in Table 4.1.

Table 4.1 Comparison of the XRD pattern of portion 'D' of id: MW6 (fig. 4.1) with those of AsS, As₂S₅ and Al.

Portion 'D'		AsS [1]		As ₂ S ₅ [2]		Al [3]	
2θ	I / %	2θ	I / %	2θ	I / %	2θ	I / %
27.31	100.0	27.94	25.2				
36.80	16.0			36.4	17.11		
				36.10	14.0		
38.47	14.00					38.47	12.5
56.50	15.5			55.81	19.22		
65.09	45.00					65.09	10.58

Since the DMO heating is not homogeneous it is supposed that some of the sulfur evaporated from the lower part of the ampoule and deposited on the upper and slightly colder part of the ampoule forming crystals of aggregated sulfur. The colour of the upper friable mass (portion 'D' of id: MW6 (fig. 4.1)) was more yellowish than the lower part portion 'C' of fig 4.1, suggesting the deposition of sulfur.

Further work was carried out to check the amorphous nature of the product id: MW6. The portions 'A' and 'D' were each subjected to selected area electron diffraction (SAED) using transmission electron microscopy (TEM). Fig. A-1 [Appendix A] shows the TEM SAED for portion 'A' of id: MW6, of fig. 4.1, and it can be seen that there is an absence of sharp diffraction rings confirming the amorphicity and supporting the XRD pattern of portion 'A' (fig. 4.2a).

The upper friable orange mass that is portion 'D' (id: MW6) of fig. 4.1 was also subjected to TEM SAED. Diffuse rings were obtained (fig. A-2, [Appendix A]) showing that portion 'D' exhibited slightly more structuring than portion 'A' for id: MW6 (compare figs. A-1 and A-2 of Appendix A), again supporting the results from XRD (figs 4.2a and 4.2b, respectively).

4.1.4 Differential thermal analysis (DTA) of the unannealed deep red glassy mass (portion 'A' of id: MW6 (fig. 4.1)).

DTA analysis (see section 3.3.3) of the as-prepared chunk portion 'A' id: MW6 (fig. 4.1) before it was annealed indicated at least three glass transition temperatures (T_g) of extrapolated onset temperature 166°C, ~194°C (broad) and 300°C in the first run (note that the T_g observed at ~166°C might be a noise very small (see fig. 4.3a)) suggesting that the

sample was inhomogeneous and consisted of more than one glass composition. During the first DTA run the sample temperature was raised to 600°C before cooling. The cooling rate was not controlled and was achieved by switching of the DTA equipment and allowing it to cool naturally with the DTA sample still inside the DTA head. The sample was then rerun in the DTA equipment

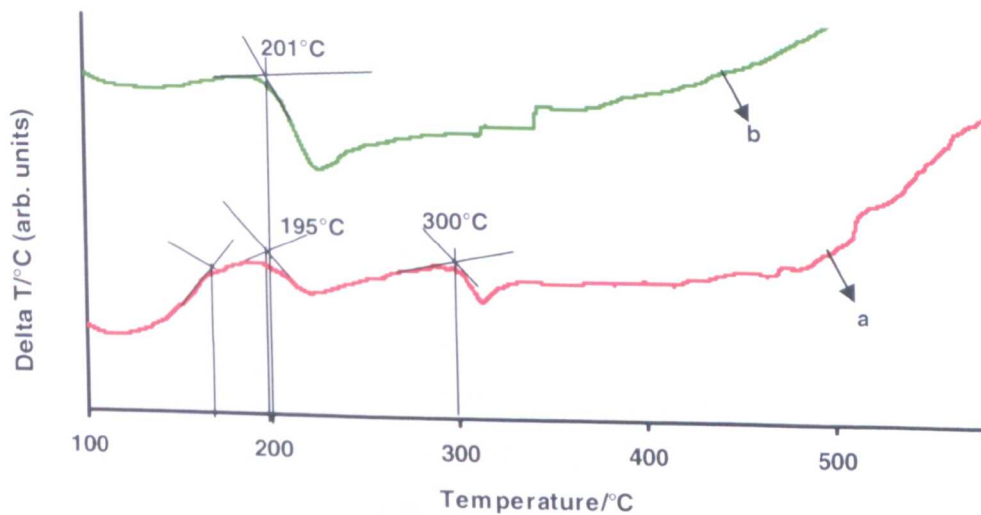


Figure 4.3

- (a) Differential thermal analysis (DTA) curve of the as-quenched, unannealed portion 'A' of the As-S product prepared in the domestic microwave oven (DMO) (see Fig. 1).
- (b) Re-run of DTA curve of portion 'A' of the As-S product prepared in the DMO (see Fig. 1) after it had undergone: (i) the DTA run shown in (a); (ii) continued heating inside the DTA equipment to above the liquidus of As_2S_3 ; (iii) cooling to 100°C *in situ* inside the DTA equipment.

under the same DTA conditions as the first run. A single Tg was observed of extrapolated onset $202^\circ\text{C} \pm 5^\circ\text{C}$ in the second DTA run (fig. 4.3b). (The error on the measurement is an estimate, given the typical error found for repeat DTA measurements of Tg of other glasses in later work (see chapter 5)).

As-S has a wide glass-forming composition range and the ampoule containing the precursors was not rocked during the microwave-assisted synthesis. Hence it is concluded that the 'A' portion of the product id: MW6 as-prepared was inhomogeneous consisting of three or more glasses. The multiple Tg events were at extrapolated onset temperatures of 166°C , $\sim 194^\circ\text{C}$ and 300°C . Others have observed the Tg of As-S glasses to range from 34°C for $\text{As}_{0.11}\text{S}_{0.89}$ to 205°C for $\text{As}_{0.4}\text{S}_{0.6}$ (atomic fractions) [4, 5]. The variation of glass transition temperature of As_2S_3 with change in stoichiometry of the composition is given in Table 4.2 [4, 5].

Table 4.2 Variation of T_g of As_xS_{1-x} glass with change in stoichiometry [4, 5].

Composition for As _x S _{1-x} samples	T _g /°C
x = 0.11 ± 0.01	34 ± 5
x = 0.19 ± 0.01	85 ± 5
x = 0.33 ± 0.01	160 ± 5
x = 0.40 ± 0.01	205 ± 5

From Table 4.2 it is concluded that the three T_gs observed at 166°C, ~194°C and 300°C for the as-prepared portion 'A' of id: MW6 corresponded to glasses of As / S stoichiometries of ~ As_{0.33}S_{0.67}, As_{0.38}S_{0.62} and As_{>>0.4}S_{<<0.6}, respectively. Hence there will have been some sulfur-rich regions compared to the ideal As_{0.4}S_{0.6} glass and some sulfur-deficient regions in the glassy 'A' portion of id: MW6.

For the observed DTA T_g of 202°C, of the second DTA run, then the calculated liquidus (T_L) of the sample was, according to the "2 / 3 Rule" (*i.e.* [(T_g / K) + (T_L / K)] = 2/3), 440°C [6]. During the first DTA run, portion 'A' id: MW6 was heated to a maximum temperature of ~ 600°C before cooling at the end of the run. Therefore, prior to the second DTA run, the inhomogeneous liquid portion 'A' had an opportunity to homogenise above the liquidus, during the first DTA run inside the sealed DTA silica glass ampoule, and this accounts for the single T_g event observed during the second DTA run. The single T_g of 202°C ± 5°C was close to that expected for As₂S₃ id: MW6 of 205°C [4, 5], indicating that the microwave synthesised glass, after it had been homogenised above the liquidus, was close to the desired stoichiometry. This point is taken up later when ESEM EDX is used to quantify the homogeneity of this sample (see 4.4.2).

It is supposed that since in the DMO the silica ampoule was not rocked the reactants were not heated uniformly and not mixed therefore an inhomogeneous glass was formed. This is in contrast to the interpretation of Sivakumaran *et. al.* [7] who suggested liquid-liquid phase separation was occurring during the preparation of their DMO Se-Te-Sb glass products leading to their observed double T_g. Sivakumaran *et. al.* [7] attempted some crude mixing during the DMO synthesis removing the ampoule containing the melt and manually shaking it before replacing it back in the DMO for further microwave irradiation. However, this may not have been sufficient to homogenise fully the liquid compared to several hours of rocking during conventional melting.

4.1.5 Annealing of the deep red glassy mass (portion 'A' of id: MW6 (fig 4.1)).

The deep red glassy mass (portion 'A' of id: MW6 (fig 4.1)) was washed with acetone (Fisher, 99.9 %) and wiped with clean filter paper. To release any stress the deep red glassy mass

(portion 'A' of fig. 4.1) was then annealed. The sample was re-sealed under vacuum into a fresh silica glass ampoule and then reheated slowly ($20^{\circ}\text{C}/\text{h}$) to $T_g + 10^{\circ}\text{C}$. The ampoule and contents were held isothermally for 1 h and then cooled at $5^{\circ}\text{C}/\text{h}$ to $T_g - 40^{\circ}\text{C}$, and then finally cooled down to room temperature at $20^{\circ}\text{C}/\text{h}$. For this exercise T_g was taken as the measured DTA T_g of 202°C (see fig. 4.3b).

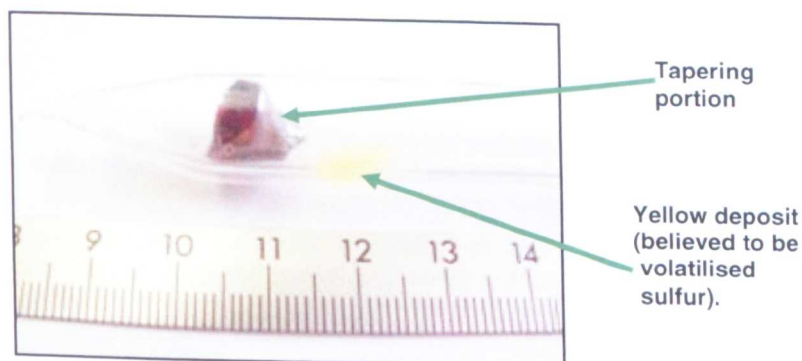


Fig. 4.4 The as-prepared glassy mass (portion 'A' of id: MW6 (fig. 4.1)) after annealing at 212°C .

A yellow deposit could be observed just above the sample on the inner surface of the silica glass ampoule after annealing. It is believed that sulfur had partially volatilised, probably from inhomogeneous sulfur-rich regions, during the annealing process and was deposited on the inner surface of the silica ampoule. Unlike the heat treatment above the liquidus during the first DTA run (fig. 4.3a), here during annealing of the bulk portion 'A', of id: MW6, there was no opportunity for homogenisation because the viscosity of the melt at $\sim T_g$ is high ($\sim 10^{12.5}$ Pa s) and the time spent at the annealing temperature was insufficient for homogenisation to take place.

4.1.6 X-ray diffractometry (XRD) and optical microscopy of the deep red glassy mass (portion 'A' of id: MW6 (fig. 4.1)) annealed at 212°C .

The tapering portion of the annealed deep red glassy mass (portion 'A' of id: MW6) as shown in fig 4.4 was cut to obtain a flat surface of the glass and the remaining part (the small conical portion of the sample) was powdered and subjected to powder XRD. The amorphous halo obtained in the XRD pattern (fig. 4.5) showed that a glass had been formed during the original DMO synthesis. However, some small XRD peaks appeared to be present (Table 4.3) at $31.73^{\circ}2\theta$, $38.42^{\circ}2\theta$, $64.95^{\circ}2\theta$, and $78.22^{\circ}2\theta$. The small peaks present in the XRD pattern (fig. 4.5) suggest that, at the very least, embryos of crystals, possibly of stoichiometry As_2S_5 [2] or aluminium [3] (from the sample holder), had been formed during the annealing at 212°C .

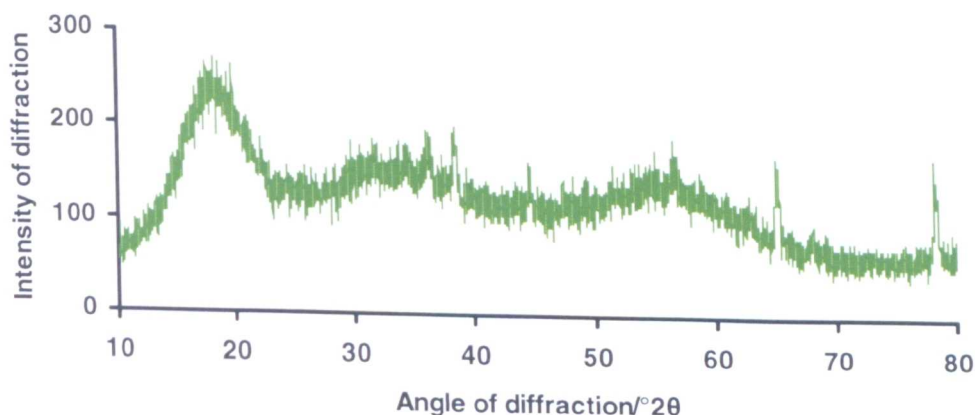


Fig. 4.5 X-ray diffraction pattern of conical part of the arsenic sulfide portion 'A' (id: MW6) deep red glassy mass after annealing at 212°C (as shown in fig. 4.4).

Table 4.3 Comparison of observed XRD peaks after annealing at 212°C of the conical part of the portion 'A' (id: MW6) deep red glassy mass of arsenic sulfide shown in fig 4.4.

Observed		As ₂ S ₅ [2]		Al [3]	
θ /°2θ	I / %	θ /°2θ	I / %	θ /°2θ	I / %
31.7	40.0				
36.4	44.4	36.3	44.0		
		36.1	40.0		
38.5	66.7			38.5	66.0
56.5	55.5	55.8	50.0		
65.1	80.0			65.1	88.9
78.2	100.0			78.3	80.0

It is important to note that the glassy portion 'A' of id: MW6 *after* annealing (fig. 4.4) was then safe to cut and polish to make a specimen suitable for transmission optical microscopy (see section 3.2.1 (g & h)). This showed clearly that that the glass was inhomogeneous. Fig. 4.6 shows a defect of the order 1 mm long. The non-unique T_g (fig. 4.3a) further supported the fact that the arsenic sulfide portion 'A' (id: MW6) prepared in the DMO (section 4.1.2), although glassy, was inhomogeneous. The wing-like structure visible in fig. 4.6 (arrowed) was surmised to be unreacted amorphous arsenic since under the optical microscope the colour of the wing structure was grey and had a slight metallic lustre.

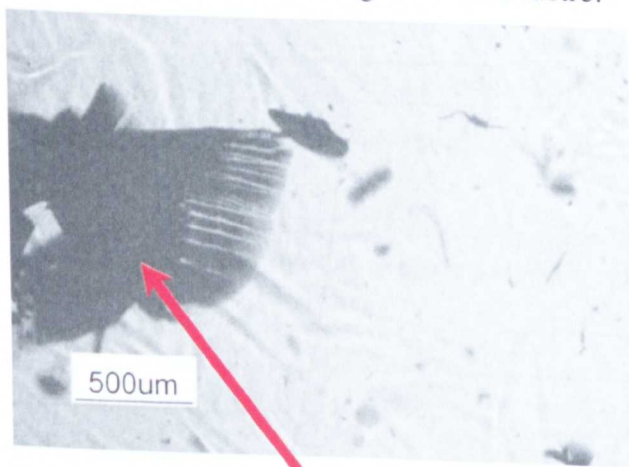


Fig. 4.6 Transmission optical microscopy of the arsenic sulfide made *via* microwave assisted synthesis (portion 'A' of id: MW6) (fig. 4.1). A defect proposed to be unreacted arsenic is arrowed.

Because the arsenic precursor was amorphous (see Table 3.2), it would not be expected to give rise to sharp XRD peaks.

4.2 Synthesis of arsenic sulfide glass *via* resistance heating.

The properties of arsenic sulfide made *via* microwave heating were compared with those of the arsenic sulfide made *via* resistance heating. The latter procedure was carried out as follows: arsenic (6.105 g, 99.9999 %, All Chemie Ltd. (amorphous)) and sulfur flakes (Testbourne Ltd., 99.999 %, 3.9405 g) taken in atomic ratio As_2S_3 were used without further purification. Arsenic was selected from the bottle, by shaking the bottle, to be less than 0.2 mm diameter particles. Sulphur flakes were crushed to powder using a clean, agate mortar and pestle inside the glove box (see section 3.1.1.3). A silica glass ampoule was rinsed with distilled water and oven dried at 70°C for six hours in the class-10,000 clean room (see section 3.1.1.1). The batch was weighed into the ampoule which was evacuated to 2.3 Pa and sealed (see section 3.1.1.3). The reactants were melted in the resistance rocking furnace (see section 3.1.1.4) according to the melting schedule shown in Table 4.4 to make several products named here 'conventionally prepared arsenic sulfide', id: CF 074 and CH25. In the early stage of the project the sample ids for the conventionally melted samples were assigned with 'CF' tag as this tag ('CF') was used in our research group and hence the naming was simply inherited from there. Note that CF074 was the first conventionally melted glass for this project. But in the later stage of the project the sample ids were tagged with 'CH' for this project as could be seen here for the sample id CH25.

Table 4.4 Melting schedule of the conventionally prepared arsenic sulfide batched as As_2S_3 (atomic ratio) id: CF 074.

Stage	Schedule
1	20°C to 90°C @ 70°C/hr
2	90°C to 650°C @ 30°C/hr
3	Dwell at 650°C for 12 hrs.
4	650°C to 570°C @ 60°C/hr
5	Hold 570°C until quench.
6	Quench ampoule in boiling water for ~30 s

The glass melt was quenched in boiling water for about 30 seconds. It was then annealed according to the schedule shown in Table 4.5.

Table 4.5 Annealing schedule of the conventionally prepared arsenic sulfide batched as As_2Se_3 , id: CF 074.

Stage	Schedule
1	200°C for 1 h
2	200°C to 150°C @ 5°C / h
3	150°C to 20°C @ 20°C / h

Fig. 4.7 shows a photograph of the typical annealed arsenic sulfide made *via* conventional heating.

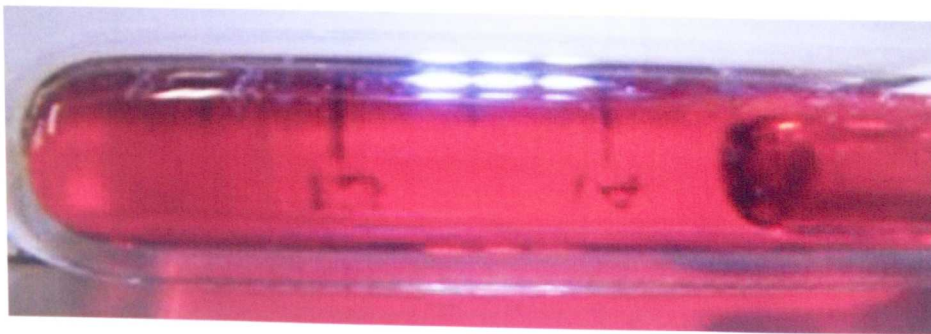


Fig 4.7 Photograph of the conventionally prepared arsenic sulfide batched as As_2S_3 (atomic ratio) id: CF 074.

4.2.1 The amorphicity of the arsenic sulfide prepared by conventional heating, id: CF 074.

The amorphicity of the arsenic sulfide product id: CF 074, prepared by conventional heating, was investigated by XRD. In fig. 4.8, the XRD pattern is composed of the broad humps and hence indicates that this product was amorphous.

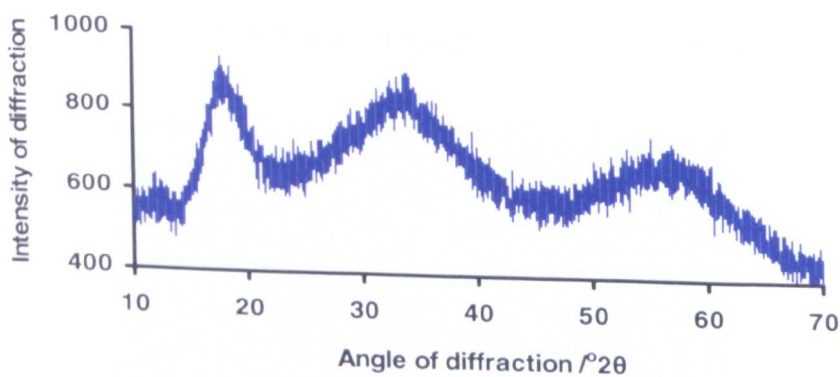


Fig. 4.8 XRD pattern of the conventionally prepared arsenic sulfide batched as As_2S_3 (atomic ratio) id: CF 074.

The amorphicity of the conventionally prepared arsenic sulfide id: CF 074 was further investigated by subjecting the sample to TEM SAED. The diffuse ring structure (fig. A-3 [Appendix A]) confirmed the absence of small crystals in the sample.

4.2.2 Thermal analysis of the conventionally prepared arsenic sulfide id: CH 25.

The extrapolated onset T_g of the conventionally prepared arsenic sulfide glass id: CH 25 was analysed using differential scanning calorimetry (DSC). To obtain the DSC curve shown in fig. 4.9, 12.05 mg of the product was enclosed in a lidded DSC aluminium pan (section 3.3.4.3).

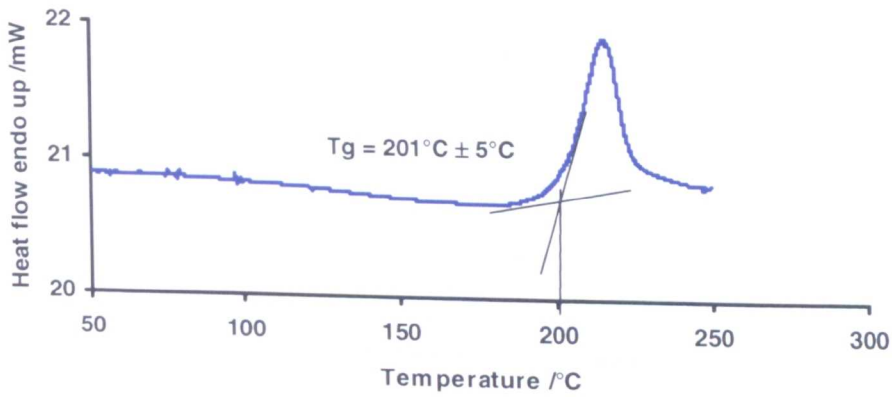


Fig 4.9 Typical DSC curve of the conventionally prepared arsenic sulfide batched as As_2S_3 (atomic ratio) id: CH25, showing the extrapolated onset Tg.

DSC curves showed the extrapolated onset Tg at $201^\circ\text{C} \pm 5^\circ\text{C}$ as calculated using Perkin Elmer software. The error bar is an assumed worst-case value from work done later on DTA within chapter 5.

4.2.3 Optical microscopy of the conventionally prepared arsenic sulfide id:CF 074.

A sample of the conventionally prepared arsenic sulfide product id: CF 074 was cut and polished (section 3.2.1 (g & h)) and then subjected to transmission optical microscopy (see (fig. 4.10)).

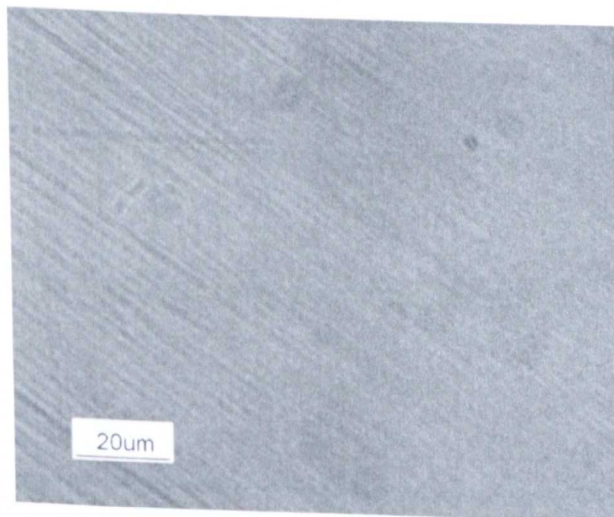


Fig. 4.10 Transmission optical microscopy of the conventionally prepared arsenic sulfide, batched as As_2S_3 (atomic ratio) id: CF 074 then ground and polished.

No defects of $\sim 0.5 \mu\text{m}$ diameter upwards were observed and the product appeared homogenous.

4.3 The optical transmission window measurement using FTIR of the conventionally prepared arsenic sulfide and as-annealed DMO arsenic sulfide.

Figure 4.11a shows the FTIR spectrum of the as-annealed conventionally prepared glass id: CF 074 and fig. 4.11b shows the FTIR spectrum of the as-annealed (see section 4.1.5) DMO product portion 'A' of id: MW6. The FTIR absorption bands obtained, together with their assignments and the literature references are listed in Table 4.4.

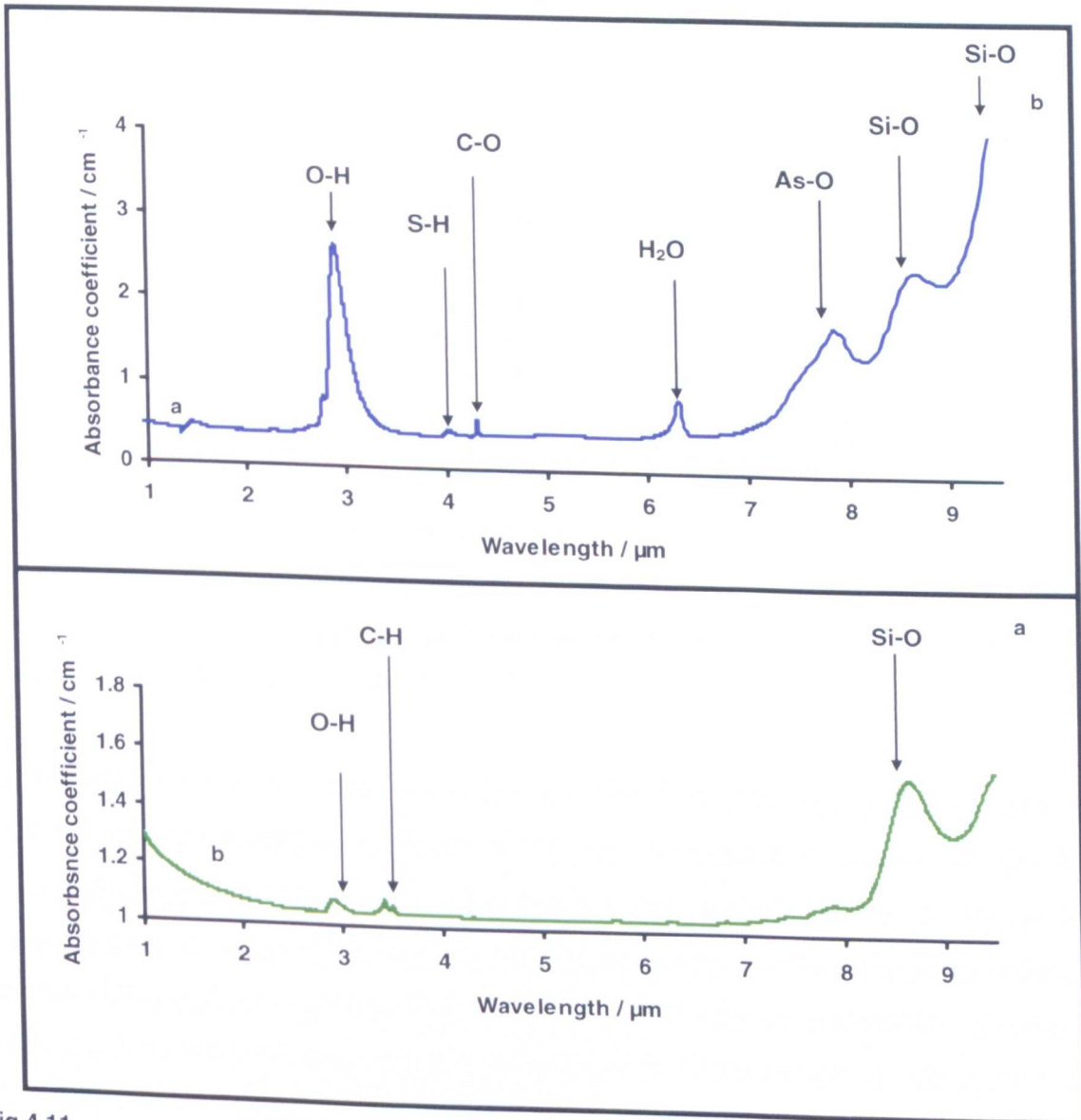


Fig 4.11

a) FTIR data of as-annealed As-S glass made through conventional heating id: CF 074 (As explained above in section 4.2 this sample was tagged with letters 'CF' as was done previously in our research group since this was the first sample made for this project).

b) FTIR spectrum of DMO As-S as-annealed glassy portion 'A' id: MW6.

As described in section 3.3.5, the spectra were treated for background absorption removal but nothing was done to manipulate the baseline and the spectra were divided by the optical pathlength of the specimen *i.e.* the mean sample thickness which was about 3 mm to 4 mm.

For Table 4.6, the quoted absorption coefficient of an absorption band was measured by taking the baseline absorption coefficient from the peak absorption coefficient.

Table 4.6 Identification of FTIR absorption bands with the literature assignments and references for both DMO and conventionally made arsenic sulfide products id: MW6 and id: CF 074, respectively.

OBSERVED				LITERATURE		
As-S conventionally-made id: CF 074		DMO As-S id: MW6		Wvlen / μm	Assign-ment	Ref.
Wvlen / μm	Absn. coeff./ cm^{-1}	Wvlen / μm	Absn. coeff./ cm^{-1}			
2.91	2.40	2.86	0.023	2.92	O-H	[8]
-	-	3.41	0.019	3.41	C-H	[9]
4.11	0.004	-	-	4.10	S-H	[10]
4.31	0.10	-	-	4.31	C-O	[11]
6.32	0.41	-	-	6.30	H ₂ O	[12]
7.92	0.72	-	-	7.90	As-O	[9]
8.75	7.75	8.75	0.2	8.70	SO ₂	[13]
9.43	8.00	-	-	9.43	Si-O	[10]

Key: Absn. Coeff. is absorption coefficient, Wvlen is wavelength. Note both the DMO and conventionally prepared glasses were FTIR analysed as-annealed.

First it must be recalled that the as-annealed glassy portion 'A' of DMO As-S id: MW6 was concluded probably to be inhomogeneous (section 4.1.5) and moreover sulfur was evolved from the product during the annealing. Therefore the spectrum shown in fig. 4.11b is of this inhomogeneous DMO glassy product.

For the conventionally prepared As-S glass id: CF074, significantly it may be seen from Table 4.6 that the absorption coefficient of the extrinsic absorption band at 2.91 μm due to [O-H] contamination was 2.40 cm^{-1} yet had diminished to 0.02 cm^{-1} at 2.86 μm for the DMO product portion 'A' of id: MW6. Thus the [O-H] contamination of the microwave synthesised glass was decreased to ~ 0.96 % of that of the glass made through conventional heating. It is interesting to consider the reason for this much lower [O-H] content for the glassy portion 'A' of the DMO As-S product id: MW6.

It is suggested that during microwave heating both physi-sorbed and chemi-sorbed water on the surface and inside the bulk of the reactants could have vaporised and collected in the colder part of the ampoule. This might have been caused by the plasma which could have displaced water vapour to the upper part of the ampoule whereas the reactants were present on the bottom of the ampoule. Thus the plasma may have prevented the water vapour (originating from the reactants and present as contamination) from being in direct contact with the reactants thereafter. In this way, the FTIR absorption due to [O-H] in the final

product was reduced in the DMO As-S glassy product compared to the conventionally prepared As-S glass made through resistance heating. During resistance heating, the ampoule was kept rocking and hence any volatilised species would have been continuously re-incorporated into the liquid melt and would have tended towards achieving an equilibrium solubility.

The band obtained at 3.41 μm obtained for the DMO As-S glassy portion 'A' id: MW6 corresponds to C-H vibrational absorption and the absorption band obtained at 9.43 μm shows that carbon was present in the system. Carbon might have come from the starting materials, especially sulfur, or from back-streaming of the oil vapour from the rotary pump attached to the evacuation system or from the walls of the silica ampoule. In addition, the grinding and polishing reagents can introduce oil and hydrocarbon solvents into the surface of the glassy product. The latter has been confirmed in our laboratory by noting the absence of C-H absorption at $\sim 3.41\mu\text{m}$ wavelength when the optical loss of chalcogenide glass fibre is measured by the cut-back method [6]. However, it is noted that the conventionally prepared glass did not appear to exhibit this C-H band at 3.41 μm and this cannot be explained at present.

For the conventionally prepared As-S glass id: CF074, sulfur hydride impurity was observed confirmed by the presence of the relatively large S-H band at 4.11 μm wavelength that exhibited an absorption coefficient 0.004 cm^{-1} (fig. 4.11b). Perhaps this hydride impurity was incorporated from the moisture present in the starting materials.

Strikingly, this S-H band was apparently absent from the spectrum of the DMO As-S id: MW6 (fig. 4.11a). It is suggested that for the DMO As-S product, the separation of moisture into the space above the reactant melt *i.e.* the upper, colder part of the ampoule, prevented the hydride contamination occurring. Thus, the same reason is proposed for both low O-H, and zero S-H, contamination of the DMO As-S when compared to the contamination present within the conventionally prepared As-S.

Now considering the FTIR oxide bands, the conventionally prepared As-S glass id: CF074 exhibited oxide impurities at 4.31 μm corresponding to C-O bond vibration, 7.9 μm corresponding to the As-O bond vibration It is believed that the oxide impurities are obtained from the reaction between either hydroxide impurities present in the starting materials at a high temperature or some of the oxide such as As-O might be present as impurity in the arsenic itself. The DMO product exhibited neither the 4.31 μm corresponding to C-O bond vibration nor the 7.9 μm corresponding to the As-O bond vibration. Again the partition of the

molecular water above the melt during the microwave processing is proposed to account for this lack of oxide contamination.

The absorption band due to SO_2 impurity at $8.7 \mu\text{m}$ (symmetric stretching mode) was observed in both the samples irrespective of the heating methodology employed for the preparation of the products. Starting materials (arsenic or sulphur) could be a source of oxygen impurity. Though, silica glass melt-ampoule might act as an oxygen supplier. Again, the level of SO_2 impurity was less in the DMO As-S product than the conventionally prepared As-S glass which could be explained with the similar logic (as was discussed earlier in this section (this section 4.3) for H_2O impurity) that plasma had displaced SO_2 to the upper part of the ampoule leaving behind the sample while the glass sample was sitting at the bottom of the ampoule.

The $9.43 \mu\text{m}$ absorption band corresponding to Si-O species are apparently present in both the DMO As-S glassy portion and the conventionally prepared As-S glass. Clearly the Si-O impurity has originated from the silica glass ampoule but it is unclear whether this is due to volatilised silicon monoxide, either during the chalcogenide glass melting or during the sealing off of the ampoule, which tends to occur at $\sim 900^\circ\text{C}$ at 1 atmosphere ($\sim 10^5 \text{ Pa}$) or due to the breaking open of the silica glass ampoule after the melting process and fine dust may have been incorporated into the chalcogenide products.

4.4 Stoichiometry of the as-annealed DMO synthesised As-S glassy portion ‘A’ id: MW6 and conventionally prepared As-S id: CF074.

4.4.1 ESEM EDX for stoichiometry of the as-annealed DMO As-S glassy portion ‘A’ id: MW6 (see section 4.1.5).

The stoichiometry of the as-annealed DMO As-S glassy product (portion ‘A’ of id: MW6, see fig. 4.1) was studied by performing energy dispersive X-ray (EDX) analysis using the environmental scanning electron microscope (ESEM) in auxiliary mode at 20 kV. The pressure of nitrogen gas inside the sample chamber was kept *ca.* 200 Pa. The annealing of the sample had been at 212°C as described in section 4.1.5.

From the ESEM images, several surface defects were observed (see fig 4.7 'a' and 'b') of approximately 50 μm to 150 μm diameter. Such defects are commonly seen during the fracture of silicate glasses and are the result of fracture. The particular shape of the fracture pattern is called "conchoidal" [14]. This is yet more evidence for the glassy nature of the DMO product portion 'A' id: MW6.

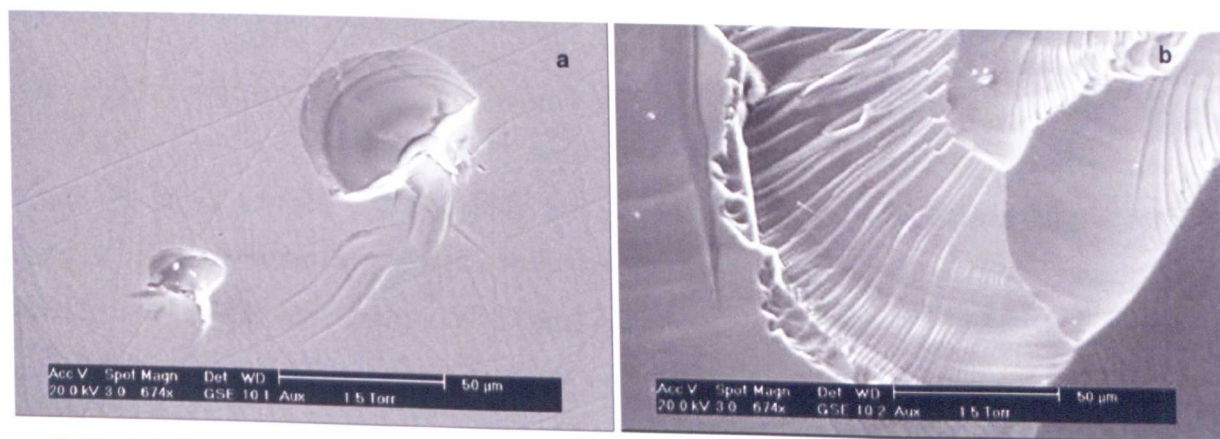


Table 4.7 Stoichiometry of as-annealed portion 'A' of DMO As-S glass (sample id: MW6) as obtained *via* ESEM EDX.

The stoichiometry of this sample as observed using ESEM EDX is shown in Table 4.7. The mean stoichiometry of the As-S glassy product was As = 58.0 and S = 42.0 (theory As = 40 at% and S = 60 at%) with a standard deviation of 1.4. These quantitative results indicate that the as-annealed DMO As-S glass was inhomogeneous, which is in conformity with the results obtained from the DTA analysis of the unannealed product (when more than one T_g was observed (see fig 4.3) and is in agreement with section 4.1.5.

Table 4.7 Stoichiometry of as-annealed portion 'A' (see fig. 4.1) as obtained *via* ESEM EDX.

Observations	Element / at%	
	As	S
1	56.0	44.0
2	57.3	42.7
3	59.0	41.0
4	57.7	42.3
5	60.0	40.0
6	58.0	42.0
Mean	58.0	42.0
Standard deviation	1.4	1.4
Theory	40.0	60.0

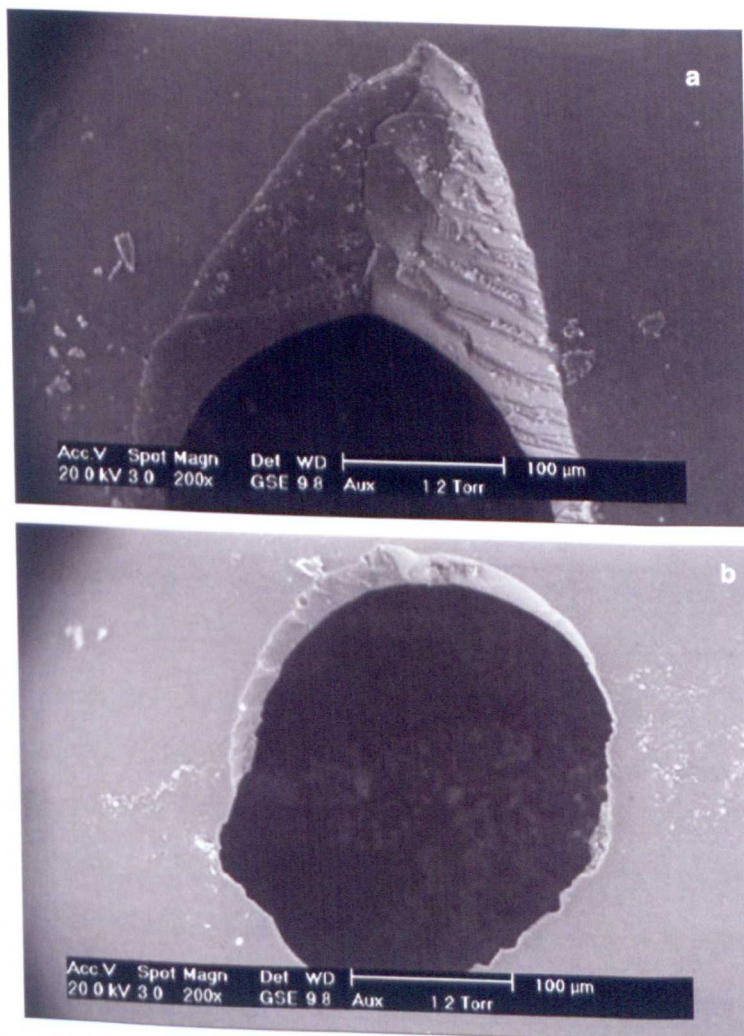
4.4.2 ESEM EDX for stoichiometry of the DTA 'homogenised' DMO As-S glassy portion 'A' id: MW6 (see section 4.1.4).

Since a single T_g value was obtained for the DMO As-S glassy portion 'A' (id: MW6) in the second DTA run (see fig 4.3b) and the result was interpreted in terms of homogenisation of

the sample above the liquidus during the first DTA run (section 4.1.4), it was decided to examine the stoichiometry of the DTA 'homogenised' glass sample. To obtain this sample, the small DTA silica-glass ampoule was carefully cut open after the second DTA run and the small chunk of chalcogenide glass inside was then subjected to ESEM EDX analysis. This small chalcogenide glass sample had exhibited a single T_g at 202°C during the second DTA run (fig. 4.3b) and hence was concluded to be 'homogeneous'.

The ESEM micrographs revealed several defects (see fig. 4.13 'a' to 'c'). The sample contained several holes up to $150\ \mu\text{m}$ diameter surrounded by smooth high quality material. Inside the upper surface of the sample was a contraction cone and inside this the surface exhibited a honeycomb-like surface structure. Perhaps some gas had been evolved due to heating to a high temperature ($\sim 600^\circ\text{C}$) during the second DTA run (fig. 4.3b).

In Table 4.8 are listed the stoichiometries observed for the DMO As-S glassy portion 'A' (id: MW6) after the second DTA run (see fig 4.3b).



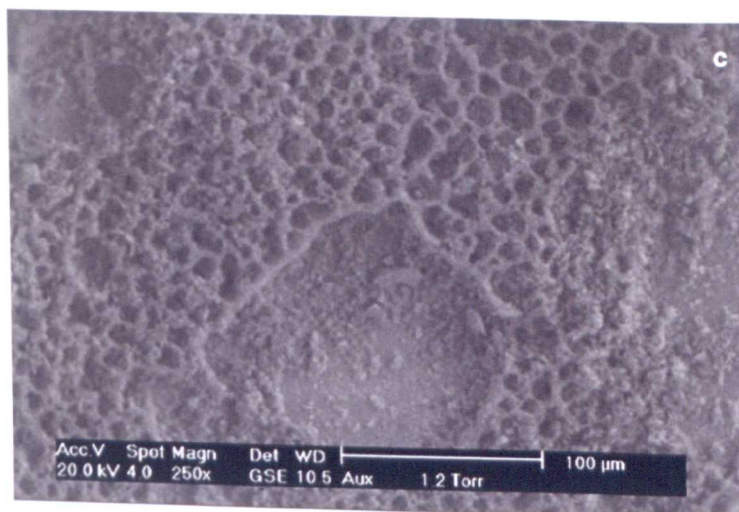


Fig. 4.13 ESEM micrographs of the DTA homogenised DMO As-S glassy portion 'A' of id: MW6: (a) and (b) showing ~ 150 μm diameter holes surrounded by smooth, high quality material and (c) the honeycomb-like structure inside the contraction cone in the upper surface of the sample as it had been orientated within the DTA silica glass ampoule, suggested gas evolution at the higher temperatures during DTA run 2 (fig 4.7).

Table 4.8 Stoichiometry of DTA annealed DMO As-S glass (sample id: MW6) as obtained *via* EDX.

Observations	Element / at %	
	As	S
1	41.0	59.0
2	44.8	55.1
3	44.6	55.4
4	68.1	31.8
5	40.6	59.4
6	48.8	51.1
7	38.3	61.6
8	38.0	62.0
9	37.5	62.5
10	43.1	56.9
11	42.6	57.4
12	44.6	55.4
13	37.4	62.6
Mean	43.8	56.2
Standard deviation	8.1	8.1
Theory	40.0	60.0

From Table 4.8 the mean at% As = 43.8 and S = 56.2, with very large standard deviations of 8.1 and 8.1, respectively. Therefore, it is evident from Table 4.8 that the glass remained slightly inhomogeneous yet much improved upon the sample which had only been as-prepared then annealed at 212°C (section 4.1.5, sample portion 'A' of id: MW6). Hence the homogenisation above the liquidus during the first DTA run (fig. 4.3a) had been successful to a certain extent. However, while performing the EDX analysis it was observed that the detector could not catch completely the X-ray radiation as the glass sample was not absolutely flat. To overcome this potential error, the DTA 'homogenised' DMO As-S glass was next cleaved and the freshly cleaved surface was analysed for the stoichiometry.

The ESEM EDX data obtained for the freshly cleaved sample are summarised in Table 4.9.

Table 4.9 ESEM EDX results obtained for the freshly cleaved DMO As-S glass (portion 'A' of id: MW6 that had been 'homogenised' during the first DTA run (fig. 4.6)).

Observations	Element / at %	
	As	S
1.	39.7	60.3
2.	43.2	56.7
3.	43.5	56.5
4.	49.2	50.8
Mean	43.9	56.1
Standard deviation	3.4	4.0
Theory	40.0	60.0

The results in Table 4.9 give mean values of the at% of As and S of 43.9 and 56.1, respectively and large standard deviations of 3.4 and 4.0, respectively.

In conclusion, all of the above ESEM EDX results (Tables 4.7 to 4.9) show that the stoichiometry of the DMO As-S glass supposedly 'homogenised' during the first DTA run (fig. 4.6) was not the same throughout the sample nor matched with the desired value ($As_{40}S_{60}$) showing that the glass was inhomogeneous.

4.4.3 ESEM EDX for stoichiometry of the conventionally prepared As-S id: CF074.

In contrast to the stoichiometry of the DMO As-S glassy samples determined by means of ESEM EDX, the As-S glass made through resistance heating using the resistance rocking furnace (id: CF074) was homogeneous and the stoichiometry was very close to the desired value. Thus from Table 4.10, the mean at % of As and S was 40.4 and 59.6, respectively with standard deviations of 0.7 and 0.7, respectively, while the theoretical value was $As_{40}S_{60}$.

Table 4.10 ESEM EDX results obtained for the conventionally prepared As-S glass id: CF074. Note: the sample analysed, was not freshly cleaved.

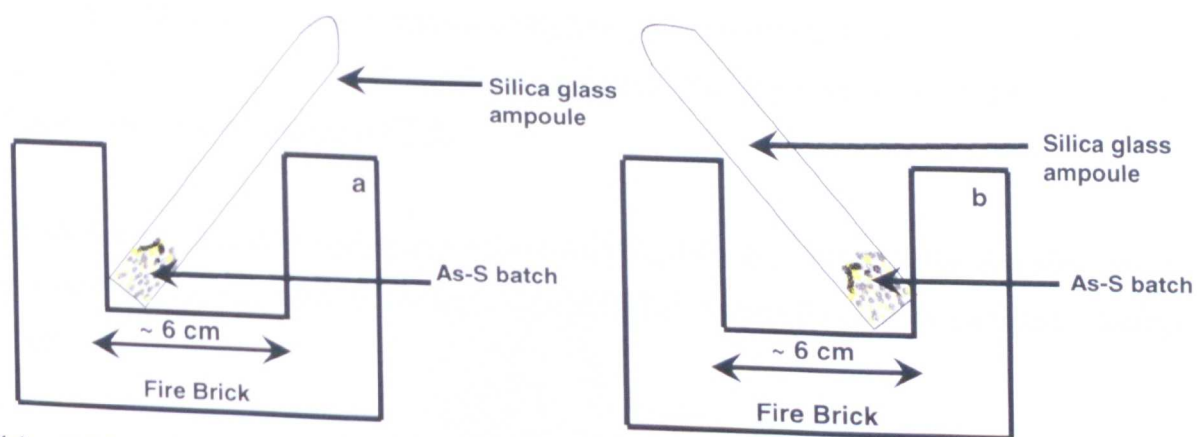
Observations	Element / at%	
	As	S
1.	41.4	58.6
2.	40.9	59.1
3.	40.2	59.8
4.	39.8	60.2
5.	39.9	60.1
Mean	40.4	59.6
Standard deviation	0.7	0.7
Theory	40.0	60.0

Table 4.10 shows that the As-S glass formed in the resistance rocking furnace has the desired stoichiometry showing that As_2S_3 glass was formed. In contrast, to that the DMO As-S glass (Tables 4.7 to 4.9) exhibited stoichiometry far from the desired value showing that the glass was inhomogeneous. During the making of As_2S_3 glass in the resistance rocking furnace, the glass-melt was rocked during melting and was given sufficient time to melt and react the complete batch mass leading to the formation of As_2S_3 glass. During the DMO preparation, only a part of the batch reacted to give DMO As-S glass but this glass was inhomogeneous. It is proposed that the inhomogeneity of the DMO glass occurred principally as the ampoule was not rocked therefore there was no mechanical mixing.

4.5 The irreproducibility of the glass-melting reaction in the DMO.

It was observed that the DMO heating was very sensitive to the position, relative to the inside surfaces of the DMO, of the silica glass ampoule containment. The requirement of the DMO type preparation was to keep the silica glass ampoule, containing the chalcogenide precursors, in a anti-node of the microwave radiation for optimum exposure.

For instance, when keeping the fire brick support in exactly the same position, relative to the inside surfaces of the DMO, arsenic sulfide glass was formed only when the ampoule was angled, as shown in fig. 4.20 (a), and not when the ampoule was angled $\sim 90^\circ$ relative to this, as shown in fig. 4.20 (b).



(a) position of the silica glass ampoule relative to the firebrick support when arsenic sulfide glass was successfully partially formed;

(b) position of the silica glass ampoule relative to the fire brick when arsenic sulfide glass was not formed.

Fig. 4.14 The importance of the position of the silica glass ampoule and firebrick support within the DMO for successful chalcogenide glass melting. Note: (i) the silica glass ampoule contained the chalcogenide precursors and (ii) the firebrick support for both (a) and (b) was kept in the same place exactly relative to the inside walls of the DMO.

4.6 Summary

Even when the As and S reactants were ground together (in atomic ratio 2:3) it was not possible to form a single homogeneous As_2S_3 glass using the DMO. Instead, an inhomogeneous arsenic sulfide glass having four different layers was formed. According to visual inspection, the lowermost part of the sample was glassy. The amorphicity of the glassy portion of the sample was confirmed by XRD and TEM SAED. The inhomogeneity of the chalcogenide glass was also observed through transmission optical microscopy and was further confirmed when at least three Tgs were observed through DTA. It is believed that since the ampoule was not rocked during heating inside the DMO, an inhomogeneous glass was formed. However, remelting the glassy part of the DMO product (in the DTA) resulted in a single Tg As-S glass whose Tg ($202^\circ\text{C} \pm 5^\circ\text{C}$) close to that expected for As_2S_3 (Tg is 205°C [4, 5]). Hence an X-ray amorphous material that exhibits one Tg can be synthesised *via* microwave heating. However, ESEM EDX revealed that the stoichiometry was not exact (s.d. = 1.4) and perfect homogeneity was not achieved.

For the DMO as-annealed glass (that was not heated above the liquidus and hence not homogenised) the FTIR optical absorption due to hydroxide contamination at $2.91\ \mu\text{m}$ wavelength was found to be diminished for the DMO arsenic sulfide glass compared to the glass made through resistance heating. It is supposed that physic-sorbed and chemi-sorbed moisture adhered to the reactants was vaporised during the DMO heating and displaced by the plasma to the colder part of the ampoule and hence the glass obtained manifested a low hydroxide impurity according to FTIR.

DMO As-S glass was inhomogeneous and was full of defects whereas an homogenous As_2S_3 glass (composition s.d. = 0.7, according to ESEM EDS) could be made in resistance rocking furnace.

References:

- [1] D.J.E. Mullen, W. Nowacki and Z. Kristallogr., *Kristallgeom., Kristallphys., Kristallchem.* **136** (1972), p. 48.
- [2] Timofeeva, *Dokl. Phys. Chem.* **190** (1970), p. 115.
- [3] Swanson and Tatge., *Natl. Bur. Stand. (U.S.), Circ.* **539 1** (1953), p. 11.
- [4] M.B. Myers and E.J. Felty, *Mater. Res. Bull* **2** (1967), p. 535.
- [5] E.L. Busse, *Phys. Rev.* **B29 6** (1984), p. 3639.
- [6] Personal Communication, A.B. Seddon, 2008.
- [7] K. Sivakumaran and C.K.S. Nair, *J. Phys. D: Appl. Phys.* **38** (2005), p. 2476.
- [8] J. Kobelke, J. Kirchhof, K. Schuster and A. Schwuchow, *J. Non-Cryst. Solids* **284** (2001), p. 123.
- [9] D. Lezal, *J. Optoelect. & Adv. Mat* **5** (2003), p. 23.
- [10] M.F. Churbanov, *J. Non-Cryst. Solids* **184** (1995), p. 25.
- [11] M.F. Churbanov, V.S. Shiryayev, I.V. Scripachev, G.E. Snopatin, V.V. Gerasimenko, S.V. Smetanin, I.E. Fadin and V.G. Plotnichenko, *J. Non-Cryst. Solids* **284** (2001), p. 146.
- [12] D. Lezal, J. Pedlikova and J. Zavadila, *Chalc. Lett.* **1** (2004), p. 11.
- [13] G.E. Snopatin, M.Y. Matveeva, G.G. Butsyn, M.F. Churbanov, E.B. Kryukova and V.G. Plotnichenko, *Inorg. Mater.* **42** (2006), p. 1388.
- [14] H. Rawson, *Glass science and technology 3, Properties and applications of glass*, Elsevier Scientific Publishing Company, Amsterdam, (1980).

Chapter 5

Microwave assisted synthesis of arsenic selenide.

This chapter discusses the synthesis of arsenic selenide *via* microwave heating. The properties of the DMO arsenic selenide were compared with those of the arsenic selenide glass made *via* conventional heating method using a rocking resistance furnace.

The amorphous nature of the products was examined by X-ray diffraction (XRD) analysis and selected area electron diffraction (SAED) using a transmission electron microscope (TEM). Differential thermal analysis (DTA) and differential scanning calorimetry (DSC) were used to determine the glass transition temperatures (T_gs) of the respective products. The stoichiometry of the product samples is discussed in section 5.3.3. Section 5.3.4 discusses the results obtained using Fourier transform infrared (FTIR) spectroscopy performed to determine the transmission window of the As-Se products. The refractive index of the DMO As-Se product was measured and is discussed section 5.3.5. Chapter 5 is summarised in section 5.5.

A list of all the As-Se products prepared is given in Table 5.1.

Several DMOs of different makes and model were used while making different samples of DMO As-Se product. Table 5.2 summarises the make, model, wattage used for the formation of DMO As-Se product, time of exposure to microwave and the physical state of the starting materials.

Table 5.1 As-Se products prepared from molar proportioned batch As/Se = 2/3.

Id:	Preparation		Resulting sample form (visual inspection)
	DMO	Conventional	
MW8	✓		Small pellets with smaller 'frozen' droplets adhering to surface
MW9	✓		"
MW10	✓		Broken shiny rod (over-quenched)
MW18	✓		Monolithic shiny rod
MW19	✓		Monolithic shiny rod with several surface pores
MW39	✓		Monolithic shiny rod
MW55	✓		"
CH12		✓	"

Key: MW microwave heating, CH conventional heating using rocking resistance furnace, DMO Domestic microwave oven, id: is identification code-number of product.

Table 5.2 List of reaction conditions under which As-Se batches were melted during microwave heating.

Id:	DMO Make/Model	Power/ W	Exposure time / mins	Physical state of starting material	
				As	Se
MW8	DeLonghi/ M8021P-B1	800	35	*	*
MW9	"	"	"	*	*
MW10	DeLonghi/ EM821AAN	"	"	*	*
MW18	"	"	"	*	*
MW19	"	"	"	+	+
MW39	"	"	"	*	*
MW55	Panasonic/ NN A554W	1000	"	*	O

Key: * manually crushed inside the glove box, + powdered reactants were bought (see section 3.1.1.2), O used without crushing. (see Table 3.2 for purities and source of starting materials)

5.1 Microwave irradiation of the arsenic and selenium and formation of DMO As-Se rods.

5.1.1 Product id: MW8.

Amorphous arsenic (All Chemie Ltd., Lot # A 3079, 99.95 %, powder < 0.2 mm diameter, 1.56 g) and selenium beads (2.49 g, Cerac, 5n, ca. 2.5 mm in diameter) were individually crushed manually inside the glove box (MBraun-150B-G, H₂O < 0.1 ppm, O₂ < 0.1 ppm) using a clean, agate mortar and pestle (Fischer) to give a total batch of 4.06 g. The arsenic powder and the selenium powder were mixed in molar proportion As:Se = 2:3 in a weighing boat (Fischer) and then poured in the silica ampoule (OD/ID = 14/10, length = ca. 200 cm). The ampoule was made in-house by heating one end of a silica tube (Multilab) in an oxypropane flame to form a tube with one closed end. This ampoule was used without further

in-house cleaning or baking. The ampoule was then evacuated and sealed (sealing vacuum = 1.8×10^{-5} torr (2.4×10^{-3} Pa)) to be about 140 to 159 mm in length. It was next heated in the DMO at 800 W for 35 minutes with the ampoule resting in the surface of sand. The height of the sand was about 2 cm in a 50 ml beaker. Several blue glows could be seen as soon as the powdered arsenic and selenium were exposed to the microwaves (see, for example, fig. 3.12). The reactants melted and the DMO As-Se melt appeared to travel upwards in the ampoule. After about 3 to 4 minutes the As-Se melt boiled and the refluxing red hot glass-melt could be seen (see, for example, fig. 3.13). The heating stopped as soon as the DMO switched off with the timer function and the As-Se melt could be seen to have coated the interior walls of the ampoule making them appear black from the outside of the ampoule (see, for example, fig. 3.9).

A few glassy-looking pellets were obtained from these first few experiments (see sec. 3.1.2.3). Fig 5.1 shows a scanning electron micrograph (SEM) of the typical shiny hemispheres of a few mm diameter with smaller droplets of $\sim 20 \mu\text{m}$ diameter (estimated) (see portion 2 of fig. 5.1) over their surfaces. The flat surfaces of the hemispheres were due to them forming on the interior wall of the silica glass ampoule.

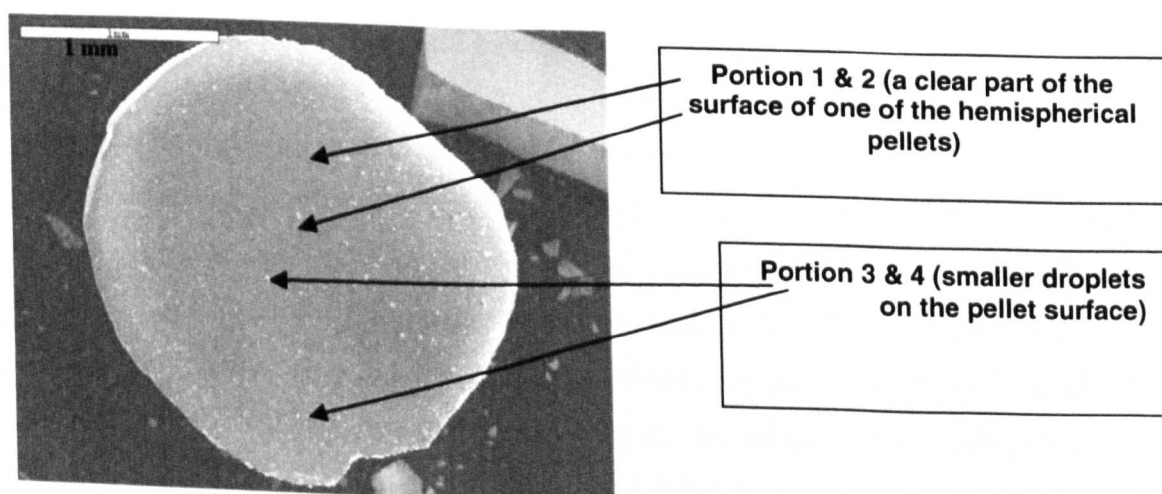


Fig. 5.1 One of the shiny hemispheres (a few mm diameter) of the product formed from the DMO preparation of As-Se. (id: MW8). There were smaller droplets (estimated to be $\sim 20 \mu\text{m}$ diameter) adhering to the surface of the hemisphere.

5.1.2 Products id: MW9; MW10; MW18; MW19.

The experimental conditions to prepare product id: MW8, as described in section 5.1.1 above, were repeated and similar “glassy-looking” pellets as shown in fig. 3.9 were obtained giving product id: MW9. These DMO As-Se products were characterised and the results obtained are summarised in section 5.2.

After the preparation of X-ray amorphous MW8 and MW9 with a T_g (see section 5.3.2.1), the main aim of the experiment was to prepare a glass rod so that a glass disc could be cut and polished (see section 3.2.3.2). The glass disc was required for the measurement of optical transmission window, as it was not possible to perform FTIR measurement for the DMO products id: MW8 and MW9 which were in the form of hemispherical pellets obtained.

To achieve this goal, during the preparation of sample id: MW10, the arsenic/selenium mixture in the atomic ratio of 2/3 of larger batch (10 g total, As: Furukawa 7x9s purity purified as in section 3.1.1.2 and Se: Cerac 5x9s) was exposed to microwaves (see Table 5.2) in a shorter ampoule (length of the ampoule for id: MW10 was *ca.* 120 mm as opposed to ~ 160 mm for id: MW8 and MW9) as it was supposed that the DMO As-Se melt formed during microwave heating would be forced to collect at the bottom of the ampoule to form a rod. According to the expectation, the DMO As-Se id: MW10 melt dripped down to the bottom of the ampoule and formed a shiny, monolithic (initially) rod (Table 5.1). Unfortunately, the ampoule containing the melt id: MW10 was over-quenched (in water) and the DMO As-Se product fractured.

Perhaps, the observed dripping was encouraged by the larger amount of batch (10 g for id: MW10 as opposed to 3 to 4 g total batch for id: MW8 and MW9). Thus, while synthesising the DMO As-Se rod id: MW10, the droplets which formed on the interior walls of the silica melt-ampoule were larger than the droplets observed to form during the synthesis of DMO As-Se products id: MW8 and MW9. Thus the ratio of surface area of each drop to the volume of each drop was smaller for id: MW10 and hence these larger liquid droplets will not have cooled so quickly as for the smaller liquid droplets of id: MW8 and id MW9. The larger droplets survived as a liquid that remained above T_g and allowed this movement under gravity until the droplets reached the bottom of the ampoule and aggregated to form a monolithic mass. This happened even though the ampoule was quenched in liquid water.

As stated above, the DMO As-Se rod id: MW 10 cracked during the water quench and it was believed that the sample was over-quenched and so the next step was to find an optimum quench to avoid cracking.

The experiment was repeated to make rod DMO As-Se id: MW18 when again 10 g total batch was microwave irradiated in *ca.* 110 mm of the ampoule (starting materials as id: MW10) but this time the melt was air quenched (the standard quenching condition for the preparation of arsenic selenide). It was observed that the id: MW18 melt collected at the bottom of the ampoule suggesting that the length of the ampoule and the amount of glass-batch was indeed

significant. Figure 5.2 shows the collection of DMO As-Se (id: MW 18) melt at the bottom of the ampoule. The DMO As-Se rod MW18 was later successfully drawn to a fibre (see chapter 8).

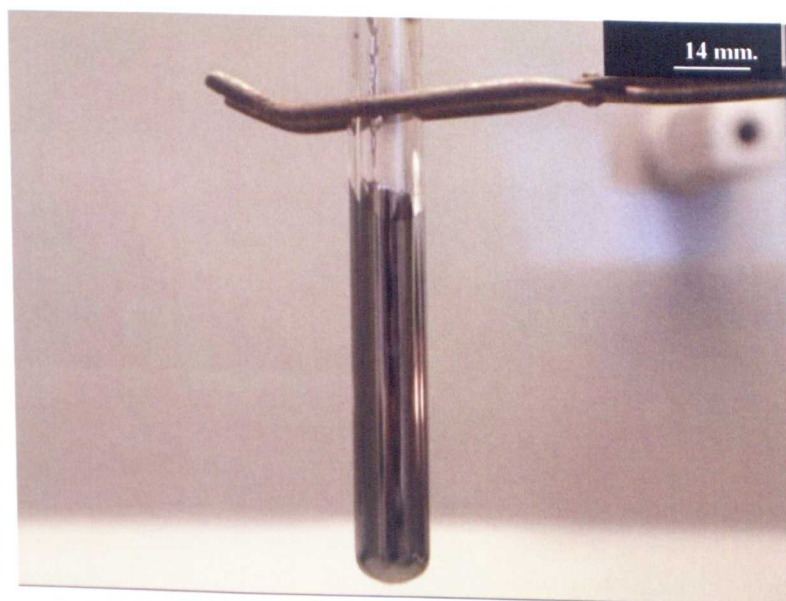
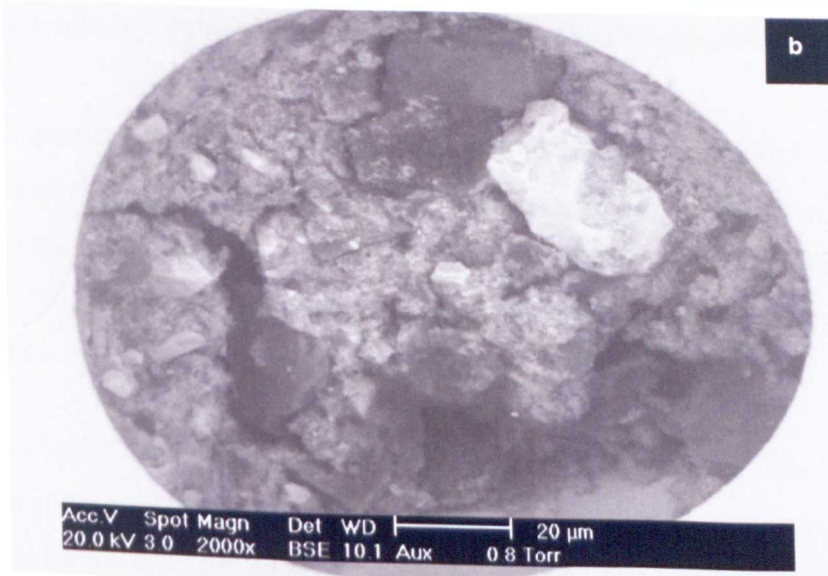
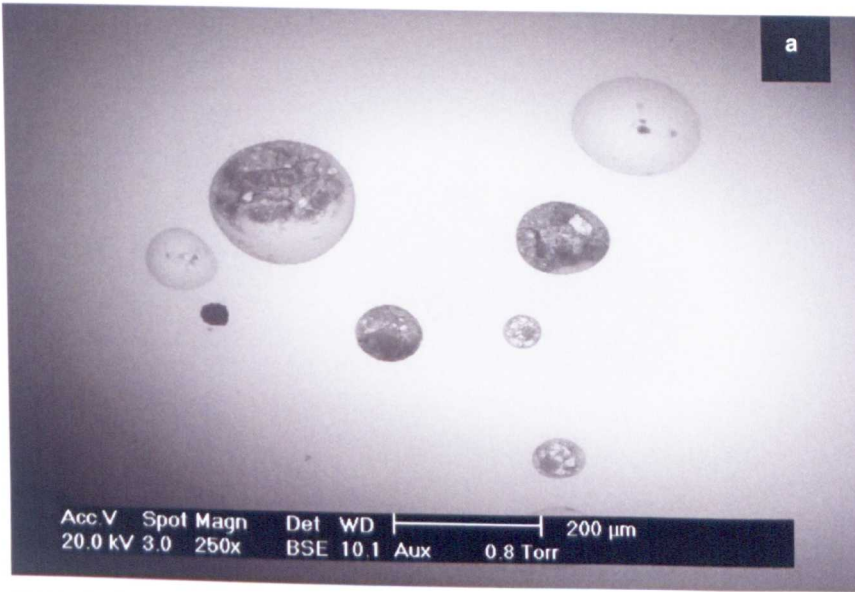


Fig. 5.2 Photograph showing the rod of DMO As-Se melt id: MW18 (10 g of the glass batch in ~110 mm silica glass melt-ampoule) collected at the bottom of the ampoule just after quenching.

For the last product discussed in this subsection, DMO As-Se id: MW19, the reactants were in powder form (As: Alfa Aesar, 100 mesh, 7.5x9s (purified as usual section 3.1.1.2) and Se: Cerac, 3mm beads, 5x9s, manually crushed). Total batch mass was 10 g and the ampoule length was ~ 110 mm.

A shiny rod was again obtained, that was annealed inside the ampoule at 180°C (see section 3.2.1). However, this time there were many pores visible to the naked eye on the surface of the DMO As-Se rod product. The product was studied using ESEM imaging (see fig. 3 (a) to (d)) and at the base of the holes there appeared to be some debris. Gas may have been evolved from the DMO As-Se rod surface during the DMO synthesis which made circular holes in the sample surface.



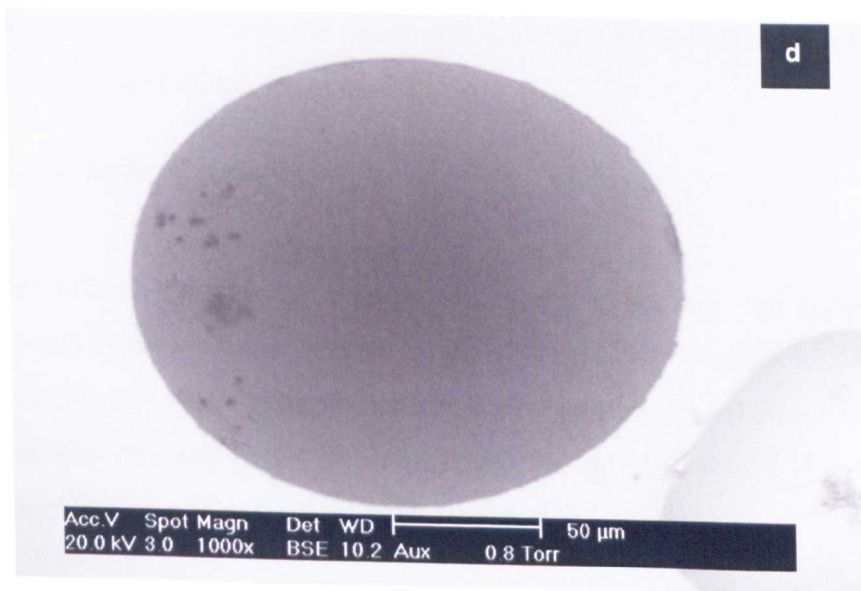


Fig 5.3 ESEM micrographs ('a' to 'd') showing holes in the DMO As-Se product with debris inside them (id: MW19).

Later in this chapter (section 5.3.3) ESEM EDX analysis will be presented of all of the DMO and conventionally prepared As-Se products prepared as in Table 5.1. However, it was thought important to present the ESEM EDX results for id: MW19 here to allow early conclusions to be given about the poor quality of the DMO product when using powdered starting materials.

Thus DMO As-Se id: MW19 was subjected to ESEM EDX analysis. The materials present inside the hole could not be analysed as the holes were deep and the X-rays apparently could not reach inside hence only the clear areas of the sample were analysed. The results obtained are summarised in Table 5.3

Table: 5.3 Stoichiometry of the DMO As-Se glass rod (sample id: MW19) with holes in the rod surface as obtained in EDX analysis.

Observations	Element / at%	
	As	Se
1.	37.3	62.7
2.	40.6	59.4
3.	38.4	61.6
4.	39.3	60.7
5.	38.2	61.8
6.	40.7	59.3
Mean	39.1	60.9
Standard deviation	1.4	1.4
Theory	40.0	60.0

Table 5.3 shows that the stoichiometry of the DMO As-Se product id: MW19 was close to the desired value (id: MW19 As mean at% = 39.1, s. d. = 1.4; Se mean at% = 60.9, s. d. = 1.4. Ideal As = 40.0 at% and Se = 60.0 at%) but the presence of the surface holes with debris

inside was not desirable and hence the powdered starting materials were not used for As-Se products in the rest of the project.

5.1.3 Product id: MW39, MW55.

For product id: MW39, which was a successful shiny glass rod, the same experimental conditions of DMO synthesis were used as for id: MW18. DMO product id: MW55 was also made under exactly the same conditions with two exceptions: the selenium was not crushed but used as beads as-received and a different DMO was used (Table 5.1). Note product id: MW55 will not be discussed further here until section 5.4.

Several blue flashes and the boiling glass melt were again seen during the DMO synthesis. The DMO As-Se melt collected at the bottom of the ampoule. It was then air quenched and annealed at 180°C (see section 3.2.1) when a glass rod was formed (id: MW39). The rod looked shiny and homogenous (see fig. 5.2).



Fig. 5.4 DMO As-Se (id: MW39) rod.

The DMO As-Se product id: MW8, MW9, MW18, MW19, MW39 and MW55. The results obtained are summarised in section 5.2.

5.2 Synthesis of arsenic selenide glass *via* resistance heating.

The properties of arsenic selenide made *via* microwave heating were compared with those of the arsenic selenide made *via* resistance heating. The latter procedure was carried out as follows: arsenic (3.88 g, Furukawa, 7x9s, manually crushed inside the glove box (section 3.1.1.3), purified as normal: section 3.1.1) and selenium (6.13 g, Cerac, 5x9s, 99.999 %, manually crushed inside the glove box) taken in atomic ratio As_2Se_3 . A silica glass ampoule was sourced from Multilab already closed at one end. The ampoule was rinsed with distilled

water and oven dried at 70°C for six hours in the class-10,000 clean room (see section 3.1.1.1) followed by air then vacuum baking (section 3.1.1.1). The batch was weighed into the ampoule which was evacuated to 2.3 Pa and sealed (see section 3.1.1.3). The reactants were melted in the resistance rocking furnace (see section 3.1.1.4) according to the melting schedule shown in Table 5.4 to make one product: id: CH12.

Table 5.4 Melting schedule of the conventionally prepared arsenic selenide batched as As_2Se_3 (atomic ratio) id: CH12.

Stage	Schedule
1	20°C to 200°C @ 200°C/hr
2	Start rocking at 250 °C to 300 °C (when Se has melted to avoid scratching inside walls of ampoule)
3	200°C to 800°C @ 40°C/hr
4	Dwell at 800°C for 12 hrs.
5	800°C to 650°C @ 40°C/hr
6	Hold 650°C for 1 to 2h.
7	Switch of rocking mechanism and hold ampoule vertical inside rocking furnace for 15 min.
8	Quench ampoule in air for ~45 - 60 s (for 10 g batch)

Each of the eight steps shown in Table 5.4 is important. The glass melt was quenched in air for about 45 to 60 seconds. It was then annealed according to the schedule shown in Table 5.5.

Table 5.5 Annealing schedule of the conventionally prepared arsenic selenide batched as As_2Se_3 , id: CH12.

Stage	Schedule
1	180°C for 1 h
2	180°C to 140°C @ 5°C / h
3	140°C to 20°C @ 20°C / h

5.3 Characterisation.

5.3.1 Amorphicity of the DMO As-Se products (id: MW8, MW9; MW10; MW18; MW19; MW39) and conventionally prepared product id: CH12 by means of XRD and TEM SAED.

5.3.1.1 DMO As-Se product.

The DMO As-Se products (id: MW9, MW10 and MW39) were ground and subjected to powder XRD when an amorphous halo was obtained suggesting that the glass had been formed. Fig 5.3 shows typical XRD patterns of MW9 and MW10.

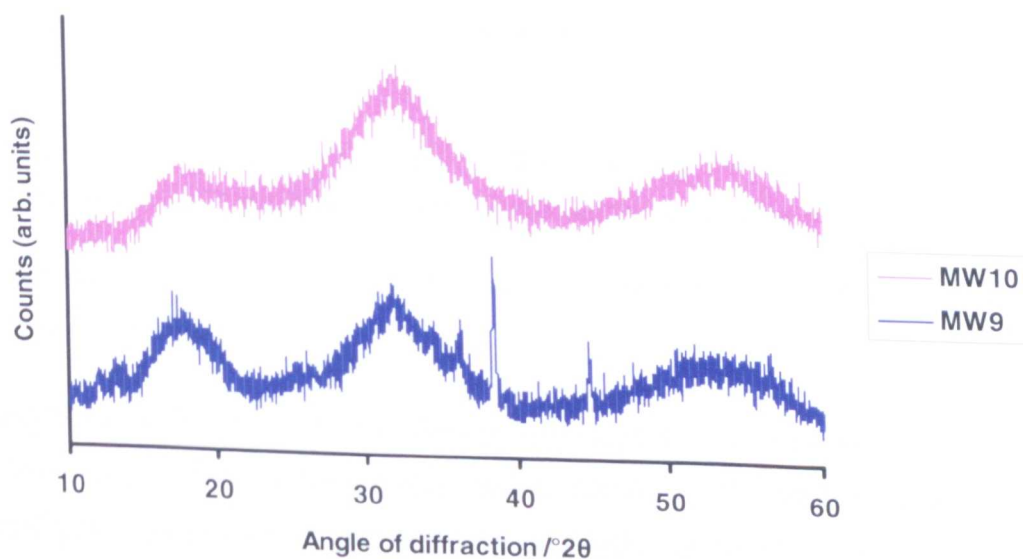


Fig. 5.5 Powder XRD patterns of DMO As-Se products (id: MW9 and MW10).

From fig. 5.3 it may be seen that the both products id: MW 9 and MW 10 exhibited the broad humps characteristic of a glass however there were also a few small, sharp peaks present for sample id: MW9. The XRD pattern of sample id: MW9 was investigated using evaluation software and the small, sharp XRD peaks obtained were found to match aluminium (Table 5.6).

Table 5.6 Identification of the small, sharp XRD peaks obtained for sample id: MW9 (see fig. 5.3).

Observed XRD $^{\circ}/2\theta$		Theoretical peaks for Al angle $^{\circ}/2\theta$ [1]
$^{\circ}/2\theta$	I %	
38.5	100.0	38.5
45.0	40.0	45.0

It is thought that the observed XRD peaks for id: MW9 were due to the aluminium holder used to hold the DMO As-Se sample while doing the X-ray diffractometry.

Fig. 5.6a shows the powder XRD pattern of part of the DMO arsenic selenide rod product id: MW39.

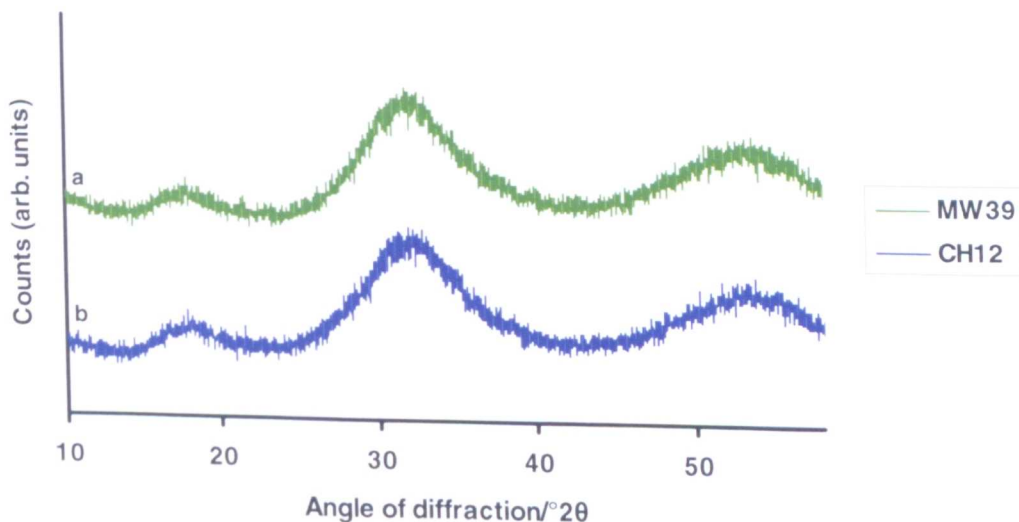


Figure 5.6

(a) XRD pattern of the as-annealed DMO As-Se product (id: MW39).

(b) X-ray diffraction (XRD) pattern of the conventionally prepared As-Se product (id: CH12).

From the broad humps observed in fig. 5.6a it is concluded that that the As-Se rod (sample id: MW39) was amorphous.

The amorphicity of the DMO As-Se products was further investigated by means of TEM SAED (see section 3.3.2). A blurred ring pattern confirmed the absence of any crystalline structure (fig. B-1 [Appendix B]) for the As-Se rod product id: MW39.

5.3.1.2 Conventionally prepared As-Se product.

The above XRD results for the DMO As-Se products (Figs. 5.5 and 5.6a) were then compared with those obtained for a typical arsenic selenide product made through conventional heating (id: CH12, Fig. 5.6b).

From powder XRD (fig. 5.6b), as for the DMO As-Se samples, broad diffraction humps were observed for the conventionally prepared As-Se product id: CH12.

Furthermore, from TEM SAED, as for the DMO As-Se samples, a blurred ring structure was observed for the conventionally prepared As-Se product id: CH12 indicating amorphicity at the nano-scale (fig. B-2 [Appendix B]).

The above XRD and TEM SAED results showed that the product obtained after heating arsenic and selenium in the DMO was amorphous and was comparable to the glass made

through conventional heating. The DMO As-Se material could be synthesised reproducibly to be amorphous according to XRD and TEM SAED.

5.3.2 Thermal analysis of the As-Se products.

5.3.2.1 DMO As-Se products.

T_g of the DMO As-Se products was investigated either *via* DTA or DSC; thus product id: MW8 was analysed using DTA (see section 3.3.3) whereas product id: MW39 was analysed using DSC (see section 3.3.4).

(a) Evaluation of T_g using DTA

The small, sealed DTA silica glass ampoule containing 82.0 mg of the product id: MW8, in the form of small chunks of ~ 2 mm diameter, was heated to 600°C at 10°C/min, when the following curve (fig. 5.7a) was obtained showing that the extrapolated onset T_g of the sample was 175°C ± 5°C. The error was estimated from manually drawing tangents on the T_g peak.

The same ampoule (DTA ampoule) was cooled *in-situ* in the DTA equipment at room temperature. This was then subjected to a second DTA run under similar heating conditions to the first DTA run to give the DTA curve in fig. 5.7b showing an extrapolated onset T_g value of again 175°C ± 5°C. The error was checked manually by drawing tangents on a large print-out and estimated at ±5°C.

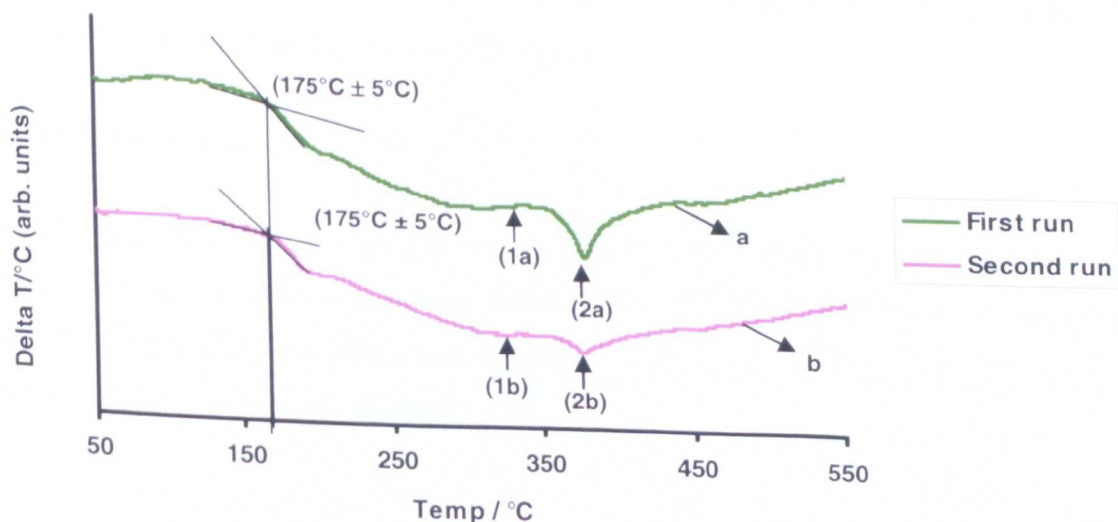


Fig. 5.7

(a) DTA curve showing that the extrapolated onset T_g of the DMO As-Se product (id: MW8) was 175°C ± 5°C from the first DTA run.

(b) DTA curve of the second run of the DMO As-Se product (id: MW8) showing that T_g was 175°C ± 5°C as found for the first run (see fig. 5.7a).

From fig. 5.7b, it can be inferred from the value of extrapolated onset T_g of $175^\circ\text{C} \pm 5^\circ\text{C}$, which matches that observed, within the bounds of error, at 178°C for As_2Se_3 glass reported by Savage [2], that the glass was of the desired stoichiometry. The single T_g value showed that the glass had been homogenised.

In the above figs. 5.7a and 5.7b, the two temperatures shown by arrows (1a), (2a) and (1b), (2b) may be discussed as follows. The temperature as shown by (1a) and (1b) in figs. 5.7a and 5.7b respectively, is possibly the return of the DTA curve to the baseline after a small amount of devitrification had taken place; the devitrification is exothermic and may show as a small exothermic hump. The temperature shown as (2a) and (2b) are the peak melting temperatures of the crystalline phase(s) and it is bigger in the first run than in the second run showing that the glass was more amorphous after it had been through the first DTA run. Applying the “2/3 rule”, the liquidus of As_2Se_3 glass is estimated to be $\sim 400^\circ\text{C}$. The DTA sample was heated to 600°C during the first DTA run, which was above the liquidus. Hence the sample could have homogenised to some extent inside the DTA silica glass ampoule during the first DTA run. This homogenisation may be the reason for the apparent increase in amorphicity of the glass during the second DTA run.

In addition, if there were some ‘already present crystals’ in the as-prepared product, then the melting of these crystals would have taken in energy and contributed to the size of the melting peak in the first DTA run. These ‘already present crystals’ may have melted at the liquidus during the first DTA run and may not have reformed on cooling the DTA sample after the first DTA run. This also would account for the DTA melting peak being smaller for the second DTA run compared to the first DTA run.

(b) Evaluation of T_g using DSC.

The T_g of As-Se made through microwave heating (id: MW39) was measured by means of DSC. 16.10 mg of glass was heated from 40°C to 250°C at $10^\circ\text{C}/\text{min}$ in the differential scanning calorimeter. The DSC curve of sample id: MW39 is shown in fig. 5.8a and shows a single extrapolated onset T_g at $180^\circ\text{C} \pm 5^\circ\text{C}$.

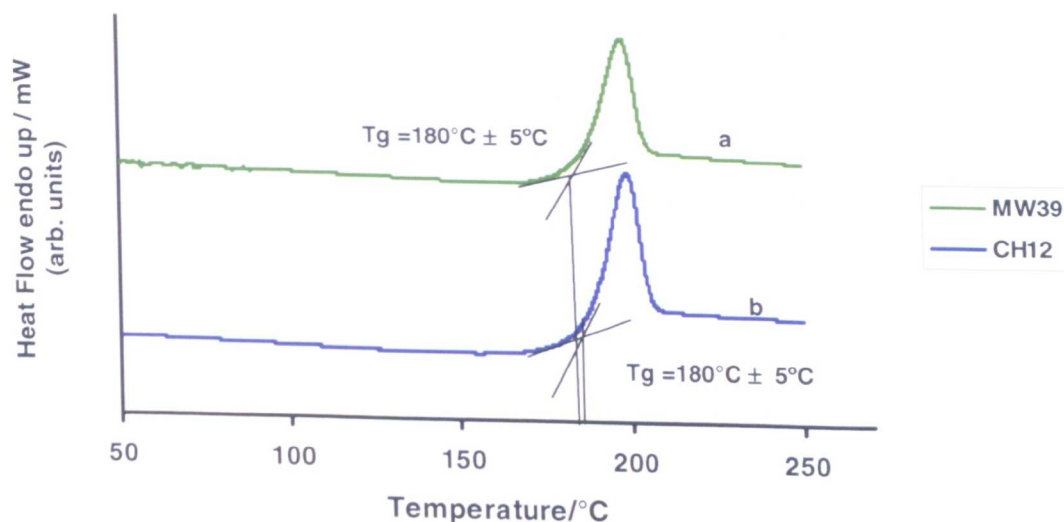


Fig. 5.8

- (a) DSC curve of DMO As-Se (id: MW39) showing a single extrapolated onset Tg at $180^{\circ}\text{C} \pm 5^{\circ}\text{C}$.
 (b) DSC curve of conventionally prepared As_2Se_3 glass (id: CH12) showing the extrapolated onset Tg at $180^{\circ}\text{C} \pm 5^{\circ}\text{C}$.

From fig. 5.8a, the numerical value of the extrapolated onset Tg was $180^{\circ}\text{C} \pm 5^{\circ}\text{C}$ as calculated by DSC software (Perkin-Elmer) for the samples. The single Tg suggested again that the DMO As-Se glass sample was homogenous. The numerical value of Tg showed that the stoichiometry of the glass was As_2Se_3 [2]. The single Tg value indicated that the glass had homogenised. It is proposed that boiling of the glass-melt (and possibly refluxing) under the microwave irradiation homogenised the glass. It is further proposed that the reaction occurred in the plasma state very rapidly as the reactants were present in an ionic state while forming the plasma.

However, it was not possible to ensure that the DSC aluminium sample pan was hermetically sealed and hence it was not possible to heat the sample of id: MW39 much above Tg. Thus it was not possible to observe whether the sample would have undergone any crystallisation during the DSC run.

5.3.2.2 As-Se product made *via* conventional heating (id: CH12).

The Tg result obtained by means of DSC for the DMO As-Se product (id: MW39) was compared with the Tg obtained when As_2Se_3 glass had been made through conventional heating. Conventionally prepared As-Se id: CH12 was subjected to evaluation of Tg using DSC (compare figs 5.8a and 5.8b). 19.76 mg of glass was heated from 40°C to 250°C at $10^{\circ}\text{C}/\text{min}$ in the differential scanning calorimeter.

The calculated value of Tg using DSC Perkin Elmer software was found to be $180^{\circ}\text{C} \pm 5^{\circ}\text{C}$ (see fig. 5.8b) which was very close to the value of $175^{\circ}\text{C} \pm 5^{\circ}\text{C}$ obtained for the DMO As-Se

glass (id: MW39) and that observed for As_2Se_3 glass of 178°C reported by Savage [2], indicating that As_2Se_3 glass had indeed been synthesised using microwave heating.

5.3.3 Stoichiometry of the DMO and conventionally prepared As-Se products by means of ESEM EDX.

5.3.3.1 DMO As-Se product.

The stoichiometry of the DMO As-Se products was examined by performing energy dispersive X-ray (EDX) analysis using the environmental scanning electron microscope in auxiliary mode. A few chunks of the prepared glasses were placed over the carbon coated sticky stubs and were inserted in the sample chamber of the microscope. The results obtained after scanning a sample of DMO As-Se sample id: MW8 are listed in Table 5.7. To recap, as in fig. 5.1, the preparation of DMO As-Se sample id: MW8 resulted in pellets of chalcogenide glass (glass - according to XRD, see section 5.3.1) with smaller 'frozen' droplets evident on some parts of the pellet surface.

It is evident from the Table 5.7, that the stoichiometry of the clear surface of the pellet the As-Se id: MW8 [mean As = 38.0 at% (s.d. = 2.6); mean Se = 62.0 at%, s.d. = 2.6] and was close to the desired value for the As_2Se_3 glass (As= 40.0 at% and Se = 60.0 at%) but the smaller droplets which had formed over the glass hemispheres *i.e.* the pellets, were selenium rich. It is suggested that the smaller droplets were formed due to vapour deposition of selenium, as the very formation of plasma was attributed to the formation of selenium vapour.

Table 5.7 Stoichiometry of DMO As-Se glass (id: MW8) as obtained via ESEM EDX. The sample as-prepared consisted of pellets of glass (glass - according to XRD and TEM SAED, sections 5.3.1) with some areas of pellets being covered in smaller 'frozen' droplets.

Observations (Portions as shown in fig. 5.1)	Element / at%	
	As	Se
1. (clear area of pellets)	41.0	59.0
2. (")	39.3	60.7
3. (tiny droplets on pellets)	36.1	63.9
4. (")	35.6	64.4
Mean	38.0	62.0
Standard deviation (s.d)	2.6	2.6
Theory	40.0	60.0

The DMO As-Se product id: MW10 was a broken rod (Table 5.1). A small chunk of this chalcogenide glass rod was analysed using ESEM EDX. The results obtained are summarised in Table 5.8.

Table 5.8 EDX analysis of the DMO prepared As-Se glass rod id: MW10, showing the stoichiometry.

Observations	Element / at%	
	As	Se
1.	40.8	59.2
2.	40.6	59.4
Mean	40.7	59.3
Standard deviation (s.d)	0.1	0.1
Theory	40.0	60.0

From Table 5.8, the results obtained from the ESEM EDX analysis for the DMO product id: MW10 (mean As = 40.7 at%, s.d. = 0.1 and mean Se = 59.3 at%, s.d. = 0.1) were close to the desired value for As_2Se_3 glass (As = 40.0 at% and Se = 60.0 at %).

The stoichiometry of the DMO rod products was further confirmed when sample id: MW39 was analysed (polished disc subsequently used for FTIR analysis, section 5.3.4). The ESEM EDX values are depicted in the following Table 5.9.

Table: 5.9 Stoichiometry of DMO As-Se glass as obtained using ESEM EDX analysis (id: MW39).

Observations	Element / at%	
	As	Se
1.	40.6	59.4
2.	39.6	60.4
3.	39.6	60.4
4.	40.4	59.6
5.	40.3	59.7
6.	40.1	59.9
Mean	40.1	59.9
Standard deviation (s. d)	0.4	0.4
Theory	40.0	60.0

The results obtained from the ESEM EDX analysis for products id: MW10 (Table 5.8) and MW39 (Table 5.9) suggested that As_2Se_3 had been formed in the required stoichiometry. It is proposed that boiling of the melt during the microwave processing homogenised the products.

To check further the homogeneity of the DMO glasses, DMO As-Se product id: MW18 and several other samples of DMO As-Se id: MW39 were subjected to ESEM EDX analysis to check the stoichiometry. One example is given in the following Table 5.10 (id: MW18). Please note that the sample of id: MW18 was in fact a piece of fibre drawn from the rod manufactured in the DMO (see chapter 8) and therefore had been through an extra process of reheating to form the fibre. Also, for the ESEM EDX results any carbon from the carbon tab support was ignored in the analysis.

Table: 5.10 Stoichiometry of DMO As-Se glass as obtained using ESEM EDX analysis (id: MW18). (Note that this sample was fibre that had been drawn from the as-annealed DMO rod product.)

Observations	Elements/ at%	
	As	Se
1.	39.8	60.2
2.	40.8	59.2
3.	41.0	59.0
4.	39.7	60.3
Mean	40.3	59.7
Standard deviation (s. d.)	0.7	0.7
Theory	40.0	60.0

Both As-Se products id: MW18 and id: MW39 formed a monolithic, shiny rod as-prepared (Table 5.1). The ESEM EDX spectra taken from each of two different areas of the same sample of the DMO As-Se product id: MW18 are shown in fig. B-3 (a) and (b) [Appendix B]. Similarly, the ESEM EDS spectrum taken from each of several different areas of the same sample of the DMO As-Se product id: MW39 are shown in fig. B-4 (a) to (f) [Appendix B]. The ESEM EDS spectral files were chosen randomly and are displayed here to illustrate their reproducible nature and that arsenic selenide was therefore formed reproducibly *via* microwave heating.

5.3.3.2 Conventionally prepared As-Se product

The arsenic selenide made through conventional heating (id: CH12, Table 5.1) was studied using the ESEM EDX to compare the stoichiometry of this with the As-Se products obtained by microwave heating. A powdered (particle size > 0.2 mm) sample of the conventionally heated As-Se product (id: CH12) was analysed performing ESEM EDX analysis. The results obtained are summarised in the following Tables 5.11 and 5.12, respectively.

Table 5.11 ESEM EDX analysis of conventionally made As-Se product (id: CH12) showing the stoichiometry. (Note that the sample had been ground to a powder of particle size < 0.2 mm diameter.)

Observations	Element / at%		
	As	Se	C
1.	13.5	19.9	66.6
2.	20.3	29.5	50.2
3.	28.8	19.6	51.6
4.	13.4	18.8	67.8
5.	22.8	15.5	61.7
Mean	19.8	20.7	59.6
Standard deviation (s. d.)	6.5	5.2	8.3
Theory	40.0	60.0	0

From Table 5.11 it can be seen that the atomic% of carbon was unexpectedly high and this must be explained.

It is believed that, because the sample was in a powdered state, and therefore perhaps more prone to charging than if it was a monolith, when the beam of electrons was focused on the sample, while the spot analysis was carried out, a part of the beam was scattered. In such a case, the beam can in general be considered to be divided into two components: scattered and unscattered. The unscattered component of the electron beam is considered to come from the surface of the sample at the desired point. The scattered electron beam comes from some broader area. These scattered electrons are usually known as “skirt”. Perhaps here, these skirt electrons collided with the carbon tab on which the sample powder was placed. The degree of scattering of the electrons depends upon the pressure of the gas in the ESEM sample chamber and the distance between the electron beam aperture and the surface of the sample. The higher the pressure the greater will be the skirt. Here the ESEM sample chamber was filled with nitrogen gas (pressure = 10 torr (1.33×10^3 Pa)) which increased the possibility of skirt.

One more possible reason for the anomalously high carbon measurement is that if the beam is focused at a point on the sample surface for more than 30 to 40 seconds it may deposit carbon on the surface of the sample since the electron beam interacts with unwanted oil vapour coming from the pumps attached to the ESEM microscope. Assuming that the carbon came from the above stated sources, the stoichiometry of the glass sample was measured ignoring carbon content in the sample (see Table 5.12). The re-calculated stoichiometry of the sample (mean As at% = 40.5, s. d. = 0.2 and Se mean at% = 59.5 and s. d. = 0.2) was then close to the desired value (As= 40.0 at% and Se = 60.0 at%), on ignoring what is believed to have been an artefact.

Table: 5.12 ESEM EDX analysis of conventionally made As-Se glass (id: CH12) showing the measured atomic stoichiometry (sample id: CH12) when the atomic percentage of carbon (see Table 5.11) was not taken into account.

Observations	Elements/ at%	
	As	Se
1.	40.4	59.6
2.	40.8	59.2
3.	40.5	59.5
4.	40.4	59.6
5.	40.5	59.5
Mean	40.5	59.5
Standard deviation (s. d.)	0.2	0.2
Theory	40.0	60.0

A polished circular disc sample (used later for FTIR, section 5.3.4) of the same conventionally prepared As-Se product (id: CH12) of diameter 10 mm was analysed with the aim of reducing the electron skirt. The sample was cut using a diamond saw (see section 3.2.3.1) and was ground and polished as discussed in section 3.2.3.2. The sample was dried

under vacuum overnight inside the small antechamber of the glove box (see section 3.1.2.3). The sample was then analysed to verify stoichiometry. The ESEM was kept under similar conditions to those used for the powdered id: CH12 (see Tables 5.11 and 5.12) regarding the pressure of the nitrogen gas in the sample chamber *ie.* 10 Torr (1.33×10^3 Pa). The results obtained are listed in Table 5.13.

Table 5.13 EDX analysis of conventionally made As_2Se_3 glass disc showing the stoichiometry (sample id: CH12).

Observations	Elements/ at%		
	As	Se	C
1.	41.6	58.4	0.0
2.	40.7	59.3	0.0
3.	41.0	59.0	0.0
Mean	41.1	58.9	0.0
Standard deviation (s. d.)	0.5	0.5	0.0
Theory	40.0	60.0	0.0

The results in Table 5.13 show that no carbon was found for the monolithic product id: CH12 as opposed to carbon found for the powdered sample (Table 5.11). This result suggests that the presence of carbon in the EDX analysis was indeed due to the scattering of electrons off the carbon tab sample support when a powdered sample was used.

5.3.3.3 Conclusions.

The above results (Tables 5.9 to 5.13) demonstrate that the stoichiometry of the arsenic selenide glass made through microwave heating was similar to that of the desired value of As_2Se_3 as well as to the arsenic selenide glass made through resistance heating. In summary, the above results prove that arsenic selenide glass can be made through microwave heating having similar stoichiometry as that of the glass made through resistance heating method.

5.3.4 Measurement of the optical infrared transmission window of DMO and conventionally prepared As-Se products.

Arsenic selenide glass samples, made through microwave heating, as well as resistance heating, were cut (see section 3.2.3.1) and polished as described in section 3.2.3.2. Infrared radiation of wavelength in the range of $2 \mu\text{m}$ to $12 \mu\text{m}$ was passed through the samples using the FTIR spectrometer (see section 3.3.5). The spectra obtained for the conventionally (through resistance heating) prepared arsenic selenide id: CH12 is depicted in fig. 5.9a and the DMO As-Se glass id: MW39 in fig. 5.9b.

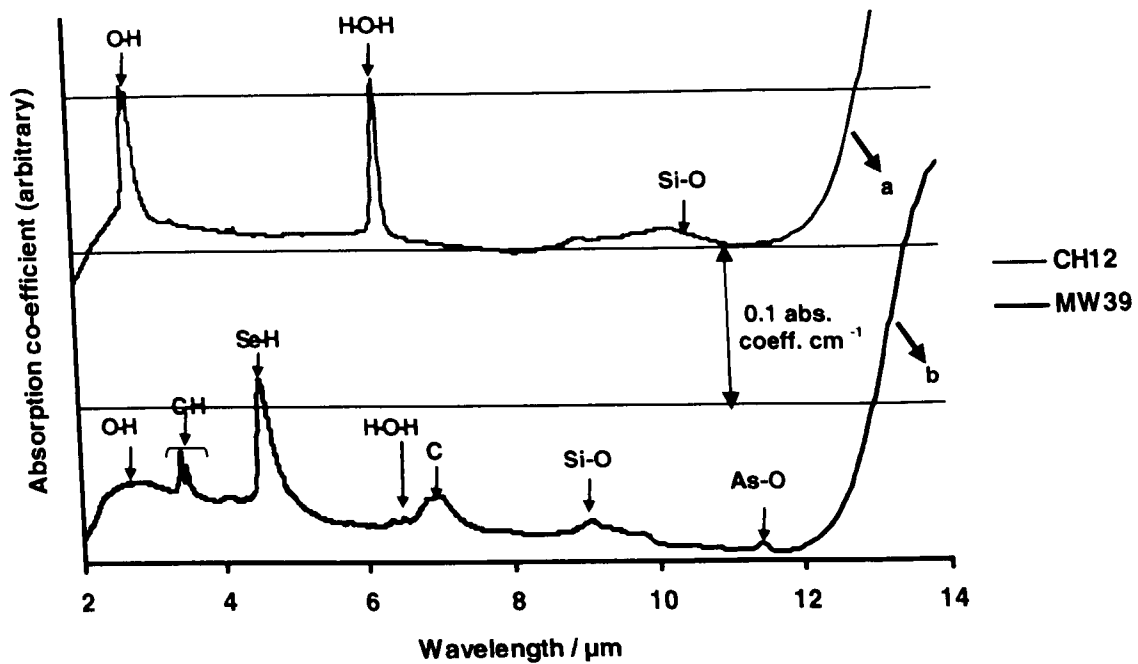


Figure 5.9

(a) Fourier transform infrared (FTIR) spectroscopy of the conventionally prepared As-Se glass (id: CH12).

(b) FTIR spectroscopy of the as-annealed As-Se product prepared in the domestic microwave oven (DMO) (id: MW39).

From figs. 5.9a and 5.9b, the absorption bands obtained for the DMO prepared and, conventionally prepared, As-Se glasses id CH12, and MW39 respectively, due to the extrinsic impurities are labelled and the literature assignments are summarised in Table 5.14.

Table 5.14 The impurity bands obtained for the conventionally prepared and DMO As-Se products, id: CH12 and MW39, respectively in the FTIR absorption spectrum.

OBSERVED				LITERATURE		
As-Se conventionally made (id: CH12)		DMO As-Se (id: MW39)		Wave length/ μm	Assign.	Ref.
Wave length/ μm	Absn. coeff./ cm^{-1}	Wave length/ μm	Absn. coeff./ cm^{-1}			
2.87	0.7	-	-	2.9	O-H	[3]
-	-	3.40	0.02	3.4	C-H	[4]
-	-	3.51	0.01	3.51	C-H	[4]
-	-	4.59	0.06	4.6	Se-H	[5]
6.30	0.9	-	-	6.3	O-H of the molecular H_2O	[6]
-	-	6.91	0.1	6.89	C	[7]
-	-	7.06	0.1	7.07	C	[7]
9.09	0.002	9.09	0.002	9.09	Si-O	[8]
-	-	9.89	0.001	9-10 (broad)	Si-O	[7]
-	-	11.47	0.002	11.5	As-O	[9]

From Table 5.14 absorption bands due to OH as hydroxide or water contamination at 2.9 μm and molecular water contamination at 6.3 μm exhibits smaller absorption coefficients for the

DMO As₂Se₃ glass than for the As₂Se₃ glass made through conventional heating. This is similar to the result for DMO As-S (id: MW6 portion A) (section 4.3) when a very small OH bond (absorption coefficient = 0.023 at 2.86 μm) was obtained as compared to conventionally prepared As₂S₃ glass which exhibited a much longer OH (absorption coefficient 2.40 at 2.91 μm). The explanation proposed was that the microwave plasma displaced water vapour to the upper part of the ampoule, and away from the chalcogenide product. The water vapour may also be displaced away from the product during the DMO synthesis of As-Se, thereby accounting for the lower level of OH in the DMO product (id: MW39) compared to the conventionally prepared product (id: CH12).

The absorption band at around 4.57 μm confirms the presence of Se-H species in the DMO As₂Se₃ glass. It is supposed that the selenium was contaminated during crushing as the reactants were crushed, using a mortar and pestle, before they were exposed to the microwaves. To investigate this proposition, the shiny rod product: DMO As-Se id: MW55 was also investigated by means of FTIR. This is because id: MW55 was made from uncrushed selenium (see section 5.1.3). In fact the FTIR spectrum of id: MW55 (not shown) was very similar to that of id: MW39 except that the Se-H band was slightly smaller. However, the conventionally prepared glass (id: CH12) exhibited no Se-H band. For As-S (section 4.3), the DMO As-S product (id: MW6 portion A) exhibited no S-H band whilst the conventionally made As₂S₃ glass exhibit a very small S-H band (absorption coefficient 0.004 at 4.11 μm). Thus the results differ regarding the chalcogenide hydride band for As-S and As-Se glasses.

The weak bands present at 3.4 μm and 3.51 μm indicate the presence of C-H bonds in the glass whereas the weak bands present at 6.89 μm and 7.07 μm depict the presence of carbon. Churbanov *et. al.* [7] suggested that the carbon comes in the reaction system due to the pumps used for the evacuation of the ampoule before sealing. Previous work in our laboratory has also demonstrated that grinding and polishing fluids can leave C-H contamination [10]. The absorption bands present in the wavelength region 9.09 μm to 9.89 μm proves the presence of the Si-O group. It is believed that Si-O contamination came from the silica ampoule. Some of the silicon monoxide vapour might have been trapped within the ampoule during ampoule sealing because above ~950°C the following decomposition is favoured:



and silica monoxide may react readily with the chalcogenide batches and the glass-melt. The Si-O band was found to be stronger for the DMO arsenic selenide glass than the arsenic

selenide glass made through resistance heating. Since, the silica ampoules for the microwave heating procedure were deliberately kept as small as possible; the point of sealing was very near to the reactants which perhaps accounts for the extra contamination of the reactants with the silicon monoxide vapour.

5.3.5 Refractive indices.

The refractive index dispersion curves of DMO As-Se product id: MW39 (monolithic, shiny rod on preparation, see Table 5.12) and conventionally prepared As-Se product id: CH12 were kindly measured at the University of Pardubice in the Czech Republic by the group of Professor Tomas Wagner. Both of these samples were ground and polished and then pressed in-house equipment in our laboratories under vacuum. The conditions of the heating, pressing and cooling regimes are depicted in Table 5.15.

Table 5.15: Heating schedule, conditions for vacuum pressing and cooling regime.

Steps during vacuum pressing.			
Step 1	The polished DMO As ₂ Se ₃ disc was kept between the two silicon wafers (supplied by Professor Catrina Bryce, Optoelectronics Research Group, Department of Electronics and Electrical Engineering, The University of Glasgow)		
Step 2 to step 4 was done under vacuum (see section 3.5.2).			
Step 2	Heating of the glass above its T_g to make the sample soft.		
	Stage	Schedule	
	1.	From room temperature to 245°C in 1 hr	
	2.	Dwell at 245°C for 5 minutes	
Step 3	Application of load.		
	Sample id	Stage	Schedule
	MW39	1.	60 N for 15 mins
		2.	Pressure released.
Step 4	Annealing of the pressed sample.		
	Stage	Schedule	
	1.	Step to 180°C from 245°C	
	2.	Dwell at 180°C for 1 hr	
	3.	From 180°C to 140°C @ 5°C	
	4.	From 140°C to room temperature @ 20°C	

The results (see fig. 5.10) obtained show that the refractive index dispersion for the conventionally prepared AS-Se and DMO As-Se are almost identical except in the region of the bandgap. The bandgap absorption depends on the nature of the electron clouds within the bonding of the glass itself and so this may suggest a subtle difference in the bonding between the DMO and the conventionally prepared As-Se glasses. However, there is a sample to sample variation in measured refractive indices by the elipsometry.

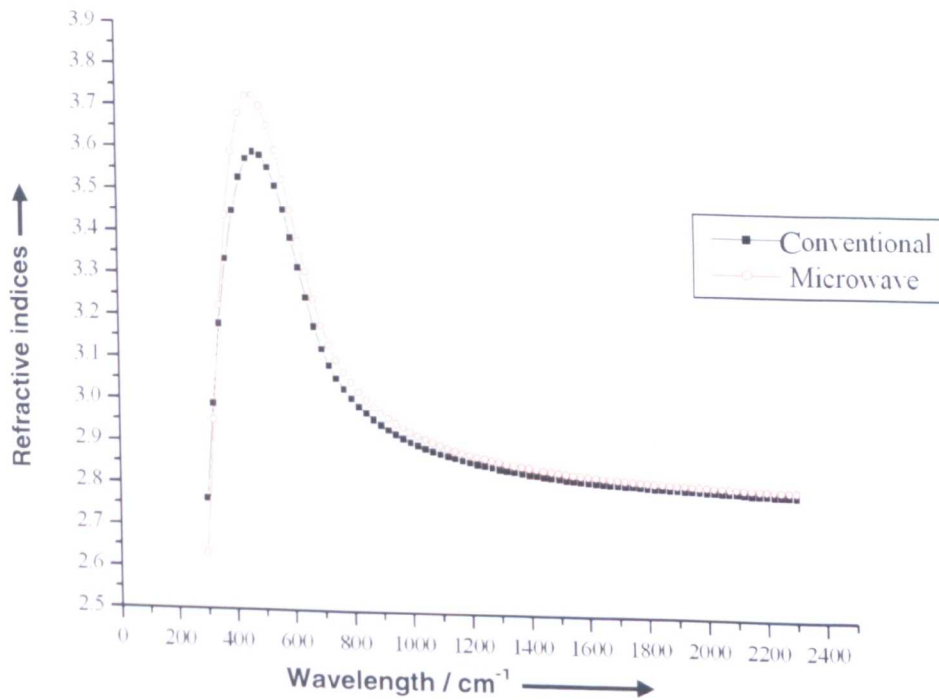


Fig. 5.10 Refractive indices of arsenic selenide at different wavelengths.

5.4 Further discussion

Since microwaves do not couple with the silica ampoule during the DMO synthesis, the temperature of the walls of the silica ampoule therefore must be lower during microwave heating than during the conventional heating; hence the heat flow from the glass-melt to the atmosphere is a favoured process. Hence, it is likely that the glass-melt was quenched more rapidly through the temperature range between the liquidus and T_g during microwave assisted synthesis than in the conventional heating. This could lead to formation of an amorphous material of slightly different molecular arrangement than the material formed through the conventional heating method. Concentrating only on the DMO rod product id: MW39, this was shown to be homogenised by means of ESEM EDS and was shown to be fully amorphous by means of XRD and TEM SAED. From DSC, the DMO rod product id: MW39 exhibited only one T_g and this matched that observed for the conventionally prepared id: CH12. Hence overall it is concluded here that the DMO product MW39 was indistinguishable from the conventionally prepared product id: CH12. Thus the evidence presented here tends to suggest that the DMO synthesis has not led to formation of an amorphous material of slightly different molecular arrangement than the material formed through the conventional heating method.

FTIR showed that the DMO As-Se product exhibited no OH band at about $2.9 \mu\text{m}$ nor molecular water band at $6.3 \mu\text{m}$ yet the conventionally prepared As_2Se_3 glass exhibited both

these bands. It is proposed that arsenic and selenium reacted during the early stage of the DMO heating, when the plasma formed, leading to the formation of the glass-melt and exclusion of *ie.* water did not dissolve into the glass-melt. Thus, because molecular water was excluded then the water did not hydrate the glass (bending vibrational absorption at 6.3 μm). Furthermore, water did not form hydroxide *via* hydrolysis (splitting of water molecule) because it failed to hydrate hence leading to the lower intensity band at 2.9 μm . The reaction time and temperature could be an important factor. While, making a chalcogenide glass through the resistance heating method, the glass-melt was in close contact with the silica glass ampoule for a long time as it had to be heated for about 32 hours at a high temperature. It is proposed that, due to the long reaction time, hydroxide and/or absorbed water contamination present in the surface of the silica ampoule was dissolved in the As-Se glass-melt. During microwave assisted synthesis the reactants were heated for only 35 mins furthermore the silica glass ampoule remained cool as it was not coupled into by the microwaves and hence reaction with hydroxide and/or water contamination adhered on the walls of the silica ampoule did not get much time nor were at high temperature to dissolve in the glass-melt leading to the diminished hydroxide and water bands.

The difference in the results obtained between the glasses from the conventional heating method and the microwave heating method could also may be attributed to the fact that the surface area of the powdered reactants (for the DMO reaction) were larger than the chunk reactants (used for conventional heating) which increased the possibility of the reaction with the carbon present in the evacuation line. It is not really understood why the DMO As-Se product exhibited FTIR bands due to carbon and C-H, whereas the conventionally prepared As_2Se_3 glass did not exhibit these bands. Perhaps, some carbon impurity was incorporated in the glass batch from the mortar and pestle during mechanical crushing of the reactants or from the oil pumps vapour during evacuation of the ampoule, but these effects are equally likely to occur for the DMO products as for the conventionally prepared products.

5.5 Summary

The above results showed that arsenic selenide glass of similar properties to those of conventionally prepared As_2Se_3 glass can be made through microwave heating in 35 minutes which gives a time advantage with respect to the conventional method which normally takes 32 hours. XRD demonstrates that DMO As-Se product was amorphous. In contrast to the DMO arsenic sulfide glass the DMO arsenic selenide (see section 4.1.4) glass showed a single glass transition temperature (T_g). The value of T_g of the DMO arsenic selenide glasses matched with the literature values as well as the conventionally prepared arsenic selenide glass. DMO arsenic selenide glass was observed by means of EDX to have close to the desired stoichiometry. This desired stoichiometry of the DMO arsenic selenide glass was obtained reproducibly. The hydroxide contamination was less in the DMO arsenic selenide glasses than the conventionally prepared arsenic selenide glasses. This result is consistent with the result obtained while preparing DMO arsenic sulfide glass (see section 4.3). Refractive indices of the DMO arsenic selenide glass were found to be slightly higher in the anomalous wavelength region (close to the optical band gap) than found for the conventionally prepared glass. Good agreement of refractive index in the normal spectral region, away from absorption bands, was found between the DMO and conventionally prepared glasses.

One sample of the DMO arsenic selenide glass was drawn to fibre successfully but unfortunately no signal throughput was obtained using FTIR (see later section 8.1) so this aspect would require greater investigation. The DMO arsenic selenide was hot embossed successfully when channels of depth were formed showing that the glass could be hot embossed (see latter section 8.2).

References

- [1] Swanson and Tatge., *Natl. Bur. Stand. (U.S.), Circ. 539* **1** (1953), p. 11.
- [2] J.A. Savage, *Infrared optical materials and their antireflection coatings*, Adam Hilger Ltd., Bristol, (1985).
- [3] W.A. King, A.G. Clare and W.C. LaCourse, *J. Non-Cryst. Solids* **181** (1995), p. 231.
- [4] D. Lezal, *J. Optoelect. & Adv. Mat* **5** (2003), p. 23.
- [5] C.T. Moynihan, P.B. Macedo, M.S. Maklad, R.K. Mohr and R.E. Howard, *J. Non-Cryst. Solids* **17** (1975), p. 369.
- [6] D. Lezal, J. Pedlikova and J. Zavadila, *Chalc. Lett.* **1** (2004), p. 11.
- [7] M.F. Churbanov, *J. Non-Cryst. Solids* **184** (1995), p. 25.
- [8] V.S. Shiryayev, S.V. Smetanin, D.K. Ovchinnikov, M.F. Churbanov, E.B. Kryukova and V.G. Plotnichenko, *Inorg Mater.* **41** (2005), p. 308.
- [9] M.F. Churbanov, V.S. Shiryayev, S.V. Smetanin, V.G. Pimenov, E.A. Zaitseva, E.B. Kryukova and V.G. Plotnichenk, *Inorg. Mater.* **37** (2001), p. 1188.
- [10] A.B. Seddon and C.A. Miller, Unpublished work, 2006.

Chapter 6

Microwave assisted synthesis of germanium arsenic selenide.

The synthesis of products from two different batch compositions composed of: germanium arsenic selenide, Ge/As/Se = 17/18/65 and Ge/As/Se = 33/12/55 at%, was attempted through microwave heating. Also glasses of these two batch compositions were prepared by conventional heating in a rocking resistance furnace. This chapter illustrates the observations made during the microwave irradiation of the starting materials, as well as the properties of the products made through the microwave heating method and those of products made *via* conventional resistance heating. In contrast to previous experience during the microwave assisted synthesis of arsenic selenide, when small glassy pellets were obtained (see section 5.1.2), a monolithic rod was always formed with these Ge-As-Se compositions because a short silica glass melting ampoule was always used (see section 6.1). Resistance melting of the compositions is presented in section 6.2. The results obtained for Ge/As/Se = 17/18/65 (at%) prepared *via* microwave heating are described in section 6.3.1 whereas the results obtained when effort was made to prepare Ge/As/Se = 33/12/55 (at%) *via* microwave heating are discussed in section 6.3.2.

6.1 Microwave irradiation of the starting materials and the formation of product rods.

Germanium, arsenic and selenium batch elements, of the specifications as described in section 3.1.1.2, as at% of Ge/As/Se = 17/18/65 and in the at% of Ge/As/Se = 33/12/55, were powdered individually manually (visually estimated diameter of the particles of the powdered reactants ≤ 0.2 mm) using a clean agate mortar and pestle (Fischer) in the ambient atmosphere inside the glove box (see section 3.1.1.3). The powdered reactants were mixed together in a plastic weighing boat (Fisher) using a clean stainless steel spatula (Fischer) before pouring into the silica glass ampoule. The ampoule, containing the reactants was evacuated and sealed as described in section 3.1.1.3. The silica glass ampoules, used for the preparation of Ge/As/Se products, irrespective of the heating method and composition, were purified as discussed in section 3.1.1.1. As discussed earlier the lengths of the silica glass melt-ampoules

were kept as small as possible so that the Ge/As/Se DMO-melt could collect at the bottom of the ampoule and a glass rod could be formed (see section 3.1.2.4 and see section 5.1). The length of the silica glass melt-ampoule was kept approximately at 10 cm in each experiment while making DMO Ge/As/Se product (see fig. 6.2 and fig. 6.3). The purity of reactants used for the preparation of Ge/As/Se products, irrespective of the microwave heating method, and the batch composition is described in section 3.1.1.2. Crushed arsenic was purified for the preparation of DMO products as described in section 3.1.1.2. Flashing could be seen within the first couple of seconds of heating for both of the compositions (fig 6.1) indicating that a plasma had formed. The DMO Ge/As/Se-melt was seen in both cases.



Fig. 6.1 An example of formation of plasma when a mixture of germanium, arsenic and selenium in the molar% of Ge/As/Se = 33/12/55 was exposed to microwaves is displayed.

A list of Ge/As/Se products prepared is given in Table 6.1.

Table 6.1 List of Ge/As/Se products prepared in this project.

Id	Batch Composition	Preparation		Resulting sample form (visual inspection)
		DMO	Conventional	
MW29	Ge ₁₇ As ₁₈ Se ₆₅	✓		Shiny rod divided into two parts Monolithic shiny rod
MW31	"	✓		
MW41	"	✓		
CH13	"		✓	"
CH14	"		✓	"
MW38	Ge ₃₃ As ₁₂ Se ₅₅	✓		"
MW46	"	✓		"
CH15	"		✓	"

Table 6.2 Summary of the make/model used for the preparation of DMO Ge/As/Se products, time of exposure to microwaves and the physical state of the starting material.

Id	DMO Make/Model	Power/ W	Exposure time / mins	Physical state of starting material		
				Ge	As	Se
MW29	DeLonghi/ EM821AAN	800	24 min 12 sec.	*	*	*
MW31	"	"	9 mins 50 sec.	*	*	*
MW41	Panasonic/ NN A554W (Convection DMO)	1000	11 mins. 20 sec	*	*	*
MW38	"	"	10 mins	*	*	*
MW46	"	"	8 mins 30 sec.	*	*	*

Key: * manually crushed inside the glove box.

The formation of the rod product from a batch in the atomic ratio of Ge/As/Se = 17/18/65 will be discussed in section 6.1.1 and the formation of rod product from batch in the atomic ratio Ge/As/Se = 33/12/55 is discussed in section 6.1.2.

6.1.1 Formation of DMO Ge/As/Se = 17/18/65 (at%) rod (id: MW29).

~ 5 minutes (though time not recorded) after the start of the DMO processing of the Ge/As/Se = 17/18/65 at% (id: MW29), the uppermost and the lowermost parts of the inside of silica-glass ampoule appeared black. A boiling red-coloured DMO Ge/As/Se = 17/18/65 melt was observed in the middle of the silica glass ampoule. After about 10 minutes, the uppermost black region started increasing in length downwards and the black region of the lower part of the ampoule was seen to be decreasing in length. It seems that the DMO Ge/As/Se = 17/18/65 melt that had reached the top of the ampoule perhaps could not trickle down due to the relatively high viscosity of the DMO Ge/As/Se = 17/18/65 melt (isoviscous temperature higher than arsenic selenide glass melt, T_g of As₂Se₃ is 180°C (see section 2.4.1.1 and section 5.3.2) whereas T_g of Ge₁₇As₁₈Se₆₅ is 245°C ± 5°C (see section 2.4.1.1 and section 6.3.1.2). The DMO Ge/As/Se = 17/18/65 melt remained stuck at the top of the ampoule presumably due to the high viscosity. After 11 minutes 23 seconds again a blue glow was observed in the middle of the ampoule. The upper part of the ampoule became heavier than the lower part as the plasma appeared responsible for pushing the Ge/As/Se = 17/18/65 DMO melt to the upper part of the ampoule. In fact the plasma force lifted the ampoule a couple of times. The ampoule was taken out of the DMO after 24 minutes and 12 seconds. The Ge/As/Se = 17/18/65 DMO melt (id: MW29) was air quenched and annealed *in situ* inside the ampoule at 245°C. Fig. 6.2 shows the ampoule after annealing containing the two zones of chalcogenide product: named here MW29 bulk_upper and MW29 bulk_lower.

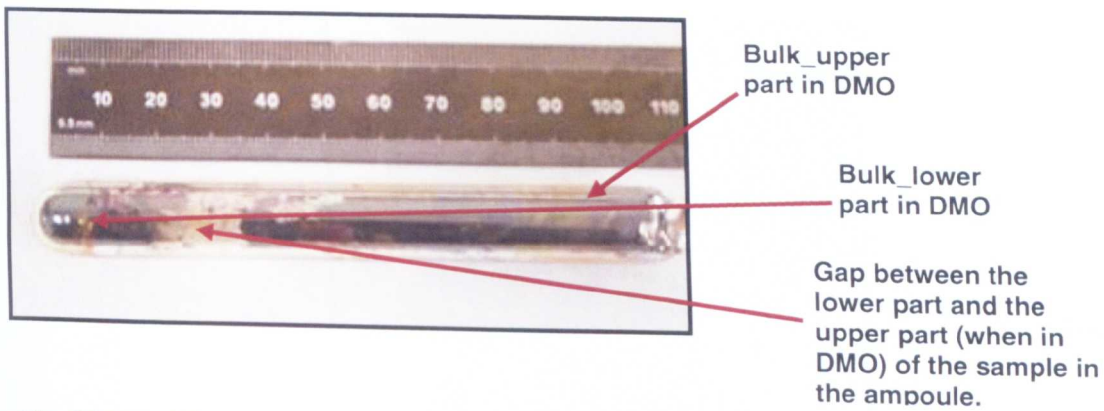


Fig. 6.2 The silica glass ampoule (coated inside with the chalcogenide product) and having two distinct regions: *bulk_upper* and *bulk_lower* (id: MW29, Ge/As/Se = 17/18/65 at%).

Ge/As/Se = 17/18/65 at% was again prepared (id: MW31) and again the boiling melt was observed. Again, after about 10 minutes of heating (exact time 9 minutes 50 seconds), the upper black portion of the ampoule was seen to be starting to increase in length downwards. The DMO was switched off after 9 minutes and 50 seconds and the DMO Ge/As/Se = 17/18/65 melt was air quenched *in situ* inside the ampoule followed by annealing *in situ*, again at 245°C. Figures 6.3 and 6.4 show the chalcogenide product (id: MW31) inside the silica glass melting ampoule after annealing and it is seen that in contrast to the previous product (id: MW29), the product was a monolithic rod. However, as discussed in the later section 6.3.1.3, some of the rod near the contraction cone adhered to the inner silica glass wall of the melting ampoule and exhibited some small holes at the rod surface (see fig. 6.21).

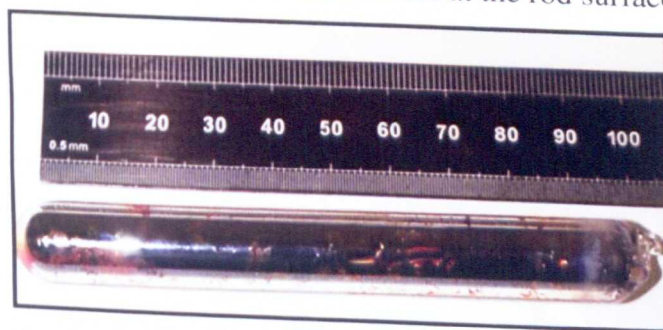


Fig. 6.3 The silica glass ampoule (coated with Ge/As/Se = 17/18/65 at% product) showing no zone separation (id: MW31). Compare fig. 6.2.



Figure 6.4 The chalcogenide product (id: MW31, Ge/As/Se = 17/18/65 at%) rod inside the silica glass ampoule partway through the process of removing it from the ampoule.

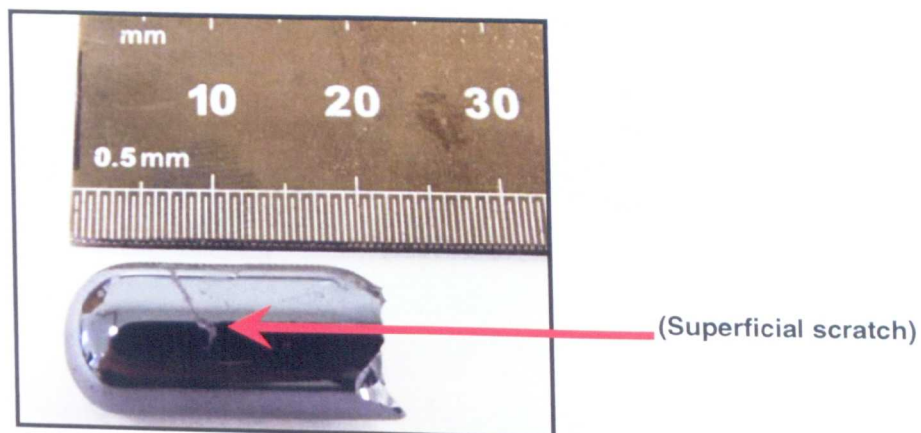


Fig. 6.5 The DMO Ge/As/Se = 17/18/65 product rod (id: MW31). (The product rod was scratched accidentally while taking it out from the silica glass melting ampoule.)

A Ge/As/Se = 17/18/65 (at%) batch (id: MW41) was then prepared using convection DMO when the reactants were heated to 220°C using the convection current before the microwave heating was started. The DMO took about 10 mins to achieve this temperature (220°C). The convection heating was switched off while the microwave heating was switched on. It was observed that the amount of chalcogenide glass adhering to the walls of the ampoule was less than in the previous experiments. Perhaps, the more elevated initial temperature helped raise the temperature of the silica glass container the DMO Ge/As/Se = 17/18/65 and helped the melt to drip down to the bottom of the ampoule. A glossy DMO Ge/As/Se = 17/18/65 rod was formed in this experiment.

6.1.2 Formation of Ge/As/Se = 33/12/55 (at%) rod (id: MW38 and MW46).

Similar to the above experiment (section 6.1.1), it was observed that for the Ge/As/Se batch at% 33/12/55 (id: MW 38), the melt started accumulating at the upper part of the silica glass melting ampoule after about 4 to 5 minutes (though exact time not recorded). Again the plasma appeared to be responsible for pushing the molten material to the upper part of the ampoule. The DMO was switched off after 10 minutes and id: MW38 was prepared. The DMO Ge/As/Se = 33/12/55 melt was air quenched and then annealed at 365°C *in-situ* inside the ampoule. Note that the DSC T_g was 365 °C ± 5°C see later section 6.3.2.2 and section 2.4.1.1. A DMO product rod was formed from Ge/As/Se = 33/12/55 mol%. A DMO Ge/As/Se = 33/12/55 rod (id: MW46) of the same nominal batch composition could be made using the convection microwave oven in 8 minutes 30 seconds (see fig. 6.6). The DMO was heated to 220°C before the start of the microwave heating which took ~ 10 minutes followed microwave irradiation for 8 minutes 30 seconds.

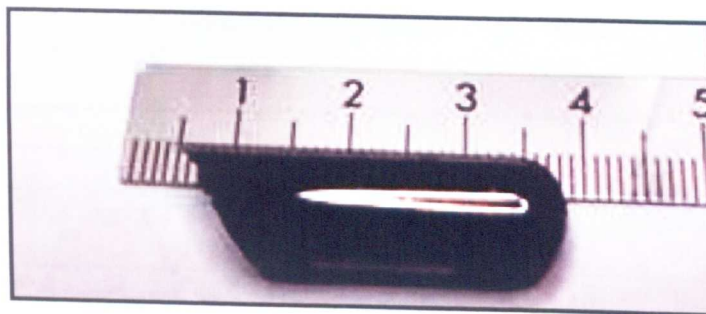


Fig. 6.6 The DMO $\text{Ge}_{33}\text{As}_{12}\text{Se}_{55}$ product rod (id: MW46).

The properties of DMO $\text{Ge}/\text{As}/\text{Se} = 17/18/65$ and $\text{Ge}/\text{As}/\text{Se} = 33/12/55$ (at%) products were compared with those of the $\text{Ge}_{17}\text{As}_{18}\text{Se}_{65}$ and $\text{Ge}_{33}\text{As}_{12}\text{Se}_{55}$ glasses made through conventional heating using rocking resistance furnace. The method of preparation *via* resistance heating is described in the next section 6.2.

6.2 Synthesis of $\text{Ge}_{17}\text{As}_{18}\text{Se}_{65}$ and $\text{Ge}_{33}\text{As}_{12}\text{Se}_{55}$ glasses *via* resistance heating.

The method of preparation of $\text{Ge}_{17}\text{As}_{18}\text{Se}_{65}$ glass through conventional heating is described in section 6.2.1 and that of $\text{Ge}_{33}\text{As}_{12}\text{Se}_{55}$ is described in section 6.2.2.

6.2.1 Synthesis of $\text{Ge}_{17}\text{As}_{18}\text{Se}_{65}$ glasses (id: CH13 and CH14) *via* resistance heating.

The ampoules were purified as discussed in section 3.1.1.1. The purity, and amount, of starting materials taken for the preparation of each of the $\text{Ge}_{17}\text{As}_{18}\text{Se}_{65}$ glasses (id: CH13 and CH 14) *etc.* is given in Table 6.3.

Table 6.3 Information about the materials taken for the preparation of $\text{Ge}_{17}\text{As}_{18}\text{Se}_{65}$ glasses (id: CH13 and CH14).

Id	Elements	Amount /(g)	Purity (%)	Source	Physical state
CH13	Ge	1.616	99.999	Cerac	*
	As	1.749	99.99999 ^P	Furukawa	*
	Se	6.652	99.999	Cerac	*
CH14	Ge	1.604	99.999	Cerac	*
	As	1.756	99.99999 ^P	Furukawa	*
	Se	6.656	099.999	Cerac	*

Key: *materials were crushed manually. ^P arsenic was purified after crushing (see section 3.1.1.2).

The starting materials as in Table 6.3 were taken in the purified silica glass ampoules. Each ampoule was then evacuated ($\sim 2.5 \times 10^{-4}$ Pa) and sealed as discussed in section 3.1.1.3. The batch was then melted according to the heating schedule in Table 6.4.

Table 6.4 Melting schedule of the conventionally prepared germanium arsenic selenide batched as $\text{Ge}_{17}\text{As}_{18}\text{Se}_{65}$ (atomic ratio) id: CH13 and CH14.

Stage	Schedule
1	20°C to 200°C @ 200°C/h
2	Start rocking at 250°C to 300°C (when Se has melted to avoid scratching inside walls of ampoule)
3	200°C to 930°C @ 40°C/h
4	Dwell at 930°C for 12 h
5	930°C to 800°C @ 40°C/h
6	Hold at 800°C for 1 to 2h
7	Switch of rocking mechanism and hold ampoule vertical inside rocking furnace for 15 min
8	Quench ampoule in air for ~ 45 s to ~ 60 s (for 10 g batch)

The quenched chalcogenide melt was placed in a preheated annealing furnace at 245°C and annealed according to the cooling schedule in Table 6.5.

Table 6.5 Annealing schedule of the conventionally prepared germanium arsenic selenide batched as $\text{Ge}_{17}\text{As}_{18}\text{Se}_{65}$ (at%), id: CH13 and CH14.

Stage	Schedule
1	Dwell at 240°C for 1 h
2	From 240°C to 200°C @ 5°C / h
3	200°C to 20°C @ 15°C / h

6.2.2 Synthesis of $\text{Ge}_{33}\text{As}_{12}\text{Se}_{55}$ glass (id: CH15) via resistance heating.

$\text{Ge}_{33}\text{As}_{12}\text{Se}_{55}$ glass (id: CH15) was prepared through conventional heating using the resistance rocking furnace. The method of preparation was as follows: germanium (3.14 g, Cerac, 5x9s), arsenic (1.18 g, Furukawa, 7x9ns purified as discussed in section 3.1.1.1), selenium (5.68 g, Cerac, 5x9s) were taken in a purified ampoule (see section 3.1.1.2). The ampoule was then evacuated ($\sim 2.5 \times 10^{-4}$ Pa) and sealed as described in section 3.1.1.3. It was then heated according to the schedule in Table 6.6.

Table 6.6 Melting schedule of the conventionally prepared germanium arsenic selenide batched as $\text{Ge}_{33}\text{As}_{12}\text{Se}_{55}$ (atomic ratio) (id: CH15).

Stage	Schedule
1	20°C to 200°C @ 200°C/h
2	Start rocking at 250°C to 300°C (when Se has melted to avoid scratching inside walls of ampoule)
3	200°C to 930°C @ 40°C/h
4	Dwell at 930°C for 12 h
5	930°C to 800°C @ 40°C/h
6	Hold at 800°C for 1 to 2h
7	Switch of rocking mechanism and hold ampoule vertical inside rocking

Stage	Schedule
	furnace for 15 min
8	Quench ampoule in air for ~45 - 60 s (for 10 g batch)

The quenched chalcogenide melt (id: CH15) was annealed according to the cooling schedule in Table 6.7.

Table 6.7 Annealing schedule of the conventionally prepared germanium arsenic selenide batched as Ge₃₃As₁₂Se₅₅ (at%), id: CH15.

Stage	Schedule
1	Dwell at 365°C for 1 h
2	From 365°C to 315°C @ 5°C / h
3	315°C to 20°C @ 15°C / h

6.3 Product characterisation.

The properties observed of DMO Ge/As/Se = 17/18/65 products (id: MW29, MW31 and MW41) were compared with those of the conventionally prepared Ge₁₇As₁₈Se₆₅ glass (id: CH13 and CH14) and are discussed in section 6.3.1. Similarly, DMO Ge/As/Se = 33/12/55 products (id: MW38 and MW46) were characterised and the results obtained were compared with conventionally prepared Ge₃₃As₁₂Se₅₅ glass (id: CH15) and as described in section 6.3.2.

6.3.1 Characterisation of DMO Ge/As/Se = 17/18/65 products (id: MW29, MW31 and MW41) and conventionally prepared products (id: CH13 and CH14).

6.3.1.1 Amorphicity.

The amorphous nature of the DMO Ge/As/Se = 17/18/65 product was observed through two techniques: i) powder X-ray diffraction (XRD) discussed in section 6.3.1.1.1 and ii) selected area electron diffraction (SAED) using the transmission electron microscope (TEM) discussed in section 6.3.1.1.2.

6.3.1.1.1 XRD.

The DMO chalcogenide product (Ge/As/Se = 17/18/65 (at%), id: MW29) was collected in three different parts (see section 6.1.1); each part was characterised separately, as follows:

- i) the chalcogenide product, as a visually shiny, small rod, obtained from the bottom of the silica glass melting ampoule formed from the melt collected there which will be called MW29 bulk_lower.

ii) the visually shiny product collected from the upper part of the silica glass melting ampoule formed from the glass-melt that reached the top of the ampoule during the boiling inside the DMO but could not trickle down apparently due to the high viscosity of the melt. This part will be named as MW29 bulk_upper;

iii) the visually shiny, curved thin film, that collected on the walls of the silica glass melting ampoule which will be named MW29_wall.

In contrast to the DMO As-S glass (id: MW6, see section 4.1.2) when the different parts of the DMO As-S product were visually different, here a similar looking product was obtained in all three parts of the sample in terms of the surface quality but not physical shape.

All three parts of the sample showed amorphous halos in the XRD pattern indicating that the product was amorphous throughout. Thus fig. 6.7 (a) shows the XRD pattern obtained from the lower part of the sample (id: MW29 bulk_lower) whereas fig. 6.7 (b) and fig. 6.7 (c) show the X-ray diffraction patterns of the upper part of the sample (id: MW29 bulk_upper) and the DMO chalcogenide product obtained from the walls of the sample (id: MW29_wall). The X-ray diffraction patterns (see figs. 6.7 (a) to 6.7 (c)) of the different portion of the product id: MW29 matched with each other and with the X-ray diffraction pattern of the conventionally prepared (see sec. 6.2.1) product id: CH14 (see fig. 6.7 (g)).

To confirm the reproducibility of the DMO reaction the well-established (by conventional melting) glass forming composition $\text{Ge}_{17}\text{As}_{18}\text{Se}_{65}$ was prepared repeatedly and then subjected to powder XRD. Two examples (id: MW31 and MW41) are displayed here (figs. 6.7 (d), 6.7 (e) and 6.7 (f), respectively) to provide more evidence that an amorphous material having batch composition $\text{Ge}/\text{As}/\text{Se} = 17/18/65$ could be prepared by DMO similar to that prepared by conventional resistance heating (fig 6.7 (g)) except for the product id: MW31 (fig. 6.7 (d)) where there is no hump at the angle of diffraction 2θ value 15° in the first run of the X-ray diffraction measurement. The reason for this was unclear. The sample (id: MW31) was again subjected for the powder X-ray diffraction when exactly similar pattern (hump at 15°) was obtained (see fig. 6.7 (g)) (data obtained on June 2009).

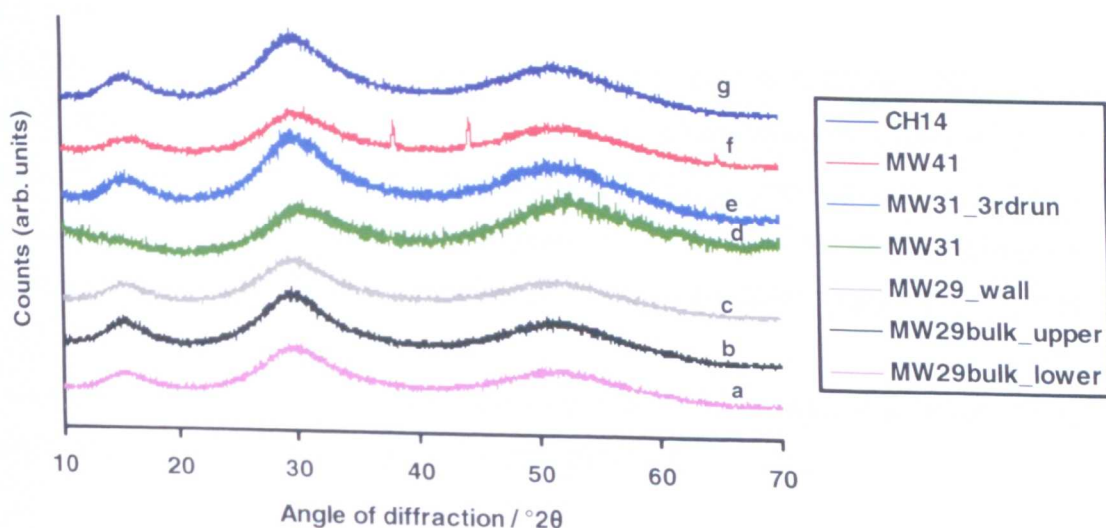


Fig. 6.7 The powder XRD pattern of

- the lower part of the DMO Ge/As/Se = 17/18/65 rod (id: MW29 bulk_lower).
- the upper part of the DMO Ge/As/Se = 17/18/65 rod (id: MW29 bulk_upper).
- DMO Ge/As/Se = 17/18/65 product (id: MW29_wall) showing it was amorphous.
- DMO Ge/As/Se = 17/18/65 product (id: MW31) showing that it was amorphous. Data multiplied with a factor of 3.
- DMO Ge/As/Se = 17/18/65 product (id: MW31) showing that it was amorphous.
- the glassy-looking DMO Ge/As/Se = 17/18/65 product (id: MW41) showing that it was amorphous. Note: sharp peaks are due to aluminium holder (see Table 6.8).
- the conventionally melted $\text{Ge}_{17}\text{As}_{18}\text{Se}_{65}$ glass (id: CH14)

The crystalline peaks observed in the XRD pattern obtained for product id: MW41 (see fig. 6.7 (f)) were analysed using Evaluation software and the results (Table 6.8) match peaks due to aluminium [1].

Table 6.8 Identification of the XRD peaks obtained for id: MW41 (see fig. 6.11).

Observed peaks angle $^{\circ}/2\theta$	Theoretical peaks for Al angle $^{\circ}/2\theta$ [1]
38.42	38.47
44.68	44.74

It is believed that, since an aluminium holder was used to hold the id: MW41 some of the X-rays might have reached the sample holder.

The XRD patterns of the DMO Ge/As/Se = 17/18/65 amorphous products were indistinguishable from that of conventionally melted $\text{Ge}_{17}\text{As}_{18}\text{Se}_{65}$ glass (figures 6.7 (a) to 6.7 (f)) could be compared with figure 6.7 (g)). The amorphicity of the DMO glass was further investigated by performing selected area electron diffraction (SAED) using transmission electron microscopy (TEM) and is discussed below in section 6.3.1.1.2.

6.3.1.1.2 TEM SAED.

TEM SAED was performed to investigate further the amorphicity of the DMO Ge/As/Se = 17/18/65 rods compared with the results obtained for conventionally melted glass. Blurred electron diffraction rings were obtained from TEM SAED (see fig. C-1 and fig. C-2 of [Appendix 'C']) showing that the DMO products id: MW29 and MW31 were amorphous and suggesting the absence of any fine crystalline structure in the DMO Ge/As/Se = 17/18/65 rods.

The conventionally melted Ge₁₇As₁₈Se₆₅ glass (id: CH14) was subjected to TEM SAED when a blurred structure was obtained (fig. C-3 [Appendix 'C']).

The above TEM SAED results suggested that an amorphous material could be made from the batch composition Ge/As/Se = 17/18/65 *via* microwave heating including combined convection and microwave heating and that it was of similar amorphous nature to that of the conventionally melted Ge₁₇As₁₈Se₆₅ glass.

6.3.1.2 Thermal analysis of DMO Ge/As/Se = 17/18/65 products (id: MW29, MW31) and conventionally melted product Ge/As/Se = 17/18/65 (id: CH13).

The glass transition temperature (T_g) of DMO Ge/As/Se = 17/18/65 products was evaluated using differential scanning calorimetry (DSC) (see section 3.3.3) and with differential thermal analysis (DTA) (see section 3.3.4). Thus sample id: MW31 (DMO Ge/As/Se = 17/18/65) was analysed using both methods DTA and DSC whereas sample id MW29 (DMO Ge/As/Se = 17/18/65) and sample id: CH13 (conventionally melted Ge₁₇As₁₈Se₆₅ glass using rocking resistance furnace) were analysed using only DSC. The result obtained from DTA for DMO product id: MW31 is described in section 6.3.1.2.1 and the results obtained from DSC analysis for DMO products id: MW29 and MW31 and CH13 are described in section 6.3.1.2.2. The DSC result for conventionally prepared product id: CH13 is presented in section 6.3.1.2.3.

6.3.1.2.1 Evaluation of T_g of DMO Ge/As/Se = 17/18/65 (id: MW31) using DTA.

140.0 mg of the DMO product Ge/As/Se = 17/18/65 (id: MW31) was subjected to DTA. At T_g the sample temperature will tend to be lower than the reference temperature. Figure 6.8 displays the DTA curve (the sample and the reference DTA ampoules were heated at a rate of $10^\circ\text{C}/\text{min}$).

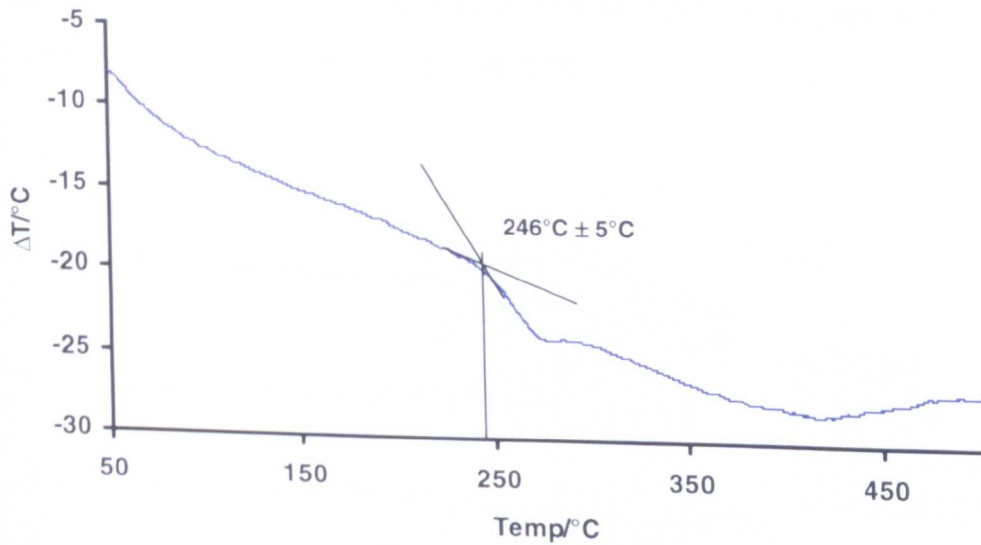


Fig 6.8 DTA curve showing the T_g value of DMO Ge/As/Se = 17/18/65 (id: MW31).

The onset of T_g was evaluated to be 246°C using DTA software (Perkin Elmer). The T_g value matched with the literature value of 236°C for $\text{Ge}_{17}\text{As}_{18}\text{Se}_{65}$ (see section 2.4.1.1) [2]. This shows that the stoichiometry of the glass was close to $\text{Ge}_{17}\text{As}_{18}\text{Se}_{65}$. This suggests that $\text{Ge}_{17}\text{As}_{18}\text{Se}_{65}$ glass was prepared through microwave heating. The above results were further confirmed by the measurement of T_g using DSC, since DSC is a more sensitive and quantitative method than DTA. In DSC, the samples were cold-sealed in aluminium pans which provided a better thermal contact with the thermocouples inside the calorimeter than in the DTA where the samples were sealed in silica glass ampoules (*ca.* 1 mm wall thickness see section 3.3.3) under vacuum. Silica is a worse conductor of heat than aluminium and vacuum increased the thermal inertia of the system. In addition, the greater mass of sample used for the DTA measurement also provides greater thermal inertia. DSC identifies the change in phase with the amount of heat absorbed (or released) by the sample than the reference.

6.3.1.2.2 Evaluation of T_g Ge/As/Se = 17/18/65 (at %) products.

T_g values for Ge/As/Se = 17/18/65 (at %) products (irrespective of the heating method) were evaluated using DSC. Table 6.9 enlists the amounts of products taken for this purpose.

Table 6.9 Amounts of products taken for evaluation of Tg using DSC.

Sample id	Amount of the sample taken in DSC pan / mg
CH13	13.13
MW31	12.84
MW29_bulk upper	11.93
MW29_bulk lower	12.53

The above stated amounts of products (see Table 6.9) were sealed in an aluminium pan covered with an aluminium lid and heated from 40°C to 300°C at the rate of 10°C/minute. The DSC curves obtained are shown in fig. 9 (a) to (d).

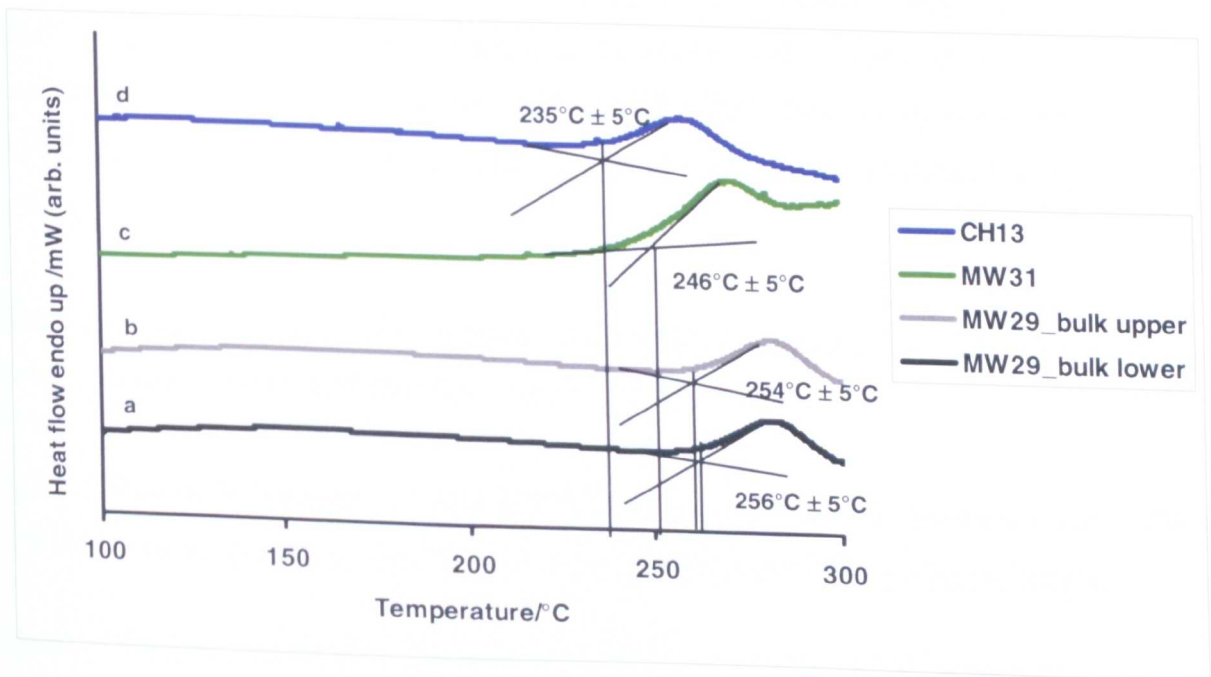


Fig. 6.9 DSC curve showing the Tg value of

- DMO Ge/As/Se = 17/18/65 product (id: MW29 bulk_lower).
- DMO Ge/As/Se = 17/18/65 product (id: MW29 bulk_upper).
- DMO Ge/As/Se = 17/18/65 product (id: MW31).
- conventionally melted $\text{Ge}_{17}\text{As}_{18}\text{Se}_{65}$ glass (id: CH13).

The onset of Tg was calculated using the software provided by Perkin and Elmer. It was observed that the DSC Tg value for MW29_bulk lower and MW29_bulk lower was $254^\circ\text{C} \pm 5^\circ\text{C}$ and $256^\circ\text{C} \pm 5^\circ\text{C}$, respectively, for the two zones.

DSC runs of different samples taken from the DMO melt product (id: MW31) (see fig. 6.9 (c)) showed Tg at $246^\circ\text{C} \pm 5^\circ\text{C}$ which was the same as the DTA Tg for this product (see fig. 6.8). The DSC Tg value obtained for DMO Ge/As/Se = 17/18/65 amorphous material may be compared with literature value 236°C [2].

The above results, of DTA and DSC Tg of the DMO products, were compared with that of the conventionally melted $\text{Ge}_{17}\text{As}_{18}\text{Se}_{65}$ glass (id: CH13) (fig. 6.9 (d)). From fig. 6.9 (d), the DSC Tg of the conventionally prepared $\text{Ge/As/Se} = 17/18/65$ (at %) (id: CH13) was measured to be $235^\circ\text{C} \pm 5^\circ\text{C}$ (see section 2.4.1.1).

This DSC Tg of the conventionally prepared product of $235^\circ\text{C} \pm 5^\circ\text{C}$ was lower than the DSC and DTA Tg observed for the DMO product id: MW31 of $246^\circ\text{C} \pm 5^\circ\text{C}$ and DSC Tg observed for the DMO product id: MW29 of $255^\circ\text{C} \pm 6^\circ\text{C}$ (mean value). Because the DMO product id: MW29 separated into two zones during the preparation it is suggested that the Tg result of DMO product id: MW31, which formed a monolithic rod, is more reliable. Taking into consideration the errors $\pm 5^\circ\text{C}$, then the DSC and DTA Tg of DMO product id: MW31 ($246^\circ\text{C} \pm 5^\circ\text{C}$) was reasonably close to the DSC Tg of the conventionally prepared glass ($235^\circ\text{C} \pm 5^\circ\text{C}$).

The stoichiometry of the DMO products was further investigated by ESEM EDX and the results are discussed in the following section 6.3.1.3.

6.3.1.3 The stoichiometry of the DMO and conventionally prepared $\text{Ge/As/Se} = 17/18/65$ (at%) products (id: MW29 and MW31, and CH13, respectively).

Some of the DMO $\text{Ge/As/Se} = 17/18/65$ (at%) products were analysed for stoichiometry using ESEM EDX (see section 3.4.6). For DMO product id: MW31 (see fig. 6.5), although a product in the form of a complete rod was obtained, some of the rod near the contraction cone adhered to the silica glass wall of the melting ampoule and exhibited some small 'holes' at the rod surface. Section 6.3.1.3.1 discusses the ESEM EDX of this rod near to the holes and section 6.3.1.3.2 discusses a more representative sample of the bulk rod.

6.3.1.3.1 EDX analysis of the DMO $\text{Ge/As/Se} = 17/18/65$ (at%) rod product(id: MW31) that had adhered to the silica glass melting ampoule.

As discussed above (section 6.3.1.3), the surface of the DMO glass (sample id: MW31) that adhered to the ampoule exhibited some holes (see fig. 6.10 a & b).

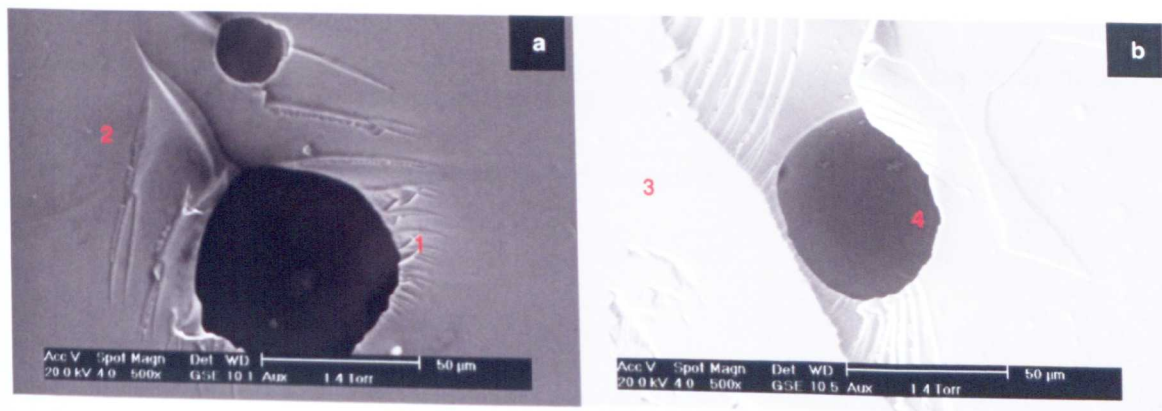


Fig. 6.10 (a&b) ESEM micrographs showing $\sim 20\ \mu\text{m}$ – $\sim 50\ \mu\text{m}$ diameter holes in the surface of the DMO Ge/As/Se = 17/18/65 (at%) rod product (id: MW31) where the rod had adhered to the inside wall of the silica glass melting ampoule. The periphery of the holes was analysed using EDX (see Table 6.8).

The holes, imaged in fig. 6.10, show that there may have been some bubbles trapped in the DMO melt (id: MW31) as it cooled, possibly from boiling of the melt in the DMO. One fractured surface, where the surface of the rod had been adhered to the walls of the silica glass ampoule (fig. 6.11) was analysed using EDX (Table 6.10).

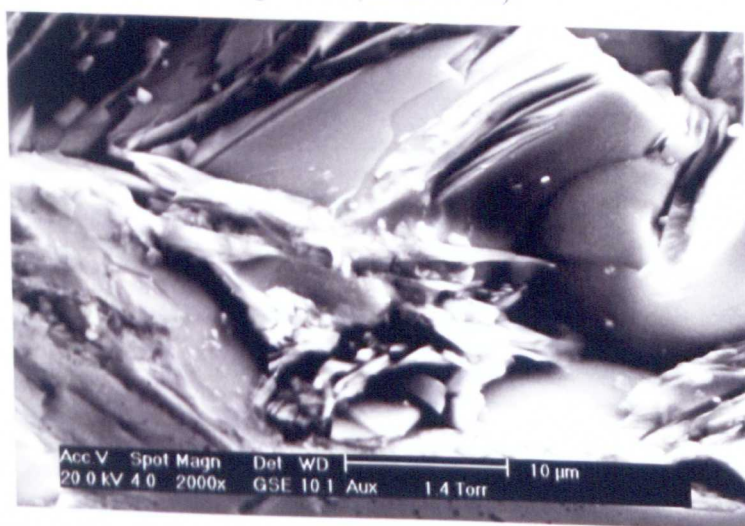


Fig. 6.11 ESEM micrograph showing the fracture surface of the DMO Ge/As/Se = 17/18/65 (at%) (id: MW31) where it had adhered to the inner walls of the silica glass melting ampoule. This fracture surface was analysed using EDX (Table 6.10).

During the ESEM EDX analysis of this sample, it was observed that the X-ray intensity captured by the detector was low giving low counts per second and hence the data obtained were not very reliable, though all values obtained are listed below in Table 6.10. The extreme of this phenomenon was again observed when the inner surface of the holes of the sample were attempted to be analysed and the X-rays captured by the detector (counts per second) were extremely low and hence the data were not reliable (verbal communication Dr. Nigel Neate and Mrs. Nikky Weston).

Table 6.10 Stoichiometry of the DMO Ge/As/Se = 17/18/65 (at%) product adhered to the silica glass melting ampoule (id: MW31).

Obs.*	Area chosen for analysis	Counts/ s ⁻¹	Elements / at%			
			Ge	As	Se	Total
1.	Clean surface at the edge of the hole as shown by the number '1' in the image 6.10 (a).	1680 (low)	21.3	14.9	64.0	100.2
2.	Clean surface away from the hole as shown by the number '2' in the image 6.10 (a).	Acceptable > 2000	17.3	18.3	64.4	100.0
3.	Clean surface at the edge of the hole as shown by the number '1' in the image 6.10 (a).	"	17.6	17.8	64.7	100.1
4.	Surface inside the hole as shown by the number '4' in the image 6.10 (b).	> 1300	Unreliable data.			
5.	Fractured surface (fig. 6.11). The overall area was analysed.	1387 (Low)	20.6	22.6	56.8	100.0
Theory			17.0	18.0	65.0	100.0

*Key: Obs: Observation.

From Table 6.10 it is evident that the stoichiometry of the fractured part of the DMO Ge₁₇As₁₈Se₆₅ glass (MW31) deviated from the expected value as did the interior of the observed holes in the glass rod surface. As described previously in this section this unexpected result might be attributable to the shape (either holes or fracture) of the glass sample from where the required amounts of X-rays are not generated, and hence the results are spurious and probably due to artefacts.

6.3.1.3.2 EDX analysis of the middle part of the DMO Ge/As/Se = 17/18/65 (at%) rod product (id: MW31) compared to that of the conventionally prepared Ge/As/Se = 17/18/65 (at%) product (id: CH13).

The DMO Ge/As/Se = 17/18/65 (at %) rod product (id: MW31) was cut using a diamond wafering blade. The sample was flat and no holes were observed and during EDX analysis the X-ray counts per second were found to be large enough to be relied upon. The results obtained are summarised in Table 6.11.

Table 6.11 Stoichiometry according to ESEM EDX analysis of middle part of the DMO Ge/As/Se = 17/18/65 (at%) (id: MW31).

Observation	Elements/ at%			
	Ge	As	Se	Total
1.	17.3	19.1	63.6	100.0
2.	17.2	19.7	63.1	100.0
3.	17.2	19.0	63.8	100.0
4.	16.7	19.7	63.6	100.0
Mean	17.1	19.4	63.5	
Standard deviation	0.3	0.4	0.3	
Theory	17.0	18.0	65.0	100.0

Table 6.11 shows that the atomic percentage of selenium in the bulk glass was slightly less (mean 63.5) than the desired value (65.0). To investigate the reproducibility of the DMO preparation of Ge/As/Se = 17/18/65 (at%) was repeated and the stoichiometry of the new rod product (id: MW41) was studied using EDX. Table 6.12 enlists the observed values and again it was found that the mean observed selenium content (63.5) was lower than that batched (65.0).

Table 6.12 Stoichiometry according to ESEM EDX of middle part of the DMO Ge/As/Se = 17/18/65 (at%) (id: MW41).

Observation	Elements/ at%			
	Ge	As	Se	Total
1.	17.4	18.4	64.2	100.0
2.	18.2	18.2	63.0	99.4
3.	18.0	18.9	63.2	100.1
4.	18.0	18.2	63.8	100.0
5.	17.9	19.3	62.9	100.1
6.	18.3	18.9	62.8	100.0
7.	17.8	17.3	64.9	100.0
Mean	17.9	18.5	63.5	
Standard deviation	0.3	0.6	0.8	
Theory	17.0	18.0	65.0	100.0

From Tables 6.11 and 6.12 it can be concluded that the stoichiometry of the DMO products id: MW31 and id: MW41 exhibits a lower amount of selenium than the expected value. The standard deviation for id: MW41 was higher (0.8) than that of id: MW 31 (0.3), but still acceptable for the analytical method.

Possibly, some of the material was lost as the gas H_2Se during the DMO preparation. But a simpler explanation is that during crushing of the selenium shot for batching some was lost due to the difficulty of crushing and also of batching powder in the dry atmosphere of the glovebox which led to static problems. Hence, to compare this result with the conventionally melted glass and to examine whether this deviation in the stoichiometry was due to the batching procedure, the starting materials (germanium, arsenic, selenium) were crushed, before conventional heating in a rocking resistance furnace of product Ge/As/Se = 17/18/65

(at%) id:CH13. The ESEM EDX stoichiometry results obtained for product id: CH13 are summarised in Table 6.13.

Table 6.13 Stoichiometry by means of ESEM EDX of conventionally melted $\text{Ge}_{17}\text{As}_{18}\text{Se}_{65}$ glass (id: CH13).

Observation	Elements/ at%			
	Ge	As	Se	Total
1.	17.8	18.9	63.3	100.0
2.	17.9	19.1	63.0	99.4
3.	17.3	19.2	63.5	100.1
4.	17.7	18.5	63.7	100.0
5.	18.0	19.8	62.2	100.1
6.	17.1	19.4	63.6	100.0
Mean	17.6	19.2	63.2	100.0
Standard deviation	0.4	0.4	0.5	
Theory	17.0	18.0	65.0	100.0

Table 6.13 reveals that the conventionally melted $\text{Ge}_{17}\text{As}_{18}\text{Se}_{65}$ glass (id: CH13) also showed deviation in the observed selenium value (63.2 at% mean) from the expected value (65.0 at%). The atomic percentage of selenium was less than the required value. Thus a deviation in the measured stoichiometry of the $\text{Ge}_{17}\text{As}_{18}\text{Se}_{65}$ glass, irrespective of the heating methodology may be attributed to the batching methodology where the starting materials were crushed and eventually some of the material is not transferred effectively which is reflected in the EDX analysis of the samples.

A second explanation is that H_2Se irreversibly vaporised into the silica glass melting ampoule and hence was lost from the melt.

Thus the stoichiometry of the DMO Ge/As/Se = 17/18/65 products was comparable to that of conventionally melted $\text{Ge}_{17}\text{As}_{18}\text{Se}_{65}$ glass.

Some of the EDX spectra files obtained for stoichiometry measurement of DMO Ge/As/Se = 17/18/65 product id: MW31 using ESEM are displayed (see fig. C-4 (a) to (d) of [Appendix C]) here in evidence that this was made through microwave heating.

6.3.1.4 Measurement of optical transmission window using FTIR.

Since $\text{Ge}_{17}\text{As}_{18}\text{Se}_{65}$ glass is an infrared transmitting material, the samples prepared here (irrespective of heating methodology) were cut and polished and subjected to Fourier transform infrared (FTIR) spectroscopy to study the range of wavelengths in the infrared region in which glass transmits the light and the influence of impurities. The glass samples were cut and polished as described in section 3.2.3.2. Infrared spectra were collected in the

wavelength region of 2 μm to 12 μm as described in section 3.3.5. Fig 6.24 displays the FTIR spectrum of DMO Ge/As/Se = 17/18/65 (at %) id: MW31 and fig 6.25 presents the FTIR spectrum of Ge₁₇As₁₈Se₆₅ glass id: MW13 made through conventional heating.

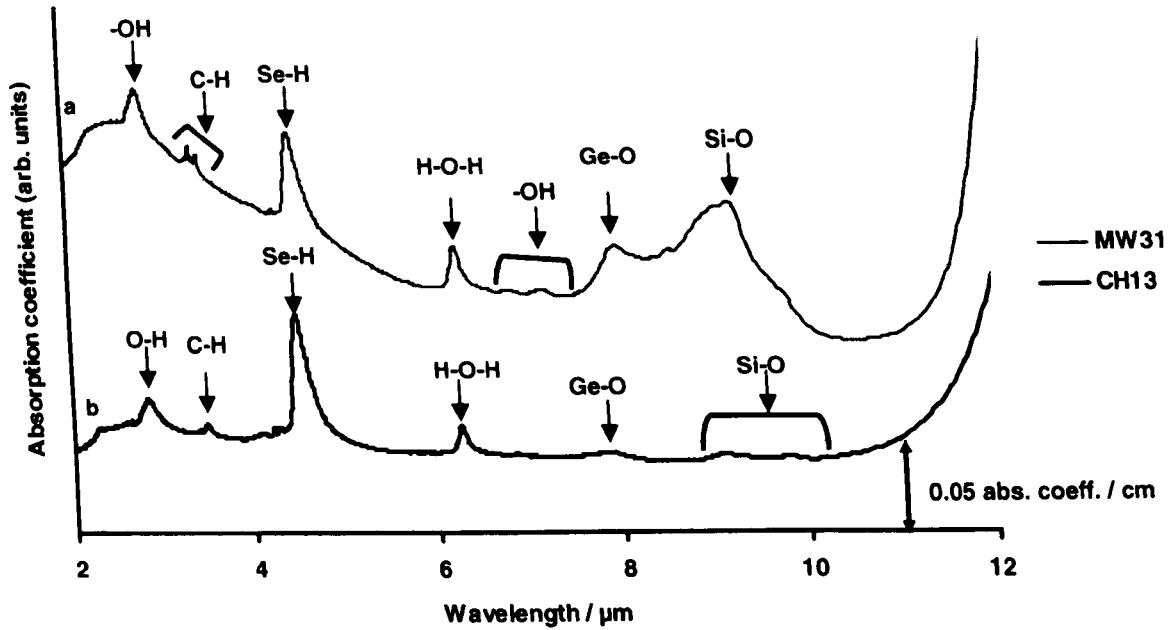


Fig. 6.12 FTIR absorption spectrum of

(a) DMO Ge/As/Se = 17/18/65 (at%) (id: MW31, path length of sample = 3.2 mm).

(b) Conventionally prepared Ge₁₇As₁₈Se₆₅ glass (id: CH13, path length of the sample = 6.15 mm).

Figs. 6.12 (a) and 6.12 (b) show the absorption bands of impurities present for the products and the observed bands are listed and assigned in the following Table 6.14.

Table 6.14 FTIR absorption bands observed for in the DMO product Ge/As/Se = 17/18/65 at % id: MW31 and the conventionally prepared Ge₁₇As₁₈Se₆₅ glass id: CH13.

OBSERVED FTIR BANDS				LITERATURE		
DMO prepared		Conventionally prepared		Wv / μm	Assign.	Ref.
Ge/As/Se = 17/18/65		Ge ₁₇ As ₁₈ Se ₆₅ glass				
Wv / μm	Abs coeff / cm^{-1}	Wv / μm	Abs coeff / cm^{-1}			
2.88	0.010	2.88	0.010	2.9	O-H	[3]
3.43	0.003	-	-	3.4	C-H	[4]
3.52	0.060	3.52	0.010	3.5	Se-H	[5]
4.53	0.050	4.53	0.060	4.5	Se-H	[6]
6.29	0.010	6.29	0.020	6.3	H-O-H	[6]
6.95	0.010	-	-	7.0	C-H	[3]
7.28	0.002	-	-	8.0	Ge-O	[7]
8.05	0.01	7.95	0.001	8.0	Se-O	[7]
9.29	0.02	9.20	0.001	9.3	Si-O	[3]

Key: Wv / μm : Wavelength / μm , Abs coeff / cm^{-1} = Absorption coefficient per cm

The absorption band at 2.9 μm due to hydroxide contamination in the DMO Ge/As/Se = 17/18/65 (at%) product (id: MW31) was the same intensity as for the $\text{Ge}_{17}\text{As}_{18}\text{Se}_{65}$ glass made through conventional heating. The $\sim 6.3 \mu\text{m}$ H-O-H bending absorption band was very slightly broader for the $\text{Ge}_{17}\text{As}_{18}\text{Se}_{65}$ glass made *via* conventional heating method but again of similar intensity. This result is similar to the results obtained when comparisons of FTIR OH, H-O-H absorption bands for DMO As_2Se_3 and conventionally prepared As_2Se_3 (section 5.3.4). The intensity of absorption due to hydroxide and water contamination here cannot be attributed to the heating methodology as discussed in the previous chapters (see section 4.3 and section 5.3.4).

The appearance of the C-H absorption band at 3.4 μm and at 6.95 μm in the FTIR spectrum of the DMO Ge/As/Se = 17/18/65 (at%) id: MW31 product could not be attributed to the batching methodology which was kept the same while making the DMO $\text{Ge}_{17}\text{As}_{18}\text{Se}_{65}$ glass (sample id: MW31) and $\text{Ge}_{17}\text{As}_{18}\text{Se}_{65}$ glass made through the conventional heating method (sample id: CH13). It should not be attributed to the arsenic purification method as well since the same method of arsenic purification was employed irrespective of the heating method (for comparison purposes). It cannot be argued that the appearance of C-H impurity in id: MW31 is due to the arsenic purification method where arsenic was purified after crushing and it could be said that that during purification under vacuum arsenic crushed arsenic (having more reaction sites where the exposed surface area is more than the lump arsenic) might have reacted with the carbon coming from the oil of the pumps attached with the evacuation line as arsenic was purified after crushing irrespective of the method. Perhaps, the mortar and pestle used for crushing the other two reactants (germanium and selenium while batching the material) contained traces of acetone, as acetone was used to clean the mortar and pestle or the weighing boat used might have some contamination. It might also be possible that the silica ampoule used for the synthesis of DMO Ge/As/Se = 17/18/65 (at%) id: MW31 glass was not as pure as the silica ampoule used for the preparation of $\text{Ge}_{17}\text{As}_{18}\text{Se}_{65}$ glass *via* conventional heating method. Though it may be considered that due to the formation of blue plasma the reactants attain a very high temperature and form ions. These ions collide with the walls of the silica ampoule and carbon adhered to the walls of the ampoule dissolved in the glass-melt. Importantly, it has been found in previous work in our laboratory that the carbon can be present at the surface of samples due to the diamond paste used for polishing of glass samples for FTIR measurement [8].

The impurity absorption bands for Se-H bond at 3.5 μm and 4.5 μm were obtained for both the samples: MW31 and CH13. It is believed that this contamination came from the starting material. Similarly, an absorption band of Ge-O was observed at 8 μm for both samples, and

the oxide was believed to be present in the starting materials. One weak absorption band due to Si-O was observed at $9.2\ \mu\text{m}$ and a strong absorption band was observed at $9.3\ \mu\text{m}$ in the DMO $\text{Ge}_{17}\text{As}_{18}\text{Se}_{65}$ glass yet was not present in the spectrum of conventionally prepared glass. This difference in results might have been due to the formation of plasma during the DMO processing when the very hot ionic reactants collided with the walls of the silica glass melting ampoule resulting in some dissolution of silica in the glass-melt. It might also have been possible that some silica fume was trapped during the silica ampoule sealing as described in the previous chapter (see section 5.3.4).

The DMO $\text{Ge}_{33}\text{As}_{12}\text{Se}_{55}$ glass was also characterised and the results obtained are discussed in the following section 6.2.2.

6.3.2 Characterisation of DMO Ge/As/Se = 33/12/55 product (id: MW38) and conventionally prepared product (id: CH15).

6.3.2.1 Amorphicity.

The DMO product Ge/As/Se = 33/12/55 (at%) (id: MW38) obtained (see section 6.1.2 for preparation) was powdered and subjected to X-ray diffraction (XRD) (see section 6.3.2.1.1) and selected area electron diffraction (SAED) using transmission electron microscopy (TEM) (see section 6.3.2.1.2) to investigate amorphicity of the sample compared to that of the conventionally prepared glass $\text{Ge}_{33}\text{As}_{12}\text{Se}_{55}$ id: CH15 .

6.3.2.1.1 XRD.

The DMO Ge/As/Se = 33/12/55 (at%) (id: MW38) as prepared rod was cut, powdered and subjected to powder XRD when amorphous humps were observed with one crystalline peak at $32.5^\circ 2\theta$ (fig.6.13 (a)).

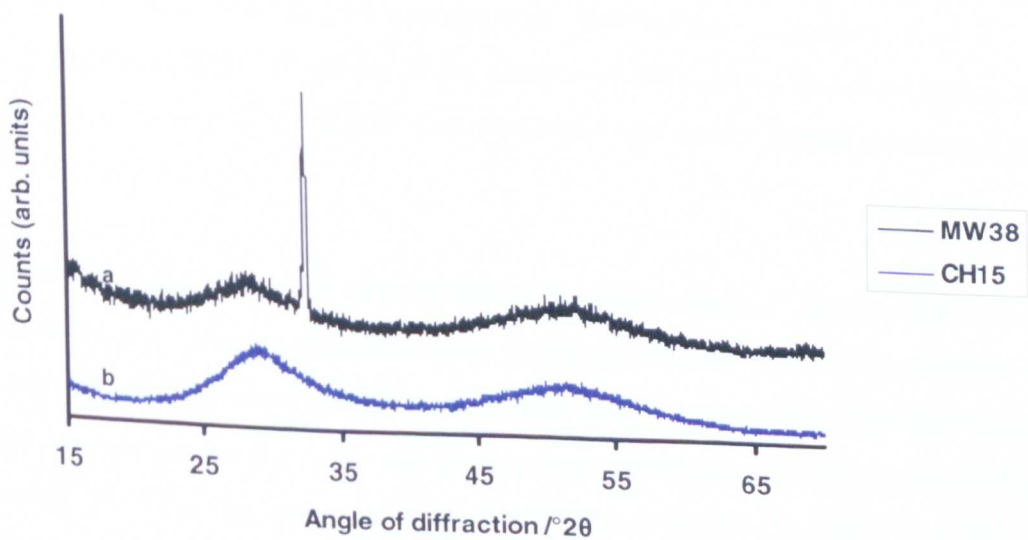


Fig. 6.13 XRD pattern of the
(a) DMO Ge/As/Se = 33/12/55 product (id: MW38).
(b) conventionally prepared $\text{Ge}_{33}\text{As}_{12}\text{Se}_{55}$ product (id: CH15).

The $32.5^\circ\theta$ peak obtained in the XRD pattern matches with no known species and therefore the contaminant is unknown. It is possibility that the DMO melt did not dissolve all of the bath elements which remained in their crystalline form as when batched. This suggests that the DMO melt should be exposed to the microwaves for a longer period of time. In contrast to the above result, a conventionally melted $\text{Ge}_{33}\text{As}_{12}\text{Se}_{55}$ glass (id: CH15) was found to be completely amorphous without any crystalline peaks (see fig. 6.13 (b)).

6.3.2.1.2 TEM SAED.

The DMO sample $\text{Ge}/\text{As}/\text{Se} = 33/12/55$ (at%) (id: MW38) was subjected to TEM SAED when a blurred ring structure was obtained showing the absence of any crystalline structure (fig. C-5 [Appendix C]). Thus, since in SAED a few microns area of the sample could be studied there is the chance of missing important information such as the presence, in other areas of the sample, of the crystalline selenium.

The conventionally melted $\text{Ge}/\text{As}/\text{Se} = 33/12/55$ (at%) (id: CH15) product was found to have no crystallinity according to TEM SAED (fig. C-6 [Appendix C]) which is consistent with the result using XRD (fig. 6.13 (b)).

From the above results it can be concluded that a $\text{Ge}/\text{As}/\text{Se} = 33/12/55$ (at%) product could be made through microwave heating with partial success. The T_g of the DMO product was determined using DSC (see section 6.3.2.2).

6.3.2.2 Thermal analysis of DMO $\text{Ge}/\text{As}/\text{Se} = 33/12/55$ (at%) product (id: MW38) and conventionally melted product $\text{Ge}_{33}\text{As}_{12}\text{Se}_{33}$ (id: CH15).

T_g of the DMO $\text{Ge}/\text{As}/\text{Se} = 33/12/55$ product (id: MW38) was evaluated using differential scanning calorimetry (DSC). 15.98 mg of the material (DMO $\text{Ge}/\text{As}/\text{Se} = 33/12/55$, sample id: MW38) was heated from 40°C to 400°C at $10^\circ\text{C}/\text{min}$ in a sealed, lidded aluminium pan (see section 3.3.4) (fig. 6.14 (a)).

From fig. 6.14 (a), the numerical value of the extrapolated onset of T_g was $368^\circ\text{C} \pm 5^\circ\text{C}$, as calculated using the software (Perkin Elmer) supplied with the DSC. Observation of a T_g showed that the DMO product was at least partially glassy and that the glass that had formed was mainly homogeneous (i.e. only one glass composition present) because multi- T_g s were not observed. This may be compared with that observed by W. Pan (W J Pan PhD thesis). From XRD (see fig. 6.13 (a)), at least one crystalline species is known to be present in this

product but the DSC curve in fig. 6.14 (a) would not have been affected by this unless the crystals had melting point below 368°C.

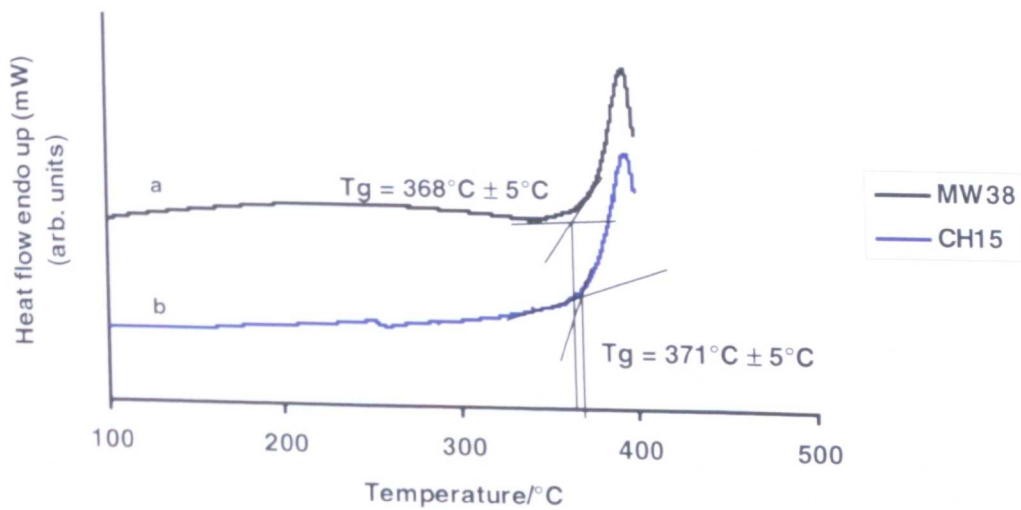


Fig. 6.14 The DSC curve showing the Tg value of
(a) DMO Ge/As/Se = 33/12/55 (at%) product (id: MW38).
(b) conventionally prepared Ge₃₃As₁₂Se₅₅ product (id: CH15).

A Ge/As/Se = 33/12/55 (at %) (id: CH15) product, made through conventional heating (id: CH15), was subjected to thermal analysis to make a comparison (compare figs. 6.14 (a) and 6.14 (b), respectively).

Figs. 6.14 (a) and 6.14 (b) showed that the Tg value of the DMO Ge/As/Se = 33/12/55 product (id: MW38) of 368°C ± 5°C is comparable to the Tg value observed of 371°C ± 5°C of Ge₃₃As₁₂Se₅₅ glass (id: CH15) made through conventional heating.

The stoichiometry of the DMO product was further studied through ESEM EDX analysis and is discussed in the next section 6.3.2.3.

6.3.2.3 ESEM EDX analysis of the DMO Ge/As/Se = 33/12/55 product (id: MW38 and id: CH15).

The stoichiometry of the DMO product Ge/As/Se = 33/12/55 (id: MW38) was analysed by means of EDX analysis using FEG-ESEM. The results obtained from seven different areas of the same sample are listed in the Table 6.15.

Table 6.15 Stoichiometry of the DMO Ge/As/Se = 33/12/55 product (id: MW38) as obtained from ESEM EDX analysis of different areas of the same sample.

Observation	Elements/ at%			
	Ge	As	Se	Total
1.	34.4	9.4	56.3	100.1
2.	35.0	9.0	56.1	100.1
3.	35.1	8.8	56.1	100.0
4.	32.4	6.4	61.2*	100.0
5.	35.8	12.1	52.2*	100.1
6.	24.7	17.7	57.6	100.0
7.	31.9	12.6	55.5	100.0
Mean	32.8	11.0	56.4	
s.d	3.8	3.7	2.7	
Mean (ignoring *)	32.8	11.0	56.3	
Standard deviation (ignoring *)	1.5	2.2	0.8	
Theory	33.0	12.0	55.0	100.0

Table 6.15 shows that the stoichiometry of the DMO Ge/As/Se = 33/12/55 product deviated from the desired value and was rather variable *eg.* mean Se = 56.4 at% with a large standard deviation 2.7. Ignoring the starred selenium results which were rather high (61.2 at%) and low (52.2 at %) and may have been associated with the crystals which were present according to XRD (fig. 6.13 (a) and Table 6.15) the mean and standard deviation (s.d) are still 56.3 at% and 0.8 at%, respectively.

To compare this result, the conventionally made Ge₃₃As₁₂Se₅₅ (id: CH15) glass was analysed by performing ESEM EDX analysis (see Table 6.16).

Table 6.16 Stoichiometry of the conventionally Ge₃₃As₁₂Se₅₅ (at%) glass (id: CH15) as obtained in the ESEM EDX analysis.

Observation	Elements/ at%			
	Ge	As	Se	Total
1.	33.5	11.7	54.8	100.0
2.	32.3	12.1	55.6	100.0
3.	34.7	13.3	52.0	100.0
4.	34.8	11.9	53.3	100.0
5.	33.6	12.4	54.0	100.0
6.	34.2	13.0	52.7	99.9
7.	33.4	13.3	53.3	100.0
8.	34.7	12.7	52.6	100.0
9.	33.0	12.4	54.5	99.9
Mean	33.8	12.5	53.6	
Standard deviation	0.9	0.6	1.2	
Theory	33.0	12.0	55.0	100.0

In contrast to the results obtained for thermal analysis, where T_g for the DMO Ge/As/Se = 33/12/55 product (T_g = 368°C ±5°C) was comparable to the T_g value observed of 371°C ±5°C of Ge₃₃As₁₂Se₅₅ glass (id: CH15) made through conventional heating, the ESEM EDX

Analysis showed that the stoichiometry of the DMO product (id: MW38) was different from that of the conventionally made Ge/As/Se = 33/12/55 (id: CH15).

The atomic percentages as obtained in the ESEM EDX analysis suggested that the conventionally prepared id: CH15 product (mean = $\text{Ge}_{33.8}\text{As}_{12.5}\text{Se}_{53.6}$) was closer in mean analysis to the desired value ($\text{Ge}_{33.0}\text{As}_{12.0}\text{Se}_{55.0}$) and with lower standard deviations of Ge, As, and Se of 0.9, 0.6 and 1.2 at%, respectively. In contrast, the DMO product id: MW38 showed mean analysis of $\text{Ge}_{32.8}\text{As}_{11.0}\text{Se}_{56.4}$ with very high standard deviations of Ge, As, and Se of 1.8, 3.7 and 2.7 at% suggesting it had far greater inhomogeneity and could be made with only partial success through microwave heating. The inhomogeneity of the DMO product might be attributed to the high viscosity of the melt. It is proposed that the DMO melt did not boil effectively to make a homogenous glass. This was also reflected in the X-ray diffraction pattern as well when a crystalline peak due to unmelted batch was observed for the DMO Ge/As/Se = 33/12/55 MW38 product (see section 6.3.2.1.1).

Smaller standard deviations could be calculated for the DMO product id: MW38 (see Table 6.15) if some of the more widely differing ESEM EDX results were ignored.

Also it should be noted that even for the conventionally prepared product id: CH15 the mean selenium value (53.6 at%) was again rather low compared to the theoretical value (55 at%) as noted for the previous composition Ge/As/Se = 17/18/65 (at%) id: MW31 in section 6.2.1.3.2 in Table 6.13.

Some of the ESEM EDX spectra obtained for the stoichiometry measurements for the inhomogeneous DMO Ge/As/Se = 33/12/55 product (id: MW38) using ESEM EDX are displayed here (see fig. C-7 (a) to (b) of [Appendix C]).

6.3.2.4 The optical transmission window measurement by means of FTIR.

Though the DMO product obtained from batch Ge/As/Se = 33/12/55 (at %) (id: MW38) exhibited a crystalline peak on the XRD pattern, and undesirable, inhomogeneous, stoichiometry, the sample was found to be transparent to infrared radiation.

The DMO Ge/As/Se = 33/12/55 (at %) rod product (id: MW38) was sectioned and polished as described in section 3.2.3.2. The FTIR spectrum of the DMO product, as obtained from the batch Ge/As/Se = 33/12/55 (mol %) (id: MW38), is displayed in fig. 6.15 (a). The conventionally prepared $\text{Ge}_{33}\text{As}_{12}\text{Se}_{55}$ (id: CH15) glass was also cut and polished for

comparison (see section 3.2.3.2). The FTIR spectrum obtained for id: CH15 is displayed in fig. 6.15 (b).

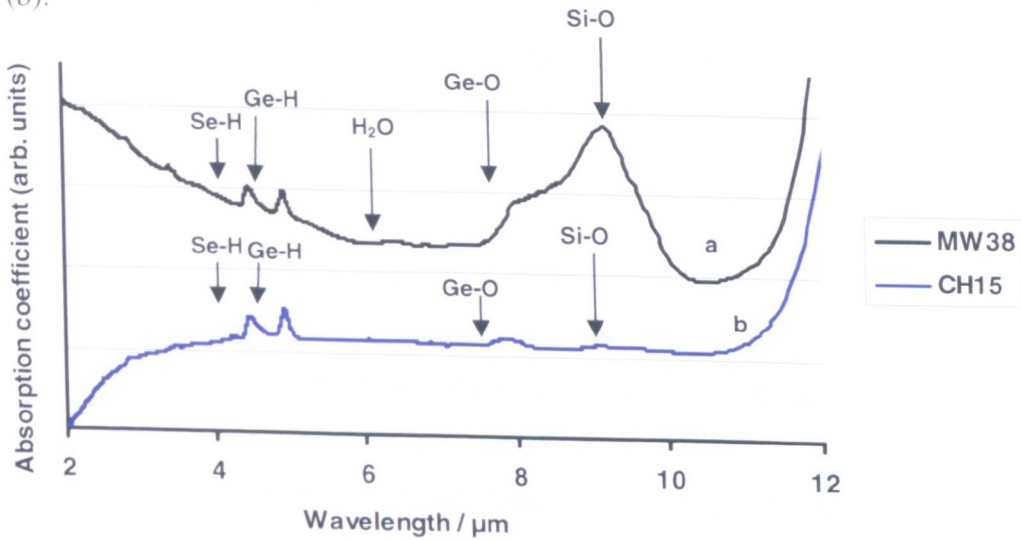


Fig. 6.15 FTIR absorption spectrum of
(a) DMO Ge/As/Se = 33/12/55 product (id: MW38, path length of sample = 3.5 mm).
(b) conventionally prepared Ge/As/Se = 33/12/55 glass (id: CH15, path length of sample = 4.5 mm).

The impurity absorption bands obtained in the above spectra (see fig. 6.15 (a) and 6.15 (b)) are listed in the following Table 6.17.

Table 6.17 FTIR absorption bands observed for in the Ge/As/Se = 33/12/55 mol % products:
id: MW38 made in DMO and id: CH15 made conventionally.

OBSERVED FTIR BANDS				LITERATURE		
DMO prepared		Conventionally prepared		Wv / μm	Assign.	Ref.
Ge/As/Se = 33/12/55 (at%) (id: MW38)		Ge/As/Se = 33/12/55 (at%) (id: CH15)				
Wv / μm	Abs coeff $/\text{cm}^{-1}$	Wv / μm	Abs coeff $/\text{cm}^{-1}$			
4.50	0.020	4.50	0.010	4.5	Se-H	[6]
4.95	0.020	4.95	0.030	4.9	Ge-H	[3]
-	-	7.90	0.010	7.9	Ge-O, As ₄ O ₆	[5]
9.19	0.130	9.19	0.001	9.1, 9.2	Si-O	[9]

Key: Wv / μm : Wavelength / μm , Abs coeff $/\text{cm}^{-1}$ = Absorption coefficient per cm, Assign. = Assignment, Ref. = Reference

Table 6.17, and also figs. 6.15 (a) and 6.15 (b), show that the number of impurities present in the DMO Ge/As/Se = 33/12/55 (mol %) product and conventionally made Ge/As/Se = 33/12/55 (mol %) product are much lower than the other chalcogenides prepared in this project (see section 4.3, 5.3.4 and 7.3.4). Most strikingly the hydroxide (2.9 μm) and/or water (6.3 μm) impurities were almost absent in these products.

The ampoules used, for the preparation of both the DMO and conventionally prepared chalcogenide products, were made of silica glass of specification by the manufacturer of less than 0.1 ppm of OH contamination. Perhaps, the low hydroxide and water content of both the DMO, and the conventionally prepared, products were due to this very low contamination of the original ampoules.

In addition, these silica glass melting ampoules were air baked for at least two schedules (see section 3.1.1) by human error but then the silica glass melt-ampoules were vacuum baked twice deliberately to study the effect of ampoule purification on the quality of glass. Thus not only were the silica melt ampoules of low water and hydroxide content as source, but they were also especially dried in the laboratory prior to the DMO and resistance heating of the chalcogenide products.

Moreover, it can be seen here that the absorption bands at 4.50 μm and 4.95 μm are smaller than the absorption bands obtained in the chalcogenide glasses prepared in this project (see section 4.3, 5.3.4 and 7.3.4). The loss due to hydride impurity Se-H bond vibration at 4.50 μm and 4.95 μm was almost the same for both the DMO and conventionally prepared products (id: MW38 and CH14, respectively). The slight difference observed may have been due to (slightly) different starting materials or batching methodology.

The absorption band due to Ge-O species can be seen in the spectrum of the conventionally prepared $\text{Ge}_{33}\text{As}_{12}\text{Se}_{65}$ glass at 7.9 μm (fig. 6.15 (b)). It is proposed that perhaps 32 hours of melting at a high temperature facilitated the process of dissolution of the oxide impurity from the silica glass (an oxide glass) ampoule in the glass-melt.

However, a huge absorption band due to Si-O bond at 9.19 μm could be seen in the spectrum (fig. 6.15 (a)) of the DMO product obtained from the batch $\text{Ge/As/Se} = 33/12/55$ (mol %) (id: MW38). It is always possible that the mouth of the silica glass ampoule broke due to human error while evacuating ampoule and dropped in the batch then reflected in the FTIR spectrum as a big absorption band.

6.4 Summary

The DMO preparations from batches of Ge/As/Se = 17/18/65 and Ge/As/Se = 33/12/55 were attempted. The properties of the resulting products were compared with those of the same nominal batches melted by conventional resistance heating.

(i) Ge/As/Se = 17/18/65

The DMO $\text{Ge}_{17}\text{As}_{18}\text{Se}_{65}$ glass product (id: MW31) overall showed comparable properties to that of the $\text{Ge}_{17}\text{As}_{18}\text{Se}_{65}$ chalcogenide glass made through conventional heating. The DMO product was made in the form of a monolithic rod through microwave heating in less than 30 minutes as compared with 32 hours by resistance heating. The fast melting of the reactants and the occurrence of reaction may be attributed to the formation of plasma which was of very high temperature which in turn was responsible for the formation of the melt. The silica glass melting ampoule after the DMO preparation was found to be coated with chalcogenide glass probably because of the high viscosity of the melt. The DMO product: was an X-ray amorphous material; was amorphous at the nano-scale according to TEM SAED; exhibited DSC and DTA $T_g = 246^\circ\text{C} \pm 5^\circ\text{C}$; had stoichiometry according to ESEM EDX of typically $\text{Ge}_{17.8}\text{As}_{18.5}\text{Se}_{63.5}$ (theory $\text{Ge}_{17.0}\text{As}_{18.0}\text{Se}_{65.0}$) with standard deviation < 1 at%. These properties may be compared with those of the conventionally prepared glass (id: CH 13) which was also amorphous according to XRD and TEM SAED but exhibited the slightly lower DSC T_g of $235^\circ\text{C} \pm 5^\circ\text{C}$ and the stoichiometry: $\text{Ge}_{17.6}\text{As}_{19.2}\text{Se}_{63.6}$. From the ESEM EDX, both the DMO and the conventionally prepared products exhibited slight lower Se content than expected (~ 63.5 at% (theory 65 at%)) and the reason for this is not clear at present. As observed during the DMO and conventional preparation of arsenic selenide (see section 5.4), here also impurity absorption bands due to hydroxide and/or water, C-H and H-Se contamination were observed using FTIR. Si-O contamination was greater in the DMO $\text{Ge}_{17}\text{As}_{18}\text{Se}_{65}$ glass than the conventionally melted $\text{Ge}_{17}\text{As}_{18}\text{Se}_{65}$ glass but the reason for this is not known.

In conclusion, $\text{Ge}_{17.8}\text{As}_{18.5}\text{Se}_{63.5}$ glass was made in a domestic microwave oven.

(ii) Ge/As/Se = 33/12/55

$\text{Ge}_{33}\text{As}_{12}\text{Se}_{55}$ could be made with only partial success in a domestic microwave oven. The DMO product obtained from the batch Ge/As/Se = 33/12/55 (mol %) (id: MW38) and the conventionally prepared $\text{Ge}_{33}\text{As}_{12}\text{Se}_{55}$ glass (id: CH15) showed: from XRD that the DMO

product was mainly amorphous but there was one large diffraction peak showing that at least one crystal phase was present and this may have been unmelted batch; the DMO product was amorphous according to TEM SAED but this was for a very small sample that may have been unrepresentative and the crystalline inclusion, found from XRD, could have been missed; from ESEM EDX the mean stoichiometry of the DMO product was reasonably acceptable *i.e.* $\text{Ge}_{32.8}\text{As}_{11.0}\text{Se}_{56.4}$ compared to conventionally prepared $\text{Ge}_{33.8}\text{As}_{12.5}\text{Se}_{53.6}$ and theoretical $\text{Ge}_{33.0}\text{As}_{12.0}\text{Se}_{55.0}$, however the standard deviation (s.d.) for the DMO product was extremely high (Ge s.d. = 3.8 at%; As s.d. = 3.7 at% and Se s.d. = 3.8 at%) indicating it was heterogeneous; almost zero loss, from FTIR, due to hydroxide contamination which can be attributed to sourcing lower OH-containing ampoules and to the ampoule purification method when the ampoules were baked (air and vacuum see section 3.1.1) twice. The DSC T_gs of the DMO and conventionally prepared products were close (DSC T_g = 365°C ± 5°C and DSC T_g = 371°C ± 5°C, respectively) indicating that the DMO product mainly successfully formed glass.

Overall it is concluded that although the DMO product was glassy it was not homogeneous and possibly contained undissolved selenium batch. It is suggested that the Ge/As/Se = 33/12/55 melt could not boil properly in the DMO as it was probably more viscous at the melting temperature than the Ge/As/Se = 17/18/65 composition which could be successfully prepared. Thus the DSC T_g = 365°C ± 5°C for the DMO Ge/As/Se = 33/12/55 product whereas the DSC T_g = 246°C ± 5°C for the DMO Ge/As/Se = 17/18/65 product.

The selenium crystallinity obtained in the DMO Ge/As/Se = 33/12/55 (at %) (id: MW38) product could possibly be avoided by: i) careful crushing of the starting materials - perhaps the smaller the particle size the easier it would melt and hence be dissolved and ii) it could be solved by using a DMO with higher output power or perhaps the convection DMO (please see Table 5.2 for the specification of convection DMO).

References:

- [1] S. Gredelj, A.R. Gerson, S. Kumar and G.P. Cavallaro, *Appl. Surf. Sci.* **174** (2001), p. 240.
- [2] S.D. Savage, C.A. Miller, D. Furniss and A.B. Seddon, *J. Non-Cryst. Solids* **354** (2008), p. 3418.
- [3] M.F. Churbanov, *J. Non-Cryst. Solids* **184** (1995), p. 25.
- [4] D. Lezal, *J. Optoelect. & Adv. Mat* **5** (2003), p. 23.
- [5] J.S. Sanghera and I.D. Aggarwal, *Infrared fiber optics*, CRC Press LLC, Washington D.C., (1998).
- [6] P.J. Webber and J.A. Savage, *J. Non-Cryst. Solids* **20** (1976), p. 271.
- [7] A.M. Reitter, A.N. Sreeram, A.K. Varshneya and D.R. Swiler, *J. Non-Cryst. Solids* **139** (1992), p. 121.
- [8] A.B. Seddon and C.A. Miller, Unpublished work, 2006.
- [9] A.G. Whittaker and D.M.P. Mingos, *J. Chem. Soc. Dalton Trans.* (1995), p. 2073.

Chapter 7

Microwave assisted synthesis of tellurium arsenic selenide.

The syntheses of arsenic selenide (see Chapter 5) and germanium arsenic selenide (see Chapter 6) *via* microwave heating using a domestic microwave oven, confirmed that the arsenic selenium mixture (in the molar ratio of As/Se = 40/60) and germanium, arsenic and selenium mixture (in the molar ratio of Ge/As/Se = 17/18/65 and in the molar ratio of Ge/As/Se = 33/12/55) coupled with microwaves to form a glass. To study the behaviour of tellurium exposed to microwaves, and to verify whether a tellurium containing glass could be formed in domestic microwave oven, the well-established glass forming system containing tellurium in the atomic% Te/As/Se = 20/30/50 was exposed to microwaves using a domestic microwave oven. Plasma formed and a chalcogenide glass-melt was formed which upon quenching followed by annealing produced a tellurium arsenic selenide product. The tellurium arsenic selenide product made using the domestic microwave oven will be called DMO TAS glass; and tellurium arsenic selenide glass prepared using a resistance rocking furnace will be termed TAS glass made through conventional heating. The latter was prepared to compare typical properties of TAS glass made through conventional heating with the properties of the DMO TAS products. This chapter explores the amorphous nature of the TAS products, glass transition temperature (T_g), stoichiometry and transmission window (see section 7.3).

7.1 Microwave irradiation of the starting materials and the formation of a chalcogenide rod product.

Several attempts were made to synthesise the product Te/As/Se = 20/30/50 (atomic %) and these are summarised in Table 7.1.

Table 7.1 The form of Te-As-Se samples obtained under different DMO reaction conditions.

Product id:	Te/As/Se / atomic %	Time of exposure to microwaves / min	Annealing temp / °C (see Table 7.4)	Comments
MW 30	20/30/50	5	150	<ul style="list-style-type: none"> • Ampoule supported in sand in a silica beaker. • Sample annealed horizontally which caused slumping. • Shiny, deformed rod resulted with bubble impressions up to ~1 mm diameter in surface in contact with the ampoule during annealing.
MW33	..	30	..	<p>Ampoule supported in silica containing a small amount of sand ~10 mm depth.</p> <ul style="list-style-type: none"> • Sample annealed vertically. • Shiny rod.
MW36

Table 7.2 summarises the make, model, wattage used for the formation of DMO Te/As/Se = 20/30/50 (atomic %) product, time the physical state of the starting materials.

Table 7.2 List of reaction conditions under which Te/As/Se = 20/30/50 glass batches were melted during microwave heating.

Product id:	DMO Make/Model	Power/W	Physical state of starting material		
			Te	As	Se
MW30	DeLonghi/ EM821AAN	800	*	*	*
MW33	*	*	*
MW36	*	*	*

Key: * manually crushed inside the glove box.

The Te, As and Se starting materials of purity as described in section 3.1.1.2, were powdered individually using a clean agate mortar and pestle (Fischer) manually in mol % and then mixed together in a plastic weighing boat (Fischer) using a stainless steel spatula (Fischer) and placed in a silica glass ampoule. The ampoule containing these reactants was evacuated and sealed as described in section 3.1.1.3. Purity of the chemicals is described in section 3.1.1.2 and the silica ampoules were purified as described in section 3.1.1.1.

7.1.1. $\text{Te}_{20}\text{As}_{30}\text{Se}_{50}$ product (id: MW30).

Several blue glows were seen as soon as the DMO was switched on. The reactants melted and the melt could be seen to rise upwards within the ampoule. After about 5 minutes the glass-melt settled down and a black mass at the bottom of the ampoule was observed. A blue spark was then observed in the lower part of the ampoule. Since during the formation of DMO $\text{Ge}_{17}\text{As}_{18}\text{Se}_{65}$ (id: MW29; section 6.1.1.) it was observed that the plasma pushed the glass-melt to the upper end of the ampoule, which was undesirable for making a rod-shaped product, it was decided to switch off the microwave heating. Therefore the total time of irradiation of the chalcogenide batch in the DMO was approximately 5 minutes.

The melt was air quenched for about 20 seconds and then was annealed at 150°C in a resistance furnace (Carbolite, Serial no. 5/86/667, Type ESF 12/10; following the schedule described in Table 7.4, section 7.2). In this furnace the silica glass ampoule holding the chalcogenide glass-melt could be kept only horizontally and not vertically. The following photographs (fig. 7.1 a & b) show the chalcogenide rod product (sample id: MW30) formed during this experiment.

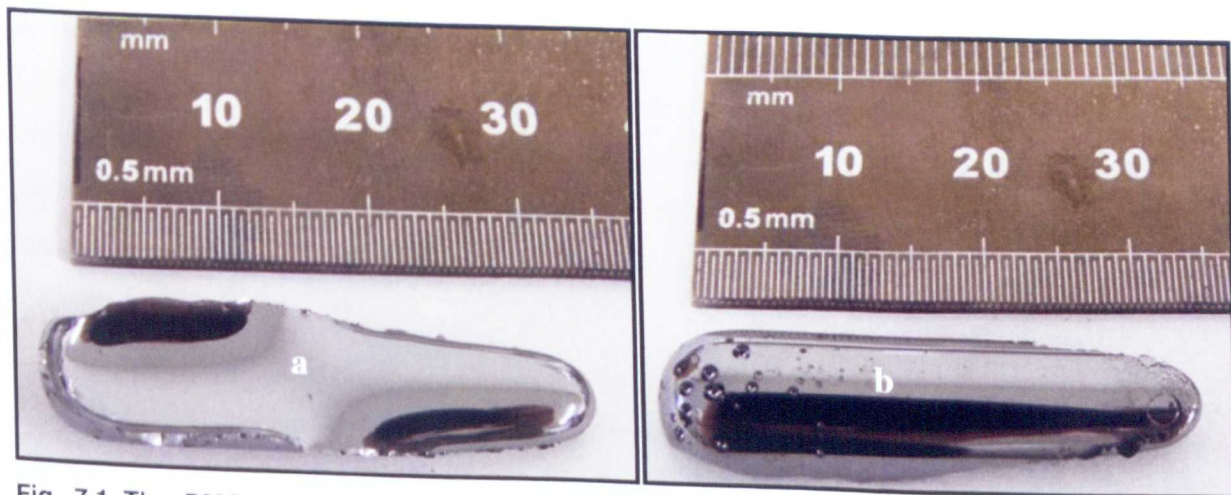


Fig. 7.1 The DMO $\text{Te}_{20}\text{As}_{30}\text{Se}_{50}$ (id: MW30) chalcogenide rod product formed *via* microwave heating (sample id: MW 30): (a) upper side of the product showing some sag due to gravity probably occurred during annealing, which was carried out with the sample in the same orientation as shown here and (b) underside of the chalcogenide rod product which had been in direct contact with the wall of the silica ampoule during the annealing; note bubble impression up to ~ 1 mm diameter.

The elongated drop shape exhibiting sagging of the rod product which was proposed to be due to the silica ampoule being kept horizontally in the annealing furnace. It is suggested that the chalcogenide melt flowed under gravity and sagged to form the shape of an elongated drop because the annealing temperature of 150°C was too high. T_g of the $\text{Te}_{20}\text{As}_{30}\text{Se}_{50}$ product id: MW30 was later shown to be $133^\circ\text{C} \pm 5^\circ\text{C}$ according to DSC (see section 7.3.2). Fig. 7.1 (a) shows the upper part of the chalcogenide rod and is in the same orientation as it was in the annealing furnace. Fig. 7.1 (b) shows under-part where the chalcogenide rod was in contact

with the silica glass ampoule and the imprints left by bubbles could be observed on this undesirable surface of the chalcogenide rod.

In this experiment the glass-melt had been allowed to boil for only 5 minutes. The stoichiometry of this product was evaluated by performing EDX analysis using ESEM; this DMO TAS glass (id: MW30) was inhomogeneous (see later section 7.3.3).

7.1.2 $\text{Te}_{20}\text{As}_{30}\text{Se}_{50}$ products (id: MW33 and MW36).

Earlier, during the formation of DMO As_2Se_3 , the melt had been allowed to boil for about 30 minutes which, it was proposed, helped to make the glass homogenous (see sections 5.1.2 and 5.1.3). Therefore, to improve the homogeneity of the TAS product id:MW30 here, in a new preparation the TAS system (id: MW33) was exposed to the microwaves for 30 minutes. It was thought that perhaps the sand (kept in the beaker over which the silica ampoule was placed) would become hotter, by conduction, during the longer irradiation and therefore the chalcogenide melt in close contact with the sand would be better insulated and remain hotter, *via* conduction, than the chalcogenide melt present in the upper part of the ampoule. To study the behaviour of the chalcogenide melt when exposed to microwave irradiation, during a fresh TAS preparation the silica ampoule was instead kept in an empty silica beaker (Fisher) without the sand present. It was observed that the reaction started with the formation of plasma and the starting materials boiled. The sample (id: MW33) was annealed vertically in a resistance furnace (INSTRON SFL/ TF 105/1 ZF, Serial No. - 0001541) at 150°C (see Table 7.4, section 7.2).

The DMO TAS preparation was repeated with a similar result (id: MW36). Fig. 7.2 shows a photograph of the DMO TAS product (id: MW 36) that resulted. From fig. 7.2 it can be seen that a good quality rod ~ 10 mm diameter and 25 mm long was prepared with a shiny surface.

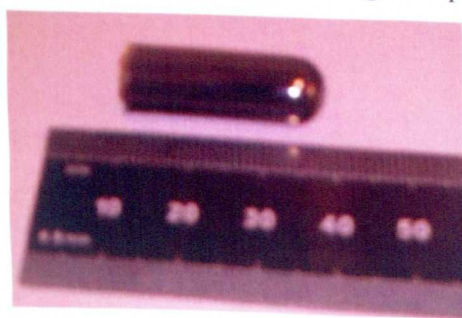


Fig. 7.2 DMO $\text{Te}_{20}\text{As}_{30}\text{Se}_{50}$ chalcogenide rod product formed *via* microwave heating (id: MW 36).

7.2 The synthesis of Te/As/Se = 20/30/50 in a rocking resistance furnace.

7.2.1 Te₂₀Se₃₀Te₅₀ product (id: CH20).

The Te/As/Se = 20/30/50 product (id: CH20) was prepared in a rocking resistance (see section 3.1.1) in order to compare the properties of the DMO synthesised TAS product with that of the conventionally prepared TAS glass. The chemicals, of purity as in section 3.1.1.2, were weighed in the atomic % ratio Te/As/Se = 20/30/50 with an aim to prepare 10 g of glass. Arsenic was purified as discussed in section 3.1.1.2. The required amounts of purified starting materials were poured into a cleaned silica glass ampoule. The ampoule was cleaned as described in section 3.2.1.1. The ampoule with the starting materials was then evacuated discussed in section 3.1.2.3. It was then heated according to the schedule in Table 7.3.

7.3 Heating schedule used for the conventional preparation of Te/As/Se = 20/30/50 product (id:CH20) in a rocking resistance furnace.

Stage	Schedule
1.	RT to 200°C @ 200°C/h
2.	200 to 750°C @ 40°C/h
3.	Start rocking at 250°C to 300°C (when Se has melted to avoid scratching inside walls of ampoule)
4.	Dwell at 750°C for 12h
5.	750 to 600°C @ 40°C/h
6.	Hold 600°C for 1 to 2h
7.	Switch off rocking mechanism and hold ampoule vertical inside rocking furnace for 15 min
8.	Quench ampoule in air for ~ 45 - 60 s (for 10 g batch)

The glass melt was quenched, *in situ* inside the ampoule, in air and annealed. Annealing was done according to the cooling schedule in Table 7.4 when a shiny chalcogenide rod, without bubbles, was formed.

Table 7.4 Annealing schedule for Te/As/Se = 20/30/50 (atomic %) DMO, and conventionally prepared, products (id: MW30, MW33, MW36 and CH20, respectively).

Stage	Schedule
1.	Dwell for 1 hr at 150°C
2.	From 150°C to 120°C @ 5°C/hr
3.	From 120°C to 15°C @ 20°C/hr

The above DMO and conventionally prepared TAS products were characterised. The results obtained are discussed in the following sections.

7.3 Characterisation of the DMO, and conventionally prepared, Te/As/Se = 20/30/50 (atomic %) products.

7.3.1. Amorphicity of the DMO Te/As/Se = 20/30/50 (atomic %) products (MW30, and MW33) and conventionally prepared Te/As/Se = 20/30/50 (atomic %) product (id: CH20).

Amorphicity of the DMO (id: MW30, MW33) and conventionally prepared (id: CH20) Te/As/Se = 20/30/50 (at%) products were studied through the following methods:

- Powder X-ray diffractometry (XRD), when a few grammes of sample could be examined for the amorphicity of the sample (see section 7.3.1.1) and
- Selected area electron diffraction (SAED) using a transmission electron microscope (TEM), when the presence of any crystalline substance in the sample could be examined at a nanoscopic level (see section 7.3.1.2).

7.3.1.1 Powder XRD.

Powder XRD was carried out to investigate the amorphicity of the products. The DMO TAS samples were crushed to a fine powder and put in an aluminium holder. The XRD pattern in fig. 7.3 (a) was obtained for sample MW30 showing that the DMO Te/As/Se = 20/30/50 was X-ray amorphous.

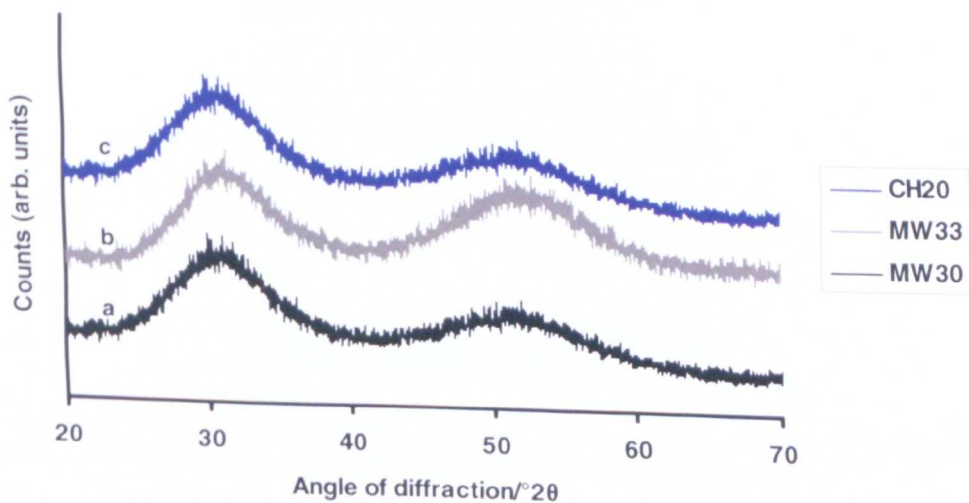


Fig. 7.3 XRD pattern obtained for the

- DMO Te/As/Se = 20/30/50 product (id: MW30).
- DMO Te/As/Se = 20/30/50 (id: MW33).
- conventionally melted TAS glass (id: CH20).

The reproducibility of the DMO reaction was established by making the TAS glass again through microwave heating using a DMO. The MW33 sample obtained was subjected powder XRD when again the product was found to be X-ray amorphous (see fig. 7.3 (b)).

The above results obtained were compared with the X-ray diffraction pattern obtained when a conventionally melted Te/As/Se = 20/30/50 (atomic %) glass (id: CH20) was subjected to XRD analysis (see fig. 7.3 (c)).

The diffraction patterns displayed in figured 7.3 (a) to 7.3 (c) are very similar and hence it can be concluded that an X-ray amorphous material could be prepared reproducibly *via* microwave heating from the well-established glass forming mixture in the molar ratio of Te/As/Se = 20/30/50 (atomic %).

7.3.1.2 TEM SAED.

The amorphicity of the DMO Te/As/Se = 20/30/50 (atomic %) was investigated at the nanometer scale by subjecting the sample to SAED using TEM. The DMO product: id: MW30 showed crystalline structure in one micrograph out of six micrographs. The MW30 sample was imaged at ten different areas. Fig. D-1 [Appendix D] shows the blurred electron diffraction pattern structure indicating the amorphous character of the DMO glass sample but fig. 7.4 shows the presence of some crystalline structure in the sample.

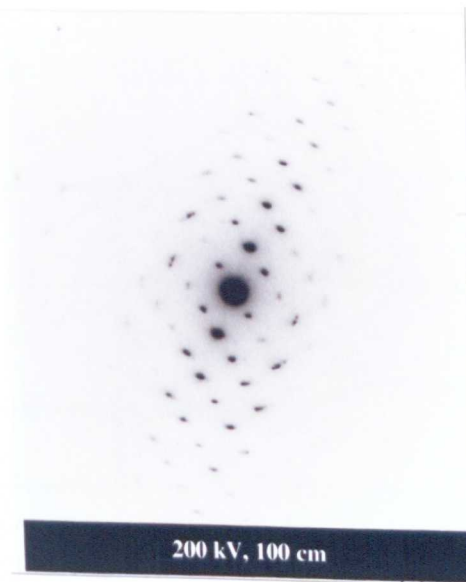


Fig. 7.4 TEM SAED pattern showing the presence of some crystalline structure in the DMO Te/As/Se = 20/30/50 (atomic %) product (id: MW 30).

It is believed that since the batch materials for DMO product id:MW30 were heated only for 5 minutes (see section 7.1.1), some of the tellurium may not have melted. The evidence for it being tellurium is from TEM EDX (not shown). No crystalline structure (see fig. D-2 and fig. D-3 of [Appendix D]) was observed when for DMO products (Te/As/Se = 20/30/50) id: MW33 and MW36 made again (section 7.1.2) and the melts were boiled for 30 minutes (sample id: MW33 and MW36).

These results suggest that boiling and prolonged heating of the Te/As/Se = 20/30/50 (at %) melt in the DMO is important not only for homogenising the melt but also for melting the starting materials completely. The amorphicity of the conventionally prepared Te₂₀As₃₀Se₅₀ (CH20) was also examined for comparison purposes and found to be amorphous at the nanometer scale (see fig. 3 [Appendix D]).

The above results suggest that, though the DMO reaction system attains a very high temperature due to the formation of plasma and the reactants melted very fast, a prolonged microwave exposure of 30 minutes provides complete melting of the reactants. It is concluded that the Te/As/Se = 20/30/50 (atomic %) as batched chalcogenide glass could be synthesised in the DMO to be amorphous reproducibly.

7.3.2 Thermal analysis of the glass.

The T_g of the TAS glasses, irrespective of the method of preparation, was evaluated using differential scanning calorimetry (DSC). Fig. 7.5 (a) shows the DSC curve of the DMO TAS product (id: MW30).

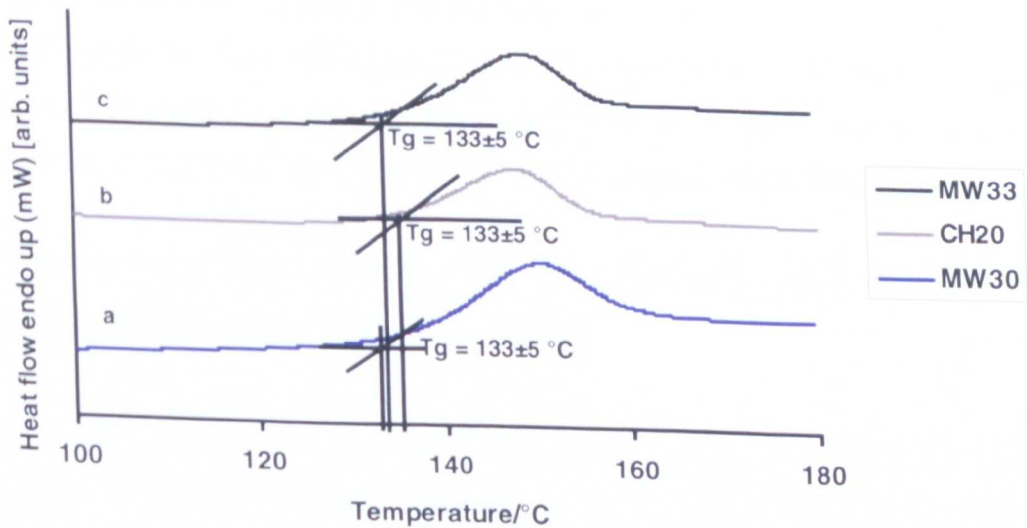


Fig. 7.5 DSC curves showing the T_g value of:

(a) DMO TAS product (id: MW30).

(b) conventionally melted TAS glass (id: CH20).

(c) DMO TAS product (id: MW33) and hence proving the reproducibility of the DMO synthesis.

The value of T_g of the DMO TAS (id: MW30) was calculated using the software provided with DSC equipment from Perkin Elmer and was found to be $133^\circ\text{C} \pm 5^\circ\text{C}$. This value of T_g matched the literature value of 135°C for $\text{Te}_{20}\text{As}_{30}\text{Se}$ reported by Luc-Adam *et al.* [1]. Conventionally melted TAS glass was subjected to T_g measurement using DSC for comparison purposes (see fig. 7.5 (b)).

The two DSC curves in fig. 7.5 (a) and 7.5 (b) show that the T_g value of DMO TAS glass is apparently the same as that of the conventionally melted TAS glass. This suggests that the desired stoichiometry of the TAS glass can be achieved *via* microwave heating.

To confirm the reproducibility of the DMO TAS reaction, another product (id: MW33) was subjected to thermal analysis for the determination of T_g (see fig. 7.5 (c)).

Comparison of the DSC curves in figs. 7.5 (a) and 7.5 (c) for DMO TAS id: MW33 and MW30, respectively, gives evidence that $\text{Te}_{20}\text{As}_{30}\text{Se}_{50}$ glass could be made reproducibly *via* microwave heating.

Finally, it should be noted that DMO TAS products id: MW30 and MW33 were annealed at 150°C . Clearly as the DSC T_g was measured to be only $133^\circ\text{C} \pm 5^\circ\text{C}$ then these DMO TAS products (and DMO TAS id: MW36) as well as the conventionally prepared TAS glass (id: CH20) were all annealed at a too high temperature (Table 7.4) and this would account for the sagging (see fig. 7.1) of DMO TAS id: MW30 observed during the horizontal annealing.

7.3.3 Stoichiometry of the DMO and conventionally prepared $\text{Te}_{20}\text{As}_{30}\text{Se}_{50}$ products (id: MW30 and MW36 respectively).

The stoichiometry of the DMO $\text{Te}_{20}\text{As}_{30}\text{Se}_{50}$ chalcogenide products (id: MW30, MW33 and MW36) prepared was investigated using the field emission gun environmental scanning electron microscope (FEG-ESEM) *via* energy dispersive X-ray (EDX) analysis. The samples were studied in auxiliary mode with the sample chamber filled with nitrogen gas; the pressure was kept to be 1.3×10^3 Pa. One sample of each DMO TAS product (id: MW30, MW33 and MW36) was subjected to the ESEM EDX analysis for the determination of stoichiometry. The results obtained are presented in Tables 7.1 to 7.3.

The data for DMO TAS (id: MW30), as shown in observation 1 of Table 7.1 were not reliable as the counts per second were very low (verbal communication of technical support staff Dr. Nigel Neate and Mrs. Nikki Weston). The data depicted as observations 2 to 10 in Table 7.5

show a deviation from the desired value; for instance the atomic percentage of tellurium observed varied from a minimum value of 19.3 to a maximum value of 22.2; this indicates that there were inhomogeneities in this DMO TAS product (id: MW30). This result provokes the question of whether more prolonged exposure to microwaves facilitates the process of boiling which in turn homogenises the melt to form a homogenous glass. The mean atomic percentage of arsenic was found to be more than the desired value (32.6, rather than the theoretical batch value of 30) everywhere in this sample DMO TAS id:MW30 whereas the mean atomic percentage of selenium was less than the desired value (47.8 rather than the ideal of 50.0). The difference in the observed atomic percentage from the desired value may be attributed to the batching methodology where the starting material had to be crushed and mixed in the weighing boat before pouring into the melt ampoule. It could just be possible that one batch material was left in the boat and in the mortar and pestle more than the others due to adhesive force of the material probably due to the static and particle shape.

Table 7.5 ESEM EDX determination of the stoichiometry of the DMO TAS product (id: MW30).

Observation	Counts/sec.	Elements/ at%			Total
		Te	As	Se	
1.	Low (> 1374)	12.0	35.2	52.8	100.0
2.	> 1000	21.5	32.5	46.1	100.0
3.	„	22.2	31.7	46.2	100.0
4.	„	19.3	32.9	47.9	100.0
5.	„	19.3	32.1	48.6	100.0
6.	„	19.6	32.5	47.8	100.0
7.	„	20.9	32.2	46.9	100.0
8.	„	19.8	32.4	47.8	100.00
9.	„	20.7	32.5	46.8	100.0
10.	„	21.0	32.0	47.0	100.0
Mean		19.6	32.6	47.8	100.0
Standard deviation		2.8	1.0	1.9	-
Theory		20.0	30.0	50.0	100.0

However, probably the lack of homogeneity of the sample was due mainly to lack of proper mixing during the melting process and this is reflected in the large standard deviations shown in Table 7.5 for Te and Se (2.8 and 1.9, respectively).

To study the effect of microwave exposure time on the properties of TAS glass, the starting materials were exposed in the DMO for 30 minutes to produce DMO TAS products id: MW33 and MW36. The results obtained are listed Table 7.2; all counts/sec were acceptably high.

Table 7.6 ESEM EDX determination of the stoichiometry of the DMO TAS product (id: MW36).

Observation	Elements/ at%		
	Te	As	Se
1.	19.5	30.8	49.6
2.	19.3	30.9	49.8
3.	19.7	30.3	50.0
4.	20.4	30.7	48.9
5.	19.3	30.4	50.2
6.	19.1	29.6	51.3
7.	19.8	30.0	50.2
Mean	19.6	30.4	50.0
Standard deviation	0.4	0.5	0.7
Theory	20.0	30.0	50.0

Comparison of Tables 7.5 and 7.6 illustrates that the homogeneity of the TAS glass improved on increasing the duration of microwave exposure from 5 minutes to 30 minutes. The above results show that $\text{Te}_{20}\text{As}_{30}\text{Se}_{50}$ chalcogenide glass could be made homogeneously through microwave heating for 30 minutes. Thus, the effect of duration of the DMO heating cannot be neglected in the homogenisation of the glass-melt. Here for DMO TAS glasses, when the melt boiled, a homogenous product was obtained.

Fig. D-4 'a' to 'd' [Appendix D] display some of the ESEM EDX spectra obtained while studying the DMO TAS glasses. The spectra files were chosen randomly.

7.3.4 Optical transmission using FTIR.

DMO TAS glass samples were polished using silicon carbide powder and diamond paste a $1\mu\text{m}$ finish as described in Chapter 3 (section 3.2.3.2) and were subjected to determination of the optical transmission window using FTIR.

Fig. 7.6 (a) shows the FTIR spectrum of DMO TAS glass (id: MW30), which was heated by microwave exposure for only 5 minutes and was shown to be inhomogeneous by means of ESEM EDX. It may be compared with the results obtained for DMO TAS glass when the melt was allowed to boil for 30 minutes (DMO TAS product id: MW36) (see Fig. 7.6 (b)).

The absorption bands obtained and identified from the FTIR spectra of the DMO TAS products id: MW30 and MW36 shown in figs. 7.6 (a) and 7.6 (b), respectively, are summarised in Table 7.7. Note - the FTIR bands quoted from the literature were all observed for chalcogenide glasses made by conventional resistance heating.

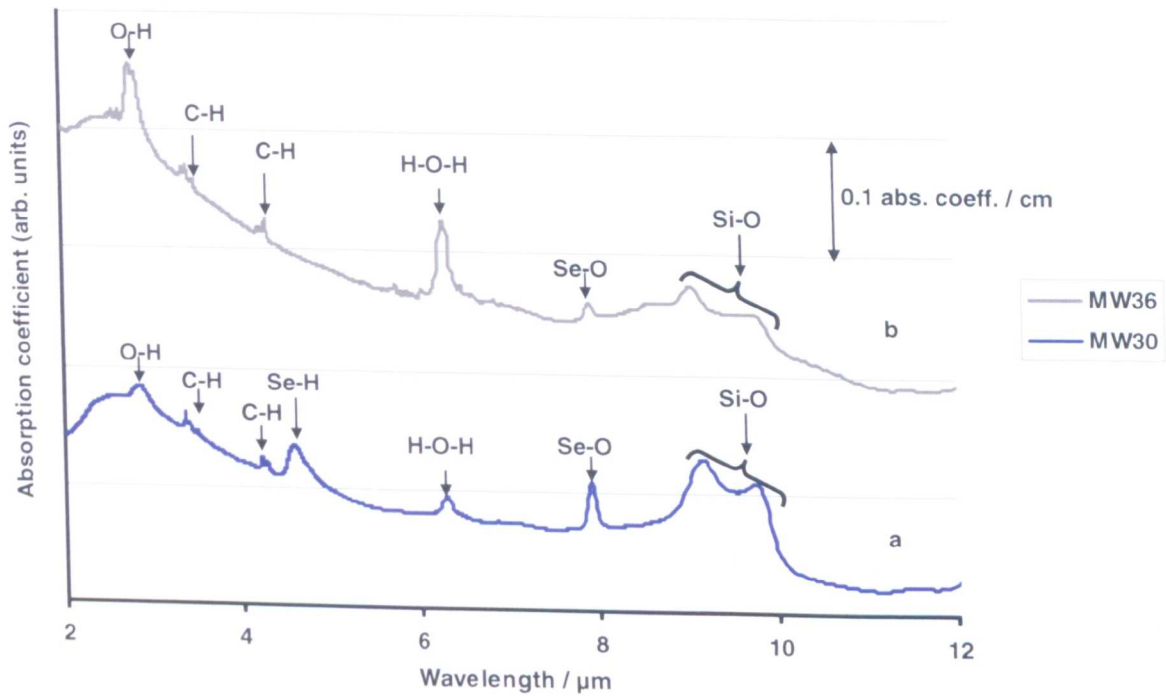


Fig. 7.6 FTIR spectrum showing

- (a) DMO TAS bulk glass transmission window and impurity bands (id: MW30, path length = 2.15 mm).
 (b) DMO TAS bulk glass transmission window and impurity bands (id: MW36, path length = 2.85 mm).

The absorption due to hydroxide, or molecular water impurity, at 2.9 μm , and due to molecular water at 6.3 μm , was less intense for product id: MW30 where the melt was exposed to microwaves for only 5 minutes. It is proposed that this may be evidence for some dissolution of hydroxide ion (chemisorbed and physisorbed) from the inner surface of the silica-glass melt-ampoule diffusing into the melt. During the preparation of product id: MW30 the melt was heated only for 5 minutes and hence less hydroxide and water impurity might have been incorporated in the glass by this mechanism which is reflected in the infrared spectrum of the DMO TAS product (id: MW30).

Table 7.7 Summary of impurity absorption bands arranged in increasing order of wavelength, as obtained in the FTIR spectra of DMO TAS glasses: id: MW30 and MW36 shown in figs. 7.6 (a) and 7.6 (b), respectively.

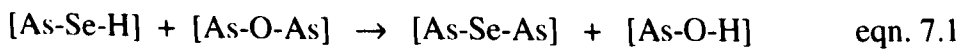
Observed bands				Literature		
Product id: MW30 [5 mins in DMO]		Product id: MW36 [30 mins in DMO]		Wavelength/ μm	Assignment	Ref.
Wavelength/ μm	Absn. coeff. / cm^{-1}	Wavelength/ μm	Absn. coeff. / cm^{-1}			
2.9	0.62	2.9	0.04	2.9	O-H	[2]
3.4	0.01	3.4	α	3.4	C-H	[3]
4.3	0.01	4.3	α	4.3	C-O	[4]
4.6	0.03	-	-	4.57	Se-H	[2, 3]
6.3	0.01	6.3	0.07	6.3	O-H	[4]

Observed bands				Literature		
Product id: MW30 [5 mins in DMO]		Product id: MW36 [30 mins in DMO]		Wavelength/ μm	Assignment	Ref.
Wavelength/ μm	Absn. coeff. / cm^{-1}	Wavelength/ μm	Absn. coeff. / cm^{-1}			
8.0	0.03	8.0	\square	8.0	SeO ₂	[5]
-		9.1	0.01	9 -10	Si-O	[2]
9.2	0.05	-	-	9 - 10	Si-O	[2]
9.8	0.04	9.8	0.01	9 - 10	Si-O	[2]
12.5	0.05	12.5	0.01	12.5	As ₂ O ₃	[5]

Key : \square Too small to calculate.

This result is in some agreement with the results obtained while making arsenic selenide through microwave heating. There, a lower loss due to hydroxide impurity was observed for the DMO arsenic selenide glass (see section 5.3.4) compared to the arsenic selenide glass made through the conventional heating method (see section 5.3.3). The arsenic selenide melt spent less time in contact with the silica glass ampoule walls during the DMO heating than during the conventional heating.

However, after 5 minutes' microwave irradiation of DMO TAS id: MW30, there was a larger Se-H absorption band (fig. 7.6 (a)) than for DMO TAS id: MW36 (fig. 7.6 (b)) which had been microwave irradiated for 30 minutes. In fact, for the latter DMO TAS product id: MW36, there was no detectable Se-H. Yet the molecular water band at 6.3 μm wavelength was much larger after 30 mins irradiation. Hence, it can also be proposed that during DMO irradiation, the Se-H impurities transform with time by reaction with impurity oxide present in the melt to form OH impurities *e.g.*:



The spectral loss due to C-H bond impurity at 3.4 μm is reduced for DMO TAS product id: MW36 compared to the DMO TAS product id: MW30. However, in the past we have shown that this C-H is due to polishing media by comparing fibre (unpolished) and bulk glass spectra [6]. In fact, the product id: MW30 had distorted during annealing (see fig. 7.1) and required rather more polishing than average.

The absorption bands at higher wavelengths 9 μm to 12 μm are due to Si-O impurity, and the interaction with the silica melt-ampoule could also be responsible for the presence of these absorption bands, as well as O-H and molecular water (see above, in this section). Again it can be seen that the optical loss in this region is more for DMO TAS product id: MW30 than

The absorption bands at higher wavelengths 9 μm to 12 μm are due to Si-O impurity, and the interaction with the silica melt-ampoule could also be responsible for the presence of these absorption bands, as well as O-H and molecular water (see above, in this section). Again it can be seen that the optical loss in this region is more for DMO TAS product id: MW30 than for product DMO TAS id: MW36. The reason behind this could not therefore be attributed to the DMO plasma formation which could cause silica vapour to dissolve in the melt since the time of exposure to microwaves was much higher for the DMO TAS product id: MW36 (30 minutes) than DMO TAS product id: MW30 (5 minutes). It could not be attributed to the length of the ampoule as well where it could be argued that, since the sealing point of the ampoule is very close to the reactants (as the silica glass melt-ampoule had to be kept as small as possible so that the chalcogenide melt could be collected at the bottom of the ampoule to form a rod, see section 3.1.2) and silica vapour formed during the sealing process contaminated the glass-batch as the length of the silica glass ampoule in both the experiments were almost the same. The length of the silica glass melt-ampoule was *ca.* 90 mm for DMO TAS id: MW30 whereas the length of silica glass melt-ampoule was *ca.* 93 mm for DMO TAS product id: MW36.

It is suggested that perhaps the edges of the silica glass melt-ampoule were cracked, or some other similar defect was present in the silica glass ampoule, while making DMO TAS id: MW30 (as the edges of the silica glass melt-ampoule were not flame glazed) during the evacuation process due to human error while making DMO TAS product id: MW30 and may be it is this phenomenon that is reflected in the FTIR absorption spectrum.

The mid-infrared transmission window of a conventionally made TAS glass (id: CH20) is displayed in fig. 7.7.

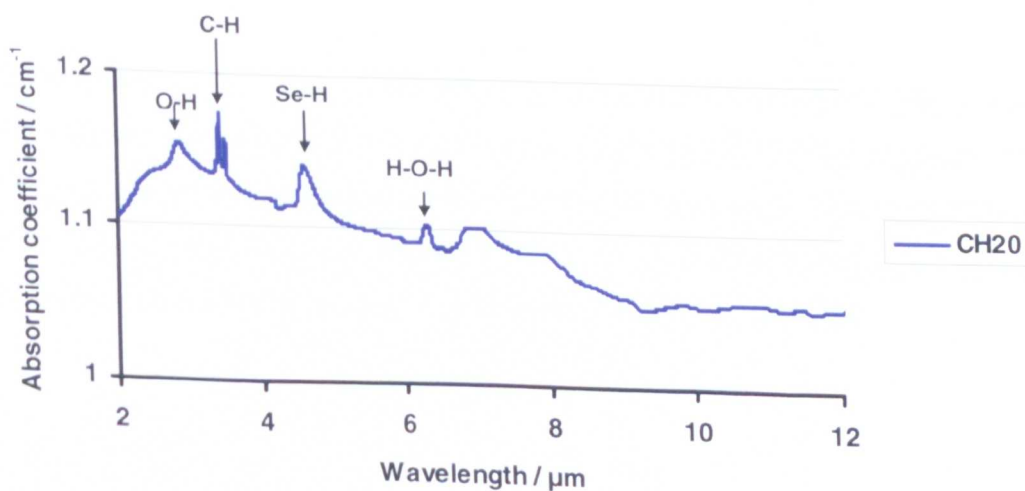


Fig. 7.7 FTIR spectrum showing conventionally prepared TAS bulk glass transmission window and impurity bands (id: CH20, path length = 3.0 mm).

The impurity absorption bands present in the conventionally prepared TAS glass id:CH20 are summarised in Table 7.8. Table 7.8 and Table 7.7 will be compared and discussed, with the FTIR spectra of both the DMO glasses id:MW 30 (microwave irradiation time 5 mins) and id:MW33 (microwave irradiation time 30 mins.).

Table 7.8 Summary of impurity absorption bands arranged in increasing order of wavelength, as obtained in the FTIR spectra of conventionally made TAS glass: id: CH20 shown in fig. 7.7.

Observed bands		Literature		
Product id: CH20				
Wavelength/ μm	Absn. coeff. / cm^{-1}	Wavelength/ μm	Assignment	Ref.
2.9	∞	2.9	O-H	[2]
3.4	0.04	3.4	C-H	[3]
4.6	0.02	4.6	Se-H	[2]
6.3	∞	6.3	H-O-H	[4]

Key : ∞ Too small to calculate.

Comparison of Table 7.8 with Table 7.7, and fig. 7.7 with figs. 7.6 (a) and 7.6 (b), shows that the conventionally made TAS glass (id: CH20) has almost the same purity level except the impurity levels at higher wavelengths due to oxide impurities (see Table 7.7) was higher in the DMO TAS glasses than the conventionally prepared TAS glass (id: CH20)

7.4 Further discussion.

Whittaker *et. al.* [7] explained the formation of sulfur and selenium containing chalcogenides accompanied with the plasma formation. It is suggested in the paper that the plasma was formed due to the formation chalcogen vapour and disappearance of plasma provides a convenient indication of the reaction completion. Since the TAS glass composition contain 30 at% of selenium the DMO was switched off as soon as the plasma disappeared while making the DMO MW30 product.

As observed earlier in the chapter, the effect of duration of the DMO heating cannot be neglected in the homogenisation of the glass-melt. Here for DMO TAS products, when the melt boiled, a homogenous product was obtained. This reinforces the same observation when synthesising arsenic selenide (see chapter 5). Sample id:MW18, MW39 and MW55 were irradiated for 35 minutes when an almost homogenous glass was obtained.

7.5 Summary.

From the XRD, TEM SAED and ESEM EDX results, tellurium arsenic selenide ($\text{Te}_{20}\text{As}_{30}\text{Se}_{50}$) glass can be prepared as a homogeneous glass rod through microwave heating using a DMO. It was observed that the time of exposure to the microwaves of the starting materials is significant for preparation of TAS glasses. It not only affects the homogeneity of the glass but also the starting materials (particularly Te (see section 7.3.1.2) took sometime to complete melting and 30 minutes of exposure including giving the melt time to boil was necessary. Using DSC, T_g of the DMO TAS glasses ($133^\circ\text{C} \pm 5^\circ\text{C}$) was identical to that of TAS glass made through conventional heating method using a resistance rocking furnace. From FTIR, the DMO TAS product formed after 5 mins. Exhibited a large Si-O bond which is believed to be due to some error during sealing of the silica glass melt-ampoule. The DMO TAS glasses showed lowered Se-H yet great H_2O ($6.3 \mu\text{m}$ absorption band) after 30 mins in the DMO compared to the after 5 mins in the DMO. Thus transformation of hydride and oxide impurities to form molecular water during the microwave processing is proposed.

References.

- [1] D.L. Coq, C.B. Plédel, G. Fonteneau, T. Pain, B. Bureau and J.L. Adam, *J. Non-Cryst. Solids* **326-327** (2003), p. 451.
- [2] M.F. Churbanov, *J. Non-Cryst. Solids* **184** (1995), p. 25.
- [3] D. Lezal, *J. Optoelect. & Adv. Mat* **5** (2003), p. 23.
- [4] J.S. Sanghera and I.D. Aggarwal, *J. Non-Cryst. Solids* **213-214** (1997), p. 63.
- [5] A.M. Reitter, A.N. Sreeram, A.K. Varshneya and D.R. Swiler, *J. Non-Cryst. Solids* **139** (1992), p. 121.
- [6] A.B. Seddon and C.A. Miller, Unpublished work, 2006.
- [7] A.G. Whittaker and D.M.P. Mingos, *J. Microwave Power and Electromag. Eng.* **29** (1994), p. 195.

Chapter 8

Processing of the DMO As_2Se_3 glass for photonic use.

One sample of DMO As_2Se_3 glass was drawn to fibre and another sample was hot embossed to examine whether a DMO chalcogenide could be further shaped for the photonic applications. The results obtained from the fibre drawing are discussed in subsection 8.1 and the results obtained from the hot embossing are discussed in subsection 8.2. Chapter 8 is summarised in section 8.3.

8.1 The fibre drawing of the DMO As_2Se_3 glass.

Sample id: MW18 was drawn to fibre in an inert atmosphere of white spot nitrogen (BOC) in class 1000 clean room (see section 3.1.1.1). Nitrogen was passed through a copper coil immersed in liquid nitrogen (BOC) to remove any residual water. The furnace was then cooled using cold water maintained at 18°C . The preform (10 mm OD) was fed in a graphite ring (15 mm OD) and was positioned in such a way that it was 5mm below the graphite ring. The graphite ring was heated using radio frequency waves which in turn heats up the glass preform. The chalcogenide glass preform was heated to $\sim 290^\circ\text{C}$ (approximately $\sim 100^\circ\text{C}$ above the T_g of the glass as T_g of arsenic selenide is $\sim 180^\circ\text{C}$). As soon as the preform was heated to the above specified temperature ($\sim 290^\circ\text{C}$) the viscosity of the reduced to $\sim 10^{-4.5} \text{ Pa s}^{-1}$ a glass gob with a long tail had dropped under gravity (see fig 8.1).

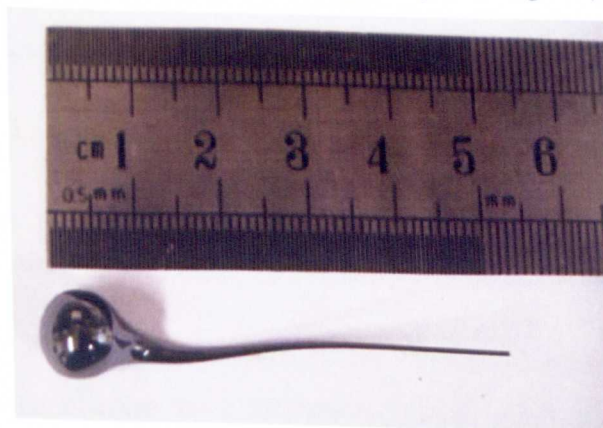


Fig. 8.1 The DMO As_2Se_3 glass gob with a tail dropped while fibre drawing (sample id: MW18).

The DMO As_2Se_3 glass was drawn to a tail was drawn in the shape of the fibre. The fibre was cooled immediately so that the shape of the fibre (diameter) could be maintained. A fibre of

200 μm was drawn here. It was then wound in the polystyrene drum (1 m diameter, see fig. 8.2).

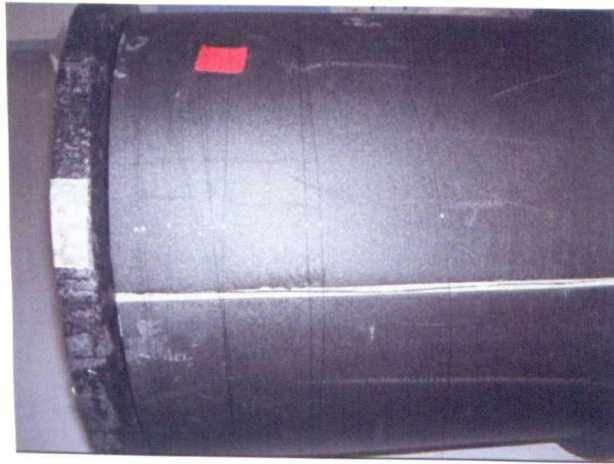


Fig. 8.2 The DMO As_2Se_3 glass fibre wound on a polystyrene drum (sample id: MW18).

A piece of fibre was observed under ESEM (see fig. 8.3 (a) and 8.3 (b)) and was found to have debris on its surface.

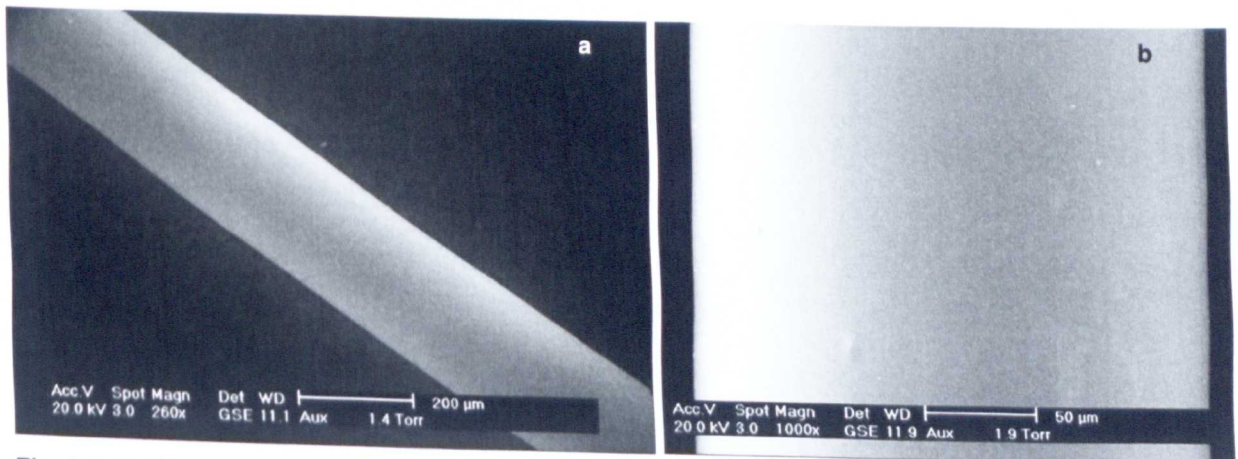


Fig. 8.3 ESEM micrograph of (a) the fibre drawn from the DMO As_2Se_3 (sample id: MW18).

(b) showing lumps and debris on the surface of the fibre drawn from the DMO As_2Se_3 sample id: MW18)

The fibre did not show any sign of formation of skin on its surface though few lumps and dirt was observed on its surface in the ESEM micrographs (see fig. 8.3 (b)).

Unfortunately, the above drawn fibre did not transmit light.

8.2 The vacuum pressing of the DMO As_2Se_3 glass

The DMO arsenic selenide glass was pressed under vacuum at a temperature higher than the T_g of the glass, to verify whether the DMO chalcogenide glass (arsenic selenide) could be used for the fabrication of rib waveguides. As described in section 3.4.2 a vacuum pressing machine designed in-house by Dr. D. Furniss was used for this purpose. The following

procedure was employed for the formation of channels and ribs on the surface of the DMO As_2Se_3 glass.

1. The arsenic selenide glass (sample id: MW39) was cut into thin disc of about 2 mm thickness and 10 mm diameter (diameter remaining the same as the internal diameter of silica glass melt-ampoule) as described in section 3.2.3.1.
2. One side of the disc was then polished using silicon carbide powder and diamond paste (see section 3.2.3.2).
3. The polished chalcogenide glass (sample id: MW39) was placed on the lower aluminium plate cleaned using acetone (Fischer, 99%). A thin film of silicon (supplied by Professor Catrina Bryce, Optoelectronics Research Group, Department of Electronics and Electrical Engineering, The University of Glasgow) was placed over the aluminium plate over which the polished DMO chalcogenide sample was placed keeping the polished face of the sample facing towards the upper aluminium plate.
4. The mould having ribs and channel was kept on the top of the DMO arsenic selenide glass. The complete arrangement is shown in fig. 8.4.

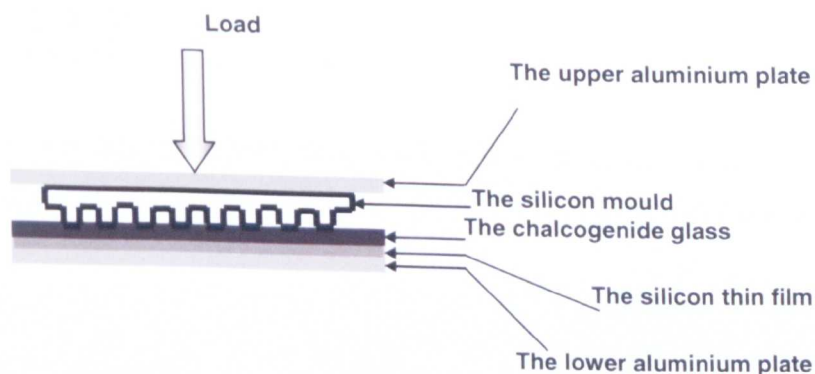


Fig 8.4 The arrangement of different elements used during vacuum pressing.

5. The upper and lower aluminium plates were heated to a temperature of $245^{\circ}C$. This temperature was maintained for approximately 5 mins so that the glass sample should also achieve the same high temperature in order to make the glass sample soft as it was easy to press soft glasses. The plates were heated to a temperature higher than the T_g of the chalcogenide glass since it was easy to press a soft glass.
6. Once the glass became soft it was pressed by applying force. Two discs of the same sample (sample id: MW39) of the glass rod was pressed to verify the reproducibility of the process. One sample (id: MW39 P1) was pressed using 30 N force whereas the other sample (id: MW39P2) was pressed using 60 N force. The whole process was done under vacuum. The

following Table 8.1 enlists the whole procedure of vacuum pressing which include that the pressure was applied in two different ways while pressing two different slices of the same sample.

Table 8.1 The procedure for vacuum pressing.

Steps during vacuum pressing.				
Step 1	Stacking of the different elements used for pressing (see fig. 8.4).			
Step 2 to step 4 was done under vacuum.				
Step 2	Heating of the glass above its T _g to make the sample soft.			
	Stage	Schedule		
	1.	From room temperature to 245°C in 1 hr		
	2.	Dwell at 245°C for 5 minutes		
Step 3	Application of load (done in different ways for different samples)			
	Sample id	Stage	Schedule	
	MW39P1	1.	30 N for 10 mins	
		2.	30 N to 15 N after 10 mins	
		3.	Pressed for 9 mins at 15 N	
		4.	Pressure released	
	Sample id	Stage	Schedule	
MW39P2	1.	60 N for 15 mins		
	2.	Pressure released.		
Step 4	Annealing of the pressed sample (remain same for both samples).			
	Stage	Schedule		
	1.	Step to 180°C from 245°C		
	2.	Dwell at 180°C for 1 hr		
	3.	From 180°C to 140°C @ 5°C		
	4.	From 140°C to room temperature @ 20°C		

It was observed that channels and ribs were formed in both samples thus confirming that a DMO As₂Se₃ glass can hot embossed. The hot embossed samples were studied under ESEM (figs. 8.5 ('a' & 'b') and 8.7).

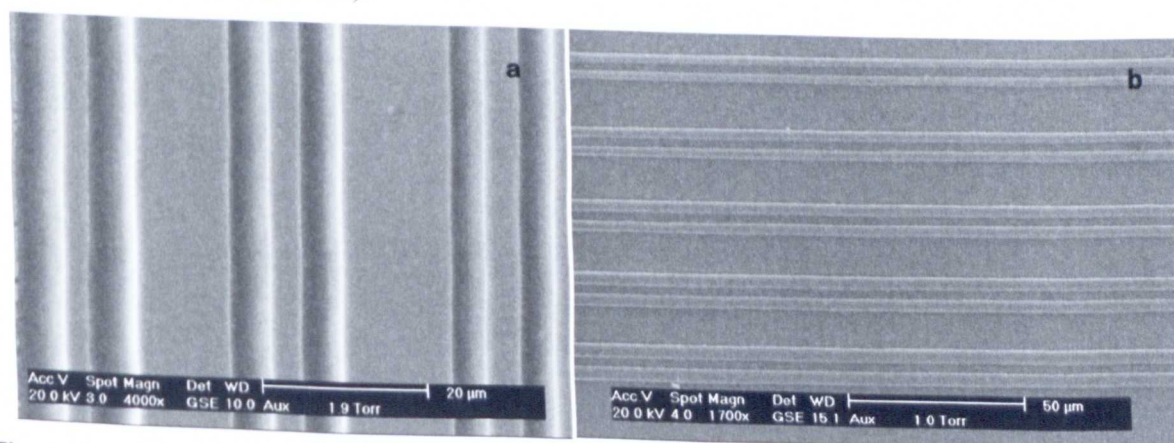


Fig. 8.5 ('a' and 'b') The ESEM micrograph of the sample id MW39P1 showing the imprints of hot embossing.

By comparing figs. 8.5 and 8.6 it was observed that the edges of sample id: MW39P2 pressed at higher load for shorter time were more deflated than MW39P1. Perhaps due to application

of higher pressure the DMO As_2Se_3 glass (sample id: MW30P2) was more distorted than the sample id MW39P1 though the channels and the ribs were formed.

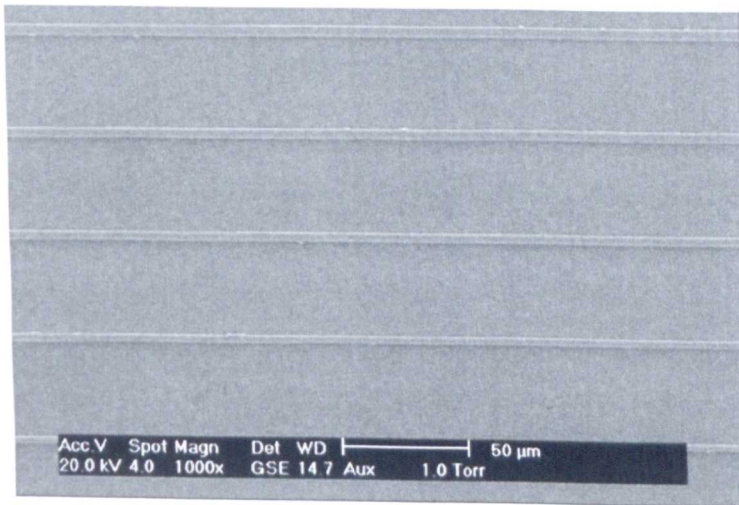


Fig. 8.6 ESEM micrograph of the sample id: MW39P2 showing the channels and ribs formed on the surface of the glass.

8.3 Summary

A DMO As_2Se_3 glass can be drawn to a fibre and can be hot embossed. The DMO As_2Se_3 glass fibre did not transmit infrared light as observed through FTIR (see section 3.).

Chapter 9

Conclusions.

This chapter summarises the conclusions of the project based upon the summaries at the end of each Chapter 4 to 8 (see section 9.1) and suggests possible future work (see section 9.2).

9.1 Conclusions.

The DMO synthesis of As_2S_3 , As_2Se_3 , $Ge_{17}As_{18}Se_{65}$, $Ge_{33}As_{12}Se_{55}$ and $Te_{30}As_{20}Se_{50}$ glasses was investigated and compared to the conventional synthesis in a resistance furnace. The DMO chalcogenide products were made in the order of less than 35 minutes whereas conventional heating method takes about 1.5 days showing that the application of microwave heating exhibited great time saving [1]. However, the time saving was at the expense in some cases of decreased glass product quality compared to the glass products made through conventional resistance heating.

The increased rate of reaction in the DMO compared to that in the resistance furnace was attributed to the formation of plasma which caused a very high temperature ($> 1000^\circ C$) of the reaction system leading to the almost instant melting of the some reactants. For example, in an effort to make As_2Se_3 (id: MW39), arsenic and selenium melted within 30 seconds as soon as the reactants were exposed to microwaves when $As_{40.1}Se_{59.9}$ was formed (according to the results obtained in EDX ESEM).

It is proposed here that the formation of plasma may be attributed to the presence of metalloids *i.e.* arsenic in the batch when the heat is produced due to the skin-effect (2.9.3) [2]. It may also due to vaporised chalcogens such as sulfur, selenium present in the reaction system [3].

It should be noted that the reactants were crushed to powder and the individual elemental batch elemental powders were mixed intimately together keeping the idea of skin effect into mind [2] and heat could be produced in the reaction. Since, the melting points of sulfur ($119^\circ C$), selenium ($221^\circ C$) and tellurium ($450^\circ C$) [4], it is supposed that these reactants melted during the formation of plasma. Arsenic sulfide could be synthesised with partial success only (see Chapter 4). It is proposed that sulfur (unlike the selenium) does not melt

'cleanly' thus it polymerises and becomes intractable - maybe that is why it is difficult to get a glass melt without the agitation just because the sulfur liquid is too viscous to move around and find new arsenic to react with whereas in the resistance furnace the movement keeps the potential for the sulfur reacting with free arsenic ever-present.

Below is very briefly summarised the result of comparing the amorphicity, homogeneity and T_g of each chalcogenide composition type made in the DMO as opposed to resistance furnace. After these short sections some more overall points which will include glass transmission window are discussed about the general observations during the DMO heating.

(i) Batch As₂S₃ (see chapter 4)

In an attempt to make As₄₀S₆₀ glass, As_{43.9}S_{56.1} X-ray amorphous material (see fig 4.2) (with standard deviation of 3.4 in at% of As and standard deviation of 3.9 in at% of sulfur (see Table 4.9)) was made irreproducibly with partial success. A glass rod was not formed (id: MW6). In contrast to that a homogenous glass rod of As_{40.4}S_{59.6} (with standard deviation of 0.7 in at% of As and standard deviation of 0.7 in at% of sulfur (see Table 4.9)) was prepared by conventional heating. The DMO As-S glass exhibited several DTA T_gs whereas the conventionally prepared As₂S₃ glass exhibited a single DSC T_g value of 201°C ± 5°C.

(ii) Batch As₂Se₃ (see chapter 5).

As₄₀Se₆₀ batched glass rods were made using a domestic microwave oven and were X-ray amorphous (see fig. 5.6) e.g. As_{40.1}Se_{59.9} glass rod (id: MW39) with standard deviation of arsenic and Se of 0.4 (see Table 5.9) was synthesised. A conventionally prepared glass rod of As_{41.1}Se_{58.9} with standard deviation 0.5 of arsenic and selenium (see Table 5.13) was formed. The DMO As-Se glass had a DSC T_g of 180°C ± 5°C and the DSC T_g of conventionally prepared glass was found to have the same T_g 180°C ± 5°C (see fig. 5.12 and 5.13).

(iii) Batch Ge₁₇As₁₈Se₆₅ (see chapter 6).

In an effort to make Ge₁₇As₁₈Se₆₅ glass rod, an X-ray amorphous (see fig. 6.10) Ge_{17.1}As_{19.4}Se_{63.5} glass rod with a standard deviation of 0.3 in the at% of Ge, a standard deviation of 0.4 in the at% of As and a standard deviation of 0.3 in the at% of selenium (see Table 6.10) was formed (sample id: MW31). Similarly, a Ge_{17.6}As_{19.2}Se_{63.2} amorphous glass rod (see fig. 6.10) with a standard deviation of 0.4 in the at% of Ge, a standard deviation of 0.4 in the at% of As and a standard deviation of 0.5 in the at% of selenium (see Table 6.12) was formed by conventional melting. The measured DSC T_g value for the DMO

$\text{Ge}_{17.1}\text{As}_{19.4}\text{Se}_{63.5}$ was $246^\circ\text{C} \pm 5^\circ\text{C}$ (see fig. 6.19) however the DSC Tg value of a conventionally prepared glass $\text{Ge}_{17.6}\text{As}_{19.2}\text{Se}_{63.2}$ was $235^\circ\text{C} \pm 5^\circ\text{C}$ (see fig. 6.20).

(iv) Batch $\text{Ge}_{33}\text{As}_{12}\text{Se}_{55}$ (see chapter 6).

In an effort to make $\text{Ge}_{33}\text{As}_{12}\text{Se}_{55}$ glass rod, $\text{Ge}_{32.8}\text{As}_{11.0}\text{Se}_{56.4}$ (id: MW38) with a standard deviation of 3.8 in the at% of Ge, a standard deviation of 3.7 in the at% of As and a standard deviation of 2.7 in the at% of selenium (see Table 6.14) was prepared. However this DMO rod glass rod exhibited a large X-ray crystalline peak at $32.5^\circ 2\theta$ in X-ray diffraction pattern (id: MW38) (see fig. 6.26); the crystal peak is unknown. In contrast to that, a completely X-ray amorphous glass rod (see Fig. 6.27 (id: CH 15)) with stoichiometry $\text{Ge}_{33.8}\text{As}_{12.5}\text{Se}_{53.6}$ (with a standard deviation of 0.9 in the at% of Ge, a standard deviation of 0.6 in the at% of As and a standard deviation of 1.2 in the at% of selenium (see Table 6.15)) glass rod was formed with the conventional heating method. The DSC Tg value for the DMO prepared $\text{Ge}_{32.8}\text{As}_{11.0}\text{Se}_{56.4}$ glass rod was found to be $368^\circ\text{C} \pm 5^\circ\text{C}$ (see fig. 6.30 (id: MW38)) whereas the conventionally prepared $\text{Ge}_{33.8}\text{As}_{12.5}\text{Se}_{53.6}$ had a DSC Tg value of $371^\circ\text{C} \pm 5^\circ\text{C}$ (see fig. 6.31(id: CH15))

(v) Batch $\text{Te}_{20}\text{As}_{30}\text{Se}_{50}$ (see chapter 7).

In trying to make $\text{Te}_{20}\text{As}_{30}\text{Se}_{50}$ glass, $\text{Te}_{19.6}\text{As}_{30.4}\text{Se}_{50.0}$ (see Table 7.6) X-ray amorphous (see fig.7.4) glass in form of rod (id: MW36) (with a standard deviation of 0.4 in the at% of Te, a standard deviation of 0.5 in the at% of As and a standard deviation of 0.7 in the at% of selenium (see Table 7.6)) was prepared. The DSC Tg value of both the DMO TAS and conventionally prepared TAS glass was $133^\circ\text{C} \pm 5$ (see fig. 7.9 to 7.11).

Once it was proved that As_2Se_3 bulk glass could indeed be made in the DMO of good optical quality and equivalent in properties to As_2Se_3 bulk glass made by resistance heating, then further investigation had to be carried out in order to form in the DMO a monolithic chalcogenide glass rod. It was found that formation of a rod was dependent upon the length of the silica glass melt-ampoule (see section 5.1) as it was important to stand the ampoule just of vertical (see section 5.1) and for the glass-melt to trickle down and collect at the bottom of the ampoule. The melt could then be quenched and annealed to form a chalcogenide glass rod. This success was in part due to the fact that during the microwave heating method the heating stopped as soon as the DMO was switched off and the chalcogenide glass-melt then was stuck to the walls of the silica glass melt-ampoule. This collection technique may be compared to what happens during the conventional resistance furnace glass melting when the silica glass

melt-ampoule was kept vertical at a temperature much higher than the corresponding T_g value (of the respective glass) for more than 15 minutes with the aim to collect the chalcogenide glass-melt at the bottom of the silica glass melt-ampoule.

All the selenium containing glasses boiled during microwave heating. Boiling of chalcogenide glass-melt affected the amorphicity of the glass. For example, DMO As_2Se_3 and $Te_{30}As_{20}Se_{50}$ glass-melts which boiled upon exposure to the microwaves for 35 minutes exhibited neither crystalline peaks in XRD analysis nor crystalline structure by SAED.

$Te_{30}As_{20}Se_{50}$ showed some crystalline structure in SAED when the reactants were exposed to microwaves only for about 5 minutes and could not boil well.

DMO Ge-As-Se glasses irrespective of the composition were not allowed to have a long exposure to the microwaves. This was because, since the melt accumulated at the upper-part of the silica melt-ampoule, it could not trickle down due to its high viscosity. Thus chalcogenide melt was found to have divided as a glass rod into two portions. Hence to make a single glass-rod, the reactants were exposed to microwaves for approximately 10 minutes. However, again, for one of the samples of $Ge_{33}As_{12}Se_{55}$ a crystalline peak was observed in X-ray diffraction pattern when the reactants were exposed only for about 10 minutes. Hence, time of exposure to the microwaves is very important and affects the overall quality and properties of the DMO products and whether or not good glasses are produced.

The arsenic sulfur composition mixture never boiled when exposed to microwaves and it is proposed that this was the primary reason that the chalcogenide glass product was found to be inhomogeneous.

Again it is postulated that plasma-induced boiling resulted in the formation of a homogeneous glass-melt. For example, the as-annealed As-Se DMO glass-rods showed no distinct macro-separated regions whereas as-annealed DMO As-S glass had three distinct regions. Also, the thermal analysis showed at least three T_g values for the DMO As-S glass which is in contrast to the observation where a single T_g value was always observed when an As-Se containing glass was prepared through microwave heating.

The stoichiometry of the DMO chalcogenide glasses were studied by performing EDX analysis using ESEM. Again, it was observed that the DMO As-Se chalcogenide glasses showed stoichiometry which was in agreement with the desired value whereas the DMO As-S

glass showed a large deviation from the desired values. Thus As-Se almost homogenous glass was made through microwave heating.

The transmission windows of all the glasses were measured using FTIR spectroscopy. It was observed that all the DMO chalcogenide glasses were transparent in the mid-infrared region. This showed that these glasses might be used for photonic applications in future which suggested that some *useful* glasses can be made through microwave heating. Moreover it was observed that the loss due to –OH bond at 2.9 μm and loss due to H-O-H at 6.3 μm was less in the DMO chalcogenide glasses than the chalcogenide glasses made through conventional heating method. Most strikingly this loss was least in DMO As-S glass which never boiled and hence perhaps had very little interaction with water vapour which perhaps had evaporated. In DMO As_2Se_3 glass the loss due to C-H bond at 4.3 μm was higher than for the conventional heating method [5, 6] which is perhaps due to the long reaction time for reasons unknown at present.

The quality and the purification of the ampoule were important while preparing chalcogenide glasses. The as-received powdered materials were found to be full of impurities and it was decided that as-sourced powdered starting materials would not be used during the project (see section 5.1).

The DMO As_2Se_3 was processed further for photonic applications for example it was drawn to a fibre and hot embossed (see chapter 8). Unfortunately, the fibre did not transmit any light and the reasons for this are not known at present; clearly more work is needed to establish that good optical quality optical fibre can be drawn from DMO rod preforms or the DMO approach is called into question.

However, the variation of refractive indices with wavelength (*i.e.* the dispersion) of DMO As_2Se_3 glass is in good agreement with that of the As_2Se_3 glass made through conventional heating method. Refractive index in general is extremely sensitive to composition and so this is an encouraging result for concluding that the glass was of good homogeneity and extremely similar at the molecular level to glasses made by resistance heating.

The microwave heating method gave great energy saving. The preparation of 10 g of chalcogenide glass needed about 28 K Watt h through the conventional heating method whereas the microwave heating consumed less than 1 K Watt h. Hence, the DMO preparations of As_2S_3 , As_2Se_3 , $\text{Ge}_{17}\text{As}_{18}\text{Se}_{65}$, $\text{Ge}_{33}\text{As}_{12}\text{Se}_{55}$, $\text{Te}_{20}\text{As}_{30}\text{Se}_{50}$ such as shown here, was fast and environmentally friendly.

9.2 Future work.

1. Try making other chalcogenide glasses through microwave heating such as pure selenium glass.
2. Try to hot emboss DMO As_2Se_3 as wave guide and whether examine whether it can be used as a photonic device.
3. The DMO $\text{Ge}_{17}\text{As}_{18}\text{Se}_{65}$, DMO $\text{Ge}_{33}\text{As}_{12}\text{Se}_{55}$ and $\text{Te}_{20}\text{As}_{30}\text{Se}_{50}$ can be further purified, they can be distilled and purified for instance removal of oxygen by heating the glass in the presence of aluminium to be suitable for photonic applications [7].
4. Try making photonic devices of all the DMO chalcogenide glasses.
5. Measure the refractive indices and dispersion of all the DMO chalcogenide glasses and compare the value with the literature value.

References:

- [1] K. Sivakumaran and C.K.S. Nair, *J. Phys. D: Appl. Phys.* **38** (2005), p. 2476.
- [2] <http://www.tan-delta.com/>, Last accessed 28/1/2009.
- [3] A.G. Whittaker and D.M.P. Mingos, *J. Microwave Power and Electromag. Eng.* **29** (1994), p. 195.
- [4] F.A. Cotton and G. Wilkinson, *Advanced inorganic chemistry*, A Wiley Interscience Publication, 5th edition, New York, (1976).
- [5] D. Lezal, *J. Optoelect. & Adv. Mat* **5** (2003), p. 23.
- [6] J.S. Sanghera and I.D. Aggarwal, *J. Non-Cryst. Solids* **213-214** (1997), p. 63.
- [7] H. Rowe, Ph.D. Thesis, University of Nottingham, (2004-2008).

APPENDICES

Appendix A



Fig. A-1 TEM SAED of portion 'A' of id: MW6 (fig. 4.1).



Fig. A-2 TEM SAED of portion 'D' id: MW6 (of fig 4.1).



Fig A-3 TEM SAED of the conventionally prepared arsenic sulfide batched as As_2S_3 (atomic ratio) id: CF 074.

Appendix B

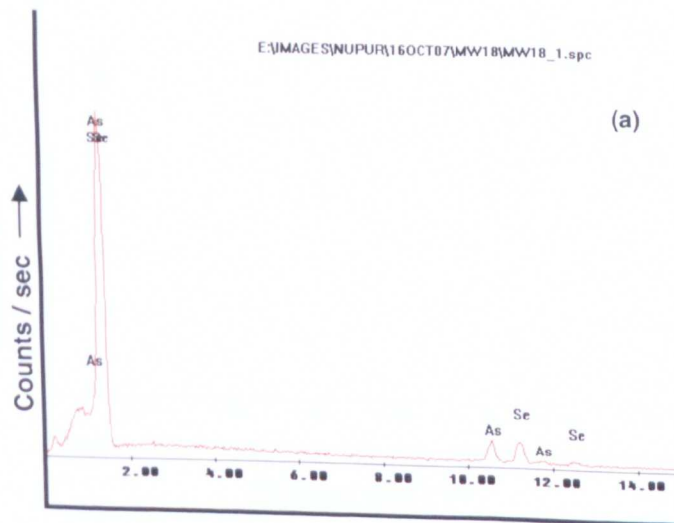


Fig. B-1 TEM SAED pattern of DMO As-Se rod product (id: MW39).



Fig. B-2 TEM SAED pattern of the As-Se product (id: CH12) made in resistance rocking furnace.

Fig. B-3 The ESEM EDX spectrum of: (a) one area of a sample of the DMO As-Se product id: MW18 and (b) the ESEM EDX spectrum of a different area of the same sample, showing reproducibility.



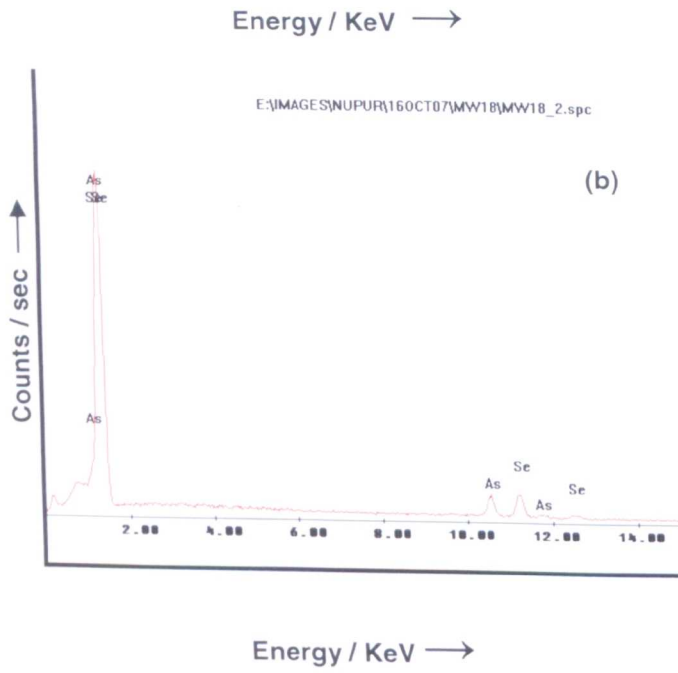
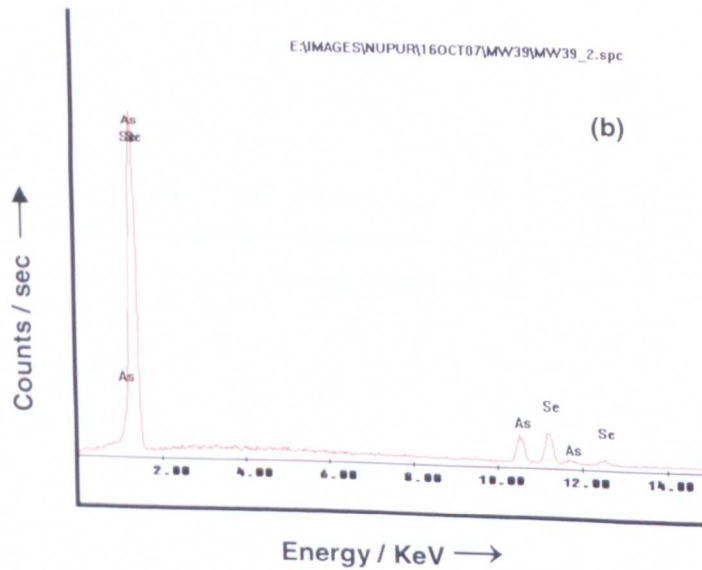
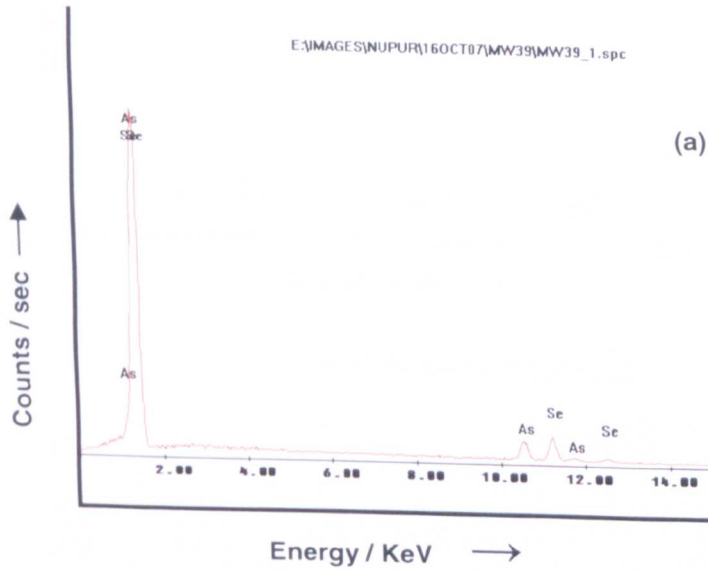
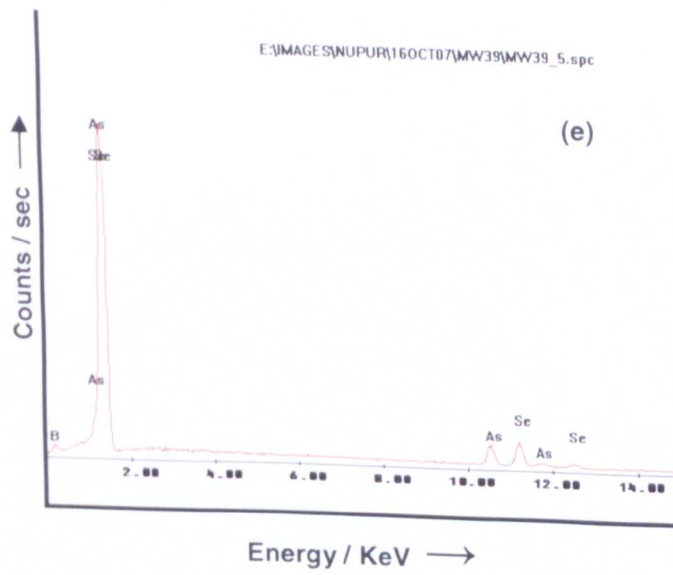
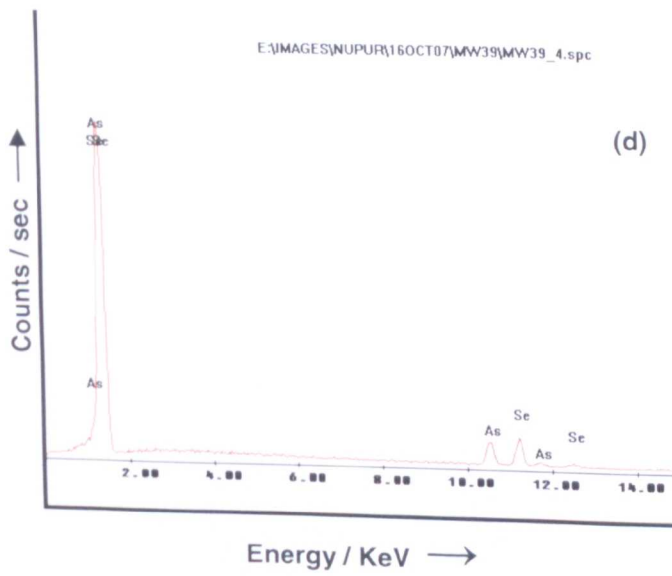
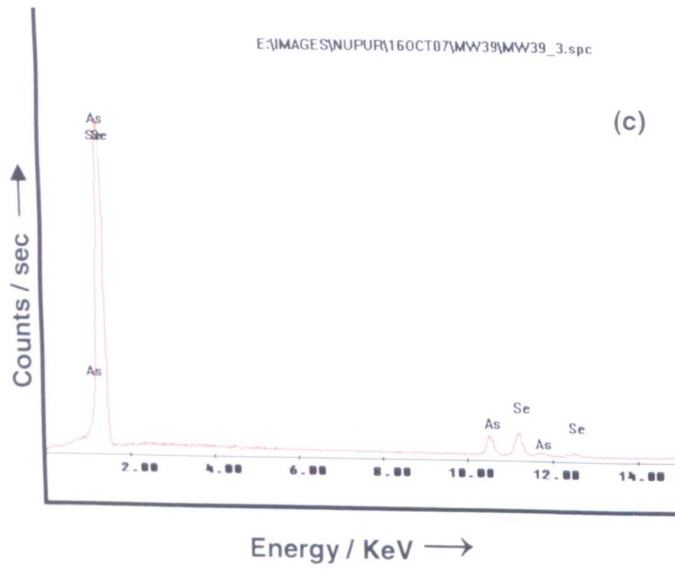
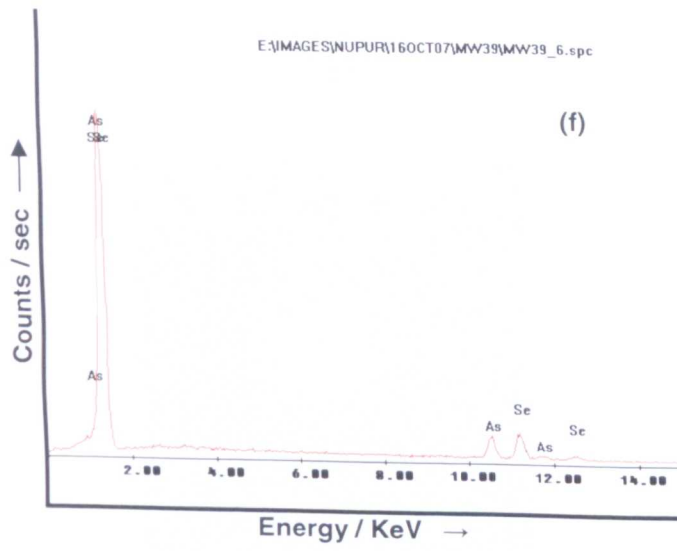


Fig. B-4 (a) to (f) are ESEM EDX spectra taken from different areas of the same sample of the DMO As-Se product id:MW39, showing reproducibility of these results.







Appendix C



Fig. C-1 TEM SAED pattern of DMO Ge/As/Se = 17/18/65 product (id: MW29 bulk_upper), indicating an amorphous structure.

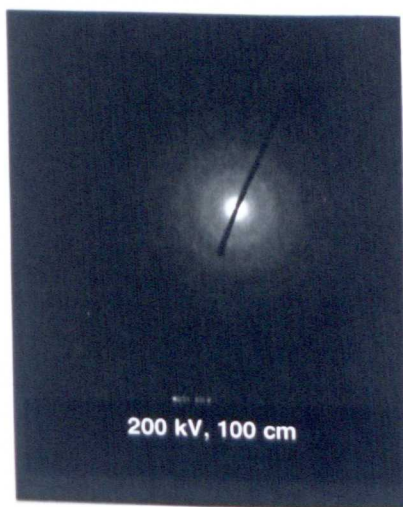


Fig. C-2 TEM SAED of DMO Ge/As/Se = 17/18/65 product (id: MW31), indicating an amorphous structure.

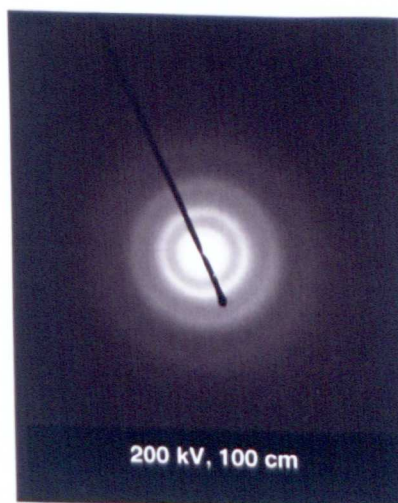
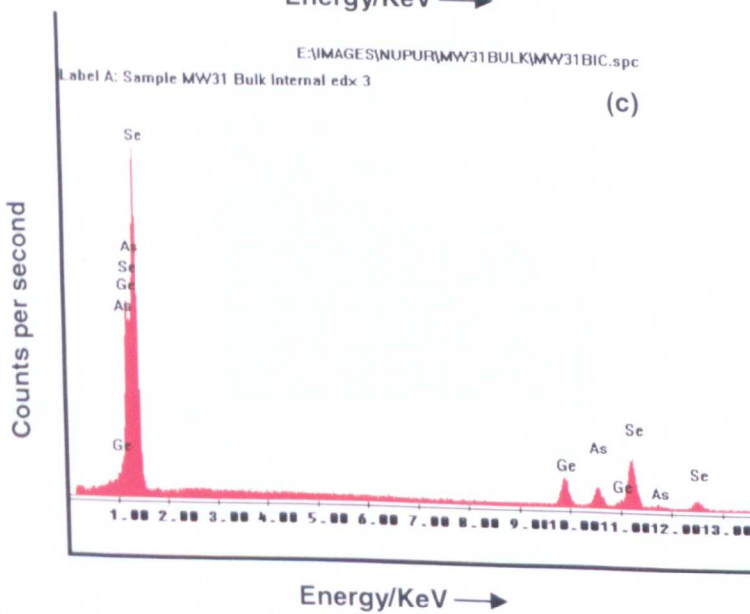
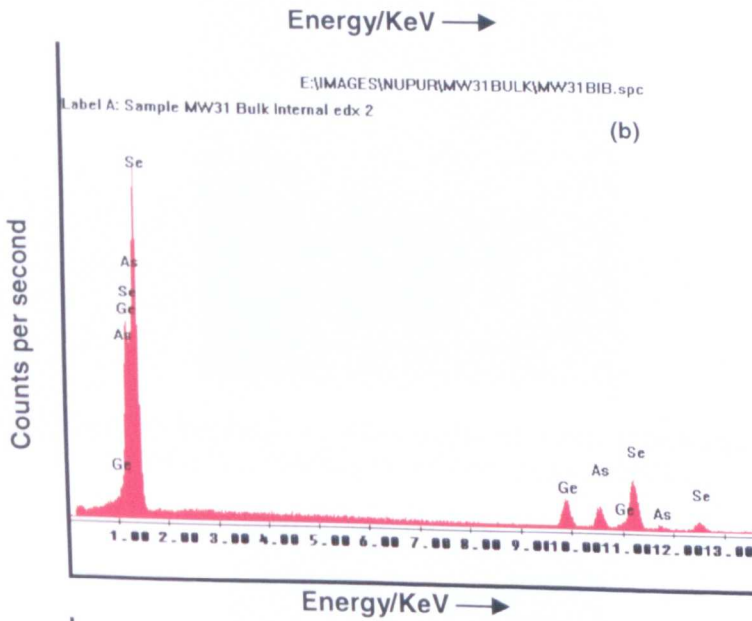
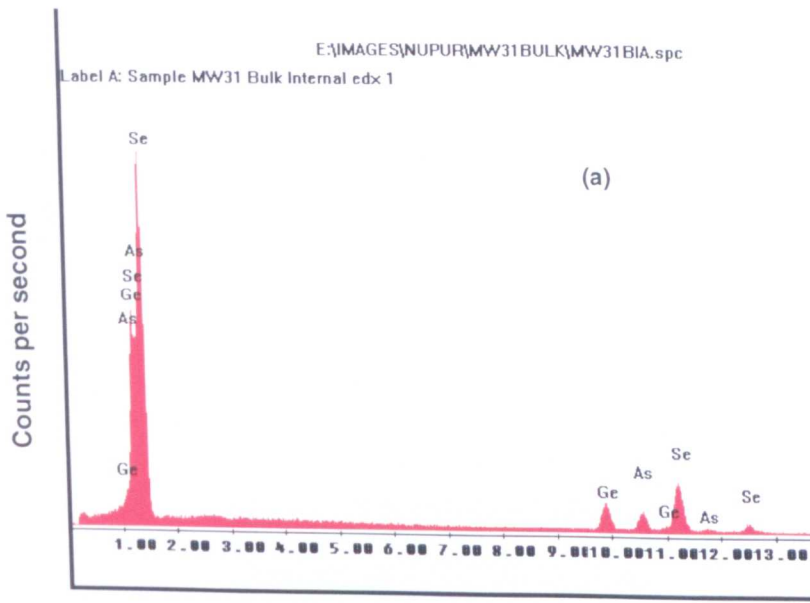


Fig. C-3 TEM SAED pattern of $\text{Ge}_{17}\text{As}_{18}\text{Se}_{65}$ glass made using resistance rocking furnace (id: CH14), indicating an amorphous structure

Fig. C-4 The spectra of DMO Ge/As/Se = 17/18/65 (at%) id: MW31 obtained for different regions ((a) to (d)) of the sample during ESEM EDX analysis of the sample.



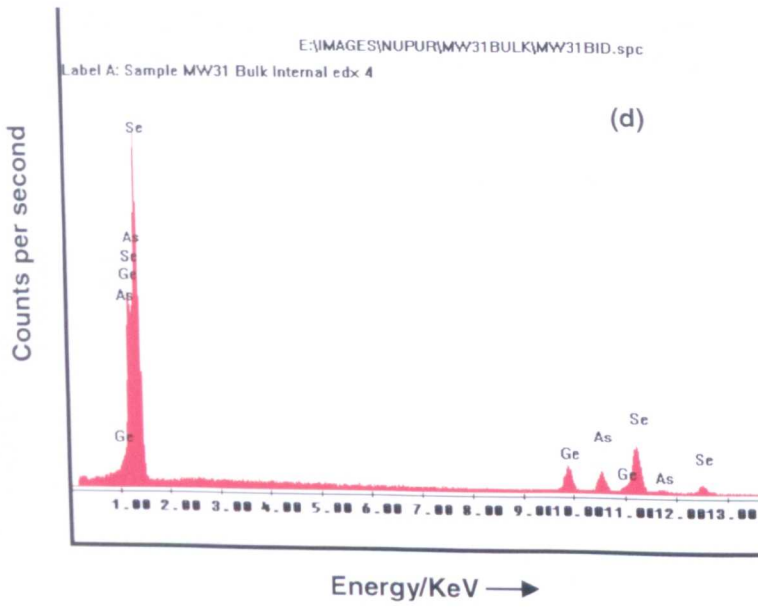


Fig. 5 TEM SAED pattern of $\text{Ge}_{33}\text{As}_{12}\text{Se}_{55}$ glass made using the resistance rocking furnace (id: MW38), indicating an amorphous structure.

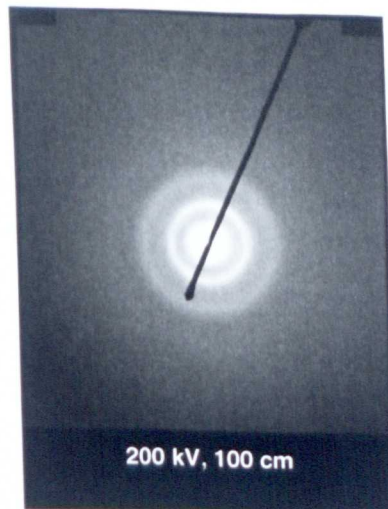
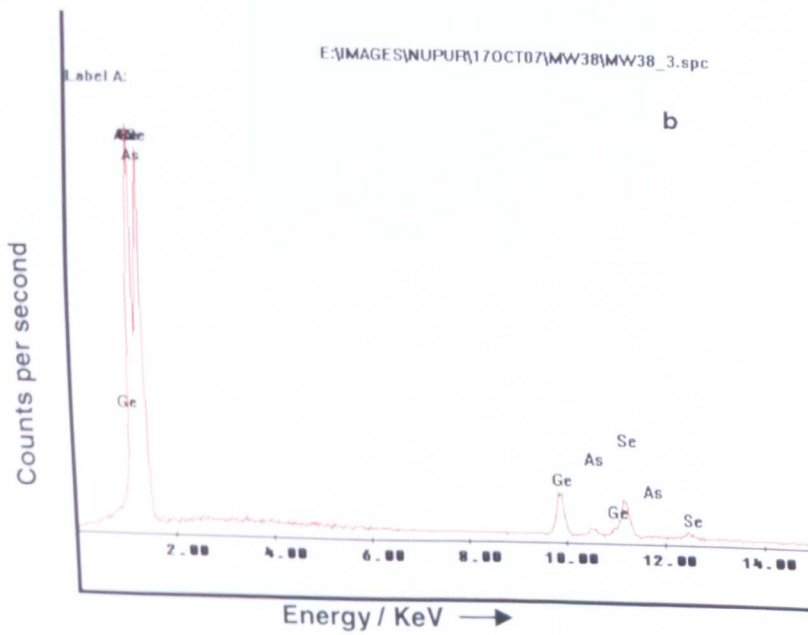
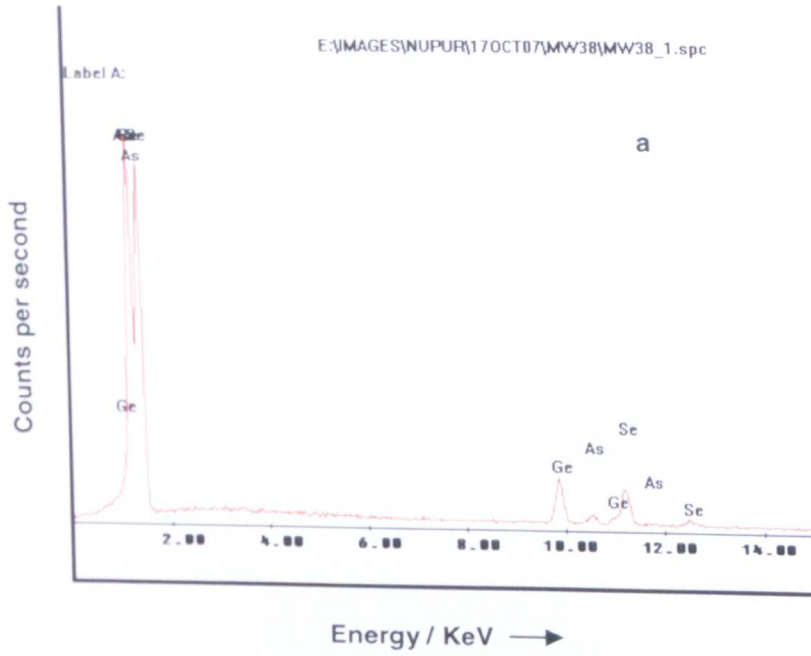


Fig. 6 TEM SAED of $\text{Ge}/\text{As}/\text{Se} = 33/12/55$ (at%) product made through conventional heating showing the lack of crystallinity (id: CH15).

Fig. 7 The spectra of DMO Ge/As/Se = 12/33/55 (at%) id: MW38 obtained for different regions of the sample during ESEM EDX analysis of the sample ((a) to (b)).



Appendix D

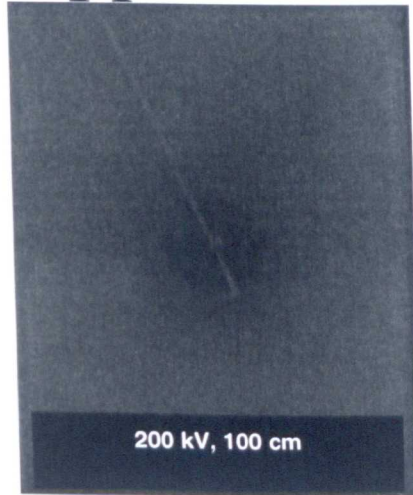


Fig. 1 TEM SAED pattern showing a typical blurred structure observed for most of the DMO Te/As/Se = 20/30/50 product (id: MW 30).

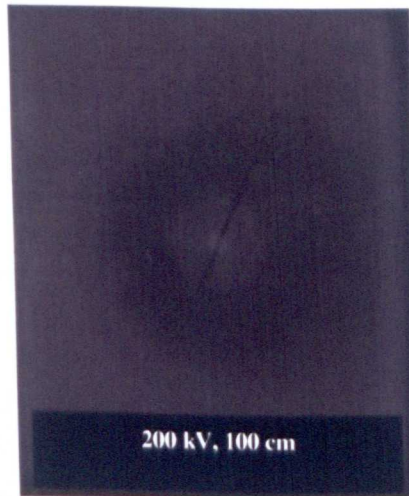


Fig. 2 TEM SAED pattern showing a blurred structure for the DMO Te/As/Se = 20/30/50 (atomic %) product (id: MW 33) when the glass melt had been boiled inside the DMO for 30 minutes.

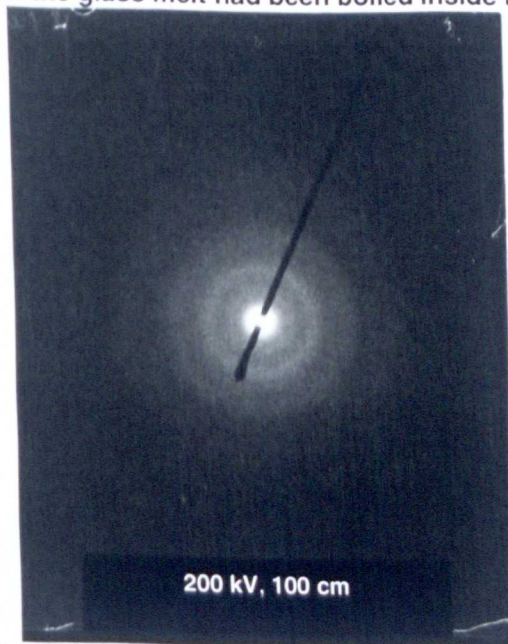
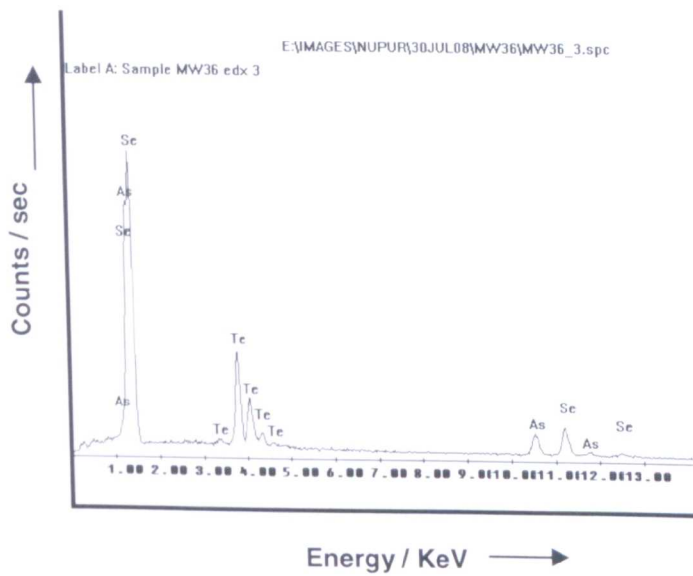


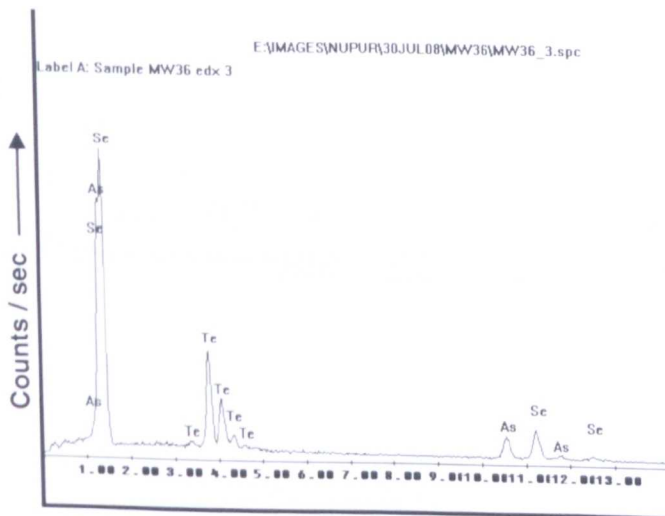
Fig. 3 TEM SAED pattern showing a blurred structure for the conventionally melted $\text{Te}_{20}\text{As}_{30}\text{Se}_{50}$ glass (id: CH20).

Fig. 4 ESEM EDX spectra (from 'a' to 'd') of randomly chosen results for DMO TAS products (id: MW33 and MW36) all of which were shown to exhibit the desired stoichiometry.

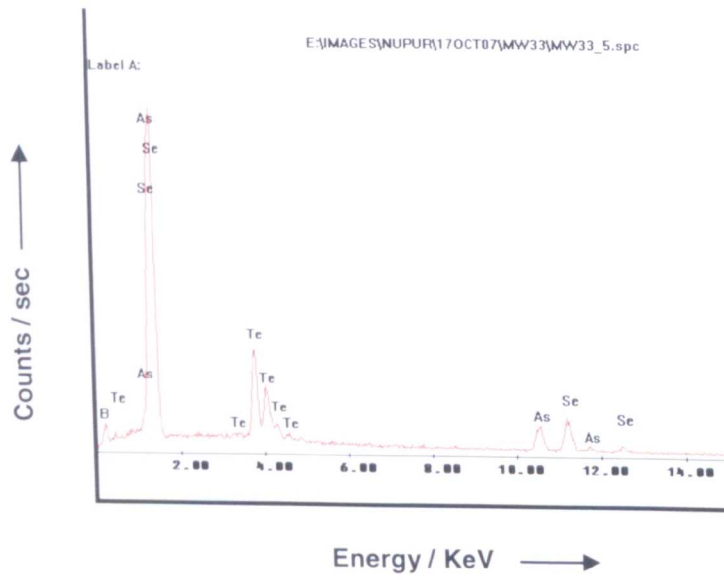
(a) DMO TAS id: MW36



(b) DMO TAS id: MW36



(c) DMO TAS id: MW33



(d) DMO TAS id: MW33

